



Universiteit
Leiden
The Netherlands

Viral gene therapy approaches for CRB1 retinal disease

Boon, N.

Citation

Boon, N. (2023, November 2). *Viral gene therapy approaches for CRB1 retinal disease*. Retrieved from <https://hdl.handle.net/1887/3655975>

Version: Publisher's Version

License: [Licence agreement concerning inclusion of doctoral thesis in the Institutional Repository of the University of Leiden](#)

Downloaded from: <https://hdl.handle.net/1887/3655975>

Note: To cite this publication please use the final published version (if applicable).

Viral Gene Therapy Approaches for *CRB1* Retinal Disease

Nanda Boon

ISBN 978-94-6483-429-1

Cover Art Nanda Boon & Hugo Veldhuizen.

Printed by Ridderprint, Alblaserdam.

The printing of this thesis was financially supported by Stichting Blindenhulp.

Copyright © Nanda Boon, 2023.

All rights are reserved. No part of this publication may be reproduced, stored or transmitted in any form or by any means without permission of the copyright owners.

Viral gene therapy approaches for *CRBI* retinal disease

Proefschrift

ter verkrijging van
de graad van doctor aan de Universiteit Leiden,
op gezag van rector magnificus prof.dr.ir. H. Bijl,
volgens besluit van het college voor promoties
te verdedigen op donderdag 2 november 2023
klokke 12:30 uur

door

Nanda Boon
geboren te Vught,
in 1994

Promotor: Prof. Dr. G.P.M. Luyten

Co-Promotor: Dr. J. Wijnholds

Leden promotiecommissie:

Prof. Dr. R.C. Hoeben

Prof. Dr. W.M.C. van Roon-Mom

Prof. Dr. C.J.F. Boon, LUMC and Amsterdam UMC

Prof. Dr. J. Verhaagen, Netherlands Institute for Neuroscience

Prof. Dr. A.A.B. Bergen, Amsterdam UMC

The research here described was conducted at the Department of Ophthalmology, at the Leiden University Medical Center (LUMC). The studies described in this thesis were financially supported by Foundation Fighting Blindness, The Netherlands Organization for Health Research and Development (ZonMw), Stichting Blinden-penning, Leiden Regenerative Medicine Platform, Rotterdamse Stichting Blindenbelangen, Landelijke Stichting voor Blinden en Slechtienden, Dutch blindness funds (Uitzicht), MaculaFonds, Stichting Blindenhulp, University of Pennsylvania Orphan Disease Center in partnership with Curing Retinal Blindness Foundation, Bontius Stichting, and HORAMA (now known as Coave Therapeutics).

Table of Contents

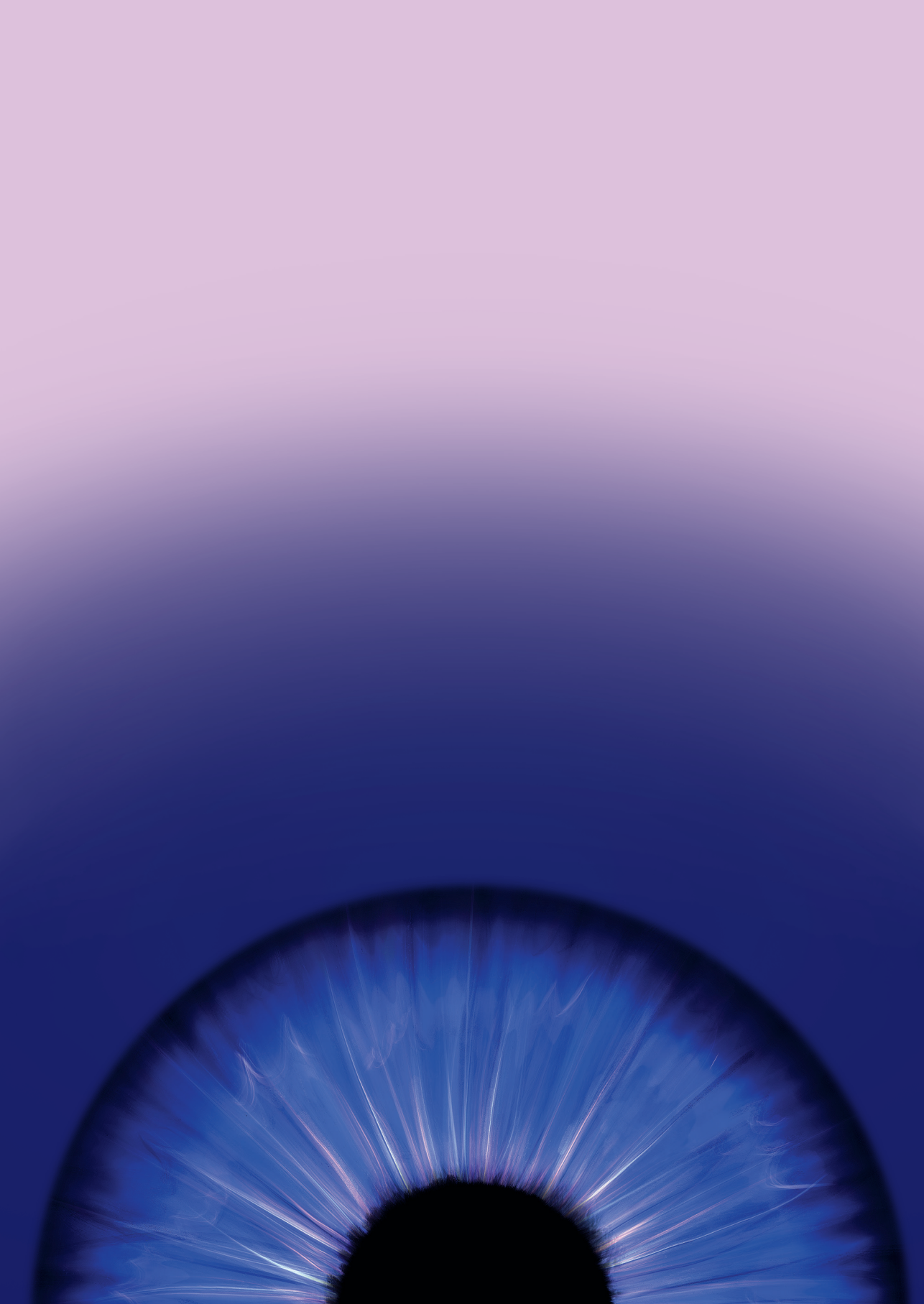
Chapter 1	General Introduction	
	1.1 Research Models and Gene Augmentation Therapy for <i>CRB1</i> Retinal Dystrophies	8
	1.2 Aims and Outline of this Thesis	
Chapter 2	CRB2 Loss in Rod Photoreceptors is Associated with Progressive Loss of Retinal Contrast Sensitivity	42
Chapter 3	Defining Phenotype, Tropism, and Retinal Gene Therapy Using Adeno-Associated Viral Vectors (AAVs) in New-Born Brown Norway Rats with a Spontaneous Mutation in <i>Crb1</i>	84
Chapter 4	AAV-Mediated Gene Augmentation Therapy of <i>CRB1</i>-Patient Derived Retinal Organoids Restores the Histological and Transcriptional Retinal Phenotype	130
Chapter 5	Characterization and AAV-Mediated Gene Therapy in Human <i>CRB1</i>^{KO} and <i>CRB1</i>^{KO}<i>CRB2</i>^{+/-} Retinal Organoids	176
Chapter 6	General Discussion	212
Chapter 7	Summary; Nederlandse Samenvatting; List of publications; Curriculum Vitae; Acknowledgements	238

Chapter 1

1.1 Research Models and Gene Augmentation Therapy for *CRB1* Retinal Dystrophies

N. Boon, J. Wijnholds, and L. P. Pellissier
Frontiers in Neuroscience, 2020, 14:860

1.2 Aims and Outline of this Thesis



Abstract

1

Retinitis pigmentosa (RP) and Leber congenital amaurosis (LCA) are inherited degenerative retinal dystrophies with vision loss that ultimately lead to blindness. Several genes have been shown to be involved in early onset retinal dystrophies, including *CRB1* and *RPE65*. Gene therapy recently became available for young RP patients with variations in the *RPE65* gene. Current research programs test adeno-associated viral gene augmentation or editing therapy vectors on various disease models mimicking the disease in patients. These include several animal and emerging human-derived models, such as human induced pluripotent stem cell (hiPSC) derived retinal organoids or hiPSC-derived retinal pigment epithelium, and human donor retinal explants. Variations in the *CRB1* gene are a major cause for early onset autosomal recessive RP with patients suffering from visual impairment before their adolescence and for LCA with newborns experiencing severe visual impairment within the first months of life. These patients cannot benefit yet from an available gene therapy treatment. In this review, we will discuss the recent advances, advantages and disadvantages of different *CRB1* human and animal retinal degeneration models. In addition, we will describe novel therapeutic tools that have been developed, which could potentially be used for retinal gene augmentation therapy for RP patients with variations in the *CRB1* gene.

CRB family members

Crumbs (*crb*) is a large transmembrane protein initially discovered at the apical membrane of *Drosophila* epithelial cells [1]. Several years later, it was found that mutations in a human homologue of the *Drosophila melanogaster* protein crumbs, denoted as CRB1 (crumbs homologue 1), was involved in retinal dystrophies in humans [2]. The human *CRB1* gene is mapped to chromosome 1q31.3, and contains 12 exons, has 12 identified transcript variants so far, 3 CRB family members, and over 210 kb genomic DNA (Den Hollander et al., 1999); http://grch37.ensembl.org/Homo_sapiens/Gene/Summary?db=core;g=ENSG00000134376;r=1:197170592-197447585). Canonical CRB1 is, like its *Drosophila* homologue,

a large transmembrane protein consisting of multiple epidermal growth factor (EGF) and laminin-globular like domains in its extracellular N-terminus (Figure 1A). The intracellular C-terminal domain contains a FERM and a conserved glutamic acid-arginine-leucine-isoleucine (ERLI) PDZ binding motives. An alternative transcript of CRB1, *CRB1-B*, is recently described and suggested to have significant extracellular domain overlap with canonical CRB1 while bearing unique 5' and 3' domains [3]. In mammals, CRB1 is a member of the Crumbs family together with CRB2 and CRB3 (Figure 1A). CRB2 display almost the same protein structure as CRB1, except a depletion of four EGF domains. CRB3A lacks the entire typical extracellular domain but contains the transmembrane domain juxtaposed to the intracellular part with the FERM-binding motif and a the ERLI PDZ sequence. A second protein (isoform CRB3B) arises from the same *CRB3* gene due to alternate splicing of the last exon, resulting in a different C-terminus with a cysteine-leucine-proline-isoleucine (CLPI) amino acid sequence, and thus lacks the PDZ domain [4, 5]. Interestingly, the CRB3B isoform is found in mammals, but not in zebrafish or *Drosophila* [4]. Further details about CRB isoform details can be found in Quinn et al. 2017 [6].

CRB localization in the retina

In mammalian tissue CRB1 and CRB2 are predominantly expressed in the retina, however CRB2 expression is also found in other tissues such as in kidney podocytes, in the subventricular zone of the brain, and in the spinal cord [7-10]. Within the retina, CRB proteins are localized at the subapical region (SAR) above the adherens junctions between photoreceptor and Müller glial cells, multiple photoreceptor cells, or between multiple Müller glial cells (MGC) [11, 12]. In addition, unlike CRB1, CRB2 is also localized in the retinal pigment epithelium (RPE). Defining the subcellular localization is essential to understand the function of CRB proteins (Figure 1B). Mouse studies have shown that full length *Crb1* protein is exclusively present in MGC at the SAR while *Crb2* and *Crb3* are present in both photoreceptor cells and MGC [13]. Serial tangential cryosectioning of the retina followed with western blotting displays *Crb1-B* transcript expression in outer segments of photoreceptor cells in mice [3]. The first ultrastructural data in postmortem human retina revealed a different localization, where CRB2 is

located in MGC at the SAR and at vesicles in photoreceptor inner segments, whereas CRB1 is located in both MGC and photoreceptor cells at the SAR [14, 15]. CRB3A was found in microvilli of MGC at the SAR and in inner segments of photoreceptor cells [14, 15]. However, recently, it was shown that CRB1 and CRB2 are located in MGC and photoreceptor cells at the SAR in the second trimester of human fetal retina and in human iPSC-derived retinal organoids, whereas in the first trimester only CRB2 was detected [16]. Single-cell RNA sequencing data of human fetal retina and RPE confirms that CRB1 is present in retinal progenitor cells and MGC but not in RPE, which is in accordance with mouse versus primate localization studies [17]. In addition, similar localization for CRB1, CRB2 and CRB3A were detected in rhesus and cynomolgus macaques [18]. CRB3A was also detected in the inner retina and RPE of both rhesus and cynomolgus macaques [18]. These recent data suggest that, in humans, CRB2 might also be present at the SAR membranes in photoreceptor cells rather than only in vesicles of photoreceptor inner segments. The discrepancies in CRB2 pattern at the SAR observed in postmortem human retinas versus monkeys, fetal and retinal organoids could be explained by the age of the donors studied, the quality of the samples (processed within 48h after death), or by technical issues. We could speculate that either CRB2 may have a different location in human aged retinas, CRB2 at the SAR might have not been detected, or CRB2 might have been endocytosed from the photoreceptor cells plasma membrane following donor death. Additional experiments with fresh human retina defining the subcellular localization of CRB1 and CRB2 could potentially resolve these differences. In summary, according to all these evidences, we hypothesize that in primates, including humans, CRB1 and CRB2 are located in both cell types at the SAR. Therefore, both MGC and photoreceptor cells should be targeted to prevent retinal degeneration in RP patients.

Recently, Crb trafficking to the correct apical location in *Drosophila* epithelium has been further investigated (Figure 1C) [19-22]. Crb is correctly localized by Rab11-containing endosomes using motor-driven transport along polarized microtubules and F-actin filaments. Interestingly, upon loss of microtubule minus-end director protein dynein, Rab11 endosomes containing Crb are transported basally rather than apically [19]. Once Crb is successfully addressed to the apical membrane, it is delivered at the

correct localization on the plasma membrane using exocyst-mediated delivery. Mutant clones for *sec15* or *sec5*, subunits of the exocyst, strongly disrupts the apical localization of Crb, confirming the essential requirement of the exocyst in delivery of Crb to the apical membrane [19]. In cultured mammalian cells, the exocyst associates with adherens junctions and PAR3 [23, 24]. Because of the known interaction between CRB, PAR6, and PAR3 in mammals, mentioned below, this trafficking model might be conserved among species. Further investigations are required to test whether the mechanisms of epithelial polarization are conserved in humans.

CRB protein function in mammalian tissues

Various research studies have shown that CRB1 and CRB2 are apical polarity factors, and apical-basal cell polarity is essential for the formation and function of epithelial tissues [25]. More research is required to define the function of the recently described CRB1-B isoform because of its distinct 5' and 3' domain. Below, we will describe the canonical function of CRB in maintaining cell adhesion and morphogenesis, and its role in cell division and development.

Maintaining cell adhesion and morphogenesis

The prototypic ERLI sequence of CRB proteins is important for interaction with key adaptor proteins. The core CRB complex is formed by interaction of CRB and protein associated with Lin Seven 1 (PALS1), also known as membrane-associated guanylate kinase p55 subfamily member 5 (MPP5), where PALS1 binds to the conserved C-terminal PDZ domain of CRB [5, 11, 26]. Ablation of *Mpp5* in mouse retinal pigment epithelium causes early-onset retinal degeneration, whereas ablation of *Mpp5* in the neural retina does not, suggesting an essential role of PALS1 at the tight junctions of RPE but not in the neural retina [27]. The core CRB complex is evolutionary conserved and regulates apical-basal polarity and maintains cell adhesion [28]. PALS1 can interact with MPP3 and MPP4 at the subapical region in the mouse retina (Figure 2A) [29-31]. *Mpp3* conditional knockout (cKO) mice with MPP3 specifically ablated in the retina showed disrupted localization and reduced levels of PALS1, indicating that MPP3 is

essential to maintain levels of PALS1 at the subapical region near the outer limiting membrane [31].

1 Additionally, binding of PALS1 and CRB can lead to the recruitment of PATJ or multiple PDZ domain protein 1 (MUPP1) to the apical membrane (Figure 2B) [26]. PATJ connects and stabilizes apical and lateral components of tight junctions in human intestinal cells [32]. In some cells, both MUPP1 and PATJ complexes co-exist, and MUPP1 regulates the cellular levels of the PALS1/PATJ polarity complex [33]. Co-immunoprecipitation studies showed that MUPP1 interacts in the retina with CRB1 and PALS1, but not or less with PATJ [11]. PATJ preferentially binds with PALS1 and partitioning defective-6 homolog (PAR6) (Figure 2B) [33, 34]. PAR6 is a key adaptor protein that interact with the ERL1 PDZ domain of CRB in mammalian cells [35, 36]. PAR6 leads to recruitment of PAR3, atypical protein kinase C (α PKC) and cell division control 42 (CDC42), known as the PAR complex [36-42]. This PAR6-CDC42 complex is required for the apical-basal polarity and cell adhesion [42].

Alternatively, the importance of a CRB-PALS1-EPB4.1L5 complex in mammals has been described [43-45]. Co-expression and co-localization studies suggested that in several epithelial derived tissues Epb4.115 interact with at least one Crumbs homologue and with PALS1 (Figure 2C). In addition, in the adult retina, Epb4.115 showed substantial overlap at the OLM with CRB1 and PALS1 [43]. Overexpression of Epb4.115 in polarized MDCK cells affects tightness of cell junctions and results in disorganization of the tight junction markers ZO-1 and PATJ [43]. However another group discovered, unlike in the zebrafish and *Drosophila* orthologues, that mouse Crumbs proteins are localized normally in absence of Epb4.115 [46]. Additional research should be performed to define its precise molecular mechanism in mammalian cells.

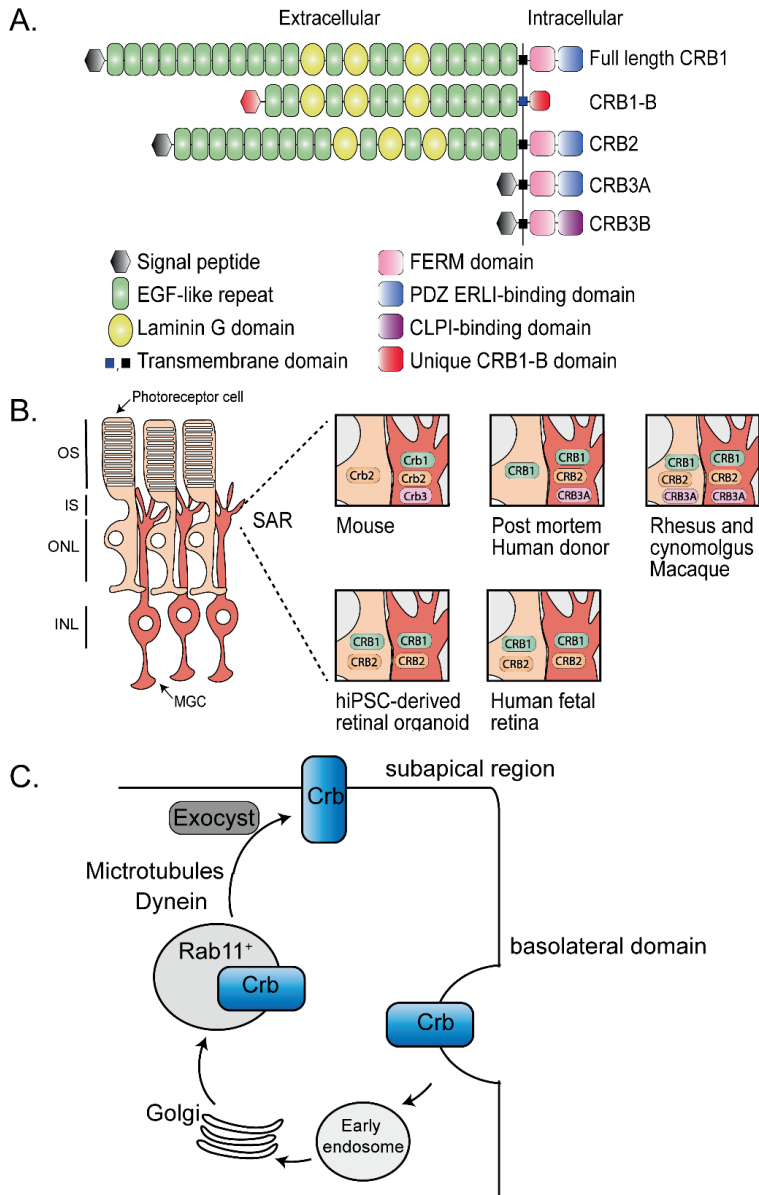


Figure 1. Schematic representation of CRB subcellular localization and proposed trafficking mechanism (A) Schematic overview of full length CRB1 (CRB1-A), CRB1-B, CRB2, CRB3A and CRB3B proteins. (B) Subcellular localization of CRB1, CRB2, and CRB3A in the retina of mouse, post mortem human donor, macaque, hiPSC, and human fetal retina. (C) Trafficking mechanism in *Drosophila* suggested to be conserved among species, adapted from

(Aguilar-Aragon et al., 2020). Note: INL = inner nuclear layer; IS = inner segments; MGC = Müller glial cell; ONL = outer nuclear layer; OS = outer segments; SAR = subapical region.

The alternative isoform CRB3B contains a distinct carboxy terminal motif namely the CLPI motif, suggesting different binding partners in epithelial cells. CRB3 is widely expressed in epithelial cells. A *Crb3* KO mouse demonstrates extensive defects in epithelial morphogenesis, the mice die shortly after birth with cystic kidneys and lung proteinaceous debris throughout the lungs [47]. Interestingly, these defects are also seen in Ezrin knockout mice, which is in line with the detected interaction between CRB3B and Ezrin in mice and mammalian cells (Figure 2D) [47, 48]. This indicates that CRB3B is also crucial for epithelial morphogenesis and plays a role in linking the apical membrane to the underlying cytoskeleton [47-49]. Therefore, the roles of the two CRB3 variants in the mouse lungs remains to be determined.

Drosophila Crb has also been found to inhibit the positive-feedback loop of phosphoinositide 3-kinase (PI-3K) and Rac1, thereby repressing the activation of Rac1 as well as PI-3K and maintaining proper apical domain and epithelial tissue integrity (Figure 2E) [50]. This process could potentially be conserved in different species, however, more research in mammalian cells is required to support this hypothesis.

CRB function in cell proliferation

In Müller glial cells of *Drosophila* and *Xenopus*, YAP plays an important role in damaged retina [51-53]. YAP is a core member of the Hippo pathway, which regulates several biological processes including cell proliferation, and survival [54]. The intracellular domain of *Drosophila* Crb interacts with Expanded and thereby regulates the activity of Hippo pathway kinases [54, 55]. In mammalian lung epithelial and breast cancer cells, CRB3 expression also correlates with the Hippo pathway [56, 57]. More specifically, CRB3 affects the Hippo pathway by interacting with Kibra and/or FRMD6 (FRMD6 is the homologue of *Drosophila* Expanded; Figure 2 F). With low CRB3 expression levels, the Hippo-pathway is inactivated, YAP is not phosphorylated and can move to the nucleus where YAP target genes are expressed leading to increased cell proliferation and decreased apoptosis [56]. Also in *Crb1^{rd8}* versus wild-type mouse retina several Hippo signaling related genes were differentially expressed [51]. In

addition, *CRB1* and *CRB2* deletion also lead to YAP signaling dysregulation in developing murine retinas [58]. These data suggest an essential role of the Hippo pathway in the control of cell proliferation.

***CRB1* and *CRB2* in retinal diseases**

Mutations in the *CRB1* gene are associated with a wide spectrum of retinal dystrophies, such as retinitis pigmentosa (RP) and Leber congenital amaurosis (LCA). RP is a clinically and genetically heterogeneous disease affecting more than 1.5 million people worldwide, where patients typically experience night blindness followed by progressive visual field loss ultimately leading to complete loss of vision in early or middle-life [59, 60]. The age at symptom onset for RP patients ranged from 0 to 47 years, with a median onset of 4 years [59]. Approximately 3 to 9% of non-syndromic cases of autosomal recessive RP are caused by a mutation in the *CRB1* gene [61-63]. LCA is a more severe retinal dystrophy, causing serious visual impairment or blindness in newborns [64]. Mutations in the *CRB1* gene account for approximately 7 to 17% of all LCA cases [61-64]. There are more than 200 different mutations described along the *CRB1* gene resulting in retinal dystrophies without a clear genotype-phenotype correlation with RP or LCA, *CRB1* patients may display unique clinical features such as pigmented paravenous chorioretinal atrophy, macular atrophy alone, retinal degeneration associated with Coats-like exudative vasculopathy, para-arteriolar preservation of the retinal pigment epithelium, or nanophthalmia [61, 62, 65]. The clinical variability of disease onset and severity, even within a patient cohort with the same homozygous mutations, supports the hypothesis that the phenotype of patients with *CRB1* mutations is modulated by other factors [66]. So far, no treatment options exist for patients with mutations in the *CRB1* gene. To study *CRB1*-related retinal dystrophies for treatment options, several models have been used. Below, *CRB1*-related human- and animal-derived retinal models are described.

Until recently, no RP patients were described with mutations in the *CRB2* gene. However, Chen *et al* discovered, using whole exome sequencing (WES), a homozygous *CRB2* p.R1249G mutation in a consanguineous Chinese family presenting RP. This mutation disturbs the stability of *CRB2* protein and thereby induces RPE degeneration,

impairs RPE phagocytosis, and accelerates RPE apoptosis [67]. However, only a limited number of patients with this mutation are described, identification of *CRB2* mutations in more RP patients is warranted to better support its pathogenicity.

Human-derived retinal models

1

The use of human-induced pluripotent stem cell (hiPSC) models for research is an emerging strategy to explore patient phenotypes *in vitro*. These techniques allow access to previously limited or inaccessible material and have been explored in many ophthalmic laboratories worldwide. A commonly used method is the differentiation of hiPSC into retinal organoids. Since the first one, numerous groups have adapted or created their own method to more efficiently generate well laminated retinal organoids [68-72]. Nevertheless, a wide variability in differentiation efficiency across hiPSC lines is often reported [73-76]. Chichagova *et al.* have shown that the ability of three different hiPSC lines to differentiate into retinal organoids in response to IGF1 or BMP4 activation was line- and method-dependent [75]. Hallam *et al.* differentiated five hiPSC lines with a variability in efficiency, but by 5 months of differentiation all the retinal organoids were able to generate light responses and contained a well-formed ONL with photoreceptor cells containing inner segments, cilia, and outer-like segments [77]. Attempts have been made to decrease this wide variability, Luo *et al.* described that the use of a Wnt signalling pathway antagonist, Dickkopf-related protein 1 (DKK-1), efficiently generated retinal organoids in all six hiPSC lines [72]. Bulk RNA-sequencing profiling of retinal organoids demonstrated that the retinal differentiation *in vitro* recapitulated the *in vivo* retinogenesis in temporal expression of cell differentiation markers, retinal disease genes, and mRNA alternative splicing [78]. These results make the retinal organoids, despite their high variability, of great interest in a wide range of applications including drug discovery, investigating the mechanism of retinal degeneration, developing cell-based therapeutic strategies and many more.

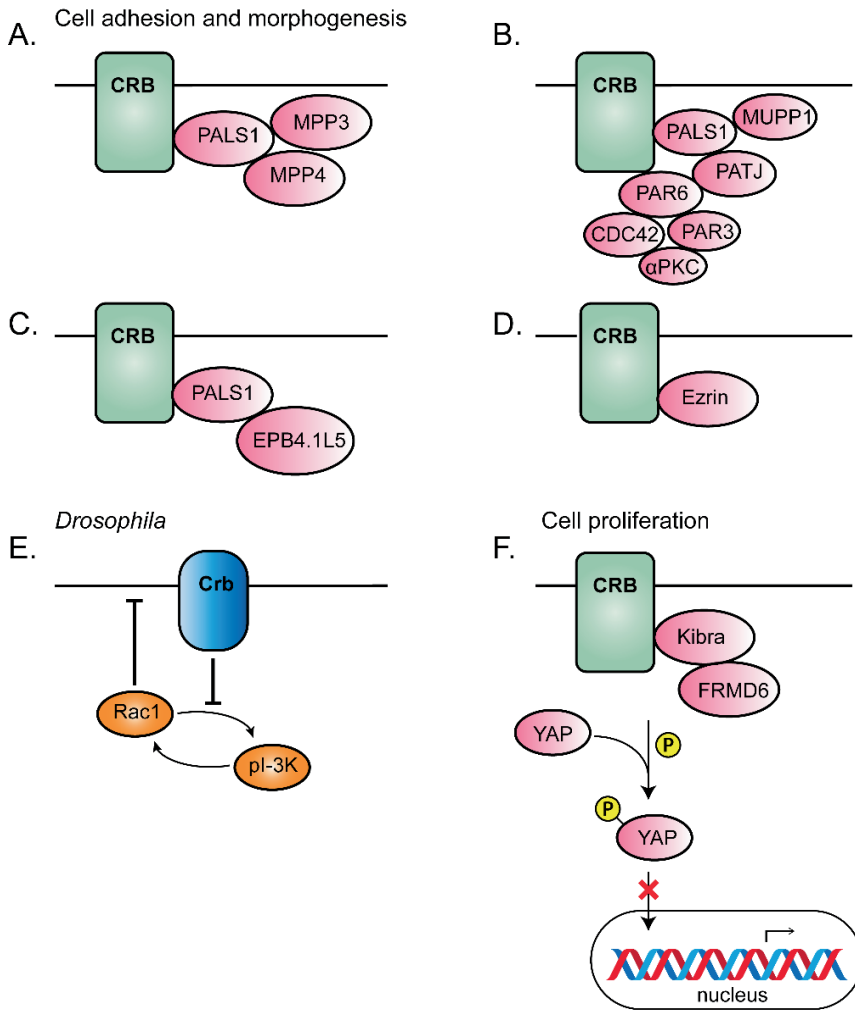


Figure 2. Schematic representation of CRB interaction partners. (A-D) Proposed interaction partners and formed CRB complexes in mammals involved in cell adhesion and morphogenesis. (E) Proposed interaction partner in *Drosophila* suggested to be conserved among species. (F) Proposed interaction partners involved in cell proliferation.

Defining the localization and onset of expression of the CRB complex members has been achieved in healthy hiPSC-derived retinal organoids. Several members of the CRB complex, CRB2, PALS1, PATJ, and MUPP1, were detected at the outer limiting membrane as early as differentiation day 28 (DD28), typical and clear puncta-like

staining patterns for CRB1 were found only after DD120. All CRB complex members together with adherens junction markers, p120-catenin and N-cadherin, were still detectable in DD180 retinal organoids [16]. The onset of CRB1 and CRB2 protein expression recapitulates those observed in the human fetal retina, with a clear onset of CRB2 expression before CRB1 expression [16].

1

Three *CRB1* patient hiPSC lines containing a homozygous missense mutation (c.3122T>C), or heterozygous missense mutations (c.2983G>T and c.1892A>G, or c.2843G>A and c.3122T>C) were successfully differentiated into retinal organoids and analyzed at differentiation day 180. Here, all three retinal layers were developed: retinal ganglion cell layer marked by Tuj1 positive dendrites, neuroblast layer marked by SOX9 positive retinal progenitor cells, and an outer nuclear layer marked by recoverin positive photoreceptor cells. However, frequently, there were ectopic recoverin positive cells found above the outer limiting membrane and all missense *CRB1* organoid lines developed small but frequent disruptions of localization of CRB complex members at the OLM that were not found in control lines [16]. Data from these *CRB1* patient hiPSC retinal organoids suggest a retinal degeneration phenotype similar to that previously found in mice lacking CRB1, mice expressing the C249W CRB1 variant, or mouse retina lacking CRB2 [11, 79, 80]. Another study shortly describes the successful differentiation of hiPSC carrying a compound heterozygous mutation in the *CRB1* gene (c.1892A>G and c.2548G>A) to retinal organoids. All three germ layers and expressed markers of retinal progenitor cells, including N-cadherin, rhodopsin, and PAX6, after 35 days of differentiation were present, but no phenotype was described in this paper [81]. To our knowledge, only these two papers have reported the generation of *CRB1* patient hiPSC-derived retinal organoids. The reproducible phenotype observed in these three *CRB1* patient lines [16] provides a good model for assessing potential gene therapy approaches.

Another frequently used method in the ophthalmic field is the differentiation of hiPSC into retinal pigment epithelium (RPE) monolayers. Efficient protocols for differentiating hiPSC into RPE monolayers using a mixture of growth factors have been established [82-84]. However, attempts are currently made to use nonbiological

products, such as small molecules, that would limit the risks of infection or immune rejection when transplanted. Maruotti *et al.* developed a protocol which uses chemotin (CTM) in combination with a previously known neural inducer nicotinamide (NIC) to efficiently differentiate hiPSC into RPE monolayers [85]. In three independent hiPSC lines, RPE differentiation was efficient, and key RPE markers such as microphthalmia-associated transcription factor (MITF), PMEL17, and tight junction protein zonula occludens 1 (ZO-1) were strongly expressed. When left longer in culture to mature, bestrophin 1 (BEST1) and retinal pigment epithelium-specific protein of 65kDa (RPE65) were also strongly expressed [85]. Using a slightly adapted protocol, Smith *et al.* differentiated six more hiPSC lines into hiPSC-RPE monolayers, all six also expressed the key RPE markers ZO-1, BEST-1, and MITF. Another study revealed by RNA sequencing data that hiPSC-RPE grouped with fetal RPE samples, indicating that their gene expression was highly correlated and similar [86]. In addition, Zahabi *et al.* provided proof-of-concept that multiple retinal-disease specific hiPSC lines, including two RP lines, can be differentiated into RPE monolayers [84]. Altogether, this data illustrates the potential of hiPSC-RPE as a model system for retinal diseases with mutations in the RPE. Related to CRB, recent studies have shown that CRB2 but not CRB1 is expressed in the human RPE during the differentiation into retinal organoids [16]. In addition, there are RP patients described with specific *CRB2* variations expressed in RPE cells [67]. Therefore, the method of generating hiPSC-RPE could be used to explore treatment possibilities for patients with specific variations in *CRB2*.

***CRB1*-related animal retinal degeneration models**

Numerous research groups focus on animal models to gain, understand, and develop gene therapy strategies that potentially can be used to treat retinal degeneration of RP and LCA patients. Over the years there are multiple animal models developed mimicking the *CRB1*-related phenotype in patients. These models vary from mild to more severe, early- to late-onset, and Müller glial cell or photoreceptor specific phenotypes. Double retinal knock-outs of *CRB1* and *CRB2*, have helped to understand the contribution of the two CRB proteins to the retinal disease etiology, and explain the relatively mild phenotype observed in *Crb1* variant mouse models [11, 79, 87, 88].

	<i>Crh1^{NO/29W}</i>	<i>Crh2^{MGC}</i>	<i>Crh1^{del-B}</i>	<i>Crh1^{fl^{off}}</i>	<i>Crh1^{KO}</i>	<i>Crh1^{null}</i>	<i>Crh2^{M rods}</i>	<i>Crh1^{KO}</i> <i>Crh2^{ARods}</i>	<i>Crh1^{KO}</i> <i>Crh2^{low-impRC}</i>	<i>Crh1^{KO}</i> <i>Crh2^{low-impRC}</i>	<i>Crh2^{MRC}</i>	<i>Crh2^{AlmPRC}</i>
Severity	+	+	-	++	++	++	++	+++	+++	+++	++++	++++
CRB1-A ablation	MGC	-	-	Natural occurring mutation	MGC	MGC	-	MGC	MGC	MGC	-	-
CRB1-B ablation	-	-	PRC & MGC	Natural occurring mutation	-	PRC & MGC	-	-	-	-	-	-
CRB2 ablation	-	MGC	-	-	-	-	Rod PRC	Rod PRC	50% in immature PRC	50% in immature PRC	RPC	Immature PRC
Morphologic phenotype onset*	8M	1M	NA	1M	P14	3M	3M	1M	P10	P10	E18.5	E15.5
ERG differences*	No	No	NA	No	No	NA	Yes (9M)	Yes (3M)	Yes (3M)	Yes (3M)	Yes (1M)	Yes (1M)
Affected areas	NA	Mainly periphery	NA	Inferior nasal quadrant	Inferior temporal quadrant	Inferior retina	Superior retina	Superior retina	Throughout retina	Throughout retina	Throughout retina	Throughout retina
OLM disruptions	Yes, sporadic	Yes	No	Yes	Yes	Yes	Yes	Yes	Yes	Yes	Yes	Yes
PRC nuclei protrusions	Yes, sporadic	Yes	No	Yes	Yes	Yes	Yes	Yes	Yes	Yes	Yes	Yes

Table 1: Schematic overview RP mouse models. MGC, Müller glial cells; PRC, photoreceptor cell; RPC, retinal progenitor cell. * The phenotype onset and ERG differences can be marginal on the indicated ages, the severity of the phenotype increases over time.

LCA-like mouse models

Four mouse models showing a *CRB1* LCA-like phenotype have been reported: *Crb1^{KO}Crb2^{ARPC}* where both *Crb1* and *Crb2* are ablated in retinal progenitor cells [58], secondly the *Crb1^{KO}Crb2^{DimPRC}* where *Crb1* is ablated in MGC and *Crb2* is ablated in immature photoreceptor cells with remaining *Crb2* levels in MGC and progenitor cells [89], thirdly the *Crb1^{KO/WT}Crb2^{ARPC}* mouse model with reduced levels of *Crb1* in MGC and ablation of *Crb2* in retinal progenitor cells [58], and finally *Crb1^{KO}Crb2^{AMGC}* in which both *Crb1* and *Crb2* are ablated in MGC [18]. All four models exhibit vision loss indicated by a reduced ERG response. In addition, retinal degeneration was observed by outer limiting membrane disruptions, abnormal retinal lamination, intermingling of nuclei of the ONL and INL, and ectopic localization of retinal cells. These mouse models show an early onset phenotype with distinct severity indicated by the order mentioned above. In short, in the most severe mouse model, *Crb1^{KO}Crb2^{ARPC}*, the phenotype onset was found as early as embryonal day 13 (E13) which was observed throughout the retina [58]. Retinal degeneration in *Crb1^{KO}Crb2^{DimPRC}* was detected at E15 in the whole retina, but in adult mice the superior retina was more affected than the inferior retina [89]. Also in *Crb1^{KO/WT}Crb2^{ARPC}* mice retinal degeneration was detected at E15, but was mostly affecting the peripheral retina [58]. Finally, the *Crb1^{KO}Crb2^{AMGC}* mice showed the first signs of degeneration at E17, where mostly the peripheral retina was affected. More subtle differences between these models are described and summarized before [18]. These data show that all four *Crb1* mouse models mimic the LCA phenotype in patients and could therefore be used for future therapy development.

RP-like mouse models

Twelve *CRB1* RP-like mouse models have been described so far, including (1) *Crb1^{KO/C249W}* with a missense variation in the *Crb1* gene [79], (2) *Crb2^{AMGC}* where only *Crb2* is ablated in MGC [90], (3) the *Crb1^{rd8}* mice with a naturally occurring nonsense mutation in the *Crb1* gene [87], (4) the *Crb1^{KO}* where the full length *Crb1* protein is ablated from retinal radial glial progenitor cells, Müller glial cells, and the rest of the

body [11], (5) the *Crb1^{del-B}* where *Crb1-B* is abolished from photoreceptor and Müller glial cells [3], (6) the *Crb1^{null}* where a deletion of alternate exon 5a up to intron 7 disrupts all *Crb1* isoforms [3], (7) *Crb2^{Arods}* where *Crb2* is ablated only in developed rod photoreceptor cells [91], (8) *Crb1^{KO}Crb2^{Arods}* where *Crb1* is ablated in MGC and *Crb2* in rod photoreceptor cells [91], (9) *Crb1^{KO}Crb2^{low-imPRC}* with absence of *Crb1* and reduced levels of *Crb2* in immature photoreceptors [89], (10) *Crb1^{KO}Crb2^{low-RPC}* with absence of *Crb1* and reduced levels of *Crb2* in retinal progenitor cells [14], (11) *Crb2^{ARPC}* where *Crb2* is ablated in retinal progenitor cells [80], and finally, (12) *Crb2^{dimPRC}* with *Crb2* ablation in immature photoreceptor cells [90]. The different Cre mouse models show variations in mosaicism (mutant adjacent to wildtype cells), but eleven out of twelve *Crb* models show disruptions at the outer limiting membrane with rows or single photoreceptor nuclei protruding into the subretinal space or ingressing into the outer plexiform layer leading to a degenerative retinal phenotype (table 1).

The *Crb1^{rd8}* mice have a naturally occurring single base deletion in exon 9 of the *Crb1* gene causing a frame shift and premature stop codon, thereby truncating the transmembrane and cytoplasmic domain of CRB1. This results in a photoreceptor degeneration mainly observed in the inferior nasal quadrant of the eye, caused by retinal folds and pseudorosettes [87]. In the *Crb1^{KO}* mouse model the retinal lamination is predominantly maintained, and degeneration is found in the inferior temporal quadrant of the retina. Degeneration is indicated by single or groups of photoreceptor cells protruding into the subretinal space, rosette formation, and neovascularization. In 18M-old mice there was no loss of overall retinal function measured by electroretinography, suggesting that a major part of the retina was not affected by loss of *Crb1* [11, 88]. Light exposure experiments reveal that light exposure doesn't initiate but rather enhances the retinal degeneration [88]. The mild phenotype observed in these *Crb1* mouse models suggest that *Crb2* protein may compensate the effect of CRB1 deletion.

In the *Crb1^{del-B}* the alternative *Crb1-B* isoform is abolished from photoreceptor cells, while the *Crb1^{null}* disrupts all potential *Crb1* isoforms [3]. The *Crb1^{del-B}* mouse do not show significant disruptions in the OLM, while the disruptions in the *Crb1^{null}* mice were comparable with *Crb1^{rd8}* [3]. Although not mentioned by Ray *et al.*, also the *Crb1^{KO}*

mice shows significant OLM disruptions strongly depending on genetic background as well as exposure to light [11, 88]. As the IrCaptureSeq suggested that *Crbl-B* is the most abundant transcript in mouse and human retina, a cross-breeding of *Crbl^{null}* with *Crbl^{del-B}* mice was performed to define the relevance of Crb1-B in the retina. This heterozygous *Crbl^{null/del-B}* showed similar OLM disruptions with the homozygous *Crbl^{null}* mouse [3]. Similar OLM disruptions were thus found in *Crbl^{rd8}*, *Crbl^{null}*, *Crbl^{null/del-B}*, and *Crbl^{KO}* mice. It is essential to perform retinal function measurements on the mouse models affecting *Crbl-B* to understand its function and to compare it with previously described *Crbl* mouse models. In addition, the most severe retinal phenotype so far derives from *Crbl* mice with concomitant loss of Crb2. Both *Crb2^{ARPC}* and *Crb2^{AimPRC}* show an early onset retinal degeneration at embryonic day 18.5 (E18.5) and E15.5 respectively, the difference is caused by the distinct expression pattern and timing of the Cre recombinase and morphological phenotypes result in differences in the scotopic and photopic ERG conditions already at 1M of age [80, 90]. Interestingly, in contrast to *Crb2^{ARPC}* mice, the lamination of Müller glial, ganglion and amacrine cells were also misplaced in *Crb2^{AimPRC}* mice. These lamination defects were also observed in *Crbl^{KO/WT}Crb2^{ARPC}* mice [58].

Another mouse model, *Crb2^{Arods}*, show a mild and late onset phenotype limited to the superior retina [91]. In some 3M and all 6M old *Crb2^{Arods}* mouse, disruptions of the outer limiting membrane, a thinned photoreceptor layer at the peripheral superior retina, and photoreceptor cells protruding into the subretinal space were observed. A reduction in ERG scotopic a-wave was observed in 9M old mice, while no difference in optokinetic head tracking response (OKT) spatial frequency or contrast sensitivity was observed. Interestingly, while most photoreceptor cells were affected, all the remaining photoreceptor cells showed mature inner- and outer-segments. Remaining rods were functional and the cones showed normal morphology. This phenotype is enhanced by a concomitant loss of Crb1 in Müller glial cells [91]. These mice, *Crbl^{KO}Crb2^{Arods}*, show a similar but enhanced phenotype in comparison to *Crb2^{Arods}* mice. Here, a reduction in ERG scotopic a-wave was observed at 3M and became more apparent at 6M onwards. In addition, a significant decrease in OKT contrast sensitivity was found from 3M of age onwards [91]. The difference in phenotype onset between all these

mouse models might be explained by the onset of Cre expression during retinogenesis and by cell-type specific ablation; ablation of Crb2 from a later time point resulted in a milder phenotype. Interestingly, when Crb2 is ablated in MGCs, *Crb2^{ΔMGC}*, a very mild morphological phenotype with no functional consequences measured using ERG was observed [90], but ablation of both CRB1 and CRB2 from Müller glial cells caused a severe LCA phenotype [18]. This data suggests that CRB2 has a redundant function in Müller glial cells, while in photoreceptor cells it is essential for proper retinal lamination and function.

Interestingly, the *Crb1^{KO}* phenotype is located at the inferior temporal quadrant whereas the *Crb2^{Δrods}* phenotype is mainly observed at the peripheral and central superior retina. These differences might be related to higher levels of CRB2 in the inferior retina while CRB1 is expressed at higher levels in the superior retina [14]. In addition, there might be modifying factors present which are enriched in either the superior or inferior retina causing the different phenotypes.

In addition to these mouse models, a rat with a spontaneous mutation in *Crb1* exon 6 was discovered mimicking human macular telangiectasia type 2 [92]. The autosomal recessive indel mutation causes an early-onset phenotype with a strongly reduced ERG response in three-week old rats. These rats showed a focal loss of retinal lamination, OLM disruptions, and photoreceptor cells, MGC and RPE alterations [92]. Differences between this and the *Crb1* mouse models could result from different types of mutations or from different genetic setups displayed by these different animal species

Gene augmentation strategies for *CRB1* retinal dystrophies

There is an emerging interest in gene augmentation strategies for retinal dystrophies. Recently, gene therapy became available for young RP and LCA patients with biallelic mutations in the *RPE65* gene. Voretigene neparvovec-rzyl, or its commercial name: LUXTURNA™, uses the adeno-associated viral vector serotype 2 (AAV2) to deliver by subretinal injection a functional copy of the *RPE65* gene into the RPE cells. *RPE65* transgene expression results in the production and correct localization of RPE65 protein in RPE cells, thereby compensating for the loss of the protein and restoring the visual

cycle in these patients [93]. Nowadays, there are numerous clinical studies ongoing which explore the use of AAV as a therapeutic vector for retinal diseases such as retinitis pigmentosa (RP), wet age-related macular dystrophy (AMD), Leber congenital amaurosis (LCA) and many more [94]. However, so far, no treatment options are available for RP and LCA patients with mutations in the *CRB1* gene. Below, we will describe novel therapeutic tools which could be promising for *CRB1* retinal gene augmentation therapy in RP patients.

Currently, AAVs are the leading platform for gene delivery in the treatment of retinal dystrophies. AAVs are mainly investigated because of their low toxicity, their capability to transduce both dividing and non-dividing cells, they do not integrate into the host genome, and AAV capsid variants display distinct cell tropisms. A complete overview of basic AAV biology, AAV vectorology, and current therapeutic strategies and clinical progress was recently reviewed by Wang *et al* [94]. The major disadvantage of AAVs is their limited package capacity, bigger gene expression cassettes than 4.5 kb are not able to fit within a single AAV. Because of this, the development of AAV-mediated *CRB1* gene therapy is also challenging. Full-length cytomegalovirus (CMV) ubiquitous promoter and *CRB1* cDNA exceeds the AAV package limitation. However, using an engineered minimal CMV promoter and codon optimized *CRB1* cDNA allowed sufficient expression levels of full-length CRB1 protein in Müller glial cells in mice [95]. Pre-clinical studies in mouse using this AAV.CMVmin.*hCRB1* have shown that expression of *CRB1* was deleterious in *CRB1* mouse models but not in wild-type mice [15]. In addition, there are more potential *CRB1* transcript variants which could be targeted [6]. Interestingly, alternative strategies using the codon-optimized structural and functional family member *CRB2* to rescue *CRB1*-related retinopathies restored retinal function and structure in *Crb1* mouse models [15]. In that study, improved photoreceptor layer morphology and ERG response was detected after *CRB2* delivery. The combination of AAV9 with a full-length CMV promoter was used to target both photoreceptor and Müller glial cells, whereas no rescue was observed when either photoreceptor or Müller glial cells were targeted with *CRB2* [15]. In addition, several groups explored the possibility to overcome the limiting AAV package capacity by dual or triple-AAV approaches [96-98] or by increasing the package capacity [99]. Yet, the

studies performed so far have shown that the dual AAV approaches have lower expression levels compared to a single AAV vector [96, 97].

Several research groups focus on AAV-mediated gene delivery to define the tropism in hiPSC-derived retinal organoids and/or RPE. Out of four different AAV capsids packaged with the CAG promoter and GFP (AAV2, AAV2-7m8, AAV8, AAV9), Garita-Hernandez *et al* showed with AAV2-7m8 infection at day 44 the most efficient transduction of the hiPSC-derived retinal and RPE organoids. Limited transduction of AAV9 was found [100]. Another study showed, using AAV-CMV-*GFP* constructs, a more efficient retinal organoid transduction at DD220 especially in MGC with AAV5 or Shh10Y445F capsids in comparison with AAV9 [16]. Recently, Lane *et al* demonstrate efficient photoreceptor cell transduction in DD150 retinal organoids using an AAV5 packaged with the CAG promoter [101]. Moreover, AAV5-mediated gene augmentation with human *RP2* was able to rescue the degeneration found in *RP2* KO retinal organoids by preventing ONL thinning and restoring rhodopsin expression [101]. Therefore, testing CRB1- or CRB2-expressing vectors in retinal organoids will aid in the discovery of *CRB* gene therapy treatment for *CRB1*-related retinal dystrophies in patients. In addition, there are different non-viral mediated approaches for gene therapy. An example is the use of nanoparticles. Three representative nanoparticles, namely metal-based, polymer-based, and lipid-based nanoparticles, were recently reviewed describing their characteristics and recent application in ocular therapy [102]. Shortly, the most extensive characterized nanoparticle is the polymer-based CK30-PEG nanoparticle, which contains plasmid DNA compacted with polyethylene glycol-substituted lysine 30-mers [103, 104]. Theoretically, these approaches have an unlimited gene packaging capacity, which display a big advantage for large genes such as *CRB1*. These nanoparticles are also able to infect RPE and photoreceptor cells, and can drive gene expression on a comparable scale and longevity than AAVs in mice [104, 105]. CK30-PEG nanoparticles have a tolerable safety profile and is nontoxic in mouse and non-human primate eyes [106, 107]. To our knowledge, there is no successful clinical study described using these nanoparticles so far. More research is required to define the clinical relevance of these nanoparticles in retinal gene therapy. Further pre-clinical research and clinical trials will aid in the discovery of new gene

therapy approaches for *Crb1*-related retinal dystrophies in patients. A retrospective *CRB1* natural history study (NHS) has been published [59], and their prospective NHS with strategies for evaluation of the efficacy of novel clinical therapeutic interventions in the treatment of *CRB1*-retinal dystrophies will be reported in the end of 2020. Recently, a French biotech company called HORAMA signed an exclusive license agreement with Leiden University Medical center targeting *CRB1* gene mutations to treat inherited retinal dystrophies. Based on current timelines, HORAMA expects initiating a Phase I/II clinical study with the drug candidate in 2023 [108].

Conclusion

In this review we have discussed (1) CRB protein function in mammalian cells, (2) recent advances and potential tools for *CRB1* human and animal retinal degeneration models, and (3) described therapeutic tools which potentially could be used for retinal gene augmentation therapy for RP and LCA patients with mutations in the *CRB1* gene.

1.2 Aims and outline of this thesis

The general aim of the research described in this thesis was describing multiple model systems for *CRB1* related retinal dystrophies, where **Chapter 2** describes the use of a mouse model, **Chapter 3** describes a rat model, and **Chapter 4 and 5** describe human-derived models. In addition, AAV-mediated *CRB* gene augmentation therapy on rats and retinal organoids was explored in **Chapter 3, 4, and 5**.

Chapter 1 serves as an introduction for this thesis, where I review (1) CRB1 and CRB2 function and localization in the retina, (2) the current status of human-derived retinal models, (3) the different generated *Crb1*-related animal retinal degeneration models, and finally (4) describe the current gene augmentation strategies and possibilities for *CRB1* retinal dystrophies.

In **Chapter 2** we describe the effect of CRB2 in rod photoreceptor cells and whether ablation of CRB2 in rods enhance the observed phenotype in *Crb1*^{KO} mouse models. For this, we assessed the morphological, retinal, and visual functional consequences of loss of CRB2 from rods with or without concomitant loss of CRB1.

Chapter 3 describes the phenotype of *Crb1* mutant rats in more detail using electroretinography (ERG), spectral domain optical coherence tomography (SD-OCT), and morphological analysis. The subcellular localization of CRB1 and CRB2 in *Crb1* mutant and control rats was explored. In addition, the tropism of three distinct viral vectors administrated in two different injection ways were analysed in *Crb1* mutant and control rats. Finally, AAV-mediated gene augmentation therapy was explored in newborn *Crb1* mutant rats.

Chapter 2 and **Chapter 3** discussed our findings on *Crb1*^{KO} mouse and *Crb1* mutant rat models, but in **Chapter 4** and **Chapter 5** we switch the focus to using human induced pluripotent stem cells (hiPSC) to differentiate into *CRB1* human derived models (retinal organoids).

Chapter 4 describes the use of hiPSCs from three different *CRB1* RP patients and isogenic controls. These *CRB1* patient derived retinal organoids were analysed for a morphological phenotype at differentiation day 210 (DD210). In addition, single cell RNA-sequencing data analysis was performed and shows disruptions in the endosomal system in Müller glial cells and rods of *CRB1*-patient derived retinal organoids. Then, AAV-mediated gene augmentation therapy was explored in these retinal organoids. AAV.h*CRB1* or AAV.h*CRB2* treatment partially improved the phenotype of *CRB1* patient derived retinal organoids, providing essential information for future gene therapy approaches for patients with mutations in the *CRB1* gene.

In **Chapter 5** retinal organoids derived from *CRB1*^{KO} and *CRB1*^{KO}*CRB2*^{+/-} iPSC show a significantly decreased number of photoreceptor nuclei in a row and a significantly increased number of photoreceptor nuclei protruding above the OLM at DD180 and DD210. AAV-mediated gene augmentation therapy showed that AAV.h*CRB2* could partially restore the phenotype observed in *CRB1*^{KO} retinal organoids.

Chapter 6 consist of the general discussion and provides future perspectives of the above mentioned chapters in this thesis, and **Chapter 7** includes the summary, the “Nederlandse samenvatting” and abbreviations, and a list of publications, curriculum vitae, and acknowledgements of the author of this thesis.

Article information

Conflict of Interest: The authors declare that the research was conducted without any commercial or financial relationship that could be construed as a potential conflict of interest. The LUMC is the holder of patent number PCT/NL2014/050549, which describes the potential clinical use of *CRB2*; JW and LPP are listed as co-inventors of this patent, and JW is an employee of the LUMC.

Author Contributions: NB, JW, and LP contributed to writing, reviewing, and editing the manuscript. NB wrote the original draft. All authors contributed to the article and approved the submitted version.

Funding: Funding was obtained from Foundation Fighting Blindness (TA-GT-0715-0665-LUMC), the Netherlands Organization for Health Research and Development (ZonMw grant 43200004), University of Pennsylvania Orphan Disease Center in partnership with Curing Retinal Blindness Foundation (MDBR-19-131-CRB1), and Stichting Blinden-Penning (Uitzicht 2014-1 to LPP and JW). LPP acknowledges funding from the European Research Council (ERC) under the European Union's Horizon 2020 research and innovation program (grant agreement No. 851231).

Abbreviations:

α PKC	Atypical protein kinase C
AAV	Adeno-associated viral vectors
AMD	Age-related macular dystrophy
BEST1	Bestrophin 1
cKO	Conditional knockout
CLPI	Cysteine-leucine-proline-isoleucine
CMV	Cytomegalovirus
CRB1	Crumbs homologue 1
CTM	Chemotin
DD	Differentiation day
DKK-1	Dickkopf-related protein 1
E13	Embryonal day 13
EGF	Epidermal growth factor
ERG	Electroretinography

ERLI	Glutamic acid-arginine-leucine-isoleucine
hiPSC	Human-induced pluripotent stem cell
LCA	Leber Congenital Amaurosis
MGC	Müller glial cells
MITF	Microphthalmia-associated transcription factor
MPP5	Guanylate kinase P55 subfamily member 5
MUPP1	Multiple PDZ domain protein 1
NIC	Nicotinamide
OKT	Optokinetic head tracking response
OLM	Outer limiting membrane
PALS1	Protein associated with Lin Seven 1
PAR6	Partitioning defective-6 homolog
PI-3K	Phosphoinositide 3-kinase
RP	Retinitis pigmentosa
RPE	Retinal pigment epithelium
RPE65	RPE-specific protein of 65kDa
SAR	Subapical region
WES	Whole exome sequencing
YAP	Yes-associated protein 1
ZO1	Zonula occludens-1

References

1. Tepass, U.; Theres, C.; Knust, E. crumbs encodes an EGF-like protein expressed on apical membranes of Drosophila epithelial cells and required for organization of epithelia. *Cell* **1990**, 61, 787–799, doi:10.1016/0092-8674(90)90189-L.
2. Den Hollander, A.I.; Ten Brink, J.B.; De Kok, Y.J.M.; Van Soest, S.; Van Den Born, L.I.; Van Driel, M.A.; Van De Pol, D.J.R.; Payne, A.M.; Bhattacharya, S.S.; Kellner, U.; et al. Mutations in a human homologue of Drosophila crumbs cause retinitis pigmentosa (RP12). *Nat. Genet.* **1999**, 23, 217–221, doi:10.1038/13848.
3. Ray, T.A.; Cochran, K.; Kozlowski, C.; Wang, J.; Alexander, G.; Cady, M.A.; Spencer, W.J.; Ruzycski, P.A.; Clark, B.S.; Laeremans, A.; et al. Comprehensive identification of mRNA isoforms reveals the diversity of neural cell-surface molecules with roles in retinal development and disease. *Nat. Commun.* **2020**, 11, doi:10.1038/s41467-020-17009-7.
4. Fan, S.; Fogg, V.; Wang, Q.; Chen, X.W.; Liu, C.J.; Margolis, B. A novel Crumbs3 isoform regulates cell division and ciliogenesis via importin β interactions. *J. Cell Biol.* **2007**, 178, 387–398, doi:10.1083/jcb.200609096.
5. Margolis, B. The Crumbs3 polarity protein. *Cold Spring Harb. Perspect. Biol.* **2018**, 10, 1–9, doi:10.1101/cshperspect.a027961.

6. Quinn, P.M.; Pellissier, L.P.; Wijnholds, J. The CRB1 complex: Following the trail of crumbs to a feasible gene therapy strategy. *Front. Neurosci.* **2017**, *11*, doi:10.3389/fnins.2017.00175.
7. Slavotinek, A.; Kaylor, J.; Pierce, H.; Cahr, M.; Deward, S.J.; Schneidman-Duhovny, D.; Alsadah, A.; Salem, F.; Schmajuk, G.; Mehta, L. CRB2 mutations produce a phenotype resembling congenital nephrosis, Finnish type, with cerebral ventriculomegaly and raised alpha-fetoprotein. *Am. J. Hum. Genet.* **2015**, *96*, 162–169, doi:10.1016/j.ajhg.2014.11.013.
8. Ebarasi, L.; Ashraf, S.; Bierzynska, A.; Gee, H.Y.; McCarthy, H.J.; Lovric, S.; Sadowski, C.E.; Pabst, W.; Vega-Warner, V.; Fang, H.; et al. Defects of CRB2 cause steroid-resistant nephrotic syndrome. *Am. J. Hum. Genet.* **2015**, *96*, 153–61, doi:10.1016/j.ajhg.2014.11.014.
9. Dudok, J.J.; Murtaza, M.; Henrique Alves, C.; Rashbass, P.; Wijnholds, J. Crumbs 2 prevents cortical abnormalities in mouse dorsal telencephalon. *Neurosci. Res.* **2016**, *108*, 12–23, doi:10.1016/j.neures.2016.01.001.
10. Tait, C.; Chinnaiya, K.; Manning, E.; Murtaza, M.; Ashton, J.-P.; Furley, N.; Hill, C.J.; Alves, C.H.; Wijnholds, J.; Erdmann, K.S.; et al. Crumbs2 mediates ventricular layer remodelling to form the spinal cord central canal. *PLOS Biol.* **2020**, *18*, e3000470, doi:10.1371/journal.pbio.3000470.
11. van de Pavert, S.A.; Kantardzhieva, A.; Malysheva, A.; Meuleman, J.; Versteeg, I.; Levelt, C.; Klooster, J.; Geiger, S.; Seeliger, M.W.; Rashbass, P.; et al. Crumbs homologue 1 is required for maintenance of photoreceptor cell polarization and adhesion during light exposure. *J. Cell Sci.* **2004**, *117*, 4169–4177, doi:10.1242/jcs.01301.
12. Pellikka, M.; Tanentzapf, G.; Pinto, M.; Smith, C.; McGlade, C.J.; Ready, D.F.; Tepass, U. Crumbs, the *Drosophila* homologue of human CRB1/RP12, is essential for photoreceptor morphogenesis. *Nature* **2002**, *416*, 143–149, doi:10.1038/nature721.
13. van Rossum, A.G.S.H.; Aartsen, W.M.; Meuleman, J.; Klooster, J.; Malysheva, A.; Versteeg, I.; Arsanto, J.P.; Le Bivic, A.; Wijnholds, J. Pals1/Mpp5 is required for correct localization of Crb1 at the subapical region in polarized Müller glia cells. *Hum. Mol. Genet.* **2006**, *15*, 2659–2672, doi:10.1093/hmg/ddl194.
14. Pellissier, L.P.; Lundvig, D.M.S.; Tanimoto, N.; Klooster, J.; Vos, R.M.; Richard, F.; Sothilingam, V.; Garrido, M.G.; Bivic, A. Le; Seeliger, M.W.; et al. CRB2 acts as a modifying factor of CRB1-related retinal dystrophies in mice. *Hum. Mol. Genet.* **2014**, *23*, 3759–3771, doi:10.1093/hmg/ddu089.
15. Pellissier, L.P.; Quinn, P.M.; Henrique Alves, C.; Vos, R.M.; Klooster, J.; Flannery, J.G.; Alexander Heimel, J.; Wijnholds, J. Gene therapy into photoreceptors and Muller glial cells restores retinal structure and function in CRB1 retinitis pigmentosa mouse models. *Hum. Mol. Genet.* **2015**, *24*, 3104–3118, doi:10.1093/hmg/ddv062.
16. Quinn, P.M.; Buck, T.M.; Mulder, A.A.; Ohonin, C.; Alves, C.H.; Vos, R.M.; Bialecka, M.; van Herwaarden, T.; van Dijk, E.H.C.; Talib, M.; et al. Human iPSC-Derived Retinas Recapitulate the Fetal CRB1 CRB2 Complex Formation and Demonstrate that Photoreceptors and Müller Glia Are Targets of AAV5. *Stem Cell Reports* **2019**, *12*, 906–919, doi:10.1016/j.stemcr.2019.03.002.

17. Hu, Y.; Wang, X.; Hu, B.; Mao, Y.; Chen, Y.; Yan, L.; Yong, J.; Dong, J.; Wei, Y.; Wang, W.; et al. Dissecting the transcriptome landscape of the human fetal neural retina and retinal pigment epithelium by single-cell RNA-seq analysis. *PLoS Biol.* **2019**, *17*, 1–26, doi:10.1371/journal.pbio.3000365.
18. Quinn, P.M.; Mulder, A.A.; Henrique Alves, C.; Desrosiers, M.; de Vries, S.I.; Klooster, J.; Dalkara, D.; Koster, A.J.; Jost, C.R.; Wijnholds, J. Loss of CRB2 in Müller glial cells modifies a CRB1-associated retinitis pigmentosa phenotype into a Leber congenital amaurosis phenotype. *Hum. Mol. Genet.* **2019**, *28*, 105–123, doi:10.1093/hmg/ddy337.
19. Aguilar-Aragon, M.; Fletcher, G.; Thompson, B.J. The cytoskeletal motor proteins Dynein and MyoV direct apical transport of Crumbs. *Dev. Biol.* **2020**, 459, 126–137, doi:10.1016/j.ydbio.2019.12.009.
20. Pocha, S.M.; Shevchenko, A.; Knust, E. Crumbs regulates rhodopsin transport by interacting with and stabilizing myosin V. *J. Cell Biol.* **2011**, *195*, 827–838, doi:10.1083/jcb.201105144.
21. Li, B.X.; Satoh, A.K.; Ready, D.F. Myosin V, Rab11, and dRip11 direct apical secretion and cellular morphogenesis in developing *Drosophila* photoreceptors. *J. Cell Biol.* **2007**, *177*, 659–669, doi:10.1083/jcb.200610157.
22. Kraut, R.S.; Knust, E. Changes in endolysosomal organization define a pre-degenerative state in the crumbs mutant *Drosophila* retina. *PLoS One* **2019**, *14*, doi:10.1371/journal.pone.0220220.
23. Ahmed, S.M.; MacAra, I.G. The Par3 polarity protein is an exocyst receptor essential for mammary cell survival. *Nat. Commun.* **2017**, *8*, doi:10.1038/ncomms14867.
24. Polgar, N.; Fogelgren, B. Regulation of Cell Polarity by Exocyst-Mediated Trafficking. *Cold Spring Harb. Perspect. Biol.* **2018**, 1–16, doi:10.1101/cshperspect.a031401.
25. Bazellières, E.; Aksenova, V.; Barthélémy-Requin, M.; Massey-Harroche, D.; Le Bivic, A. Role of the Crumbs proteins in ciliogenesis, cell migration and actin organization. *Semin. Cell Dev. Biol.* **2018**, *81*, 13–20, doi:10.1016/j.semcdb.2017.10.018.
26. Roh, M.H.; Makarova, O.; Liu, C.J.; Shin, K.; Lee, S.; Laurinec, S.; Goyal, M.; Wiggins, R.; Margolis, B. The Maguk protein, Pals1, functions as an adapter, linking mammalian homologues of crumbs and discs lost. *J. Cell Biol.* **2002**, *157*, 161–172, doi:10.1083/jcb.200109010.
27. Park, B.; Alves, C.H.; Lundvig, D.M.; Tanimoto, N.; Beck, S.C.; Huber, G.; Richard, F.; Klooster, J.; Andlauer, T.F.M.; Swindell, E.C.; et al. PALS1 Is Essential for Retinal Pigment Epithelium Structure and Neural Retina Stratification. *J. Neurosci.* **2011**, *31*, 17230–17241, doi:10.1523/JNEUROSCI.4430-11.2011.
28. Bulgakova, N.A.; Knust, E. The Crumbs complex: From epithelial-cell polarity to retinal degeneration. *J. Cell Sci.* **2009**, *122*, 2587–2596, doi:10.1242/jcs.023648.
29. Kantardzhieva, A.; Gosens, I.; Alexeeva, S.; Punte, I.M.; Versteeg, I.; Krieger, E.; Neefjes-Mol, C.A.; Den Hollander, A.I.; Letteboer, S.J.F.; Klooster, J.; et al. MPP5 recruits MPP4 to the CRB1 complex in photoreceptors. *Investig. Ophthalmol. Vis. Sci.* **2005**, *46*, 2192–2201, doi:10.1167/iovs.04-1417.

30. Kantardzhieva, A.; Alexeeva, S.; Versteeg, I.; Wijnholds, J. MPP3 is recruited to the MPP5 protein scaffold at the retinal outer limiting membrane. *FEBS J.* **2006**, *273*, 1152–1165, doi:10.1111/j.1742-4658.2006.05140.x.
31. Dudok, J.J.; Sanz, A.S.; Lundvig, D.M.S.; Sothilingam, V.; Garrido, M.G.; Klooster, J.; Seeliger, M.W.; Wijnholds, J. MPP3 regulates levels of PALS1 and adhesion between photoreceptors and Müller cells. *Glia* **2013**, *61*, 1629–1644, doi:10.1002/glia.22545.
32. Michel, D.; Arsanto, J.P.; Massey-Harroche, D.; Béclin, C.; Wijnholds, J.; Le Bivic, A. PATJ connects and stabilizes apical and lateral components of tight junctions in human intestinal cells. *J. Cell Sci.* **2005**, *118*, 4049–4057, doi:10.1242/jcs.02528.
33. Assémat, E.; Crost, E.; Ponsere, M.; Wijnholds, J.; Le Bivic, A.; Massey-Harroche, D. The multi-PDZ domain protein-1 (MUPP-1) expression regulates cellular levels of the PALS-1/PATJ polarity complex. *Exp. Cell Res.* **2013**, *319*, 2514–2525, doi:10.1016/j.yexcr.2013.07.011.
34. Adachi, M.; Hamazaki, Y.; Kobayashi, Y.; Itoh, M.; Tsukita, S.; Furuse, M.; Tsukita, S. Similar and Distinct Properties of MUPP1 and Patj, Two Homologous PDZ Domain-Containing Tight-Junction Proteins. *Mol. Cell. Biol.* **2009**, *29*, 2372–2389, doi:10.1128/mcb.01505-08.
35. Lemmers, C.; Michel, D.; Lane-Guermonprez, L.; Delgrossi, M.-H.; Medina, E.; Arsanto, J.P.; Le bivic, A. CRB3 Binds Directly to Par6 and Regulates the Morphogenesis of the Tight Junctions in Mammalian Epithelial Cells. *Mol. Biol. Cell* **2004**, *15*, 1324–1333, doi:10.1091/mbc.E03.
36. Hurd, T.W.; Gao, L.; Roh, M.H.; Macara, I.G.; Margolis, B. Direct interaction of two polarity complexes implicated in epithelial tight junction assembly. *Nat. Cell Biol.* **2003**, *5*, 137–142, doi:10.1038/ncb923.
37. Pichaud, F. PAR-Complex and crumbs function during photoreceptor morphogenesis and retinal degeneration. *Front. Cell. Neurosci.* **2018**, *12*, 1–9, doi:10.3389/fncel.2018.00090.
38. Whitney, D.S.; Peterson, F.C.; Kittel, A.W.; Egner, J.M.; Prehoda, K.E.; Volkman, B.F. Crumbs binding to the Par-6 CRIB-PDZ module is regulated by Cdc42. *Biochemistry* **2016**, *55*, 1455–1461, doi:10.1016/j.physbeh.2017.03.040.
39. Joberty, G.; Petersen, C.; Gao, L.; Macara, I.G. The cell-polarity protein Par6 links Par3 and atypical protein kinase C to Cdc42. *Nat. Cell Biol.* **2000**, *2*.
40. Suzuki, A.; Yamanaka, T.; Hirose, T.; Manabe, N.; Mizuno, K.; Shimizu, M.; Akimoto, K.; Izumi, Y.; Ohnishi, T.; Ohno, S. Atypical protein kinase C is involved in the evolutionarily conserved PAR protein complex and plays a critical role in establishing epithelia-specific junctional structures. *J. Cell Biol.* **2001**, *152*, 1183–1196, doi:10.1083/jcb.152.6.1183.
41. Lin, D.; Edwards, A.S.; Fawcett, J.P.; Mbamalu, G.; Scott, J.D.; Pawson, T. A mammalian PAR-3-PAR-6 complex implicated in Cdc42/Rac1 and aPKC signalling and cell polarity. *Nat. Cell Biol.* **2000**, *2*, 540–547, doi:10.1038/35019582.
42. Yamanaka, T.; Horikoshi, Y.; Suzuki, A.; Sugiyama, Y.; Kitamura, K.; Maniwa, R.; Nagai, Y.; Yamashita, A.; Hirose, T.; Ishikawa, H.; et al. PAR-6 regulates aPKC activity in a novel way and mediates cell-cell contact-induced formation of the epithelial junctional complex. *Genes to Cells* **2001**, *6*, 721–731, doi:10.1046/j.1365-2443.2001.00453.x.

43. Gosens, I.; Sessa, A.; den Hollander, A.I.; Letteboer, S.J.F.; Belloni, V.; Arends, M.L.; Le Bivic, A.; Cremers, F.P.M.; Broccoli, V.; Roepman, R. FERM protein EPB41L5 is a novel member of the mammalian CRB-MPP5 polarity complex. *Exp. Cell Res.* **2007**, 313, 3959–3970, doi:10.1016/j.yexcr.2007.08.025.
44. Laprise, P.; Beronja, S.; Silva-gagliardi, N.F.; Pellikka, M.; Jensen, M.; Mcglade, C.J.; Tepass, U. The FERM Protein Yurt Is a Negative Regulatory Component of the Crumbs Complex that Controls Epithelial Polarity and Apical Membrane Size. *Dev. Cell* **2006**, 11, 363–374, doi:10.1016/j.devcel.2006.06.001.
45. Laprise, P.; Lau, K.M.; Harris, K.P.; Silva-Gagliardi, N.F.; Paul, S.M.; Beronja, S.; Beitel, G.J.; McGlade, C.J.; Tepass, U. Yurt, Coracle, Neurexin IV and the Na⁺, K⁺-ATPase form a novel group of epithelial polarity proteins. *Nature* **2009**, 459, 1141–1145, doi:10.1038/nature08067.
46. Lee, J.D.; Silva-Gagliardi, N.F.; Tepass, U.; McGlade, C.J.; Anderson, K. V. The FERM protein Epb4.115 is required for organization of the neural plate and for the epithelial-mesenchymal transition at the primitive streak of the mouse embryo. *Development* **2007**, 134, 2007–2016, doi:10.1242/dev.000885.
47. Whiteman, E.L.; Fan, S.; Harder, J.L.; Walton, K.D.; Liu, C.-J.; Soofi, A.; Fogg, V.C.; Hershenson, M.B.; Dressler, G.R.; Deutsch, G.H.; et al. Crumbs3 Is Essential for Proper Epithelial Development and Viability. *Mol. Cell. Biol.* **2014**, 34, 43–56, doi:10.1128/mcb.00999-13.
48. Tilston-Lünel, A.M.; Haley, K.E.; Schlecht, N.F.; Wang, Y.; Chatterton, A.L.D.; Moleirinho, S.; Watson, A.; Hundal, H.S.; Prystowsky, M.B.; Gunn-Moore, F.J.; et al. Crumbs 3b promotes tight junctions in an ezrin-dependent manner in mammalian cells. *J. Mol. Cell Biol.* **2016**, 8, 439–455, doi:10.1093/jmcb/mjw020.
49. Gao, Y.; Lui, W.Y.; Lee, W.M.; Cheng, C.Y. Polarity protein Crumbs homolog-3 (CRB3) regulates ectoplasmic specialization dynamics through its action on F-actin organization in Sertoli cells. *Sci. Rep.* **2016**, 6, 1–20, doi:10.1038/srep28589.
50. Chartier, F.J.M.; Hardy, É.J.L.; Laprise, P. Crumbs controls epithelial integrity by inhibiting Rac1 and PI3K. *J. Cell Sci.* **2011**, 124, 3393–3398, doi:10.1242/jcs.092601.
51. Hamon, A.; Masson, C.; Bitard, J.; Gieser, L.; Roger, J.E.; Perron, M. Retinal degeneration triggers the activation of YAP/TEAD in reactive Müller cells. *Retin. Cell Biol.* **2017**, 58, 1941–1953, doi:10.1167/iovs.16-21366.
52. Rueda, E.M.; Hall, B.M.; Hill, M.C.; Swinton, P.G.; Tong, X.; Martin, J.F.; Poché, R.A. The Hippo Pathway Blocks Mammalian Retinal Müller Glial Cell Reprogramming. *Cell Rep.* **2019**, 27, 1637-1649.e6, doi:10.1016/j.celrep.2019.04.047.
53. Hamon, A.; García-García, D.; Ail, D.; Bitard, J.; Chesneau, A.; Dalkara, D.; Locker, M.; Roger, J.E.; Perron, M. Linking YAP to Müller Glia Quiescence Exit in the Degenerative Retina. *Cell Rep.* **2019**, 27, 1712-1725.e6, doi:10.1016/j.celrep.2019.04.045.
54. Yu, F.; Zhao, B.; Guan, K. Hippo Pathway in Organ Size Control, Tissue Homeostasis, and Cancer. *Cell* **2015**, 163, 811–828, doi:10.1016/j.physbeh.2017.03.040.
55. Yu, F.; Guan, K. The Hippo pathway: regulators and regulations. *Genes Dev.* **2013**, 27, 335–371, doi:10.1101/gad.210773.112.a.

56. Mao, X.; Li, P.; Wang, Y.; Liang, Z.; Liu, J.; Li, J.; Jiang, Y.; Bao, G.; Li, L.; Zhu, B.; et al. CRB3 regulates contact inhibition by activating the Hippo pathway in mammary epithelial cells. *Cell Death Dis.* **2017**, *8*, doi:10.1038/cddis.2016.478.
57. Szymaniak, A.D.; Mahoney, J.E.; Cardoso, W. V.; Varelas, X. Crumbs3-Mediated Polarity Directs Airway Epithelial Cell Fate through the Hippo Pathway Effector Yap. *Dev. Cell* **2015**, *34*, 283–296, doi:10.1016/j.devcel.2015.06.020.
58. Pellissier, L.P.; Alves, C.H.; Quinn, P.M.; Vos, R.M.; Tanimoto, N.; Lundvig, D.M.S.; Dudok, J.J.; Hooibrink, B.; Richard, F.; Beck, S.C.; et al. Targeted Ablation of *Crb1* and *Crb2* in Retinal Progenitor Cells Mimics Leber Congenital Amaurosis. *PLoS Genet.* **2013**, *9*, doi:10.1371/journal.pgen.1003976.
59. Talib, M.; van Schooneveld, M.J.; van Genderen, M.M.; Wijnholds, J.; Florijn, R.J.; ten Brink, J.B.; Schalijs-Delfos, N.E.; Dagnelie, G.; Cremers, F.P.M.; Wolterbeek, R.; et al. Genotypic and Phenotypic Characteristics of *CRB1*-Associated Retinal Dystrophies: A Long-Term Follow-up Study. *Ophthalmology* **2017**, *124*, 884–895, doi:10.1016/j.ophtha.2017.01.047.
60. Verbakel, S.K.; van Huet, R.A.C.; Boon, C.J.F.; den Hollander, A.I.; Collin, R.W.J.; Klaver, C.C.W.; Hoyng, C.B.; Roepman, R.; Klevering, B.J. Non-syndromic retinitis pigmentosa. *Prog. Retin. Eye Res.* **2018**, *66*, 157–186, doi:10.1016/j.preteyeres.2018.03.005.
61. Corton, M.; Tatu, S.D.; Avila-Fernandez, A.; Vallespín, E.; Tapias, I.; Cantalapiedra, D.; Blanco-Kelly, F.; Riveiro-Alvarez, R.; Bernal, S.; García-Sandoval, B.; et al. High frequency of *CRB1* mutations as cause of Early-Onset Retinal Dystrophies in the Spanish population. *Orphanet J. Rare Dis.* **2013**, *8*, doi:10.1186/1750-1172-8-20.
62. Bujakowska, K.; Audo, I.; Mohand-Säid, S.; Lancelot, M.E.; Antonio, A.; Germain, A.; eveillard, T.L.; Letexier, Melanie; Saraiva, J.P.; Lonjou, C.; et al. *CRB1* mutations in inherited retinal dystrophies. *Hum. Mutat.* **2012**, *33*, 306–315, doi:10.1002/humu.21653.
63. Vallespin, E.; Cantalapiedra, D.; Riveiro-Alvarez, R.; Wilke, R.; Aguirre-Lamban, J.; Avila-Fernandez, A.; Lopez-Martinez, M.A.; Gimenez, A.; Trujillo-Tiebas, M.J.; Ramos, C.; et al. Mutation screening of 299 Spanish families with retinal dystrophies by leber congenital amaurosis genotyping microarray. *Investig. Ophthalmol. Vis. Sci.* **2007**, *48*, 5653–5661, doi:10.1167/iovs.07-0007.
64. Den Hollander, A.I.; Davis, J.; Van Der Velde-Visser, S.D.; Zonneveld, M.N.; Pierrottet, C.O.; Koenekoop, R.K.; Kellner, U.; Van Den Born, L.I.; Heckenlively, J.R.; Hoyng, C.B.; et al. *CRB1* mutation spectrum in inherited retinal dystrophies. *Hum. Mutat.* **2004**, *24*, 355–369, doi:10.1002/humu.20093.
65. Henderson, R.H.; Mackay, D.S.; Li, Z.; Moradi, P.; Sergouniotis, P.; Russell-Eggitt, I.; Thompson, D.A.; Robson, A.G.; Holder, G.E.; Webster, A.R.; et al. Phenotypic variability in patients with retinal dystrophies due to mutations in *CRB1*. *Br. J. Ophthalmol.* **2011**, *95*, 811–817, doi:10.1136/bjo.2010.186882.
66. Mathijssen, I.B.; Florijn, R.J.; Van Den Born, L.I.; Zekveld-Vroon, R.C.; Ten Brink, J.B.; Plomp, A.S.; Baas, F.; Meijers-Heijboer, H.; Bergen, A.A.B.; Van Schooneveld, M.J. Long-term follow-up of patients with retinitis pigmentosa type 12 caused by *CRB1* mutations: A severe phenotype with considerable interindividual variability. *Retina* **2017**, *37*, 161–172, doi:10.1097/IAE.0000000000001127.

67. Chen, X.; Jiang, C.; Yang, D.; Sun, R.; Wang, M.; Sun, H.; Xu, M.; Zhou, L.; Chen, M.; Xie, P.; et al. CRB2 mutation causes autosomal recessive retinitis pigmentosa. *Exp. Eye Res.* **2019**, *180*, 164–173, doi:10.1016/j.exer.2018.12.018.
68. Zhong, X.; Gutierrez, C.; Xue, T.; Hampton, C.; Vergara, M.N.; Cao, L.H.; Peters, A.; Park, T.S.; Zambidis, E.T.; Meyer, J.S.; et al. Generation of three-dimensional retinal tissue with functional photoreceptors from human iPSCs. *Nat. Commun.* **2014**, *5*, doi:10.1038/ncomms5047.
69. Meyer, J.S.; Howden, S.E.; Wallace, K. a; Verhoeven, A.D.; Wright, L.S.; Capowski, E.E.; Pinilla, I.; Martin, J.M.; Tian, S.; Stewart, R.; et al. Optic Vesicle-like Structures Derived from Human Pluripotent Stem Cells Facilitate a Customized Approach to Retinal Disease Treatment. *Stem Cells* **2011**, *29*, 1206–1218.
70. Nakano, T.; Ando, S.; Takata, N.; Kawada, M.; Mugeruma, K.; Sekiguchi, K.; Saito, K.; Yonemura, S.; Eiraku, M.; Sasai, Y. Self-formation of optic cups and storable stratified neural retina from human ESCs. *Cell Stem Cell* **2012**, *10*, 771–785, doi:10.1016/j.stem.2012.05.009.
71. Ovando-Roche, P.; West, E.L.; Branch, M.J.; Sampson, R.D.; Fernando, M.; Munro, P.; Georgiadis, A.; Rizzi, M.; Kloc, M.; Naeem, A.; et al. Use of bioreactors for culturing human retinal organoids improves photoreceptor yields. *Stem Cell Res. Ther.* **2018**, *9*, 1–14, doi:10.1186/s13287-018-0907-0.
72. Luo, Z.; Zhong, X.; Li, K.; Xie, B.; Liu, Y.; Ye, M.; Li, K.; Xu, C.; Ge, J. An Optimized System for Effective Derivation of Three-Dimensional Retinal Tissue via Wnt Signaling Regulation. *Stem Cells* **2018**, *36*, 1709–1722, doi:10.1002/stem.2890.
73. Capowski, E.E.; Samimi, K.; Mayerl, S.J.; Phillips, M.J.; Pinilla, I.; Howden, S.E.; Saha, J.; Jansen, A.D.; Edwards, K.L.; Jager, L.D.; et al. Reproducibility and staging of 3D human retinal organoids across multiple pluripotent stem cell lines. *Dev.* **2019**, *146*, doi:10.1242/dev.171686.
74. Mellough, C.B.; Collin, J.; Queen, R.; Hilgen, G.; Dorgau, B.; Zerti, D.; Felemban, M.; White, K.; Sernagor, E.; Lako, M. Systematic Comparison of Retinal Organoid Differentiation from Human Pluripotent Stem Cells Reveals Stage Specific, Cell Line, and Methodological Differences. *Stem Cells Transl. Med.* **2019**, *8*, 694–706, doi:10.1002/sctm.18-0267.
75. Chichagova, V.; Hilgen, G.; Ghareeb, A.; Georgiou, M.; Carter, M.; Sernagor, E.; Lako, M.; Armstrong, L. Human iPSC differentiation to retinal organoids in response to IGF1 and BMP4 activation is line- and method-dependent. *Stem Cells* **2020**, *38*, 195–201.
76. Cora, V.; Haderspeck, J.; Antkowiak, L.; Mattheus, U.; Neckel, P.H.; Mack, A.F.; Bolz, S.; Ueffing, M.; Pashkovskaia, N.; Achberger, K.; et al. A Cleared View on Retinal Organoids. *Cells* **2019**, *8*, 391, doi:10.3390/cells8050391.
77. Hallam, D.; Hilgen, G.; Dorgau, B.; Zhu, L.; Yu, M.; Bojic, S.; Hewitt, P.; Schmitt, M.; Uteng, M.; Kustermann, S.; et al. Human-Induced Pluripotent Stem Cells Generate Light Responsive Retinal Organoids with Variable and Nutrient-Dependent Efficiency. *Stem Cells* **2018**, *36*, 1535–1551, doi:10.1002/stem.2883.
78. Kim, S.; Lowe, A.; Dharmat, R.; Lee, S.; Owen, L.A.; Wang, J.; Shakoob, A.; Li, Y.; Morgan, D.J.; Hejazi, A.A.; et al. Generation, transcriptome profiling, and functional validation of cone-rich human retinal organoids. *Proc. Natl. Acad. Sci. U. S. A.* **2019**, *166*, 10824–10833, doi:10.1073/pnas.1901572116.

79. van de Pavert, S.A.; Meuleman, J.; Malysheva, A.; Aartsen, W.M.; Versteeg, I.; Tonagel, F.; Kamphuis, W.; McCabe, C.J.; Seeliger, M.W.; Wijnholds, J. A single amino acid substitution (Cys249Trp) in *Crb1* causes retinal degeneration and deregulates expression of pituitary tumor transforming gene *Pttg1*. *J. Neurosci.* **2007**, *27*, 564–573, doi:10.1523/JNEUROSCI.3496-06.2007.
80. Alves, C.H.; Sanz sanz, A.; Park, B.; Pellissier, L.P.; Tanimoto, N.; Beck, S.C.; Huber, G.; Murtaza, M.; Richard, F.; Sridevi gurubaran, I.; et al. Loss of *CRB2* in the mouse retina mimics human retinitis pigmentosa due to mutations in the *CRB1* gene. *Hum. Mol. Genet.* **2013**, *22*, 35–50, doi:10.1093/hmg/dd3398.
81. Zhang, X.; Zhang, D.; Chen, S.C.; Lamey, T.; Thompson, J.A.; McLaren, T.; De Roach, J.N.; Chen, F.K.; McLenachan, S. Establishment of an induced pluripotent stem cell line from a retinitis pigmentosa patient with compound heterozygous *CRB1* mutation. *Stem Cell Res.* **2018**, *31*, 147–151, doi:10.1016/j.scr.2018.08.001.
82. Shutova, M. V.; Surdina, A. V.; Ischenko, D.S.; Naumov, V.A.; Bogomazova, A.N.; Vassina, E.M.; Alekseev, D.G.; Lagarkova, M.A.; Kiselev, S.L. An integrative analysis of reprogramming in human isogenic system identified a clone selection criterion. *Cell Cycle* **2016**, *15*, 986–997, doi:10.1080/15384101.2016.1152425.
83. Buchholz, D.E.; Pennington, B.O.; Croze, R.H.; Hinman, C.R.; Coffey, P.J.; Clegg, D.O. Rapid and Efficient Directed Differentiation of Human Pluripotent Stem Cells Into Retinal Pigmented Epithelium. *Stem Cells Transl. Med.* **2013**, *2*, 384–393, doi:10.5966/sectm.2012-0163.
84. Zahabi, A.; Shahbazi, E.; Ahmadi, H.; Hassani, S.N.; Totonchi, M.; Taei, A.; Masoudi, N.; Ebrahimi, M.; Aghdami, N.; Seifinejad, A.; et al. A new efficient protocol for directed differentiation of retinal pigmented epithelial cells from normal and retinal disease induced pluripotent stem cells. *Stem Cells Dev.* **2012**, *21*, 2262–2272, doi:10.1089/scd.2011.0599.
85. Maruotti, J.; Sripathi, S.R.; Bharti, K.; Fuller, J.; Wahlin, K.J.; Ranganathan, V.; Sluch, V.M.; Berlinicke, C.A.; Davis, J.; Kim, C.; et al. Small-molecule-directed, efficient generation of retinal pigment epithelium from human pluripotent stem cells. *Proc. Natl. Acad. Sci. U. S. A.* **2015**, *112*, 10950–10955, doi:10.1073/pnas.1422818112.
86. Smith, E.N.; D’Antonio-Chronowska, A.; Greenwald, W.W.; Borja, V.; Aguiar, L.R.; Pogue, R.; Matsui, H.; Benaglio, P.; Borooah, S.; D’Antonio, M.; et al. Human iPSC-Derived Retinal Pigment Epithelium: A Model System for Prioritizing and Functionally Characterizing Causal Variants at AMD Risk Loci. *Stem Cell Reports* **2019**, *12*, 1342–1353, doi:10.1016/j.stemcr.2019.04.012.
87. Mehalow, A.K.; Kameya, S.; Smith, R.S.; Hawes, N.L.; Denegre, J.M.; Young, J.A.; Bechtold, L.; Haider, N.B.; Tepass, U.; Heckenlively, J.R.; et al. *CRB1* is essential for external limiting membrane integrity and photoreceptor morphogenesis in the mammalian retina. *Hum. Mol. Genet.* **2003**, *12*, 2179–2189, doi:10.1093/hmg/ddg232.
88. van de Pavert, S.A.; Sanz sanz, A.; Aartsen, W.M.; Vos, R.M.; Versteeg, I.; Beck, S.C.; Klooster, J.; Seeliger, M.W.; Wijnholds, J. *Crb1* is a Determinant of Retinal Apical Muller Glia Cell Features. *Glia* **2007**, 1486–1497, doi:10.1002/glia.
89. Quinn, P.M.; Alves, C.H.; Klooster, J.; Wijnholds, J. *CRB2* in immature photoreceptors determines the superior-inferior symmetry of the developing retina to maintain retinal structure and function. *Hum. Mol. Genet.* **2018**, *27*, 3137–3153, doi:10.1093/hmg/ddy194.

90. Alves, C.H.; Pellissier, L.P.; Vos, R.M.; Garrido, M.G.; Sothilingam, V.; Seide, C.; Beck, S.C.; Klooster, J.; Furukawa, T.; Flannery, J.G.; et al. Targeted ablation of Crb2 in photoreceptor cells induces retinitis pigmentosa. *Hum. Mol. Genet.* **2014**, *23*, 3384–3401, doi:10.1093/hmg/ddu048.
91. Alves, C.H.; Boon, N.; Mulder, A.A.; Koster, A.J.; Jost, C.R.; Wijnholds, J. CRB2 Loss in Rod Photoreceptors Is Associated with Progressive Loss of Retinal Contrast Sensitivity. *Int. J. Mol. Sci.* **2019**, *20*, 4069, doi:10.3390/ijms20174069.
92. Zhao, M.; Andrieu-Soler, C.; Kowalczyk, L.; Paz Cortés, M.; Berdugo, M.; Dernigoghossian, M.; Halili, F.; Jeanny, J.-C.; Goldenberg, B.; Savoldelli, M.; et al. A New CRB1 Rat Mutation Links Müller Glial Cells to Retinal Telangiectasia. *J. Neurosci.* **2015**, *35*, 6093–6106, doi:10.1523/jneurosci.3412-14.2015.
93. Maguire, A.M.; Russell, S.; Wellman, J.A.; Chung, D.C.; Yu, Z.F.; Tillman, A.; Wittes, J.; Pappas, J.; Elci, O.; Marshall, K.A.; et al. Efficacy, Safety, and Durability of Voretigene Neparvovec-rzyl in RPE65 Mutation-Associated Inherited Retinal Dystrophy: Results of Phase 1 and 3 Trials. *Ophthalmology* **2019**, *126*, 1273–1285, doi:10.1016/j.ophtha.2019.06.017.
94. Wang, D.; Tai, P.W.L.; Gao, G. Adeno-associated virus vector as a platform for gene therapy delivery. *Nat. Rev. Drug Discov.* **2019**, *18*, 358–378, doi:10.1038/s41573-019-0012-9.
95. Pellissier, L.P.; Hoek, R.M.; Vos, R.M.; Aartsen, W.M.; Klimczak, R.R.; Hoyng, S.A.; Flannery, J.G.; Wijnholds, J. Specific tools for targeting and expression in Müller glial cells. *Mol. Ther. - Methods Clin. Dev.* **2014**, *1*, 14009, doi:10.1038/mtm.2014.9.
96. Carvalho, L.S.; Turunen, H.T.; Wassmer, S.J.; Luna-Velez, M. V.; Xiao, R.; Bennett, J.; Vandenberghe, L.H. Evaluating efficiencies of dual AAV approaches for retinal targeting. *Front. Neurosci.* **2017**, *11*, 1–8, doi:10.3389/fnins.2017.00503.
97. Trapani, I.; Colella, P.; Sommella, A.; Iodice, C.; Cesi, G.; de Simone, S.; Marrocco, E.; Rossi, S.; Giunti, M.; Palfi, A.; et al. Effective delivery of large genes to the retina by dual AAV vectors. *EMBO Mol. Med.* **2014**, *6*, 194–211, doi:10.1002/emmm.201302948.
98. Maddalena, A.; Tornabene, P.; Tiberi, P.; Minopoli, R.; Manfredi, A.; Mutarelli, M.; Rossi, S.; Simonelli, F.; Naggert, J.K.; Cacchiarelli, D.; et al. Triple Vectors Expand AAV Transfer Capacity in the Retina. *Mol. Ther.* **2018**, *26*, 524–541, doi:10.1016/j.ymthe.2017.11.019.
99. Ding, X.; Gradinaru, V. Structure-Guided Rational Design of Adeno-Associated Viral Capsids with Expanded Sizes. *ASGCT Abstr. B.* **2020**.
100. Garita-Hernandez, M.; Routet, F.; Guibbal, L.; Khabou, H.; Toualbi, L.; Riancho, L.; Reichman, S.; Duebel, J.; Sahel, J.A.; Goureau, O.; et al. AAV-mediated gene delivery to 3D retinal organoids derived from human induced pluripotent stem cells. *Int. J. Mol. Sci.* **2020**, *21*, 1–16, doi:10.3390/ijms21030994.
101. Lane, A.; Jovanovic, K.; Shortall, C.; Ottaviani, D.; Panes, A.B.; Schwarz, N.; Guarascio, R.; Hayes, M.J.; Palfi, A.; Chadderton, N.; et al. Modeling and Rescue of RP2 Retinitis Pigmentosa Using iPSC-Derived Retinal Organoids. *Stem Cell Reports* **2020**, *15*, 67–79, doi:10.1016/j.stemcr.2020.05.007.
102. Wang, Y.; Rajala, A.; Rajala, R.V.S. Nanoparticles as Delivery Vehicles for the Treatment of Retinal Degenerative Diseases. *Adv Exp Med Biol* **2018**, *1074*, 117–123, doi:10.1016/j.physbeh.2017.03.040.

103. Fink, T.L.; Klepcyk, P.J.; Oette, S.M.; Gedeon, C.R.; Hyatt, S.L.; Kowalczyk, T.H.; Moen, R.C.; Cooper, M.J. Plasmid size up to 20 kbp does not limit effective in vivo lung gene transfer using compacted DNA nanoparticles. *Gene Ther.* **2006**, *13*, 1048–1051, doi:10.1038/sj.gt.3302761.
104. Han, Z.; Conley, S.M.; Makkia, R.; Guo, J.; Cooper, M.J.; Naash, M.I. Comparative Analysis of DNA Nanoparticles and AAVs for Ocular Gene Delivery. *PLoS One* **2012**, *7*, 1–11, doi:10.1371/journal.pone.0052189.
105. Cai, X.; Nash, Z.; Conley, S.M.; Fliesler, S.J.; Cooper, M.J.; Naash, M.I. A partial structural and functional rescue of a retinitis pigmentosa model with compacted DNA nanoparticles. *PLoS One* **2009**, *4*, doi:10.1371/journal.pone.0005290.
106. Akelley, R.A.; Conley, S.M.; Makkia, R.; Watson, J.N.; Han, Z.; Cooper, M.J.; Naash, M.I. DNA nanoparticles are safe and nontoxic in non-human primate eyes. *Int. J. Nanomedicine* **2018**, *13*, 1361–1379, doi:10.2147/IJN.S157000.
107. Ding, X.Q.; Quiambao, A.B.; Fitzgerald, J.B.; Cooper, M.J.; Conley, S.M.; Naash, M.I. Ocular delivery of compacted DNA-nanoparticles does not elicit toxicity in the mouse retina. *PLoS One* **2009**, *4*, doi:10.1371/journal.pone.0007410.
108. HORAMA HORAMA Signs Exclusive License Agreement with Leiden University Medical Center Targeting *CRB1* Gene Mutations to Treat Inherited Retinal Dystrophies **2020**.

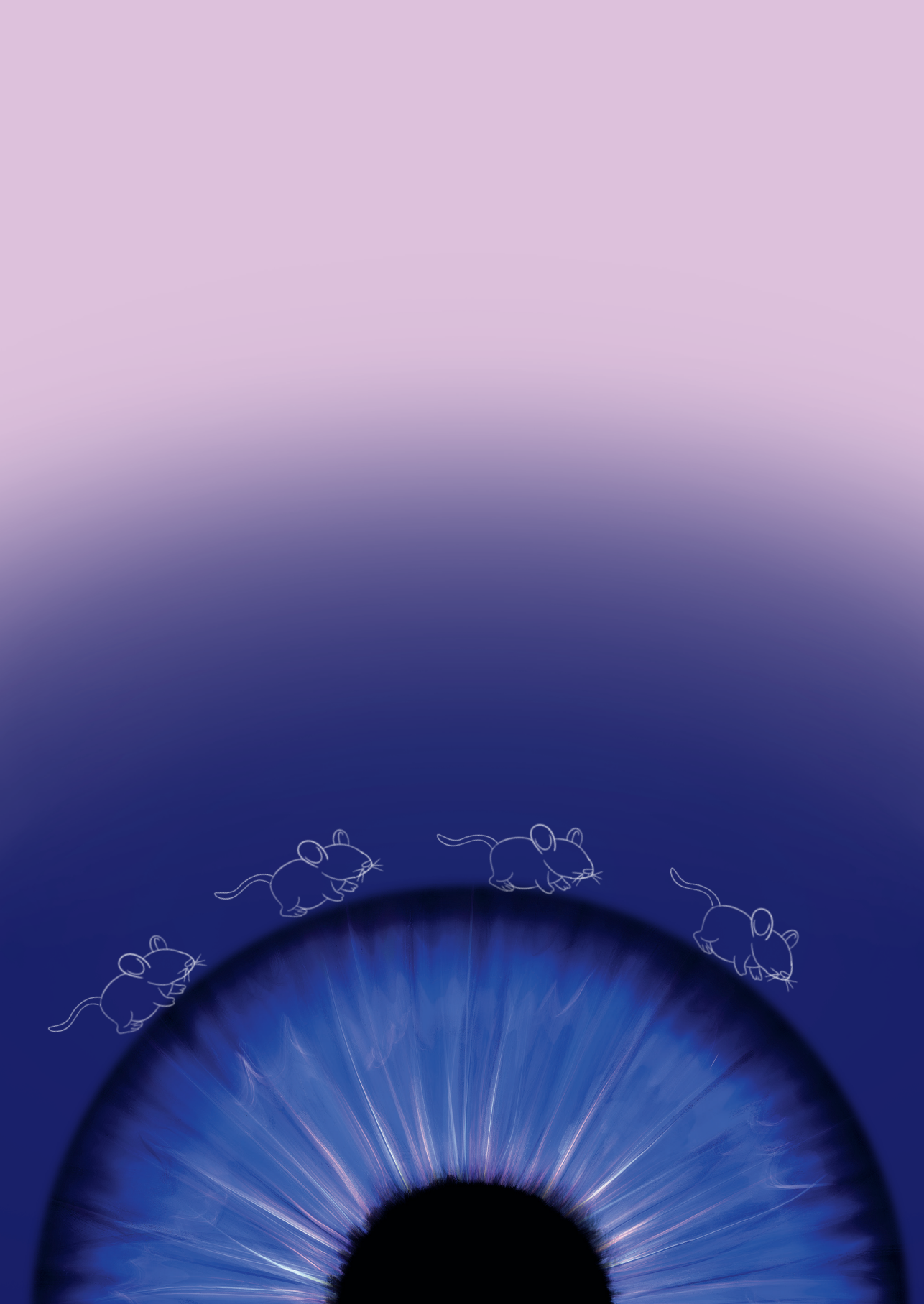
Chapter 2

CRB2 Loss in Rod Photoreceptors is Associated with
Progressive Loss of Retinal Contrast Sensitivity

C. H. Alves, **N. Boon**, A. A. Mulder, A. J. Koster, C. R. Jost,
and J. Wijnholds

Part of this study is published in:

International Journal of Molecular Sciences, 2019; 4069



Abstract

Variations in the Crumbs homolog-1 (*CRB1*) gene are associated with a wide variety of autosomal recessive retinal dystrophies including early onset retinitis pigmentosa (RP) and Leber congenital amaurosis (LCA). CRB1 belongs to the Crumbs family that in mammals includes CRB2 and CRB3. Here, we studied the specific roles of CRB2 in rod photoreceptor cells and if ablation of CRB2 in rods exacerbate the *Crb1*-disease. Therefore, we assessed the morphological, retinal and visual functional consequences of specific ablation of CRB2 from rods with or without concomitant loss of CRB1. Our data demonstrated that loss of CRB2 in mature rods resulted in RP. The retina showed gliosis and disruption of the subapical region and adherens junctions at the outer limiting membrane. Rods were lost at the peripheral and central superior retina, while gross retinal lamination was preserved. Rod function as measured by electroretinography was impaired in adult mice. Additional loss of CRB1 exacerbated the retinal phenotype leading to an early reduction of the dark-adapted rod photoreceptor a-wave and reduced contrast sensitivity from 3-months-of-age as measured by optokinetic head tracking response behaviour testing. The data suggest that CRB2 present in rods is required to prevent photoreceptor degeneration and vision loss.

Introduction

The Crumbs protein complex is essential for polarity establishment and adhesion of the retinal neural epithelium. In mammals, the Crumbs family is composed of Crumbs homolog-1 (CRB1), CRB2, and CRB3. CRB1 and CRB2 have a large extracellular domain with epidermal growth-factor-like and laminin-A globular domains, a single transmembrane domain, and an intracellular C-terminal domain of 37 amino acids; CRB3 lacks the extracellular domain [1]. The intracellular domain has a single C-terminal PDZ protein-binding motif and a single FERM-protein-binding motif juxtaposing the transmembrane domain [1]. The Crumbs proteins associate with the adaptor protein PALS1 and one of the multiple PDZ-proteins PATJ or MUPP1 to form the core of the Crumbs complex [2,3]. In the developing mouse retina, the Crumbs

proteins localize at the subapical region adjacent to the adherens junctions between retinal progenitor cells [4]. In the mature retina, the Crumbs proteins are present in photoreceptors and Müller glial cells (MGCs) [5,6]. CRB2 protein is present in photoreceptors and MGCs, whereas CRB1 protein is present only in MGCs [7,8].

Variations in the *CRB1* gene are associated with a wide variety of autosomal recessive retinal dystrophies, including retinitis pigmentosa (RP), Leber congenital amaurosis (LCA), cone-rod dystrophy, isolated macular dystrophy, and foveal retinoschisis [9,10]. So far, 310 pathogenic variations in the *CRB1* gene were identified (<http://www.LOVD.nl/CRB1>). Missense mutations in the human *CRB2* gene have been recently associated with RP [11], as well as with syndromic kidney and brain diseases [12–14].

Loss or reduced levels of the CRB1 or CRB2 proteins in retinal progenitors, immature photoreceptors, or MGCs leads to different retinal phenotypes in mice that mimic the wide spectrum of clinical features described in *CRB1*-patients, including early and late onset RP and LCA [2]. Loss of either CRB1 or CRB2 in MGCs results in mild retinal dystrophy, without impairing retinal function [6,15–17]. Ablation of *Crb2* in retinal progenitor cells, or in immature rod and cone photoreceptor cells, results in progressive thinning and degeneration of the photoreceptor layer, abnormal lamination of immature rods, and loss of retinal function [4,16,18]. Moreover, CRB2 has roles in restricting the proliferation of retinal progenitor cells and the number of rod photoreceptors and MGCs [4]. Mouse CRB2 acts as the modifying factor of *CRB1*-related retinal dystrophies, since reduction or full ablation of CRB2 in combination with loss of CRB1 results in an exacerbation of the retinal phenotype observed in *Crb1* knockout retinas [19–22]. The specific roles of CRB2 in rod photoreceptor cells still need to be elucidated. We hypothesize that CRB2 in rods is required to maintain proper retinal structure and function.

In fetal human retinas, human iPSC-derived retinal organoids, and adult non-human-primate retinas, CRB1 as well as CRB2 proteins localize at the subapical region in both photoreceptors and MGCs [22,23]. We previously showed proof-of-concept for AAV9-CMV-*CRB2*, reintroduction of CRB2 into photoreceptors and MGCs rescued the

phenotype of $Crb2^{\text{flox/flox}}\text{Chx10Cre}$ and $Crb1Crb2^{\text{F/+}}\text{Chx10Cre}$ mouse retinas [24]. Although AAV9 efficiently transduces both mouse photoreceptors and MGCs [25], AAV5 outperforms AAV9 in transducing both human photoreceptors and MGCs in cultured adult human retinal explants and human iPSC-derived retinal organoids [23]; as such, AAV5 the most suitable serotype to be used in the clinics. In mice, AAV5 only infects retinal pigment epithelium and photoreceptors; a new animal model lacking CRB2 specifically in photoreceptor cells that allows us to test the efficacy of the AAV5-CMV-*CRB2* vector is required. Therefore, to validate our hypothesis and for the ability of testing the AAV5-CMV-*CRB2* vector in the future, we generated mice lacking CRB2 specifically in adult rod photoreceptors (with remaining levels of CRB2 in MGCs and cone photoreceptors), and mice lacking CRB2 specifically in rod photoreceptors and CRB1 specifically in MGCs.

Here, we studied the effects on retinal morphology and function of loss of CRB2 specifically in rod photoreceptors with or without concomitant loss of CRB1. Our data shows that specific ablation of CRB2 in mouse rods leads to RP. The phenotype observed in these retinas was characterized by loss of photoreceptor cells and gliosis in the peripheral and central retina. The retinal degeneration was more severe in the superior than in the inferior retina. Retinal function, measured by ERG, was impaired in 9-month-old animals. Concomitant loss of CRB1 exacerbates the retinal phenotype leading to decreased retinal and visual function from 3-months-of-age. The data suggest that CRB2 in rods is required to maintain cellular adhesion between rods and prevent photoreceptor degeneration and vision loss.

Results

Rho-iCre mediates recombination specifically in rod photoreceptors

To study the specific cellular and physiological functions of CRB2 in rod photoreceptor cells, we crossed the *Crb2* floxed homozygous ($Crb2^{\text{flox/flox}}$) mice [4,18] and $Crb1^{\text{KO}}Crb2^{\text{flox/flox}}$ [19] with the *Rho-iCre* transgenic mouse line [26] to obtain $Crb2^{\Delta\text{Rods}}$ ($Crb2^{\text{flox/flox}}/\text{RhoiCre}^{+/-}$) and $Crb1^{\text{KO}}Crb2^{\Delta\text{Rods}}$ ($Crb1^{-/-}Crb2^{\text{flox/flox}}/\text{RhoiCre}^{+/-}$) animals. The *Rho-iCre* transgenic mice express CRE recombinase in rod

photoreceptors from postnatal day 7, resulting in efficient recombination at postnatal day 18 [26]. To confirm the mosaicism and specificity of the Rho-*iCre* transgenic mouse line, we crossed the *Crb2*^{ΔRods} mice with a R26-stop-EYFP reporter mouse line [27] that expresses enhanced yellow fluorescent protein (EYFP) upon CRE-mediated recombination. While in *Crb2*^{flox/flox}::*EYFP*^{flox-stop-flox/+} no EYFP signal could be detected in the retina (Supplemental Figure 1A), in *Crb2*^{ΔRods}::*EYFP* mice, EYFP fluorescence was observed in the outer nuclear layer the inner-segment layer of postnatal day 20 retinas (Supplemental Figure 1D). We checked for absence of CRE-mediated recombination in cone photoreceptors by performing co-localization studies using a cone photoreceptor marker (cone arrestin) and EYFP (Supplemental Figure 1B, C, E, F). Cone photoreceptors' cell soma and inner-segments were EYFP-negative (Supplemental Figure 1D, F; arrows), suggesting that recombination mediated by Rho-*iCre* was efficient and limited to rod photoreceptors. CRB2 was detected at the subapical region at the outer limiting membrane in postnatal day 20 control (Supplemental Figure 1G) and *Crb2*^{ΔRods} (Supplemental Figure 1H) retinas, likely due to maintained expression of CRB2 in the adjacent subapical region of wild-type MGCs and cone photoreceptors.

Ablation of CRB2 in rods with concomitant loss of CRB1 leads to retinal dysfunction and vision impairment

To study if the specific loss of CRB2 from rod photoreceptors with and without concomitant loss of CRB1 affected retinal function, we performed electroretinography (ERG) in 1-, 3-, 6-, 9-, and 12-month-old *Crb2*^{ΔRods}, *Crb1*^{KO}*Crb2*^{ΔRods}, and the respective age-matched controls (*Crb2*^{flox/flox} and *Crb1*^{KO}*Crb2*^{flox/flox}). One-month-old *Crb2*^{ΔRods} and *Crb1*^{KO}*Crb2*^{ΔRods} mice showed similar scotopic and photopic responses to the ones observed in the age-matched controls (Figure 1C, Supplemental Figure 2 and 3). In contrast, 3-month-old *Crb1*^{KO}*Crb2*^{ΔRods}, but not *Crb2*^{ΔRods} mice, showed slightly reduced amplitudes of a-wave scotopic electroretinography responses, indicating alterations of rod photoreceptor function (Figure 1A, arrow; Figure 1C). Moreover, 3-month-old *Crb1*^{KO}*Crb2*^{ΔRods} also showed reduced b-wave photopic electroretinography (Supplemental Figure 3). The reduction of the scotopic a-wave

amplitudes in $Crb1^{KO}Crb2^{\Delta Rods}$ mice became more evident at 9- and 12-months-of-age (Figure 1B–D). At these time points, a reduced a-wave was also observed in $Crb2^{\Delta Rods}$ mice (Figure 1B–D; arrows). Twelve-month-old mutants also showed a reduced b-wave (Figure 1C).

2 Three-month-old $Crb1^{KO}Crb2^{\Delta Rods}$ mice showed reduced scotopic a-wave responses, making these mice an interesting and potential suitable CRB1-disease model for future gene therapy rescue experiments. Therefore, we decided to determine whether the visual function was also affected in these mice. To do so, we used an optomotor response test (optokinetic head tracking response (OKT)) to measure the spatial frequency threshold and contrast sensitivity [28, 29]. Spatial frequency was measured by systematically increasing the spatial frequency of the grating at 100% contrast until animals no longer tracked (spatial frequency threshold). A contrast sensitivity threshold was generated by identifying the minimum contrast that generated tracking, over a range of spatial frequencies. Spatial frequency threshold and contrast sensitivity of $Crb1^{KO}Crb2^{\Delta Rods}$ mice were analysed at different time points, at 1-, 3-, 7-, and 9-month(s)-of-age. At 1- and 3-months-of-age, no differences were observed in spatial acuity between littermate controls ($Crb1^{KO}Crb2^{floxed/floxed}$) and $Crb1^{KO}Crb2^{\Delta Rods}$ mice (Figure 2A). However, at 7- and 9-months-of-age the $Crb1^{KO}Crb2^{\Delta Rods}$ showed a small but statistically significant decrease in spatial frequency thresholds, also described frequently in literature as visual acuity.

The retinas of one-month-old $Crb1^{KO}Crb2^{\Delta Rods}$ showed similar contrast sensitivity compared to $Crb1^{KO}Crb2^{floxed/floxed}$ mice at all frequencies measured (Figure 2C, Supplemental Figure 4A). However, 3-, 7-, and 9-month-old $Crb1^{KO}Crb2^{\Delta Rods}$ exhibited reduced contrast sensitivities compared to the littermate age-matched controls ($Crb1^{KO}Crb2^{floxed/floxed}$). Once $Crb1^{KO}Crb2^{\Delta Rods}$ showed impaired visual function, we wanted to evaluate if deletion of only CRB2 from rods was sufficient to induce such a deficit. Therefore, the spatial frequency threshold and contrast sensitivity of $Crb2^{floxed/floxed}$ were compared to age-matched $Crb2^{\Delta Rods}$. No differences were observed in spatial frequency threshold nor in contrast sensitivity at 3- and 5-months-of-age (Figure 2B and Supplemental Figure 4B). The data suggest that the visual function impairment

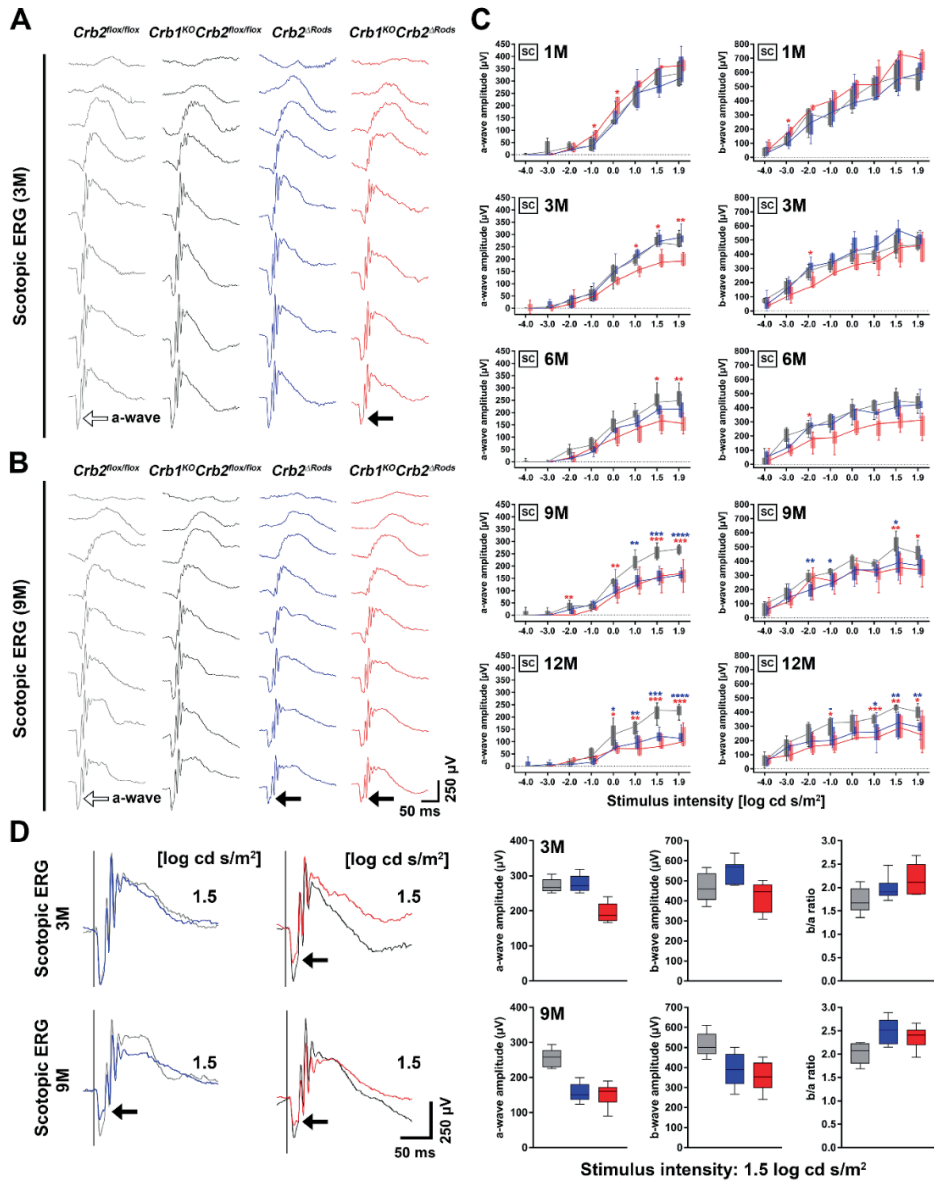


Figure 1: Progressive loss of retinal function in *Crb2*^{ΔRods} and *Crb1*^{KO}*Crb2*^{ΔRods} mice. Electroretinographic analysis of retinal function in *Crb2*^{flx/flx} (control, gray), *Crb1*^{KO}*Crb2*^{flx/flx} (control, black), *Crb2*^{ΔRods} (blue), and *Crb1*^{KO}*Crb2*^{ΔRods} (red). Scotopic single-flash intensity series from representative animals at 3-months-of-age (A) and 9-months-of-age (B). The control scotopic a-wave is indicated by the open arrow and the black arrow points to the attenuated a-wave of the *Crb1*^{KO}*Crb2*^{ΔRods} at 3-months-of-age and of the *Crb1*^{KO}*Crb2*^{ΔRods} and *Crb2*^{ΔRods} at

2

9-months-of-age (A,B; arrows). Time course single-flash ERG data from 1-, 3-, 6-, 9-, and 12-month-old *Crb2^{fllox/fllox}* (control), *Crb2^{ΔRods}* and *Crb1^{KO}Crb2^{ΔRods}* mice (C). Scotopic (SC) a-wave and b-wave amplitude are presented as a function of the logarithm of the flash intensity. Superposition of scotopic single-flash electroretinography responses (1.5 log cd*s/m²) where the black arrow points to the attenuated a-wave of the affected mice (D) (left), and the quantitative evaluation as well as the corresponding b-wave/a-wave amplitude ratio (b/a ratio) (D) (right). Boxes indicate the 25% and 75% quantile range and whiskers indicate the 5% and 95% quantiles, and the intersection of line and error bars indicates the median of the data (box-and-whisker plot). * $p < 0.05$, ** $p < 0.01$, *** $p < 0.001$, **** $p < 0.0001$.

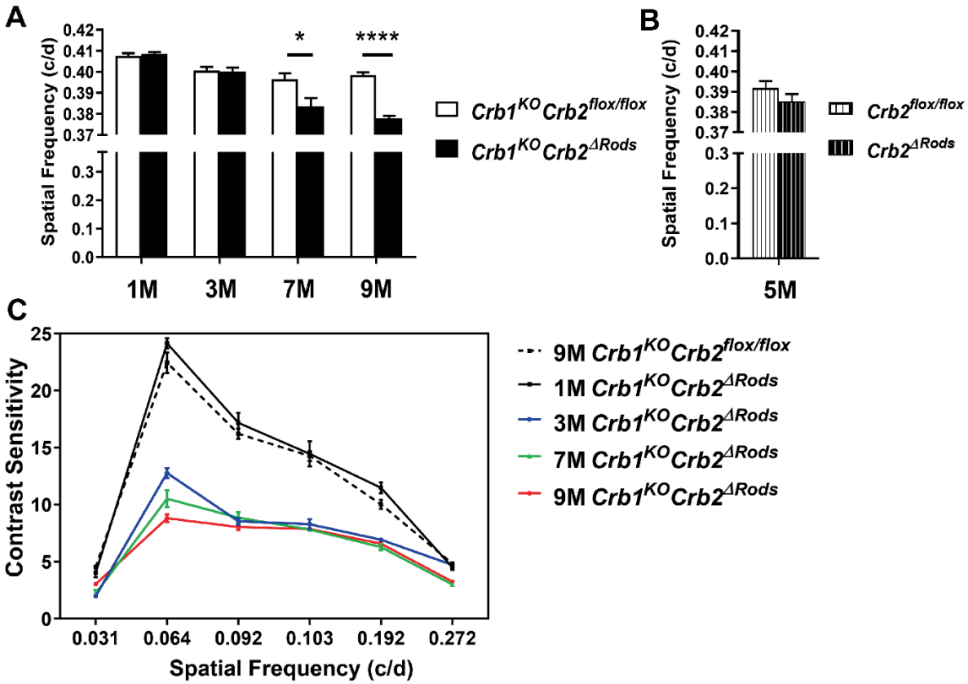


Figure 2: Visual acuity and contrast sensitivity are impaired in *Crb1^{KO}Crb2^{ΔRods}* mice. Spatial frequency thresholds (A,B) in cycles per degree (c/d) and contrast sensitivity (C) at different time points (1-month of age (1M), 3M, 5M, 7M, and 9M). Spatial frequency thresholds were reduced om 7- and 9-month-old *Crb1^{KO}Crb2^{ΔRods}* mice compared to the littermates and age-matched controls (*Crb1^{KO}Crb2^{fllox/fllox}*), at $p = 0.0274$ and $p < 0.001$, respectively (A). No differences were observed between *Crb2^{fllox/fllox}* and *Crb2^{ΔRods}* mice at 5M (B). *Crb1^{KO}Crb2^{ΔRods}* mice showed reduced contrast sensitivity compared to the littermates, and age matched controls (*Crb1^{KO}Crb2^{fllox/fllox}*) at 3-, 7-, and 9-months-of-age (C). Contrast sensitivity at: 3M (spatial frequencies: 0.031, $p = 0.7959$ (statistically non-significant); 0.064, $p < 0.0001$; 0.092, $p < 0.0001$; 0.103, $p < 0.0001$; 0.192, $p < 0.0001$; 0.272, $p = 0.0006$); 7M (spatial frequencies: 0.031, $p = 0.0121$; 0.064, $p = 0.0003$; 0.092, $p < 0.0001$; 0.103, $p = 0.004$; 0.192, $p = 0.0006$; 0.272, p

= 0.0448); and 9M (spatial frequencies: 0.031, $p < 0.0001$; 0.064, $p < 0.0001$; 0.092, $p = 0.0002$; 0.103, $p < 0.0001$; 0.192, $p < 0.0001$; 0.272, $p < 0.0001$). Error bars indicate \pm SEM, * $p < 0.05$, **** $p < 0.0001$.

observed in the $Crb1^{KO}Crb2^{\Delta Rods}$ is due to cumulative loss of CRB1 and CRB2 and not to single loss of CRB2 or due to toxicity of *iCre* expression in rod photoreceptors.

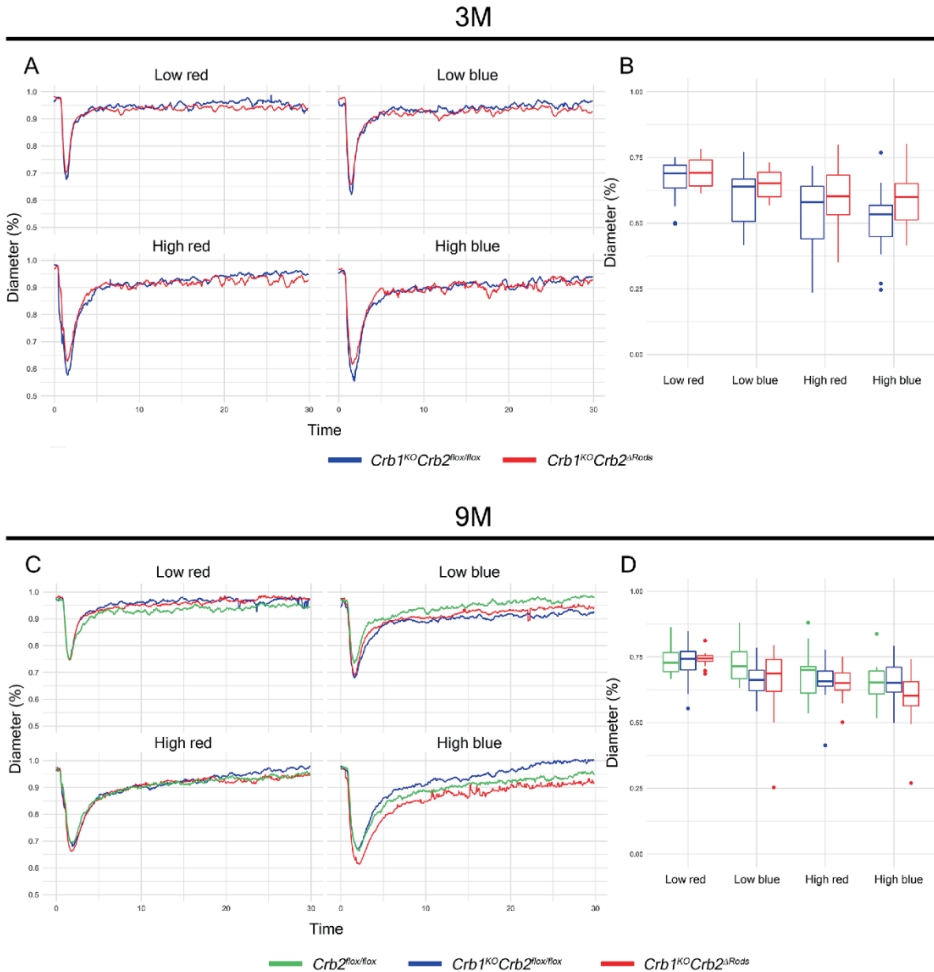
Pupil light reflex is not impaired in $Crb1^{KO}Crb2^{\Delta Rods}$ mice

To assess if pupil light reflex was affected in $Crb1^{KO}Crb2^{\Delta Rods}$ mice, we characterized the pupil response to blue and red light stimuli in dark-adapted, light-anesthetized 3- and 9-month-old $Crb1^{KO}Crb2^{\Delta Rods}$ and in control mice. Pupil response curves, contraction, and dilation after each stimulus were identical in all the experimental groups (Figure 3A, C). No differences in the maximal pupil contraction were observed between mutant and control(s) mice at any condition analysed (Figure 3B, D). These results suggest that pupil light reflex was not affected in the $Crb1^{KO}Crb2^{\Delta Rods}$ mice.

Loss of CRB2 in rods results in slow loss of photoreceptor cells, mainly in the superior retina

To study if CRB2 specific ablation in rod photoreceptors results in a morphological phenotype, histological analysis of retina sections was performed. All retinal layers were present and displayed normal organization in the $Crb2^{\Delta Rods}$ and $Crb1^{KO}Crb2^{\Delta Rods}$ mice at 1-month-of-age, suggesting that removal of CRB2 from rod photoreceptors did not affect retinal development and lamination. No morphological abnormalities were observed in the control mice ($Crb2^{flox/flox}$) (Figure 4A, A') and in the $Crb2^{\Delta Rods}$ (Figure 4B, B'), while in the $Crb1^{KO}Crb2^{\Delta Rods}$ (Figure 4C, C'; arrows), small disruptions of the outer limiting membrane were observed throughout the entire retina. Three-month-of-age retinas from control mice ($Crb2^{flox/flox}$) (Figure 4D, D') and in the $Crb2^{\Delta Rods}$ (Figure 4E, E') showed normal morphology. Ingression of photoreceptor nuclei into the inner retinal layer was frequently detected in the inferior central retina of $Crb1^{KO}Crb2^{\Delta Rods}$, as also observed in the control littermate $Crb1^{KO}Crb2^{flox/flox}$ retinas [6,15,19] (data not shown). In $Crb1^{KO}Crb2^{\Delta Rods}$, disruptions at the outer limiting membrane of the central superior retina were also observed (Figure 4F, F'; arrow). In some 3-month-old and in

all 6-month-old *Crb2*^{ΔRods} (Figure 4H, H'; arrows) and *Crb1*^{KO}*Crb2*^{ΔRods} (Figure 4F, F'; arrows) retinas, the photoreceptor layer was severely thinned at the peripheral superior area. In 9- and 12-month-old *Crb2*^{ΔRods} and *Crb1*^{KO}*Crb2*^{ΔRods}, further thinning of the outer nuclear layer was observed in the peripheral as well as central superior retina (Figure 5B, B', C, C', E, E', E'', F, F', F'').



log*lux; low blue, 0.6 log*lux; high red, 4.5 log*lux; high blue, 2.0 log*lux. X-axis: time in seconds; Y-axis: average of pupil diameter (in %) relative to baseline diameter determined from 500 ms before each stimulus (A,C). Maximal pupil contraction (B,D), boxes indicate the 25 and 75% quantile range and whiskers indicate the 5% and 95% quantiles, and the intersection of line and error bars indicates the median of the data (box-and-whisker plot).

To assess and better visualize the photoreceptor cell loss over time, the number of nuclei in rows of photoreceptors was quantified. The number of photoreceptor nuclei in a row was reduced in the entire superior retina and the inferior retina near to the optic nerve head in 6-month-old *Crb1^{KO}Crb2^{ΔRods}* compared to the *Crb2^{flx/flx}* control (Figure 5G). At 9-months-of-age, the number of photoreceptors in a row were further decreased in almost the entire superior retina and in most of the inferior retina of *Crb1^{KO}Crb2^{ΔRods}* (Figure 5H). Also at this time point, the superior retina (Figure 5H) and some areas of the inferior retina of *Crb2^{ΔRods}* mice became thinner. Twelve-month-old retinas showed almost no photoreceptor nuclei in the far peripheral superior and nearly half in the central superior retina of *Crb2^{ΔRods}* and *Crb1^{KO}Crb2^{ΔRods}*. At this time also, the inferior retina of *Crb2^{ΔRods}* and *Crb1^{KO}Crb2^{ΔRods}* mice became thinner compared to the *Crb2^{flx/flx}* control (Figure 5I).

Removal of CRB2 in rods results in loss of rods mainly at the periphery of the superior retina

The morphological phenotype observed in the *Crb2^{ΔRods}* and *Crb1^{KO}Crb2^{ΔRods}* retinas mainly affected the photoreceptor cells. In the far peripheral superior retinas of 9 month-old *Crb2^{flx/flx}* control mice, the photoreceptor cells stained positive for recoverin (Figure 6A). In the far periphery of the superior retinas of *Crb2^{ΔRods}* (Figure 6B) and *Crb1^{KO}Crb2^{ΔRods}* (Figure 6C), no photoreceptors were found. Towards the central superior retina, reduced numbers of recoverin-positive cells were detected, depicting thinning of the outer nuclear layer. Although the number of photoreceptors was reduced, the remaining photoreceptors showed matured inner- and outer-segments. Rhodopsin is normally located in the outer-segments of mature rod photoreceptor cells (Figure 6D). In areas that showed reduced numbers of photoreceptors in *Crb2^{ΔRods}* and

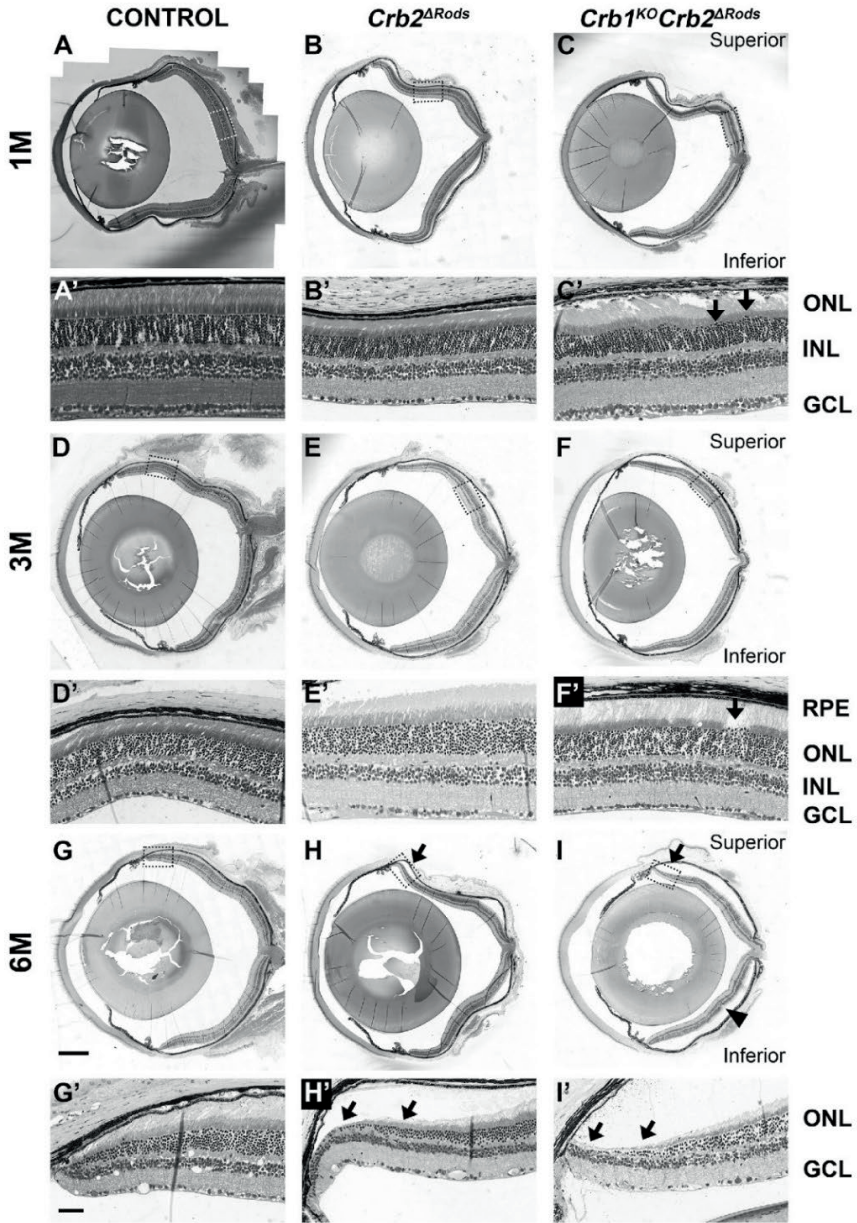


Figure 4: Loss of *Crb2* from rod photoreceptors leads to loss of photoreceptor cells, mainly in the peripheral and central superior retina. Toluidine-stained light microscopy showing retinal stitches from control (*Crb2*^{fl_{ox}/fl_{ox}) (A,D,G), *Crb2*^{ΔRods} (B,E,H) and *Crb1*^{KO}*Crb2*^{ΔRods} (C,F,I), and insets from control (*Crb2*^{fl_{ox}/fl_{ox}) (A',D',G'), *Crb2*^{ΔRods} (B',E',H'), and *Crb1*^{KO}*Crb2*^{ΔRods} (C',F',I') at different ages: (A–C) 1M; (D–F) 3M; (G–I) 6M. No abnormalities}}

were observed in the control retina. In the *Crb2*^{ΔRods} and *Crb1*^{KO}*Crb2*^{ΔRods} mice, all the retinal layers were formed and properly laminated. At 3-months-of-age, sporadic disruptions of the outer limiting membrane were found in the *Crb1*^{KO}*Crb2*^{ΔRods} in the superior retina (F,F'; arrow). The characteristic *Crb1*^{KO} phenotype, with photoreceptor dysplasia specifically in the inferior temporal retina, was also frequently observed in the inferior retina (I; arrowhead). At 6M, loss of photoreceptor cells was observed at the superior peripheral retina in both *Crb2*^{ΔRods} (H,H'; arrows) and *Crb1*^{KO}*Crb2*^{ΔRods} (I,I'; arrows) mice. Note: GCL = ganglion cell layer; INL = inner nuclear layer; ONL = outer nuclear layer; RPE = retina pigment epithelium. Scale bars: 500 μm; insets: 50 μm.

Crb1^{KO}*Crb2*^{ΔRods} retina, rhodopsin was localized in the outer segments, suggesting that the remaining rods were functional (Figure 6E, F). Cone photoreceptors can be labelled using an antibody against cone arrestin (CAR) (Figure 6D). In both knockout lines, cone photoreceptors showed normal morphology (Figure 6E, F). In the control retinas, peanut-agglutinin (PNA) stained the cone photoreceptor outer-segments and pedicles at the photoreceptor synapses (Figure 6G). PNA staining was similar in 9-month-old *Crb2*^{ΔRods} (Figure 6H) and *Crb1*^{KO}*Crb2*^{ΔRods} retinas (Figure 6I). The M-cone photoreceptor outer-segments were stained appropriately with M-opsin antibodies in the control retinas (Figure 6G) and in both mutant retinas (Figure 6H, I).

Photoreceptor cell synapses can be stained with MPP4. In the control retinas, MPP4 signal was detected in the photoreceptor synapses at the outer plexiform layer (Figure 6J, J'). In *Crb2*^{ΔRods} and *Crb1*^{KO}*Crb2*^{ΔRods} retinas, MPP4 staining was disrupted and decreased; some ectopic anti-MPP4 labelling was also detected in the outer nuclear layer (Figure 6K, K', L, L'). Protein kinase (PKC) α is abundant in retinal bipolar cells. In the control retinas, bipolar cells located at the inner nuclear layer and presented normal dendritic arborization in the outer plexiform layer (Figure 6J, J'). In the knockout retinas, bipolar cells were localized at the correct layer, but their dendritic arborization was affected (Figure 6K, K', L, L'; arrowheads).

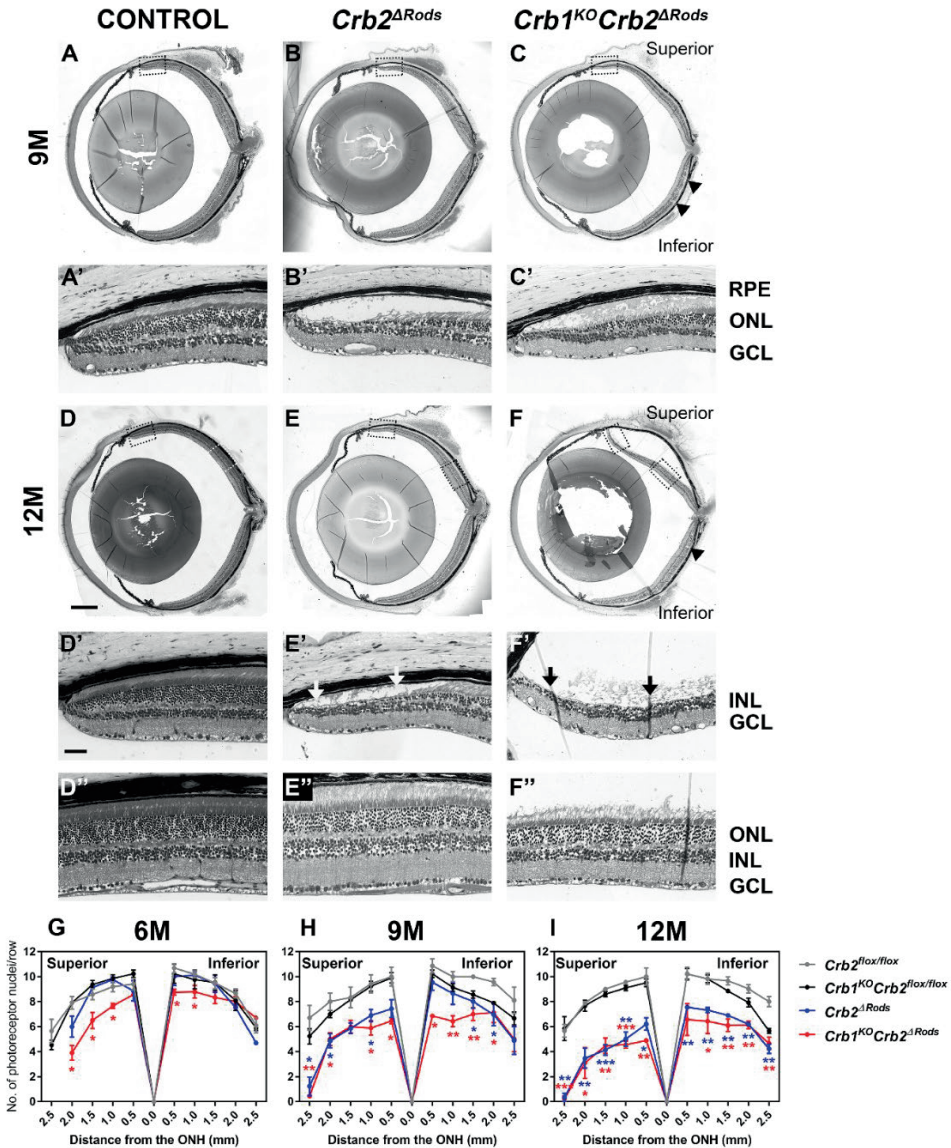


Figure 5: Aged *Crb2*^{ΔRods} and *Crb1*^{KO}*Crb2*^{ΔRods} show loss of photoreceptors in the entire retina. Toluidine-stained light microscopy showing retinal stitches from control (*Crb2*^{flx/flx}) (A,D), *Crb2*^{ΔRods} (B,E) and *Crb1*^{KO}*Crb2*^{ΔRods} (C,F) at different ages: (A–C) 9M; (D–F) 12M. The peripheral superior retina is depicted (D',E',F'); the central superior retina is depicted (D'',E'',F''). No abnormalities were observed in the control retina. At 9- and 12-months-of-age, loss of photoreceptor cells was observed, mainly in the superior peripheral retina of both *Crb2*^{ΔRods} and *Crb1*^{KO}*Crb2*^{ΔRods} mice (B,C,E,F). The characteristic *Crb1*^{KO} phenotype, with photoreceptor dysplasia specifically in the inferior temporal retina, was also frequently observed

in the inferior retina of *Crb1^{KO}Crb2^{ΔRods}* (C,F; arrowheads). Spidergram depicting the quantification of number of photoreceptor cell nuclei in a row in *Crb2^{fllox/fllox}* (grey), *Crb1^{KO}Crb2^{fllox/fllox}* (black), *Crb2^{ΔRods}* (blue), and *Crb1^{KO}Crb2^{ΔRods}* (red) at 6M (G), 9M (H), and 12M (I). A reduction in the number of photoreceptor nuclei in *Crb1^{KO}Crb2^{ΔRods}* retinas were observed from 6M in the superior peripheral retina (G). At 9M and 12M, the photoreceptor number further decreases in the superior central retina in both knockout lines (H,I). At 12M, the inferior retina also had a reduced number of photoreceptors (I). Data are presented as mean ± SEM; n = 3–4 mice, per genotype/time point. Note: GCL = ganglion cell layer; INL = inner nuclear layer; ONL = outer nuclear layer; RPE = retina pigment epithelium. Scale bars: 500 μm; insets: 50 μm. * p < 0.05, ** p < 0.01, *** p < 0.001.

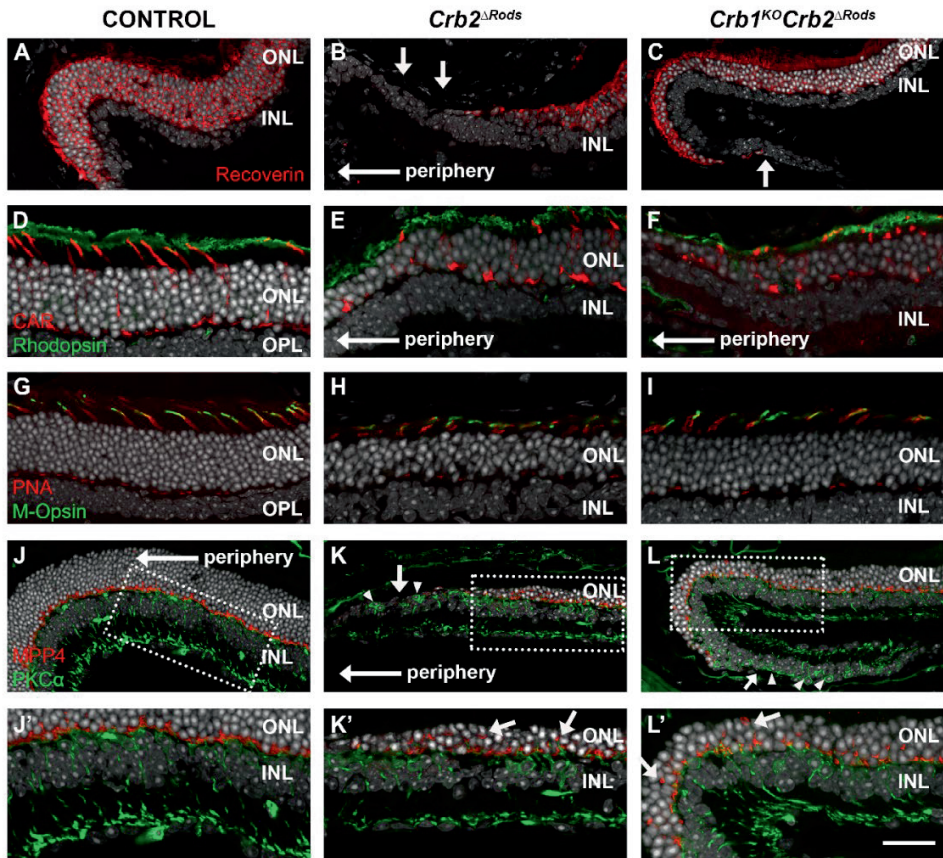


Figure 6: *Crb2^{ΔRods}* and *Crb1^{KO}Crb2^{ΔRods}* mice show loss of rod photoreceptor cells. Immunohistochemistry pictures from control (A,D,G,J), *Crb2^{ΔRods}* (B,E,H,K), and *Crb1^{KO}Crb2^{ΔRods}* (C,F,I,L) 9 month-old retinal sections stained for: recoverin (A–C), rhodopsin and cone arrestin (CAR) (D–F), peanut agglutinin (PNA) and M-opsin (G–I), MPP4 and PKCα (J–L, J'–L'). At 9-months-of-age, the number of photoreceptor cells marked by recoverin was

reduced in the *Crb2*^{ΔRods} (C) and *Crb1*^{KO}*Crb2*^{ΔRods} (D) compared to the control (A). Although the number of photoreceptors was reduced, in both mutant lines, rhodopsin was properly located in the outer-segments from rod photoreceptors (E,F). Cone photoreceptors stained with cone arresting (CAR), and with peanut agglutinin (PNA, outer segments and pedicles) and M-opsin were present in the mutant retinas and showed normal morphology (E,F,H,I; respectively). Photoreceptor synapses stained with MPP4 were lost and ectopically located in *Crb2*^{ΔRods} (K'; arrows) and *Crb1*^{KO}*Crb2*^{ΔRods} (L'; arrows); dendritic arborization of PKC α -positive cells was also affected in the mutant retinas (K,L; arrowheads). Note: INL = inner nuclear layer; ONL = outer nuclear layer; OPL = outer plexiform layer. Scale bars: (A–C) 50 μ m; (D–L) 25 μ m.

Loss of CRB2 in rods leads to disruption of the apical protein complexes

2

We previously reported that ablation of CRB2 from both immature cone and rod photoreceptor cells resulted in disruption of the apical protein complexes at the outer limiting membrane [16]. Here, we studied if removal of CRB2 specifically in rod photoreceptors is enough to lead to destabilization of the subapical region and adherens junction protein complexes at the outer limiting membrane using transmission electron microscopy and immunohistochemistry.

Using transmission electron microscopy, we showed that the structures of adherens junctions at the outer limiting membrane adjacent to photoreceptor cell nuclei were normal in retinas of 8 month-old control mice (Figure 7A, arrows; Figure 7A'), while the adherens junctions in the *Crb1*^{KO}*Crb2*^{ΔRods} mice were moderately disrupted throughout the retina (Figure 7B; arrows). Photoreceptor cell nuclei protruding the inner-/outer-segment layer were observed at sites of adherens junction disruption (Figure 7B'; blue line). In the central retina, there were more MGC apical villi visible in the *Crb1*^{KO}*Crb2*^{ΔRods} retina compared to the control retina (Figure 7C,D; asterisk). At the peripheral control retina, the MGC apical villi extend among the photoreceptor inner segments (Figure 7E; asterisk), whereas in the peripheral *Crb1*^{KO}*Crb2*^{ΔRods} retina, at regions with a diminished number of inner and outer segments, the MGC apical villi collapsed due to lack of support (Figure 7F; asterisk).

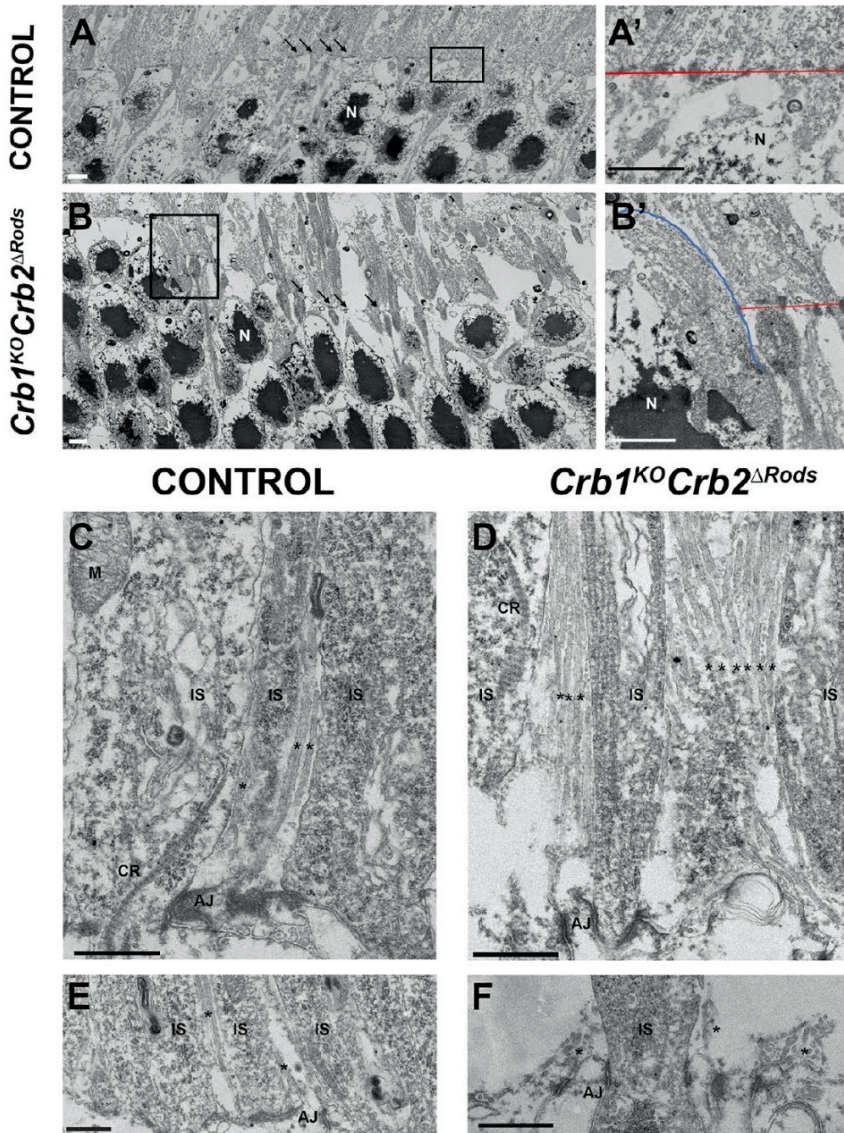


Figure 7: *Crb1*^{KO}*Crb2*^{ΔRods} retinas present disruptions in adherens junctions and MGC apical villi. Transmission electron microscopy pictures from control (*Crb2*^{flox/flox} (A,C,E) and *Crb1*^{KO}*Crb2*^{ΔRods} (B,D,F)) in 8-month-old retinal sections. The adherens junctions were present at the outer limiting membrane in the control (A,A'; arrows, red line), but they were disorganized in the *Crb1*^{KO}*Crb2*^{ΔRods} retina (B,B'; arrows, red line). Photoreceptor cell nuclei protruding from the inner-/outer-segment layers (B'; blue line). In the central retina, an increased number of

visible MGC apical villi were detected in *Crb1^{KO}Crb2^{Δrods}* compared to control retina (C,D; asterisk). In the peripheral retina, MGC apical villi were normally organized in the control retina (E; asterisk), while in *Crb1^{KO}Crb2^{Δrods}*, the MGC apical villi were collapsed (F; asterisk). Note: AJ = adherens junctions; CR = ciliary rootlets; IS = inner segments; N = nuclei; M = mitochondria; MGC = Müller glial cell. Scale bars: (A–F) 1 μ m.

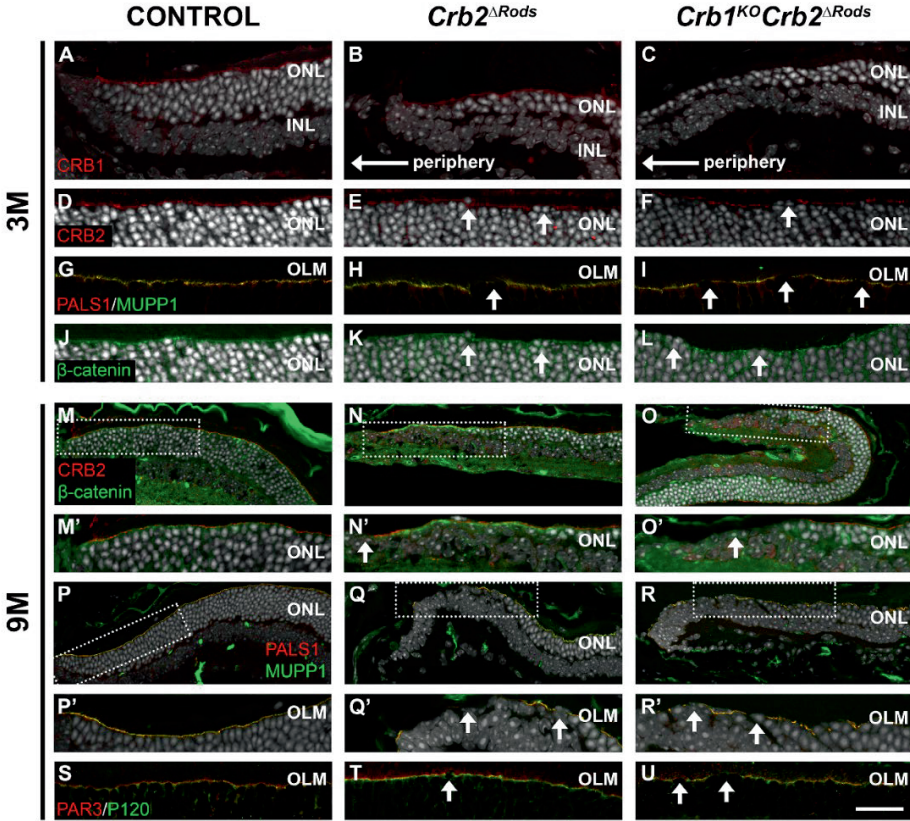


Figure 8: Specific ablation of *Crb2* from rod photoreceptors to disruptions at the subapical region and at the adherens junctions. Immunohistochemistry pictures from control (*Crb2^{fllox/fllox}*) (A,D,G,J,M,P,S), *Crb2^{Δrods}* (B,E,H,K,N,Q,T), and *Crb1^{KO}Crb2^{Δrods}* (C,F,I,L,O,R,U) at different time points: 3-months-of-age (A–L) and 9-months-of-age (M–U). Retinal sections were stained for: CRB1 (A–C), CRB2 (D–F), PALS1 and MUPP1 (G–I), -catenin (J–L), CRB2 and -catenin (M–O), PALS1 and MUPP1 (P–R), and PAR3 and P120-catenin (J–L). At 3-months-of-age, CRB1 protein was present at the subapical region above the adherens junctions in control (A) and *Crb2^{Δrods}* (B), however was absent in *Crb1^{KO}Crb2^{Δrods}* (C). CRB2 is still detected at the subapical region of *Crb2^{Δrods}* (E) and *Crb1^{KO}Crb2^{Δrods}* (F), due to the presence of CRB2 protein in MGCs and cone photoreceptor cells. However, disruptions of the subapical region were detected (E,F; arrows), mainly in the superior central retina. PALS1

and MUPP1 (H,I; arrows) were also lost at sites of disruption. Staining using the adherens junctions marker β -catenin showed disruption of the adherens junctions (K,L; arrows). Nine-month-old knockout retinas showed disruption of subapical region marker and of the adherens junctions at the superior peripheral retina (N,N',O,O',Q,Q',R,R') and superior central retina (T,U). Note: OLM = outer limiting membrane; INL = inner nuclear layer; ONL = outer nuclear layer. Scale bars: (A–C, M–O, P–R) 50 μ m; (D–L, M'–O', P'–R', S–U) 25 μ m.

At 3-months-of-age, CRB1 protein was present at the subapical region above the adherens junctions in the control (Figure 8A; arrows) and *Crb2* ^{Δ Rods} (Figure 8B; arrows) in the superior peripheral retina. In *Crb1*^{KO}*Crb2* ^{Δ Rods}, the CRB1 protein was absent, as previously found in *Crb1*^{KO} (Figure 8C). CRB2 localized at the subapical region in the control retinas (Figure 8D) and in the central superior retina of *Crb2* ^{Δ Rods} (Figure 8E) and *Crb1*^{KO}*Crb2* ^{Δ Rods} (Figure 8F). Other subapical region markers and members of the Crumbs complex, such as PALS1 and MUPP1, were correctly located at the subapical region in the control retina (Figure 8G). However, mutant retinas showed disruptions of the subapical region, labelled by CRB2, PALS1, and MUPP1 (Figure 8E, F, H, I; arrows). In the control retinas, β -catenin showed correct localization of the adherens junction (Figure 8J), while in both mutant retinas, disruptions of the adherens junctions in the central superior retina were observed (Figure 8K, L). Photoreceptor cell nuclei protruding from the inner-/outer-segment layer were observed at the site of disruption (Figure 8 arrows). In the 9-month-old control retina, CRB2 correctly localized at the subapical region just above the adherens junction marker, β -catenin (Figure 8M, M'). Also, PALS1 and MUPP1 were correctly located at the subapical region in the control retina (Figure 8P, P'). However, at the peripheral superior retina of *Crb2* ^{Δ Rods} and *Crb1*^{KO}*Crb2* ^{Δ Rods} mice, partial disruptions of the subapical region were observed (Figure 8N, N', O, O', Q, Q', R, R'), whereas adherens junctions were mainly lost in areas with loss of all photoreceptors (Figure 8N, N', O, O'). PAR3, a member of the PAR complex, and p120-catenin, an adherens junction protein, were lost at sites of disruption of the outer limiting membrane in the central superior retina (Figure 8T, U; arrows).

Removal of CRB2 from rods results in gliosis in müller glial cells

2

Müller glial cells extend throughout the entire retina and function to maintain retinal homeostasis and integrity [30]. To study the effect of CRB2 removal from rod photoreceptor cells on the morphology of MGCs, we labelled these cells with glutamine synthetase (GS), SOX9, CD44, and glial fibrillary acidic protein expression (GFAP) antibodies. In 9 month-old control retinas, MGCs stained with glutamine synthetase displayed radial alignment, with well-established apical ends (Figure 9A, A') and nuclei (SOX9-positive) located in the inner nuclear layer (Figure 9A, A'). In *Crb2*^{ΔRods} and *Crb1*^{KO}*Crb2*^{ΔRods} retinas, the radial alignment of MGCs was disturbed and SOX9-positive nuclei were located most apically (Figure 9B, B', C, C'; arrows). CD44 is highly expressed in MGC apical villi (Figure 9D, D'). In the peripheral superior knockout retinas, the radial structure of MGC apical villi was lost (Figure 9E, E', F, F'). GFAP is a marker for intermediate filaments in MGCs (Figure 9G, J, M), and an increase in GFAP occurs in gliosis. Knockout retinas showed an upregulation of GFAP in MGCs (Figure 9H, I, K, L, N, O). Increased GFAP levels were more pronounced in the peripheral (Figure 9H, I) and central (Figure 9K, L) superior retina. A moderate increase in GFAP levels was also observed in the inferior retina of *Crb2*^{ΔRods} and *Crb1*^{KO}*Crb2*^{ΔRods} (Figure 9N, O).

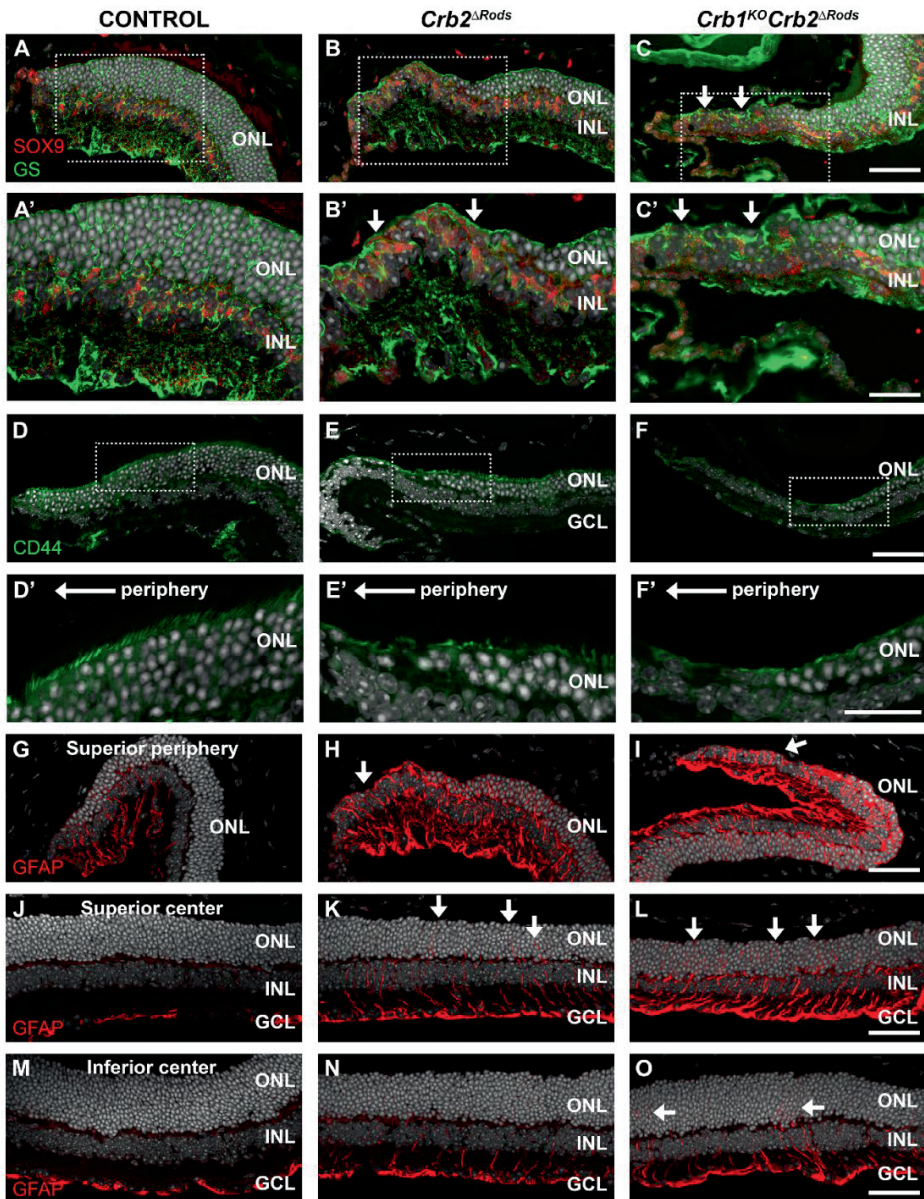


Figure 9: Loss of *Crb2* from rod photoreceptors leads to gliosis mainly in the peripheral superior retina. Immunohistochemistry pictures from 9-month-old control (*Crb2*^{fl^{ox}/fl^{ox}) (A,D,G,J,M), *Crb2*^{ΔRods} (B,E,H,K,N), and *Crb1*^{KO}*Crb2*^{ΔRods} (C,F,I,L,O) retina. Retinal sections were stained with antibodies against: SOX9 and glutamine synthetase (GS) (A–C), CD44 (D–F), and glial fibrillary acidic protein (GFAP) (G–O). Müller glial cells stained with GS showed the}

expected radial alignment (A,A'). Müller glial cell morphology was affected mainly in the superior peripheral retina of the mutant retinas (B,B',C,C'; arrows). CD44-positivemicrovilli of Müller glial cells were displaced in the *Crb2*^{Δrods} and *Crb1*^{KO}*Crb2*^{Δrods} peripheral superior retinas (E,E',F,F'), specifically where photoreceptors were lost. *Crb2*^{Δrods} and *Crb1*^{KO}*Crb2*^{Δrods} retinas showed activated Müller glial cells, detected by an increased level of GFAP, mainly in the peripheral superior retina (H,I) and in the central superior retina (K,L), with a moderately increased level of GFAP in the inferior central retina (N,O). Note: GCL = ganglion cell layer; INL = inner nuclear layer; ONL = outer nuclear layer. Scale bars: (A–C, D–F, G–O) 50 μm; (A'–C', D'–F') 25 μm.

Discussion

2

Here, we studied the effect of CRB2 removal specifically from rod photoreceptors in the mouse retina. Furthermore, we evaluated the consequences of concomitant loss of CRB1. Our key findings are: (i) loss of CRB2 from rod photoreceptors results in retinitis pigmentosa, mainly at the peripheral and central superior retina; (ii) CRB2 in rod photoreceptor cells is required to maintain the rod photoreceptor layer and retinal electrical responses; (iii) loss of CRB2 in rods and concomitant loss of CRB1 leads to an exacerbation of the retinitis pigmentosa phenotype; (iv) ablation of CRB2 from rods with concomitant loss of CRB1 results in visual function impairment.

During retinogenesis, mouse CRB2 is located in retinal radial progenitor cells [4]. In the mature retina, the protein is found in rod and cone photoreceptors and in MGCs [7]. We previously demonstrated that retinal development and lamination is affected from embryonic day 15.5, when CRB2 is removed from both immature rod and cone photoreceptors. These *Crb2*^{ΔimmPRC} mouse retinas mimicked a very early-onset retinitis pigmentosa (Supplemental Figure 5A) [16]. The *Crb2*^{ΔimmPRC} mouse retinas showed progressive thinning of the photoreceptor layer and mislocalization of retinal cells, which resulted in a severe retinal function impairment, as measured by electroretinography. Moreover, concomitant loss of CRB1 in *Crb1*^{KO}*Crb2*^{ΔimmPRC} retinas exacerbated the retinal phenotype and resulted in an LCA phenotype with thickened superior retina due to abnormal lamination of photoreceptors, intermingled photoreceptor and inner nuclear cell nuclei, and ectopic photoreceptor nuclei in the ganglion cell layer [21].

The *Crb1^{KO}Crb2^{ΔRods}* retinas described here showed moderate decrease in retinal function and a significant decrease in contrast sensitivity shortly after the onset of morphological retinal degeneration at 3-months-of-age (Supplemental Figure 5A). In these mice, specific ablation of CRB2 from rod photoreceptors was achieved by crossing *Crb2^{fllox/fllox}* mice with Rho-*iCre* transgenic mice that express *iCre* in rod photoreceptors from postnatal day 7, achieving expression in nearly all rods at postnatal day 20 [26]. The onset of CRE expression after retinogenesis might explain the moderate retinal phenotype observed in the *Crb2^{ΔRods}* and *Crb1^{KO}Crb2^{ΔRods}* mice when compared to mice with Cre-mediated ablation in retinal progenitor cells (*Crb2^{ΔRPC}*) or mice with Cre-mediated ablation in immature cone and rod photoreceptor cells (*Crb2^{ΔimmPRC}*). We previously demonstrated that short-term depletion of CRB2 from adult retinas using adeno-associated viral delivery of Cre or shRNA against *Crb2* leads to sporadic disruptions at foci of the outer limiting membrane, outer plexiform layer, and disruption of adhesion between photoreceptor cells [16]. This, together with the current data reported here, suggests that CRB2 has a function in the regulation of cellular adhesion between rod photoreceptors. Several CRB1-disease mouse models showed a gradient in phenotype severity. The entire retina is affected in *Crb2^{ΔRPC}* mice lacking CRB2 from retinal progenitors, MGCs, and photoreceptor cells, or *Crb2^{ΔimmPRC}* mice lacking CRB2 from the immature rod and cone photoreceptors [4,16]. In *Crb1^{KO}* retinas lacking CRB1 in retinal progenitors and MGCs, the phenotype is mainly located in the inferior temporal quadrant [6,15]. *Crb1^{KO}Crb2^{ΔimmPRC}* retinas lacking CRB1 and CRB2 from immature photoreceptors showed retinal dystrophy by fusion of the inner and outer nuclear layer throughout the retina. However, larger regions of ectopic photoreceptor cells were observed in the superior retina [21]. The *Crb2^{ΔRods}* and *Crb1^{KO}Crb2^{ΔRods}* mice reported here presented a retinal phenotype mainly affecting the peripheral and central superior retina. The differences observed in the different mouse *CRB1*-models might be related to the higher levels of CRB2 at the subapical region in the inferior retina, whereas CRB1 is expressed at higher levels in the superior retina [20]. Several other genes were found to be enriched in the superior retina, amongst these the photoreceptor gene endothelin 2 (*Edn2*) and the MGC genes ceruloplasmin and glial fibrillary acidic protein (GFAP) [31]. In the *Crb2^{ΔRods}* and *Crb1^{KO}Crb2^{ΔRods}*

2

mice, GFAP expression was upregulated in the superior retina, with structural changes in the subapical villi of MGC, which suggests the contribution of MGCs to the phenotype observed. Retinal function mediates visual perception, but also other vision-linked reflexes, such as the pupillary light reflex [32–34]. Previously, Kostic et al. demonstrated that low-intensity red or blue light stimulus was a good parameter to discriminate rod photoreceptor contribution for the pupil response, while the recovery time after high-intensity blue stimulus was a predictor cone contribution to the pupillary light reflex [33]. Here, we used a vision-linked reflex, the pupillary light reflex, as a retina/vision functional outcome. *Crb1*^{KO}*Crb2*^{ΔRods} mice showed a strong reduction in contrast sensitivity from 3-months-of-age onwards, which was not observed in *Crb2*^{ΔRods} mice, and a small decrease in spatial frequency from 7-months-of-age onwards, while the control *Crb1*^{KO}*Crb2*^{fllox/fllox} mice did not show a reduction at 9-months-of-age. To our knowledge, this is the first report of loss of visual function as measured by OKT in a *CRB1*-retinal disease model. The data suggest that visual contrast sensitivity might be a diagnostically accurate and practical test to detect early visual deficit in *Crb1*^{KO}*Crb2*^{ΔRods} mice. Moreover, contrast sensitivity tests might potentially be suitable for clinical studies testing candidate medicines for patients with mutations in the *CRB1* gene. The correlation between photoreceptor degeneration and OKT contrast sensitivity in different mouse models are poorly described in the literature. However, some studies used different rhodopsin mutant rat strains and demonstrated that OKT spatial frequency and contrast sensitivity did not decline until very late in the photoreceptor degeneration [35,36]. Furthermore, studies performed in mice carrying a missense point mutation in *Pde6b* (rd10), which are almost deprived of photoreceptor cells at 1-month-of-age, still presented residual spatial frequency responses at 2-months-of-age [37].

Here, we propose that loss of CRB2 leads to loss of rod-cone and rod-MGC adhesion; as a result adherens junctions are disrupted and the cytoarchitecture of the outer nuclear layer is compromised, giving rise to misplaced rod photoreceptor cells. We speculate that misplaced or “loose” rods preferentially degenerate and die or are phagocytosed by activated microglial cells. Microglia cell activation will contribute to MGC reactive gliosis, characterized by increased GFAP levels and hypertrophy, by secreting pro-

inflammatory mediators. We further speculate that the reactive MGCs from *Crb1^{KO}Crb2^{ΔRods}* and *Crb2^{ΔRods}* mice present a proliferation of fibrous processes and deposition of proteoglycans at the outer edge of the retina, inhibiting axonal regeneration and exacerbating the loss of rods (Supplemental Figure 5) [38]. Moreover, the clear deficit of contrast sensitivity may allow us to have a rigorous outcome parameter to measure functional vision gain or maintenance after AAV treatment. Therefore, *Crb1^{KO}Crb2^{ΔRods}* mice might become important resources to test therapies for retinopathies due to mutations in the *CRB1* gene.

In conclusion, we found that (i) loss of CRB2 from rod photoreceptors results in retinitis pigmentosa, mainly at the peripheral and central superior retina; (ii) CRB2 in rod photoreceptor cells is required to maintain the rod photoreceptor layer and retinal electrical responses; (iii) loss of CRB2 in rods and concomitant loss of CRB1 leads to an exacerbation of the retinitis pigmentosa phenotype; (iv) ablation of CRB2 from rods with concomitant loss of CRB1 results in visual function impairment. This clear deficit of contrast sensitivity may allow us to have a rigorous outcome parameter to measure functional vision gain or maintenance after AAV treatment. Therefore, *Crb1^{KO}Crb2^{ΔRods}* mice might become important resources to test therapies for retinopathies due to mutations in the *CRB1* gene.

Experimental procedures

Animals

All procedures concerning animals were carried out in accordance with the E.U. Directive 2010/63/EU for animal experiments and with permission from the Dutch Central Authority for Scientific Procedures on Animals (CCD), permit number 1160020172924. All mice used were maintained with a 99.9% C57BL/6J genetic background. Animals were kept in a 12 hours day/night cycle and supplied with food and water ad libitum. Mice did not have *rd8* or *pde6b* mutations.

Crb2 conditional knockout (*Crb2^{fllox/fllox}*) mice [4,18] were crossed with the Rho-*iCre* (B6;SjL-Pde6b+Tg(Rho-*iCre*)1Ck/Boc) [26] transgenic mouse line, obtained from

Jackson laboratory (IMSR Cat# JAX:015850, RRID: IMSR_JAX:015850), to specifically remove *Crb2* from rod photoreceptor cells (*Crb2*^{fl^{ox}/fl^{ox}}/Rho-iCre^{+/-}, mentioned as *Crb2*^{ΔRods}). *Crb2*^{ΔRods} were crossed with *Crb1* knockout (*Crb1*^{KO}) mice [6] to generate *Crb1*^{-/-}*Crb2*^{fl^{ox}/fl^{ox}}/Rho-iCre^{+/-} (*Crb1*^{KO}*Crb2*^{ΔRods}). Littermate age-matched *Crb2*^{fl^{ox}/fl^{ox}}/fl^{ox} or *Crb1*^{KO}*Crb2*^{fl^{ox}/fl^{ox}} were used as control. R26R-EYFP (B6.129X1-Gt(ROSA)26Sortm1(EYFP)Cos/J) (IMSR Cat# JAX:006148, RRID:IMSR_JAX:006148) reporter mice [27] were crossed with *Crb2*^{ΔRods} to generate *Crb2*^{ΔRods} *EYFP*^{fl^{ox}-stop-fl^{ox}/+} (*Crb2*^{ΔRods}::*EYFP*) mice.

2

Chromosomal DNA isolation and genotyping

Chromosomal DNA was isolated from ear biopsies. The biopsies were incubated in lysis buffer (50 mM Tris pH 8.0, 100 mM NaCl, 1% SDS) with Proteinase K (0.5 mg/ml) at 55 °C for 16 h. Chromosomal DNA was precipitated with isopropanol, washed with 80% ethanol, and rehydrated in TE buffer. Genotyping of the *Crb1*KO and *Crb2*^{fl^{ox}/fl^{ox}} transgenic animals were performed as previously described [4,6]. The following primers were used to detect the transgenic *iCre* expression: FW 5'-TCAGTGCCTGGAGTTGCGCTGTGG-3' and RV 5'-CTTAAAGGCCAGGGCCTGCTTGGC-3' (product size 650 base-pairs). R26R-EYFP mice were genotyped used the following primers: wild-type allele FW 5'-CTGGCTTCTGAGACCG-3', RV 5'-CAGGACAACGCCACACA-3' (product size 142 base-pairs), and mutant allele FW 5'-AGGGCGAGGAGCTGTTCA-3', RV 5'-TGAAGTCGATGCCCTTCAG-3' (product size 384 base-pairs).

Electroretinography (ERG)

Dark- and light-adapted ERGs were performed under dim red light using an Espion E2 (Diagnosys, LLC, Lowell MA, USA). ERGs were performed on 1-month-old (1M), 3M, 6M, 9M, and 12M in *Crb2*^{ΔRods}, *Crb1*^{KO}*Crb2*^{ΔRods}, *Crb2*^{fl^{ox}/fl^{ox}}, and *Crb1*^{KO}*Crb2*^{fl^{ox}/fl^{ox}} mice. Mice were anesthetized using 100 mg/kg ketamine and 10 mg/kg xylazine administered intraperitoneally, and the pupils were dilated using tropicamide drops (5 mg/mL). Mice were placed on a temperature regulated heating pad and reference and ground platinum electrodes were placed subcutaneously in the

scalp and the base of the tail, respectively. ERGs were recorded from both eyes using gold wire electrodes. Hypromellose eye drops (3 mg/mL, Teva., The Netherlands) were given between recordings to prevent eyes from drying. Single (Scotopic and Photopic ERG) white (6500 k)-flashes were used. Band-pass filter frequencies were 0.3 and 300 Hz. Scotopic recordings were obtained from dark-adapted animals at the following light intensities: -4, -3, -2, -1, 0, 1, 1.5, 1.9 log cd·s/m². Photopic recordings were performed following 10 minutes light adaptation on a background light intensity of 30 cd·m² and the light intensity series used was: -2, -1, 0, 1, 1.5, 1.9 log cd·s/m² [39]. The following numbers of mice were used per time point: 1-month-old (1M): (*Crb2*^{flox/flox} *n* = 4, *Crbl*^{KO}*Crb2*^{flox/flox} *n* = 5, *Crb2*^{ΔRods} *n* = 5, and *Crbl*^{KO}*Crb2*^{ΔRods} *n* = 4); 3M: (*Crb2*^{flox/flox} *n* = 5, *Crbl*^{KO}*Crb2*^{flox/flox} *n* = 6, *Crb2*^{ΔRods} *n* = 5, and *Crbl*^{KO}*Crb2*^{ΔRods} *n* = 5); 6M: (*Crb2*^{flox/flox} *n* = 6, *Crbl*^{KO}*Crb2*^{flox/flox} *n* = 5, *Crb2*^{ΔRods} *n* = 7, and *Crbl*^{KO}*Crb2*^{ΔRods} *n* = 7); 9M: (*Crb2*^{flox/flox} *n* = 5, *Crbl*^{KO}*Crb2*^{flox/flox} *n* = 4, *Crb2*^{ΔRods} *n* = 5, and *Crbl*^{KO}*Crb2*^{ΔRods} *n* = 6); 12M: (*Crb2*^{flox/flox} *n* = 6, *Crb2*^{ΔRods} *n* = 6, *Crbl*^{KO}*Crb2*^{flox/flox} *n* = 6, and *Crbl*^{KO}*Crb2*^{ΔRods} *n* = 4). Statistical analysis of the ERG data was performed using a t-test [22]. Responses of the *Crbl*^{KO}*Crb2*^{ΔRods} and *Crb2*^{ΔRods} were compared to the *Crb2*^{flox/flox} control mice at each time point analyzed.

Pupillary light reflex (PLR)

The mice were dark-adapted for 16 hours prior to experiments. Pupillary light reflex was measured under dim red light using an A2000 pupillometer (Neuroptics, Inc., Irvine, CA, USA). Pupillary light reflex was performed on 3-month-old (3M) *Crbl*^{KO}*Crb2*^{flox/flox} and *Crbl*^{KO}*Crb2*^{ΔRods} mice and on 9-month-old *Crb2*^{flox/flox}, *Crbl*^{KO}*Crb2*^{flox/flox}, and *Crbl*^{KO}*Crb2*^{ΔRods} mice. Mice were anesthetized with 50 mg/kg ketamine and 5 mg/kg xylazine injected intraperitoneally. Mice were placed on the platform, and pupil's borders were placed in focus. The following light sequence was used: red 1.2 log·lux (-1.2 log·W/m², 0.065 W/m²), blue 0.6 log·lux (-1.1 log·W/m², 0.074 W/m²), red 4.5 log·lux (2.1 log·W/m², 129.018 W/m²), blue 2.0 log·lux (0.3 log·W/m², 1.893 W/m²) [33]. Pupil diameter recording started 500 ms before the light stimulus and continued for 29 seconds after the light stimulus. The pupil diameter was determined automatically by software from Neuroptics, Inc. Pupil light reflex

measurement amounted to 320 stimuli measurements (4 stimuli per pupil), of which 17 were removed after manual curation. The numbers of animals used were as follows: 3M $Crb1^{KO}Crb2^{flox/flox}$ ($n = 56$ stimuli, $n = 8$ mice), $Crb1^{KO}Crb2^{\Delta Rods}$ ($n = 67$ stimuli, $n = 9$ mice) and 9M $Crb2^{flox/flox}$ ($n = 44$ stimuli, $n = 6$ mice), $Crb1^{KO}Crb2^{flox/flox}$ ($n = 64$ stimuli, $n = 8$ mice), and $Crb1^{KO}Crb2^{\Delta Rods}$ ($n = 72$ stimuli, $n = 9$ mice). All stimuli were normalized in percentile by the maximum dilation during the first 500 ms prior to stimulus and smoothed by running median ($k = 5$). The aggregated mean per group is shown in Figure 4A, C, and the overall maximum pupil constriction over 303 stimuli are shown in Figure 4B, D.

2

Optokinetic head tracking response (OKT)

Spatial frequency and contrast sensitivity thresholds were measured using an OptoMotry system (Cerebral Mechanics, Lethbridge, AB, Canada). One-, 3-, 7-, and 9-month-old $Crb1^{KO}Crb2^{\Delta Rods}$ and $Crb1^{KO}Crb2^{flox/flox}$ mice, and 9-month-old $Crb2^{flox/flox}$ mice were placed on a small platform in the center of four computer monitors that formed a virtual drum with a rotating vertical sine wave grating ($12^\circ/s$ (d/s)), as described previously [29]. Reflexive head movements in the same direction as the rotating gratings were considered positive responses. Spatial frequency thresholds were determined with an increasing staircase paradigm starting at 0.042 cycles/deg (c/d) with 100% contrast. Contrast sensitivity thresholds were measured across six spatial frequencies (0.031, 0.064, 0.092, 0.103, 0.192, and 0.272 c/d). The reciprocal of the contrast sensitivity threshold was used as the contrast sensitivity value at each spatial frequency.

The numbers of mice used for the OKT measurements per time point were as follows: 1M ($Crb1^{KO}Crb2^{flox/flox}$ $n = 8$ and $Crb1^{KO}Crb2^{\Delta Rods}$ $n = 4$), 3M ($Crb1^{KO}Crb2^{flox/flox}$ $n = 10$ and $Crb1^{KO}Crb2^{\Delta Rods}$ $n = 10$), 5M ($Crb2^{flox/flox}$ $n = 10$, $Crb2^{\Delta Rods}$ $n = 8$), 7M ($Crb1^{KO}Crb2^{flox/flox}$ $n = 8$ and $Crb1^{KO}Crb2^{\Delta Rods}$ $n = 9$), 9M ($Crb2^{flox/flox}$ $n = 7$, $Crb1^{KO}Crb2^{flox/flox}$ $n = 8$, and $Crb1^{KO}Crb2^{\Delta Rods}$ $n = 9$). Statistical significance was calculated by using Mann-Whitney U test.

Morphological and immunohistochemical analysis

Eyes from *Crb2*^{ΔRods}, *Crb1*^{KO}*Crb2*^{ΔRods}, *Crb1*^{KO}*Crb2*^{flox/flox}, and *Crb2*^{flox/flox} mice were collected at different time points: 1-month-old (1M), 3M, 6M, 9M, and 12M ($n = 4-6$ /age/group). For morphological analysis, the superior part of the eye was marked with a yellow dye (Davidson Marking System@dyes, Bradley Products, Bloomington, MN, USA). Thereafter, eyes were enucleated and fixed at room temperature with 4% paraformaldehyde in phosphate buffered saline (PBS) for 20 min. After fixation, the eyes were dehydrated for 30 min in 30%, 50%, 70%, 90%, and 96% ethanol, embedded in Technovit 7100 (Kulzer, Wehrheim, Germany), and sectioned (3 μm), as previously described [40]. Slides were dried, counterstained with 0.5% toluidine blue, and mounted under coverslips using Entellan (Merk, Darmstadt, Germany). Eye sections were scanned using a Panoramic 250 digital slide scanner (3DHISTECH Ltd., Budapest, Hungary) and images were processed with CaseViewer 2.1 (3DHISTECH Ltd., Budapest, Hungary).

For immunohistochemical analysis, eyes were enucleated and fixed for 20 min in 4% paraformaldehyde in PBS. Subsequently, the tissues were cryo-protected with 15% and 30% sucrose in PBS, embedded in Tissue-Tek O.C.T Compound (Sakura, Finetek, Alphen aan den Rijn, The Netherlands), and used for cryosectioning. Cryosections (8 μm) were rehydrated in PBS and blocked for 1 h using 10% goat serum, 0.4% Triton X-100, and 1% bovine serum albumin (BSA) in PBS. The primary antibodies were diluted in 0.3% goat serum, 0.4% Triton X-100, and 1% BSA in PBS, and incubated for 16 hours at 4°C. Fluorescent-labelled secondary antibodies were goat anti-mouse, goat anti-rabbit, goat anti-chicken, or goat anti-rat IgGs conjugated to Alexa 488, Alexa 555 (1:1000; Abcam, Cambridge, UK), or Cy3 (1:500) were diluted in 0.1% goat serum in PBS and incubated for 1 hour at room temperature. Nuclei were counterstained with DAPI and mounted in Vectashield Hardset mounting medium (H1500, Vector Laboratories, Burlingame, CA, USA). Sections were imaged on a Leica TCS SP8 confocal microscope. Confocal images were processed with Leica Application Suite X (v3.3.0.16799) or Adobe Photoshop CC 2018 (Adobe Photoshop, RRID: SCR_014199).

Transmission electron microscopy (TEM)

Eyes from 8-month-old *Crb1^{KO}Crb2^{ΔRods}* and respective control (*Crb2^{fllox/fllox}*) were fixed in 4% paraformaldehyde and 2% glutaraldehyde in phosphate buffer (PB) for 24 h (n = 2 per group). Eyes were cut in half along the mid-sagittal plane using a razor knife, cutting through the optic nerve. The vitreous body was removed, and the two halves were placed back in the fixative for 2 hours. After rinsing, eyes were post-fixed in 1% OsO₄/0.1M cacodylate buffer, rinsed again, and dehydrated with an ascending series of ethanol, followed by mixtures of propylene oxide and EPON (LX112). After the infiltration step with pure EPON, the halves of the eyes were positioned on the caps of large BEEM capsules filled with EPON. Ultrathin sections of the eyes, 80 nm thick, were made and stained with uranyl acetate and lead citrate and examined with a FEI Tecnai electron microscope (FEI Tecnai T12 Twin Fei Company, Eindhoven, The Netherlands; camera by OneView, Gatan) operating at 120 Kv. Overlapping images were collected and stitched together into separate images, as previously described [41].

Primary antibodies

The following primary antibodies were used: β-catenin (1:250; BD Biosciences Cat# 610153, RRID:AB_397554), catenin p120 (1:250; BD Biosciences Cat# 610134, RRID:AB_397537), CD44 (1:400; BD Biosciences Cat# 553132, RRID:AB_394647), cone arrestin (1:500; Millipore Cat# AB15282, RRID:AB_1163387), CRB1 AK2 (1:200; homemade) [6], CRB2 SK11 (1:200; homemade), glial fibrillary acidic protein (GFAP) (1:200; Dako Cat# Z0334, RRID:AB_10013382), GFP (Millipore Cat# MAB3580, RRID:AB_94936), glutamine synthetase (GS) (1:250; BD Biosciences Cat# 610518, RRID:AB_397880), MPP4 AK4 (1:300; homemade) [6], MPP5/PALS1 SN47 (1:200; homemade), MUPP1 (1:200; BDBiosciences Cat# 611558, RRID:AB_399004), M-Op sin (1:250; Millipore Cat# AB5405, RRID:AB_177456), PAR3 (1:100; Millipore Cat# 07-330, RRID:AB_2101325), PKC (1:250; BD Biosciences Cat# 610107, RRID:AB_397513), peanut agglutinin (PNA) (1:200; Vector Laboratories Cat# RL-1072, RRID:AB_2336642), recoverin (1:500; Millipore Cat#

AB5585, RRID:AB_2253622), rhodopsin (1:500; Millipore Cat#MAB5356, RRID:AB_2178961), SOX9 (1:250; Millipore Cat# AB5535, RRID: AB_2239761).

Quantification of the number of photoreceptor nuclei in a row

The number of photoreceptor cell nuclei in a row were measured every 250 μm from the optic nerve head (ONH) in 1-month-old (1M), 3M, 6M, 9M, and 12M *Crb2* Δ Rods, *Crbl*^{KO}*Crb2* Δ Rods, *Crbl*^{KO}*Crb2*^{flox/flox} and *Crb2*^{flox/flox} mice. Three sections in the optic nerve area of 3 retinas from 3–4 independent mice per group were used for the measurements. Retina sections were scanned using a Panoramic 250 digital slide scanner (3DHISTECH Ltd., Budapest, Hungary) and measurements were performed with CaseViewer 2.1 (3DHISTECH Ltd., Budapest, Hungary). The values of different sections of individual mice were averaged. The number of photoreceptor nuclei from the *Crb2* Δ Rods and *Crbl*^{KO}*Crb2* Δ Rods were compared to the *Crb2*^{flox/flox} control mice.

Statistical analysis

Normality of the distribution was tested by the Kolmogorov–Smirnov test. Statistical significance was calculated by using an unpaired t-test or by using Mann-Whitney U test if the data did not show a normal distribution. All statistical analyses were performed using GraphPad Prism version 7.02 (GraphPad Prism, RRID: SCR_002798). All values are expressed as mean \pm SEM. Statistically significant values: * $p < 0.05$, ** $p < 0.01$, *** $p < 0.001$, **** $p < 0.0001$.

Article information

Patents: The Leiden University Medical Center (LUMC) is the holder of patent application PCT/NL2014/050549, which describes the potential clinical use of CRB2. J.W. is listed as inventor on this patent, and J.W. is an employee of the LUMC

Author contributions: Conceptualization, C.H.A. and J.W.; methodology, C.H.A., N.B. and J.W.; validation, C.H.A., N.B., J.W., A.M., A.K. and C.J.; formal analysis, C.H.A., N.B. and J.W.; investigation, J.W., C.H.A. and N.B.; resources, J.W., A.K. and C.J.; data curation, C.H.A. and N.B.; writing—original draft preparation, C.H.A., N.B. and

J.W.; writing—review and editing, C.H.A., N.B. and J.W.; visualization, C.H.A., N.B. and A.T.; supervision, J.W.; project administration, J.W.; funding acquisition, J.W. and C.H.A.

Funding: This work was funded by ZonMw (grant number 43200004 to J.W.), FFB (grant number TA-GT-0715-0665-LUMC to J.W.), Leiden Regenerative Medicine Platform (grant number 2018-Project-B to J.W.), Rotterdamse Stichting Blindenbelangen, and Landelijke Stichting voor Blinden en Slechtzienenden (grant number Uitzicht-2018-6 to C.H.A. and J.W.).

Acknowledgements: We thank Macha Beijnes, Nynke van de Haar, Mees Kamps, Nienke Koot, and Eline Nagel for technical assistance and Peter M. Quinn and Thilo M. Buck for advice on the manuscript. We thank the Department of Biomedical Data Sciences for biostatistical analysis.

Conflict of interest: The authors declare no conflict of interest. The funders had no role in the design of the study; in the collection, analyses, or interpretation of data; in the writing of the manuscript, or in the decision to publish the results.

Abbreviations:

CAR	Cone arrestin
CRB1	Crumbs homolog-1
ERG	Electroretinography
EYFP	Enhanced yellow fluorescent protein
GCL	Ganglion cell layer
GFAP	Glial fibrillary acidic protein
GS	Glutamine synthetase
INL	Inner nuclear layer
LCA	Leber congenital amaurosis
MGC	Müller glial cell
OKT	Optokinetic head tracking response
OLM	Outer limiting membrane
ONL	Outer nuclear layer
PLR	Pupillary light reflex
PNA	Peanut agglutinin

RP	Retinitis pigmentosa
RPE	Retinal pigment epithelium

References

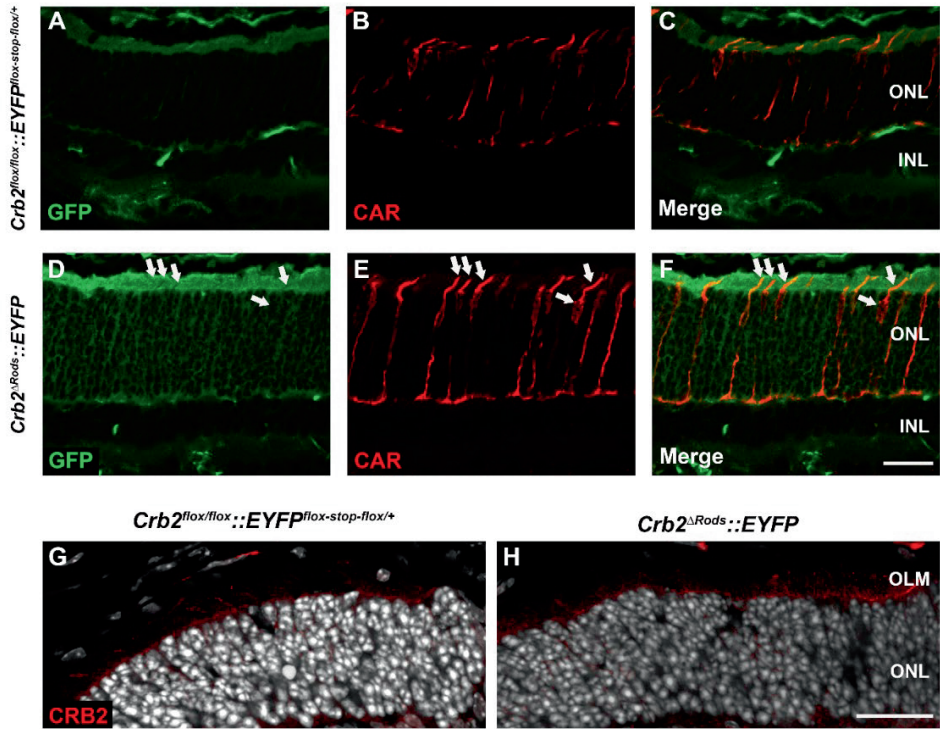
1. Tepass, U.; Theres, C.; Knust, E. crumbs encodes an EGF-like protein expressed on apical membranes of Drosophila epithelial cells and required for organization of epithelia. *Cell* **1990**, *61*, 787–799.
2. Alves, C.H.; Pellissier, L.P.; Wijnholds, J. The CRB1 and adherens junction complex proteins in retinal development and maintenance. *Prog. Retin. Eye Res.* **2014**, *40*, 35–52.
3. Alves, C.H.; Sanz Sanz, A.; Park, B.; Pellissier, L.P.; Tanimoto, N.; Beck, S.C.; Huber, G.; Murtaza, M.; Richard, F.; Sridevi gurubaran, I.; et al. Loss of CRB2 in the mouse retina mimics human retinitis pigmentosa due to mutations in the CRB1 gene. *Hum. Mol. Genet.* **2013**, *22*, 35–50.
4. Pellikka, M.; Tanentzapf, G.; Pinto, M.; Smith, C.; McGlade, C.J.; Ready, D.F.; Tepass, U. Crumbs, the Drosophila homologue of human CRB1/RP12, is essential for photoreceptor morphogenesis. *Nature* **2002**, *416*, 143–149.
5. van de Pavert, S.A.; Kantardzhieva, A.; Malysheva, A.; Meuleman, J.; Versteeg, I.; Levelt, C.; Klooster, J.; Geiger, S.; Seeliger, M.W.; Rashbass, P.; et al. Crumbs homologue 1 is required for maintenance of photoreceptor cell polarization and adhesion during light exposure. *J. Cell Sci.* **2004**, *117*, 4169–4177.
6. van Rossum, A.G.S.H.; Aartsen, W.M.; Meuleman, J.; Klooster, J.; Malysheva, A.; Versteeg, I.; Arsanto, J.P.; Le Bivic, A.; Wijnholds, J. Pals1/Mpp5 is required for correct localization of Crb1 at the subapical region in polarized Müller glia cells. *Hum. Mol. Genet.* **2006**, *15*, 2659–2672.
7. Den Hollander, A.I.; Ghiani, M.; De Kok, Y.J.M.; Wijnholds, J.; Ballabio, A.; Cremers, F.P.M.; Broccoli, V. Isolation of Crb1, a mouse homologue of Drosophila crumbs, and analysis of its expression pattern in eye and brain. *Mech. Dev.* **2001**, *110*, 203–207.
8. Motta, F.L.; Salles, M.V.; Costa, K.A.; Filippelli-Silva, R.; Martin, R.P.; Sallum, J.M.F. The correlation between CRB1 variants and the clinical severity of Brazilian patients with different inherited retinal dystrophy phenotypes. *Sci. Rep.* **2017**, *7*, 8654.
9. Talib, M.; van Schooneveld, M.J.; van Genderen, M.M.; Wijnholds, J.; Florijn, R.J.; ten Brink, J.B.; Schalijs-Delfos, N.E.; Dagnelie, G.; Cremers, F.P.M.; Wolterbeek, R.; et al. Genotypic and Phenotypic Characteristics of CRB1-Associated Retinal Dystrophies: A Long-Term Follow-up Study. *Ophthalmology* **2017**, *124*, 884–895.

10. Chen, X.; Jiang, C.; Yang, D.; Sun, R.; Wang, M.; Sun, H.; Xu, M.; Zhou, L.; Chen, M.; Xie, P.; et al. CRB2 mutation causes autosomal recessive retinitis pigmentosa. *Exp. Eye Res.* **2018**, *180*, 164–173.
11. Ebarasi, L.; Ashraf, S.; Bierzynska, A.; Gee, H.Y.; McCarthy, H.J.; Lovric, S.; Sadowski, C.E.; Pabst, W.; Vega-Warner, V.; Fang, H.; et al. Defects of CRB2 cause steroid-resistant nephrotic syndrome. *Am. J. Hum. Genet.* **2015**, *96*, 153–61.
12. Slavotinek, A.; Kaylor, J.; Pierce, H.; Cahr, M.; Deward, S.J.; Schneidman-Duhovny, D.; Alsadah, A.; Salem, F.; Schmajuk, G.; Mehta, L. CRB2 mutations produce a phenotype resembling congenital nephrosis, Finnish type, with cerebral ventriculomegaly and raised alpha-fetoprotein. *Am. J. Hum. Genet.* **2015**, *96*, 162–169.
13. Lamont, R.E.; Tan, W.H.; Innes, A.M.; Parboosingh, J.S.; Schneidman-Duhovny, D.; Rajkovic, A.; Pappas, J.; Altschwager, P.; DeWard, S.; Fulton, A.; et al. Expansion of phenotype and genotypic data in CRB2-related syndrome. *Eur. J. Hum. Genet.* **2016**, *24*, 1436–1444.
14. van de Pavert, S.A.; Meuleman, J.; Malysheva, A.; Aartsen, W.M.; Versteeg, I.; Tonagel, F.; Kamphuis, W.; McCabe, C.J.; Seeliger, M.W.; Wijnholds, J. A single amino acid substitution (Cys249Trp) in *Crb1* causes retinal degeneration and deregulates expression of pituitary tumor transforming gene *Pttg1*. *J. Neurosci.* **2007**, *27*, 564–573.
15. Alves, C.H.; Pellissier, L.P.; Vos, R.M.; Garcia Garrido, M.; Sothilingam, V.; Seide, C.; Beck, S.C.; Klooster, J.; Furukawa, T.; Flannery, J.G.; et al. Targeted ablation of *Crb2* in photoreceptor cells induces retinitis pigmentosa. *Hum. Mol. Genet.* **2014**, *23*, 3384–401.
16. Alves, C.H.; Bossers, K.; Vos, R.M.; Essing, A.H.W.; Swagemakers, S.; Van Der Spek, P.J.; Verhaagen, J.; Wijnholds, J. Microarray and morphological analysis of early postnatal CRB2 mutant retinas on a pure C57BL/6J genetic background. *PLoS One* **2013**, *8*, 1–17.
17. Pellissier, L.P.; Alves, C.H.; Quinn, P.M.; Vos, R.M.; Tanimoto, N.; Lundvig, D.M.S.; Dudok, J.J.; Hooibrink, B.; Richard, F.; Beck, S.C.; et al. Targeted Ablation of *Crb1* and *Crb2* in Retinal Progenitor Cells Mimics Leber Congenital Amaurosis. *PLoS Genet.* **2013**, *9*, e1003976.
18. Pellissier, L.P.; Lundvig, D.M.S.; Tanimoto, N.; Klooster, J.; Vos, R.M.; Richard, F.; Sothilingam, V.; Garcia Garrido, M.; Le Bivic, A.; Seeliger, M.W.; et al. CRB2 acts as a modifying factor of CRB1-related retinal dystrophies in mice. *Hum. Mol. Genet.* **2014**, *23*, 3759–3771.
19. Quinn, P.M.; Alves, C.H.; Klooster, J.; Wijnholds, J. CRB2 in immature photoreceptors determines the superior-inferior symmetry of the developing retina to maintain retinal structure and function. *Hum. Mol. Genet.* **2018**, *27*, 3137–3153.

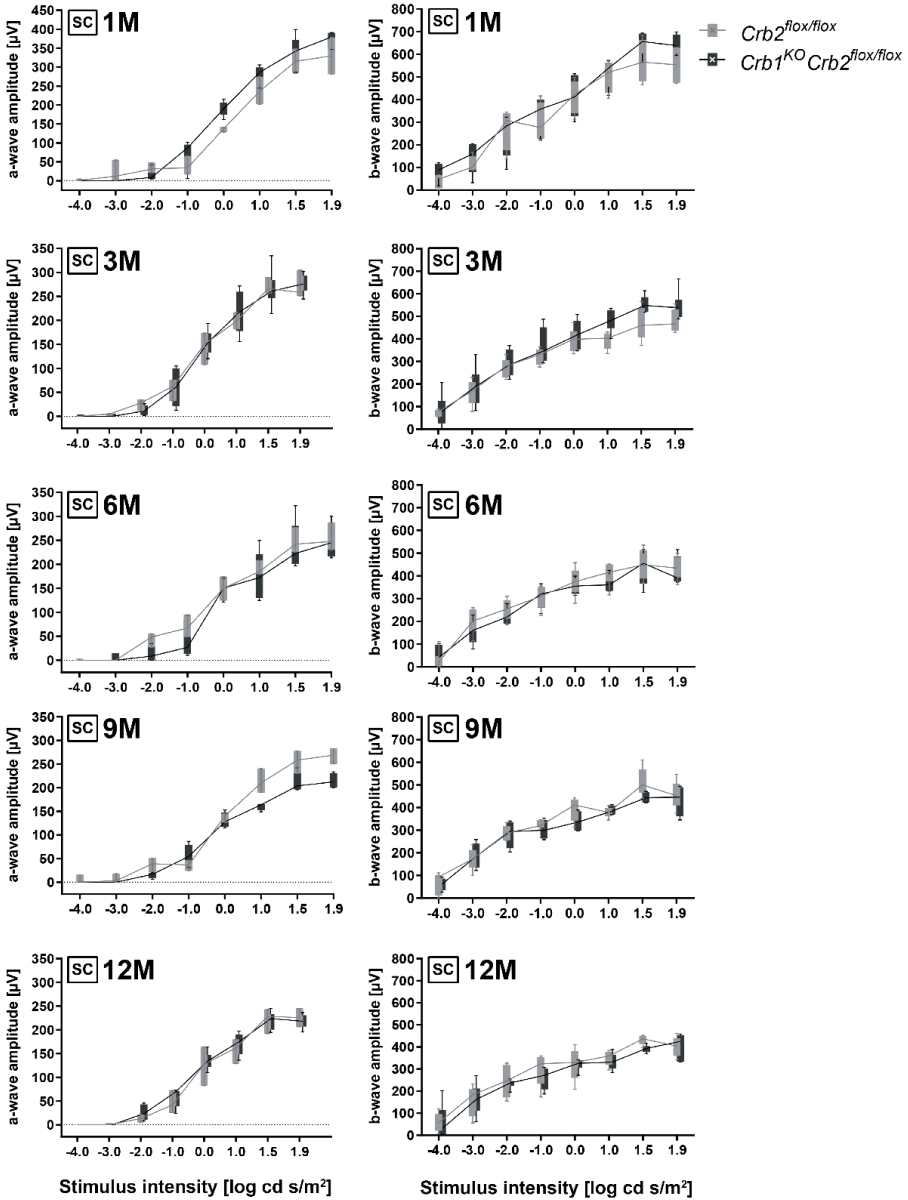
20. Quinn, P.M.; Mulder, A.A.; Alves, C.H.; Desrosiers, M.; de Vries, S.I.; Klooster, J.; Dalkara, D.; Koster, A.J.; Jost, C.R.; Wijnholds, J. Loss of CRB2 in Müller glial cells modifies a CRB1-associated retinitis pigmentosa phenotype into a Leber congenital amaurosis phenotype. *Hum. Mol. Genet.* **2019**, *28*, 105–123.
21. Quinn, P.M.; Buck, T.M.; Mulder, A.A.; Ohonin, C.; Alves, C.H.; Vos, R.M.; Bialecka, M.; van Herwaarden, T.; van Dijk, E.H.C.; Talib, M.; et al. Human iPSC-Derived Retinas Recapitulate the Fetal CRB1 CRB2 Complex Formation and Demonstrate that Photoreceptors and Müller Glia Are Targets of AAV5. *Stem Cell Reports* **2019**, *12*.
22. Pellissier, L.P.; Quinn, P.M.; Alves, C.H.; et al. Gene therapy into photoreceptors and Müller glial cells restores retinal structure and function in CRB1 retinitis pigmentosa mouse models. *Hum. Mol. Genet.* **2015**, *24*, 1–15.
23. Pellissier, L.P.; Hoek, R.M.; Vos, R.M.; Aartsen, W.M.; Klimczak, R.R.; Hoyng, S.A.; Flannery, J.G.; Wijnholds, J. Specific tools for targeting and expression in Müller glial cells. *Mol. Ther. - Methods Clin. Dev.* **2014**, *1*, 14009.
24. Li, S.; Chen, D.; Sauv e, Y.; McCandless, J.; Chen, Y.J.; Chen, C.K. Rhodopsin-iCre transgenic mouse line for Cre-mediated rod-specific gene targeting. *Genesis* **2005**, *41*, 73–80.
25. Srinivas, S.; Watanabe, T.; Lin, C.S.; William, C.M.; Tanabe, Y.; Jessell, T.M.; Costantini, F. Cre reporter strains produced by targeted insertion of EYFP and ECFP into the ROSA26 locus. *BMC Dev. Biol.* **2001**, *1*, 1–8.
26. Douglas, R.M.; Alam, N.M.; Silver, B.D.; MCGILL, T.J.; Tschetter, W.W.; Prusky, G.T. Independent visual threshold measurements in the two eyes of freely moving rats and mice using a virtual-reality optokinetic system. *Vis. Neurosci.* **2005**, *22*, 677–684.
27. Prusky, G.T.; Alam, N.M.; Beekman, S.; Douglas, R.M. Rapid quantification of adult and developing mouse spatial vision using a virtual optomotor system. *Invest. Ophthalmol. Vis. Sci.* **2004**, *45*, 4611.
28. Aleman, T.S.; Jacobson, S.G.; Chico, J.D.; Scott, M.L.; Cheung, A.Y.; Windsor, E.A.M.; Furushima, M.; Redmond, T.M.; Bennett, J.; Palczewski, K.; et al. Impairment of the transient pupillary light reflex in Rpe65^{-/-} mice and humans with leber congenital amaurosis. *Investig. Ophthalmol. Vis. Sci.* **2004**, *45*, 1259–1271.
29. Kostic, C.; Crippa, S. V.; Martin, C.; Kardon, R.H.; Biel, M.; Arsenijevic, Y.; Kawasaki, A. Determination of Rod and Cone Influence to the Early and Late Dynamic of the Pupillary Light Response. *Investig. Ophthalmology Vis. Sci.* **2016**, *57*, 2501.
30. Wendt, K.D.; Lei, B.; Schachtman, T.R.; Tullis, G.E.; Ibe, M.E.; Katz, M.L. Behavioral assessment in mouse models of neuronal ceroid lipofuscinosis using a light-cued T-maze. *Behav. Brain Res.* **2005**, *161*, 175–182.

31. Lisowska, J.; Lisowski, L.; Kelbsch, C.; Maeda, F.; Richter, P.; Kohl, S.; Zobor, D.; Strasser, T.; Stingl, K.; Zrenner, E.; et al. Development of a chromatic pupillography protocol for the first gene therapy trial in patients with CNGA3-linked achromatopsia. *Investig. Ophthalmol. Vis. Sci.* **2017**, *58*, 1274–1282.
32. Melillo, P.; Pecchia, L.; Testa, F.; Rossi, S.; Bennett, J.; Simonelli, F. Pupillometric analysis for assessment of gene therapy in Leber Congenital Amaurosis patients. *Biomed. Eng. Online* **2012**, *11*, 40.
33. Richter, P.; Wilhelm, H.; Peters, T.; Luedtke, H.; Kurtenbach, A.; Jaegle, H.; Wilhelm, B. The diagnostic accuracy of chromatic pupillary light responses in diseases of the outer and inner retina. *Graefe's Arch. Clin. Exp. Ophthalmol.* **2017**, *255*, 519–527.
34. Goldman, D. Müller glial cell reprogramming and retina regeneration. *Nat. Rev. Neurosci.* **2014**, *15*, 431–442.
35. Corbo, J.C.; Myers, C.A.; Lawrence, K.A.; Jadhav, A.P.; Cepko, C.L. A typology of photoreceptor gene expression patterns in the mouse. *Proc. Natl. Acad. Sci.* **2007**, *104*, 12069–12074.
36. Cuenca, N.; Fernández-Sánchez, L.; Sauvé, Y.; Segura, F.J.; Martí-nez-Navarrete, G.; Tamarit, J.M.; Fuentes-Broto, L.; Sanchez-Cano, A.; Pinilla, I. Correlation between SD-OCT, immunocytochemistry and functional findings in an animal model of retinal degeneration. *Front. Neuroanat.* **2014**, *8*.
37. McGill, T.J.; Prusky, G.T.; Douglas, R.M.; Yasumura, D.; Matthes, M.T.; Lowe, R.J.; Duncan, J.L.; Yang, H.; Ahern, K.; Daniello, K.M.; et al. Discordant anatomical, electrophysiological, and visual behavioral profiles of retinal degeneration in rat models of retinal degenerative disease. *Investig. Ophthalmol. Vis. Sci.* **2012**, *53*, 6232–6244.
38. Piano, I.; Novelli, E.; Gasco, P.; Ghidoni, R.; Strettoi, E.; Gargini, C. Cone survival and preservation of visual acuity in an animal model of retinal degeneration. *Eur. J. Neurosci.* **2013**, *37*, 1853–1862.
39. Nishiguchi, K.M.; Carvalho, L.S.; Rizzi, M.; Powell, K.; Holthaus, S.M. kleine; Azam, S.A.; Duran, Y.; Ribeiro, J.; Luhmann, U.F.O.; Bainbridge, J.W.B.; et al. Gene therapy restores vision in rd1 mice after removal of a confounding mutation in Gpr179. *Nat. Commun.* **2015**, *6*, 6006.
40. Alves, C.H.; Wijnholds, J. AAV Gene Augmentation Therapy for CRB1-Associated Retinitis Pigmentosa. In *Methods in molecular biology (Clifton, N.J.)*; Human Press: New York, NY, USA, **2018**; Vol. 1715, pp. 135–151.
41. Faas, F.G.A.; Avramut, M.C.; M. van den Berg, B.; Mommaas, A.M.; Koster, A.J.; Ravelli, R.B.G. Virtual nanoscopy: Generation of ultra-large high resolution electron microscopy maps. *J. Cell Biol.* **2012**, *198*, 457–469.

Supplemental information

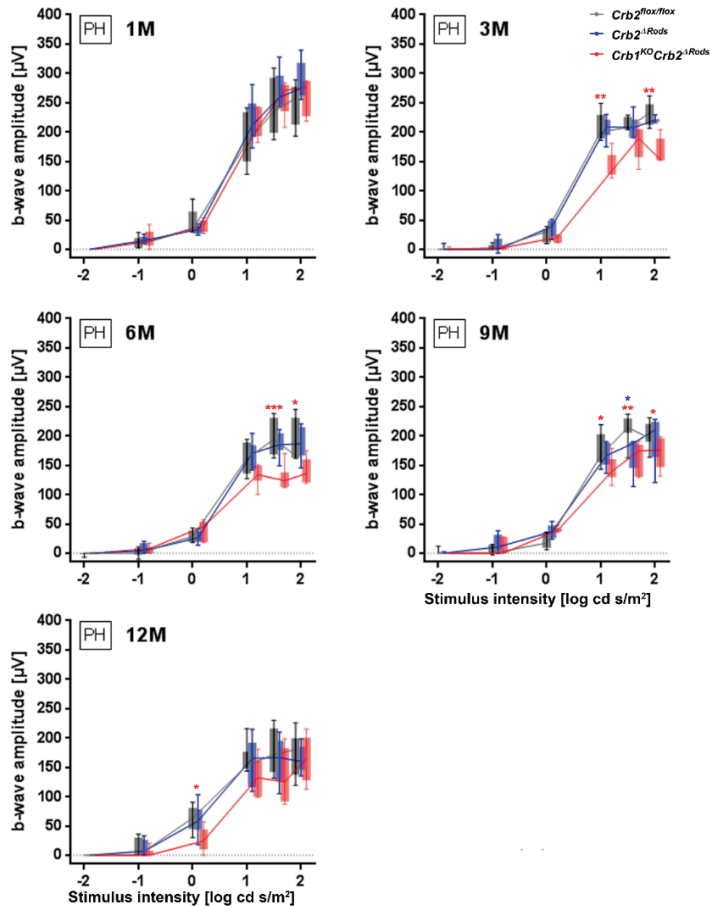


Supplemental Figure 1. Specific ablation of *Crb2* from rod photoreceptors. Evaluation of the recombination efficiency of a Rho-*iCre* mouse line (A-F). The R26-stop-EYFP mutant mice have a loxP-flanked STOP sequence followed by the Enhanced Yellow Fluorescent Protein gene (EYFP) inserted into the Gt(ROSA) 26Sor locus (*EYFP^{flox-stop-flox/+}*). When bred to mice expressing Rho-*iCre*, the STOP sequence is deleted and EYFP expression is observed in the rod photoreceptor cells of the double mutant offspring (*Crb2^{ΔRods}::EYFP*). Confocal laser scanning microscope pictures of (postnatal day 20 (P20)) retina sections from *Crb2^{flox/flox}::EYFP^{flox-stop-flox/+}* (A-C), and *Crb2^{ΔRods}::EYFP* (D-F), stained with anti-GFP and anti-cone arrestin (CAR), and sections from *Crb2^{flox/flox}::EYFP^{flox-stop-flox/+}* (G), and *Crb2^{ΔRods}::EYFP* (H), stained with anti-CRB2 antibodies. While in the *Crb2^{flox/flox}::EYFP^{flox-stop-flox/+}* (A and C) no EYFP signal could be detected, in *Crb2^{ΔRods}::EYFP* (F, arrows) retinas expression of EYFP was found only in the outer nuclear and inner-segment layers. No co-localization of EYFP with cone arrestin positive cells was observed (D, E, F, arrows), suggesting that recombination was restricted to rod photoreceptor cells. CRB2 protein was detected at the subapical region in the control retina (G). Besides the ablation of *Crb2* from rods photoreceptors, the protein could still be detected at the subapical region of mutant retinas once the protein is still expressed by wild-type Müller glial cells and cone photoreceptors (H). Note: CAR = cone arrestin; INL = inner nuclear layer; ONL = outer nuclear layer; OLM = outer limiting membrane. Scale bar: (A-H): 25 μm.

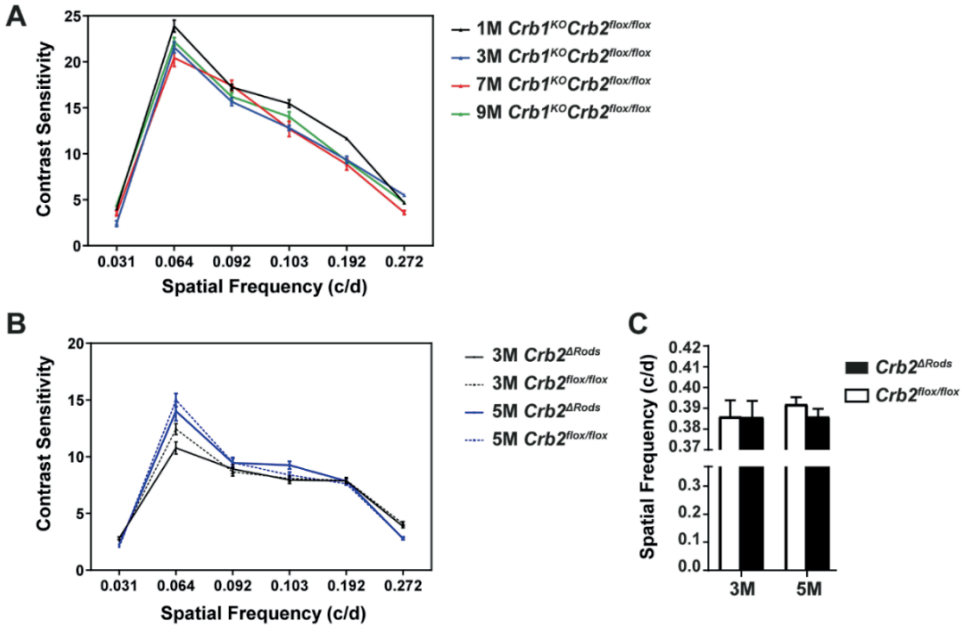


Supplemental Figure 2. *Crb1*^{KO}*Crb2*^{fl/fl} and *Crb2*^{fl/fl} mice present similar scotopic electroretinography responses. Electrophysiological analysis of retinal function in *Crb1*^{KO}*Crb2*^{fl/fl} (black) and *Crb2*^{fl/fl} (gray) mice at different time points, 1-, 3-, 6-, 9-, and 12-months-of-age. Boxes indicate the 25 and 75% quantile range and whiskers indicate the 5 and 95% quantile range.

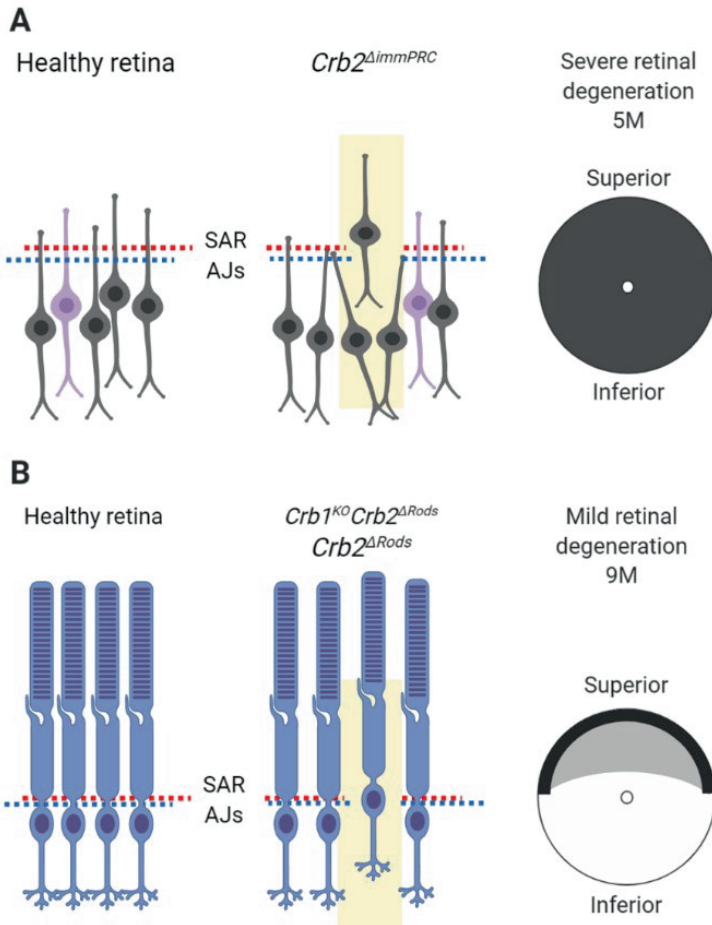
95% quantiles, the intersection of line and error bar indicates the median of the data (box-and-whisker plot).



Supplemental Figure 3. *Crb2^{ΔRods}* and *Crb1^{KO}Crb2^{ΔRods}* mice present normal photopic electroretinography responses. Electrophysiological analysis of retinal function in *Crb2^{flox/flox}* (control) (gray), *Crb2^{ΔRods}* (blue) and *Crb1^{KO}Crb2^{ΔRods}* (red) at different time points, 1-, 3-, 6-, 9- and 12-months-of-age. Boxes indicate the 25 and 75% quantile range and whiskers indicate the 5 and 95% quantiles, and the intersection of line and error bar indicates the median of the data (box-and-whisker plot).



Supplemental Figure 4. Similar contrast sensitivity for *Crb1^{KO}Crb2^{flox/flox}*, *Crb2^{flox/flox}* at all frequencies measured. (A) Contrast sensitivity in cycles per degree (c/d) from 1-month of age (1M), 3M, 7M and 9M *Crb1^{KO}Crb2^{flox/flox}*. No difference was detected between *Crb1^{KO}Crb2^{flox/flox}* mice at all frequencies and time points measured. (B) Contrast sensitivity and (C) spatial frequency from 3-, and 5-month of age *Crb2^{flox/flox}* and *Crb2^{ΔRods}*. No difference was observed between *Crb2^{flox/flox}* and *Crb2^{ΔRods}* mice. Error bars indicate \pm SEM.



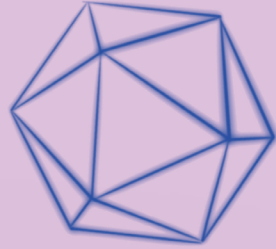
Supplemental Figure 5. Schematic overview of retinal degeneration. (A) Loss of CRB2 from immature rod and cone photoreceptors results at 5M in severe disruption of adherens junctions and nearly complete loss of photoreceptor cells throughout the entire retina (Alves et al., 2014). (B) loss of CRB2 in mature rod photoreceptors results at 9M in milder disruption of adherens junctions and photoreceptor loss especially at the far periphery especially of the superior retina (current data). The loss of CRB2 in rod photoreceptors also results at 9M in gliosis (GFAP upregulation) in the adjacent Müller glial cells.

Chapter 3

Defining Phenotype, Tropism, and Retinal Gene Therapy using Adeno-Associated Viral Vectors (AAVs) in New-Born Brown Norway Rats with a Spontaneous Mutation in *Crb1*

N. Boon, C. H. Alves, A. A. Mulder, C. A. Andriessen,
T. M. Buck, P. M. J. Quinn, R. M. Vos, A. J. Koster, C. R. Jost,
and J. Wijnholds

Part of this study is published in:
International Journal of Molecular Sciences, 2021; 3563



Abstract

Mutations in the Crumbs homologue 1 (*CRB1*) gene cause inherited retinal dystrophies, such as early-onset retinitis pigmentosa and Leber congenital amaurosis. A Brown Norway rat strain was reported with a spontaneous insertion-deletion (indel) mutation in exon 6 of *Crb1*. It has been reported that these *Crb1* mutant rats show vascular abnormalities associated with retinal telangiectasia and possess an early-onset retinal degenerative phenotype with outer limiting membrane breaks and focal loss of retinal lamination at 2 months of age. Here, we further characterized the morphological phenotype of new-born and adult *Crb1* mutant rats in comparison with age-matched Brown Norway rats without a mutation in *Crb1*. A significantly decreased retinal function and visual acuity was observed in *Crb1* mutant rats at 1 and 3 months of age, respectively. Moreover, in control rats, the subcellular localization of canonical CRB1 was observed at the subapical region in Müller glial cells while CRB2 was observed at the subapical region in both photoreceptors and Müller glial cells by immuno-electron microscopy. CRB1 localization was lost in the *Crb1* mutant rats, whereas CRB2 was still observed. In addition, we determined the tropism of subretinal or intravitreally administered AAV5-, AAV9- or AAV6-variant ShH10^{Y445F} vectors in new-born control and *Crb1* mutant rat retinas. We showed that subretinal injection of AAV5 and AAV9 at postnatal days 5 (P5) or 8 (P8) predominantly infected the retinal pigment epithelium (RPE) and photoreceptor cells; while intravitreal injection of ShH10^{Y445F} at P5 or P8 resulted in efficient infection of mainly Müller glial cells. Using knowledge of the subcellular localization of CRB1 and the ability of ShH10^{Y445F} to infect Müller glial cells, canonical *hCRB1* and *hCRB2* AAV-mediated gene therapy were explored in new-born *Crb1* mutant rats. Enhanced retinal function after gene therapy delivery in the *Crb1* rat was not observed. No timely rescue of the retinal phenotype was observed using retinal function and visual acuity, suggesting the need for earlier onset of expression of recombinant hCRB proteins in Müller glial cells to rescue the severe retinal phenotype in *Crb1* mutant rats.

Introduction

Retinitis pigmentosa (RP) and Leber congenital amaurosis (LCA) are inherited retinal degenerative diseases causing progressive vision loss, ultimately leading to blindness. Mutations in the Crumbs homolog 1 (*CRB1*) gene is a frequent cause of these retinal dystrophies in humans [1]. The *CRB1* gene, mapped to chromosome 1q31.3, encodes a large transmembrane protein and belongs to the Crumbs (CRB) family, with family members *CRB2* and *CRB3*. CRB proteins are located in the subapical region above adherens junctions at the outer limiting membrane (OLM), where it can interact with, amongst others, *PALS1* to form the canonical Crumbs complex [2–4]. *Crb1* knockout (*Crb1*^{KO}) mouse models show a mild retinal degeneration with OLM disruptions and ectopic rows of photoreceptor cell nuclei in the photoreceptor segment layers from postnatal day 14 (P14) [5]. Concomitant loss of *Crb2* in *Crb1*^{KO} mice results in a more severe RP or LCA phenotype, depending on which cell type lacks *Crb2* [6–9]. Currently, there is no treatment available for *CRB1*-related retinal dystrophies.

A Brown Norway rat strain was described with an inherited retinal degenerative phenotype caused by a spontaneous in frame insertion-deletion (indel) in exon 6 of the *Crb1* gene [10]. These *Crb1* mutant rats, expressing an alternative *CRB1*^{INDEL} protein, exhibit an early-onset loss of retinal function from 3 weeks of age. In addition, the first signs of retinal degeneration were observed from P15, including OLM disruptions and ectopic rows of photoreceptor cell nuclei in the photoreceptor segment layers. At older ages, these disruptions progress and ultimately lead to a focal loss of retinal lamination [10]. Because of its naturally occurring mutation and early-onset severe retinal phenotype, these rats are a potential attractive animal model for the development of gene therapy. Currently, gene therapy using adeno-associated viral vectors (AAVs) is the leading platform of gene delivery for the treatment of retinal dystrophies because of its low toxicity and ability to target both dividing and non-dividing cells [11]. In addition, different AAV capsids display distinct cell tropisms, making it possible to target different cell types. Moreover, previous mouse gene supplementation studies with AAV expressing human *CRB2* (*hCRB2*) have shown to preserve the retinal

morphology and function in *Crb1* RP mouse models [12,13]. Altogether, this indicates the potential use of AAV-mediated gene therapy for *CRB1*-related retinal dystrophies.

Here, we perform a thorough characterization of the morphological phenotype of newborn and adult *Crb1* mutant rats and its effect on retinal function and visual acuity in comparison with age-matched control rats. Using immuno-electron-microscopy, we show that, in control rats, canonical CRB1 localizes specifically in Müller glial cells (MGCs) at the subapical region adjacent to the adherens junctions at the outer limiting membrane (OLM), whereas the *Crb1* mutant rats barely express detectable levels of CRB1^{INDEL} at the subapical region of MGCs. In turn, CRB2 is localized at the subapical region in MGCs and photoreceptors of both control and *Crb1* mutant rats. Next, we describe the tropism of three different AAV serotypes (AAV5-, AAV9- and AAV6-variant ShH10^{Y445F}) expressing *GFP* driven by the cytomegalovirus (CMV) promoter in new-born control and *Crb1* mutant rat retinas. Tropism data at P5 and P8 shows that subretinal injection of AAV5.CMV.*GFP* and AAV9.CMV.*GFP* mainly transduces photoreceptors and retinal pigment epithelium (RPE), whereas intravitreal injection at P5 or P8 of ShH10^{Y445F}.CMV.*GFP* efficiently transduces MGCs. Based on this knowledge, AAV-mediated h*CRB1* and h*CRB2* gene therapy were explored in P5 *Crb1* mutant rats.

3

Results

The spontaneous mutation in Crb1 in brown Norway rats leads to retinal dysfunction and vision impairment

To study the retinal function of the Brown Norway rats with a spontaneous mutation in the *Crb1* gene, we performed electroretinography (ERG) in 1-, 3- and 5-month-old *Crb1* mutant rats compared to age-matched control Brown Norway rats without a mutation in *Crb1*. One-month-old *Crb1* mutant rats showed significantly reduced a- and b-wave responses under scotopic conditions (Figure 1A, C). In addition, a significant reduction in photopic b-wave was observed (Figure 1C, D). Finally, there was a significantly reduced flicker amplitude response in *Crb1* mutant rats compared to age-matched control rats in range A and B, indicating aberrations in the rod pathway

and cone pathway, respectively (Figure 1E). At 3 and 5 months of age, the retinal degeneration continued in the *Crb1* mutant rats and the ERG response was further reduced compared to the age-matched control rats (Supplemental Figure 1).

In addition, the visual function was determined using an optomotor response test (optokinetic head tracking response (OKT)). The OKT measures spatial frequency threshold, also called visual acuity, by systematically increasing the spatial frequency of the grating at 100% contrast until the animals no longer perform head tracking. In addition, contrast sensitivity can also be measured, where the minimum contrast that generated a tracking response was identified over a range of spatial frequencies [14, 15]. Three-month-old *Crb1* mutant rats showed a significantly decreased OKT spatial frequency, indicating a loss in visual function compared to control rats (Figure 1F, G). In summary, *Crb1* mutant rats presents a severely decreased retinal function and visual function within three months of age.

First signs of retinal degeneration in Crb1 mutant rats are observed from postnatal day 10

To study the morphological phenotype of new-born *Crb1* mutant rats, histological analysis of retina sections was performed and compared to age-matched controls. No abnormalities in the retinal development and lamination were observed in P5 *Crb1* mutant rats compared with the control (Figure 2A, E). In addition, immunohistochemical analysis of P5 *Crb1* mutant and control rat retinas showed similar localization of photoreceptors in the outer nuclear layer (ONL), indicated by recoverin and rhodopsin staining (Figure 2B, F); MGC localization within the inner nuclear layer (INL), indicated by SOX9 staining (Figure 2C, G); and a continuous OLM, indicated by localization of subapical region marker PALS1 and adherens junctions marker P120-catenin (Figure 2D, H). In accordance with previous data [16], glutamine synthetase (GS), a mature MGC marker, was not yet fully expressed in the P5 control nor *Crb1* mutant retinas (Figure 2C, G).

In contrast to previous findings, where the phenotype was first observed at P15 [10], here we observed focal disruptions already at P10 in the *Crb1* mutant rat retina (Figure

2M). The phenotype includes OLM breaks (Figure 2P, arrowhead) and photoreceptor cell nuclei protrusions into the photoreceptor segment layers (Figure 2N). Interestingly, PALS1 staining is more diffuse in P10 *Crb1* mutant rats in comparison to age-matched controls (Figure 2L, P). In addition, at P10, low levels of GS were detectable and appeared similar between control and *Crb1* mutant retinas (Figure 2K, O). One-month-old control rat retinas present mature photoreceptor cells, MGCs with radial processes throughout the retinal layers and a continuous OLM (Figure 2Q–T). In contrast, the retina of *Crb1* mutant rats is severely disorganized (Figure 2U), characterized by, at the foci, intermingling of nuclei from the INL and ONL and loss of photoreceptor inner and outer segments (Figure 2V, arrowhead), misplaced SOX9-positive MGC nuclei and disorganized radial MGC processes (Figure 2W). In addition, we observed OLM breaks indicated by disruptions in PALS1 and P120-catenin staining (Figure 2X, arrowhead). Similar results were obtained in 2-months-old *Crb1* mutant rats, where focal loss of retinal lamination, OLM disruptions and photoreceptor alterations were observed [10]. Altogether, these results highlight the early-onset degenerative retinal phenotype in *Crb1* mutant compared to control rats.

The Crb1 mutant rat retina develops a progressive lack of retinal lamination

Using SD-OCT imaging, the retinal degeneration was followed in vivo at P17 and 1, 2 and 3 months of age *Crb1* mutant rats in comparison with control rats. All retinal layers were correctly laminated at all ages measured in the control rat (Figure 3A', C', E', G'). At P17, retinal lamination in *Crb1* mutant rats appeared similar to control rats (Figure 3B'). At one-month-old *Crb1* mutant rats, the retinal lamination is affected mainly at the OLM indicated by a hyperreflective ONL (Figure 3D', arrowhead). Two and three months of age *Crb1* mutant rats show a further increased retinal degeneration, indicated by a hyperreflective INL and ONL, resulting in an unclear distinction between the INL and the ONL (Figure 3F', H', arrowhead). Volume intensity projection (VIP) shows disruptions throughout the *Crb1* mutant retina (Figure 3B, D, F, H). Morphological sections of the *Crb1* mutant rats show a similar degeneration, with disruptions at the OLM and intermingling of nuclei of the INL and ONL at 1 and 3 months of age rats (Figure 2M, Q, U).

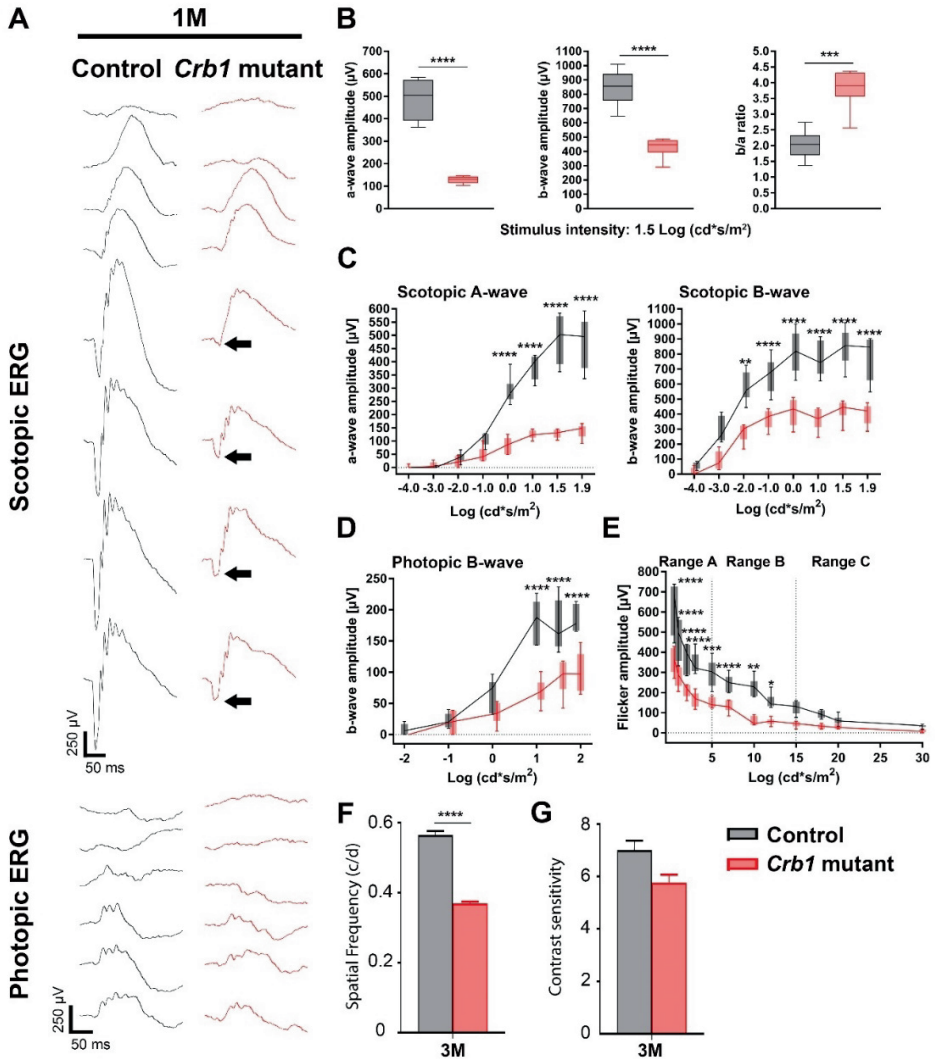


Figure 1. Significantly reduced retinal function in the *Crb1* mutant rat compared to age-matched controls. (A) Scotopic and photopic single-flash intensity series from representative rats at one month of age. The attenuated scotopic a-wave of the *Crb1* mutant rats is indicated with the black arrow. (B) Quantitative analysis of the scotopic a-wave, b-wave and b-wave/a-wave amplitude ratio (b/a ratio). Quantitative analysis of the scotopic a-wave and b-wave (C), the photopic b-wave (D) and the flicker amplitude response (E). Boxes indicate the 25 and 75% quantile range and whiskers indicate the 5 and 95% quantiles, and the intersection of line and error bar indicates the median of the data (box-and-whisker plot). Decreased visual function in 3 months of age *Crb1* mutant rats measured using the OKT spatial frequency (F) and OKT contrast sensitivity (G). Number of animals used for ERG: $n = 6$ for control and *Crb1* mutant rats; and for

OKT: control $n = 4$ and *Crb1* mutant $n = 10$. Mean \pm SEM. * $p < 0.05$; ** $p < 0.01$; *** $p < 0.001$; **** $p < 0.0001$.

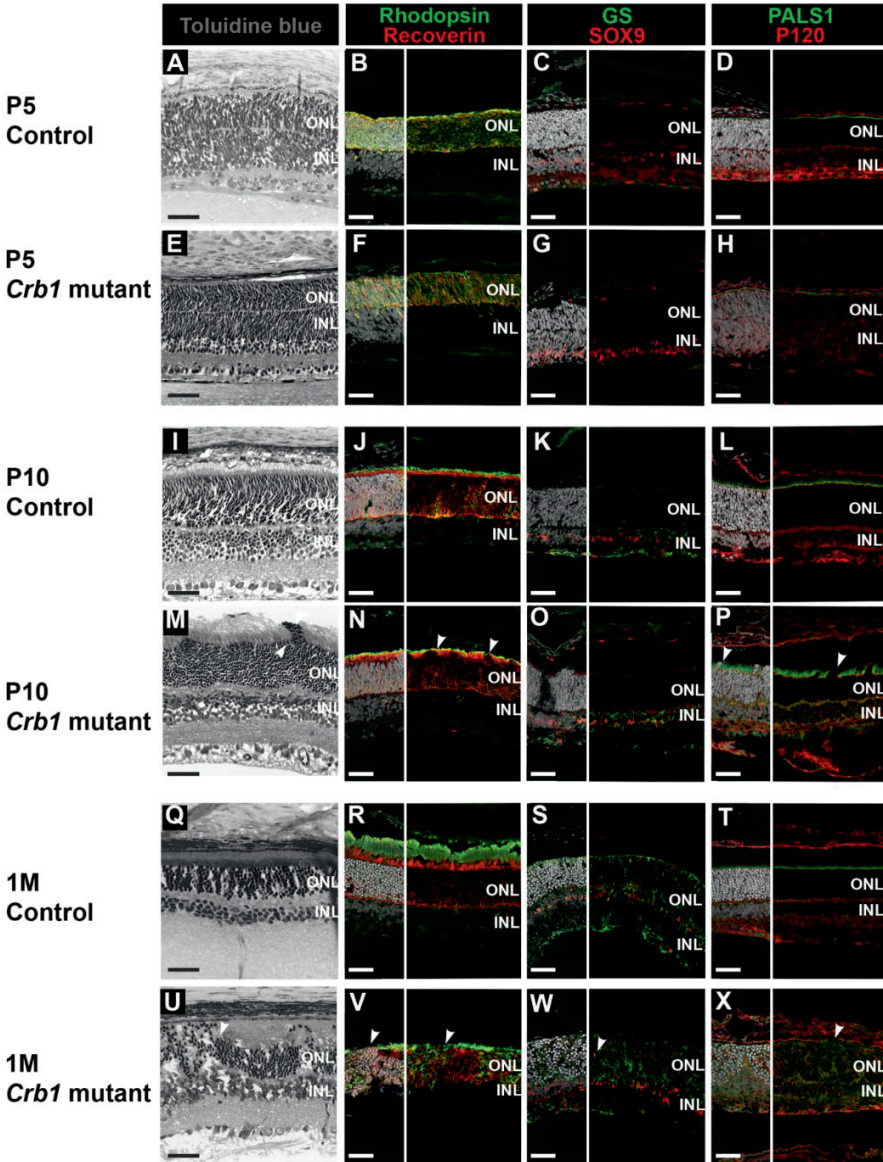


Figure 2. Retinal degeneration is observed from postnatal day 10 retinas of *Crb1* mutant rats. Light microscopy of toluidine blue-stained retinal sections from P5, P10 and 1-month-old control (A,I,Q) and *Crb1* mutant rats (E,M,U). Immunohistochemistry staining of P5, P10 and 1-

month-old retinal sections, with recoverin and rhodopsin (B,F,J,N,R,V), glutamine synthetase (GS) and SOX9 (C,G,K,O,S,W) and PALS1 with P120-catenin (D,H,L,P,T,X). No abnormalities were observed in the control retina (A-D, I-L, Q-T). In the *Crb1* mutant rats, all retinal layers were formed and properly laminated at P5 (E-H). From P10 onwards, degeneration at foci was observed in the *Crb1* mutant rat retina by photoreceptor nuclei protrusions into the photoreceptor segment layers, misplaced Müller glial cells (MGCs) and disruptions of the outer limiting membrane (OLM) (M-P,U-X; arrowheads). At least $n = 2$ eyes were used per time point. Note: GCL = ganglion cell layer; INL = inner nuclear layer; ONL = outer nuclear layer; RPE = retinal pigment epithelium. Scale bar: 40 μ m.

Quantification of the total retinal thickness at all ages revealed a significant decrease in the *Crb1* mutant compared to control rat retinas (Figure 3I). In addition, the length of disrupted and normal laminated retina was determined in both the control and *Crb1* mutant rat retina at all ages analyzed. At P17, both control and *Crb1* mutant rat retinas mainly showed a normal retinal lamination with a limited number of disruptions at the OLM and the outer plexiform layer (OPL) (Figure 3J, K). At one month of age, a significant increase in the length of degenerated retina were observed, indicated by OLM breaks (Figure 3J) or disruptions at the OPL in the *Crb1* mutant rats (Figure 3K). Finally, at two and three months of age, the length of areas of INL and ONL disruptions increased in the *Crb1* mutant rats (Figure 3L). Altogether, these data demonstrate the early-onset severe degenerative phenotype observed in *Crb1* mutant rats over time.

Ultra-structural localization of CRB1 and CRB2 proteins in the control and Crb1 mutant rat retina

CRB1 and CRB2 localization was studied by immunohistochemistry in the P5 control and *Crb1* mutant rat retinas. Canonical CRB1 was found at the OLM in control rats, while the CRB1^{INDEL} protein was below the detection level in the *Crb1* mutant rat retina (Figure 4A, B). CRB2 was detected at the OLM in both control and *Crb1* mutant rats (Figure 4C, D). Interestingly, the CRB2 staining is more diffuse in the *Crb1* mutant in comparison to control rats (Figure 4C, D). In addition, the onset of retinal function loss in the *Crb1* mutant rats is remarkably faster than in mice lacking CRB1 (*Crb1*^{KO}), mice carrying a missense CRB1 mutation (*Crb1*^{KO/C249W}) or the naturally occurring *Crb1* rd8 mouse [3,5,17,18]. Previously, we found that CRB1 or CRB2 proteins localized differently in adult human retina, fetal human retina, human iPSC-derived retinal

organoids and non-human-primate retina compared to mouse retina [8,19]. For that reason, we performed immuno-electron microscopy to determine the localization of canonical CRB1 and CRB2 in the control compared to *Crb1* mutant rat retinas. In control rats, CRB1 was abundantly present at the subapical region in MGCs but not photoreceptors at both P17 and 3 months of age (Figures 4E, G and 5A), while the CRB1^{INDEL} variant protein in *Crb1* mutant rats was only sporadically and at very low levels detected at the subapical region in MGCs (Figure 4F, H). For CRB2, a different pattern was observed: CRB2 is present at the subapical region of the MGCs and photoreceptors in both control and *Crb1* mutant retinas (Figures 4I–L and 5B). The cellular localizations of CRB1 and CRB2 are therefore similar in the mouse and rat.

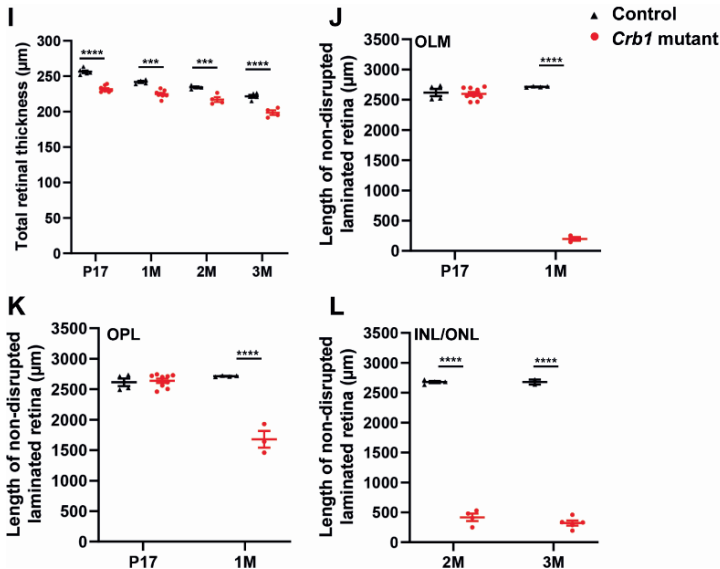


Figure 3 (I -L). *In vivo* imaging of *Crb1* mutant rats show increased retinal degeneration over time. Quantifications of total retinal thickness (I), length of non-disrupted laminated retina at the OLM in P17 and 1-month-old control and *Crb1* mutant rats (J), at the OPL (K), and in 2 and 3 months of age rats at the INL/ONL (L). Arrowheads indicate regions of retinal disorganization. Number of animals used for P17 (control $n = 6$, *Crb1* mutant $n = 9$), 1M (control $n = 4$, *Crb1* mutant $n = 9$), 2M (control $n = 4$, *Crb1* mutant $n = 4$), 3M (control $n = 2$, *Crb1* mutant $n = 5$). Values are presented as the mean \pm SEM. *** $p < 0.001$, **** $p < 0.0001$. Note: INL = inner nuclear layer; ONL = outer nuclear layer; OPL = outer plexiform layer; RPE = retinal pigment epithelium.

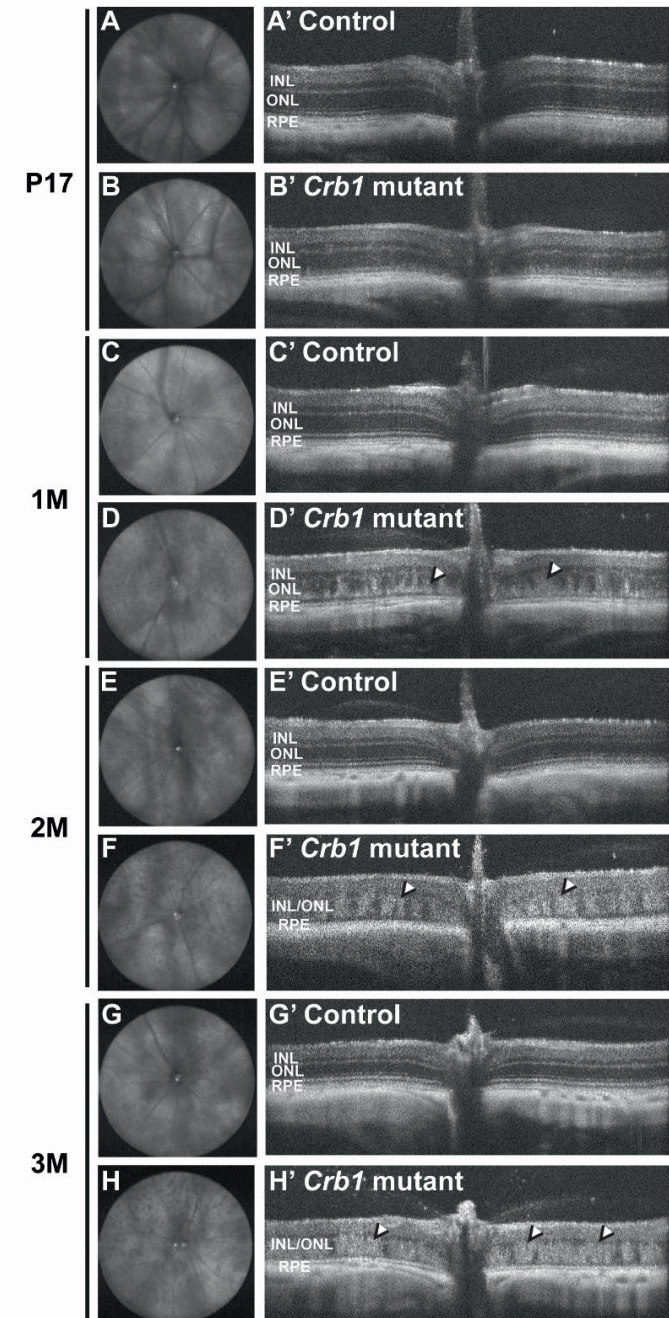


Figure 3 (A – H). *In vivo* imaging of *Crb1* mutant rats show increased retinal degeneration over time. Volume intensity projection (VIP) of the P17, and 1, 2, and 3 months of age control (A, C, E, G) and *Crb1* mutant (B, D, F, H) rat retinas; and SD-OCT B-scans of the P17 and 1, 2, and 3 months of age control (A', C', E', G') and *Crb1* mutant rat retinas (B', D', F', H').

Adeno-associated viral vector (AAV) tropism in young Brown Norway rat retina

To define the tropism of different AAV capsids, 1 μL of 1×10^{13} gc/mL AAV2.CMV.GFP expression vectors packaged into three different AAV serotypes (AAV2/5.CMV.GFP, AAV2/9.CMV.GFP and AAV2/ShH10^{Y445F}.CMV.GFP; called from now on AAV5, AAV9 and ShH10Y, respectively) were intravitreally or subretinally injected before retinal degeneration in P5 and P8 in control and *Crb1* mutant rat retinas. One month after injection, eyes were collected and analyzed using immunohistochemistry. Differences in retinal tropism were observed using the distinct application methods in new-born control and *Crb1* mutant rats; a summary of the tropism in the different serotypes, routes and time points of delivery is shown in Table 1. Interestingly, no difference in tropism was observed between control and *Crb1* mutant rats, nor the time point of the injection (P5 or P8; Table 1).

Subretinal injection of AAV5 and AAV9 at both P5 and P8 resulted in predominantly transduced RPE and photoreceptors, whereas intravitreal injection of both serotypes showed transduction of photoreceptors and, to a lesser extent, transduction of INL cells (Figure 6A–P). Furthermore, subretinal injection of ShH10Y demonstrated infection of RPE cells, photoreceptors and MGCs (Figure 6Q, R, U, V), while intravitreal injection of ShH10Y resulted mainly in transduction of MGCs and other cell types in the INL (Figure 6S, T, W, X). Co-staining with GS confirmed the transduction of mainly MGCs with all ShH10Y injections performed (Supplemental Figure 2).

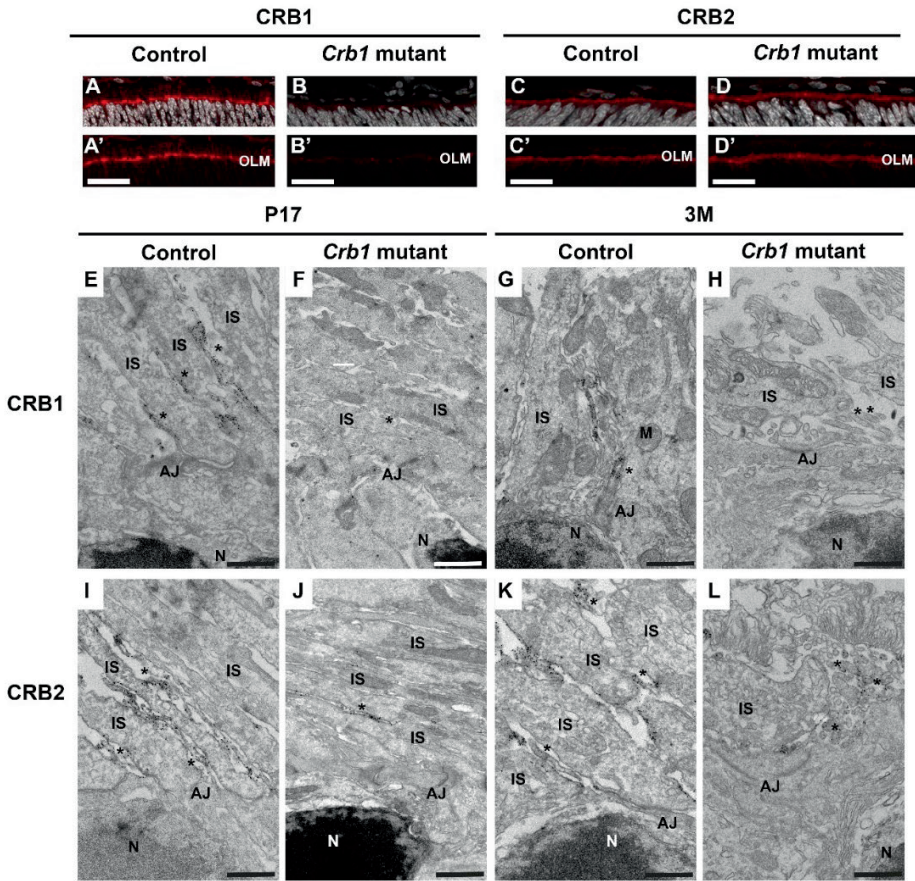


Figure 4. CRB1 is present at the subapical region (SAR) of MGCs in control rats while CRB2 is present at the SAR of both photoreceptors and MGC in control and *Crb1* mutant rats. (A–D) Immunohistochemical analysis of CRB1 (A,B) and CRB2 (C,D) in P5 control and *Crb1* mutant rats at the OLM. (E–L) Subcellular localization of CRB1 and CRB2 in control and *Crb1* mutant rats using immuno-electron microscopy. CRB1 is present at the SAR of MGC in both P17 (E) and 3M control retina (G), while the mutant CRB1^{INDEL} variant protein in *Crb1* mutant rats is sporadically detectable in P17 (F) and 3M (H). F and H show representative images lacking detectable label. CRB2 is present at the SAR of MGCs as well as photoreceptors in both control and *Crb1* mutant rat retinas at both ages (I–L). *n* = 2 animals used per time point. Note: AJ = adherens junctions; IS = inner segments; INL = inner nuclear layer; M = mitochondria; N = nucleus; OLM = outer limiting membrane; ONL = outer nuclear layer; * = Müller glial cell villi. Scale bars (A–D) = 20µm, (E–L) = 1µm.

Table 1. Summary of the retinal tropism of three different adeno-associated viral vector (AAV) serotypes, namely, AAV5, AAV9 and ShH10Y, injected via two different routes of delivery at P5 or P8 in control and *Crb1* mutant rat retina. For each serotype and route of delivery, a dose of $\sim 1 \times 10^{13}$ gc/mL was injected in a volume of 1 μ L. Quantified data are presented as follows: no GFP positive (-); 1 GFP positive (+/-); 2–5 GFP positive (+); 6–10 GFP positive (++); 11–15 GFP positive (+++); and ≥ 16 GFP positive cells (++++) per 100 μ m. Number of animals analysed: AAV5 control P5 SR $n = 6$, P5 IV $n = 2$, P8 SR $n = 2$, P8 IV $n = 2$, AAV5 *Crb1* mutant P5 SR $n = 4$, P5 IV $n = 3$, P8 SR $n = 2$, P8 IV $n = 5$; AAV9 control P5 SR $n = 3$, P5 IV $n = 2$, P8 SR $n = 3$, P8 IV $n = 3$, AAV9 *Crb1* mutant P5 SR $n = 4$, P5 IV $n = 3$, P8 SR $n = 2$, P8 IV $n = 3$; ShH10Y control P5 SR $n = 2$, P5 IV $n = 6$, P8 SR $n = 2$, P8 IV $n = 5$, ShH10Y *Crb1* mutant P5 SR $n = 3$, P5 IV $n = 4$, P8 SR $n = 2$, P8 IV $n = 3$. Note: DOI = date of injection; TOI = type of injection; GCL/RNFL = ganglion cell layer; RNFL = retinal nerve fiber layer; INL = inner nuclear layer; ONL = outer nuclear layer; RPE = retinal pigment epithelium; SR = subretinal injection; IV = intravitreal injection.

AAV	DOI	TOI	GCL/RNFL	INL	ONL	RPE	
AAV5	P5	SR	-	-	++	+	Control
	P5	SR	-	-	+	+	<i>Crb1</i> mutant
	P5	IV	-	+/-	+/-	-	Control
	P5	IV	-	-	+	-	<i>Crb1</i> mutant
	P8	SR	-	+/-	+++	+	Control
	P8	SR	-	-	+++	+	<i>Crb1</i> mutant
	P8	IV	-	-	+	-	Control
	P8	IV	-	+	+/-	-	<i>Crb1</i> mutant
AAV9	P5	SR	-	-	++	+	Control
	P5	SR	-	-	+++	+	<i>Crb1</i> mutant
	P5	IV	-	++	+/-	-	Control
	P5	IV	+/-	+	-	-	<i>Crb1</i> mutant
	P8	SR	-	-	+++	+	Control
	P8	SR	-	-	+++	+	<i>Crb1</i> mutant
	P8	IV	-	+/-	--	-	Control
	P8	IV	-	+/-	-	-	<i>Crb1</i> mutant
ShH10Y	P5	SR	-	+	+	+	Control
	P5	SR	-	+	+	+	<i>Crb1</i> mutant
	P5	IV	-	+++	+/-	-	Control
	P5	IV	-	++	+	-	<i>Crb1</i> mutant
	P8	SR	-	+	+	+	Control
	P8	SR	-	+	+	+	<i>Crb1</i> mutant
	P8	IV	-	++	-	-	Control
	P8	IV	-	++	+/-	-	<i>Crb1</i> mutant

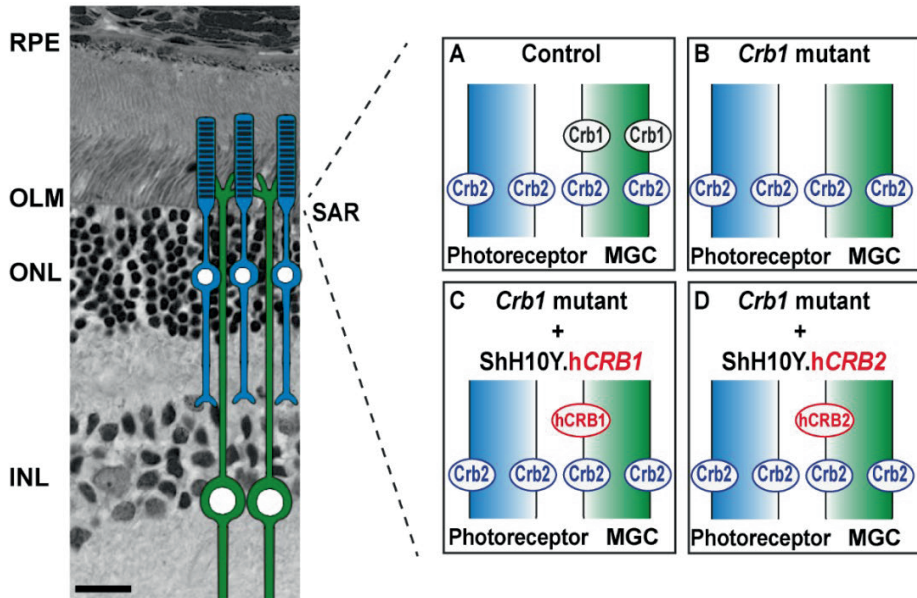


Figure 5. Graphical representation of subcellular localization of Crb1 and Crb2 proteins in Brown Norway rat retina and gene therapy approach using ShH10Y.hCRB1 and ShH10Y.hCRB2. Graphical representation of the subcellular localization of Crb1 and Crb2 in control (A) and *Crb1* mutant (B) rat retinas. Graphical representation using AAV-mediated gene therapy vectors targeting MGCs using ShH10Y-hCRB1 (C) and ShH10Y-hCRB2 (D). Scale bar: 20 μ m. Note: RPE = retinal pigment epithelium; OLM = outer limiting membrane; ONL = outer nuclear layer; INL = inner nuclear layer; SAR = subapical region; MGC = Müller glial cell.

Intravitreal delivery of ShH10Y.hCRB1 or ShH10Y.hCRB2 at P5 does not increase the retinal function in Crb1 mutant rats

Based on the subcellular localization of CRB1 and the tropism of different AAV capsids, we determined that intravitreal injection of ShH10Y is the most suitable viral vector to infect MGCs and explore gene therapy possibilities in *Crb1* mutant rats (Figure 5C, D). In addition, tropism studies in both control and *Crb1* mutant rats show that larger stretches of the retina are transduced when intravitreally injected at P5 with ShH10Y (Supplemental Figure 3A, B). For that reason, the *Crb1* mutant rats were injected at P5, with ShH10Y either with hCRB1 (ShH10Y.hCRB1) or hCRB2 (ShH10Y.hCRB2) and the other eye was injected with PBS (mock control).

Immunohistochemical analysis of 3-month-old *Crb1* mutant rats injected at P3 with ShH10Y.h*CRB1* show expression of h*CRB1* above the OLM (Supplemental Figure 3C). In addition, rats injected with ShH10Y.h*CRB2* reveal a remaining CRB2 localization at the OLM similar to the uninjected condition (Supplemental Figure 3D). The visual and retinal function were measured by OKT in 3-month-old, and ERG at 2- and 3-month-old *Crb1* mutant rats. No significant differences were observed in visual function, as measured by the OKT spatial frequency, between untreated, PBS-, ShH10Y.h*CRB1*- or ShH10Y.h*CRB2*-treated eyes at 3 months of age (Figure 7A). In addition, no significant difference in retinal function as measured by ERG was observed between ShH10Y.h*CRB1*-treated and PBS-injected eyes (Figure 7B, C). However, an increase in OKT contrast sensitivity at 0.092 c/d spatial frequency was observed in 3-month-old *Crb1* mutant rats injected with ShH10Y.h*CRB2* compared to PBS-injected rats (Figure 7A). In addition, an increased ERG response at high dark-adapted intensities (1.5 and 1.9) on the a-wave amplitude for rod photoreceptor transmission was observed in *Crb1* mutant rats treated with ShH10Y.h*CRB2* (Figure 7C).

When the retinal function within individual rats was analyzed in 2- and 3-months-old *Crb1* mutant rats, no significant differences were observed between ShH10Y.h*CRB1* and their PBS-injected eyes for both the scotopic a- and b-wave (Figure 7D and Supplemental Figure 3E). In addition, no differences were observed when treated with ShH10Y.h*CRB2* (Figure 7E and Supplemental Figure 3F). Interestingly, we observed high variations on the scotopic ERG responses between individual animals measured injected with PBS, ShH10Y.h*CRB1* or ShH10Y.h*CRB2* (a-wave range 10–100 μ V; b-wave range 50–300 μ V; Figure 7D,E); similar variations were observed when the response of the right and left eye of untreated *Crb1* mutant rats were compared (a-wave range 10–100 μ V; b-wave range 100–300 μ V; Figure 7F), indicating a variability in the scotopic ERG response between different *Crb1* mutant litters. Because of the absence of an enhanced retinal function after gene therapy delivery, we hypothesize that the injection with our viral vectors at P5 does not allow timely expression of the h*CRB1* or h*CRB2* transgenes before the onset of loss of visual or retinal function in the *Crb1* mutant rats.

As postnatal day 5 might be too close to the onset of retinal degeneration, attempts to treat the *Crb1* mutant rat earlier has been made. However, treatment with AAV2/ShH10^{Y445F}.CMV.*GFP* is only efficient when sufficient number of Müller glial cells are born to become targeted by the vectors. Previous research of murine development have shown that approximately 50% of the Müller glial cells are born at P3 [42], which might just be sufficient to rescue the observed retinal phenotype. Immunohistochemical analysis of one-month old *Crb1* mutant rat retinas injected intravitreally at P3 with ShH10.*GFP* (1 μ l of 1x10¹³ gc/ml) showed efficient Müller glial cell transduction (Supplemental Figure 4A). No significant differences were observed in visual function, as measured by OKT spatial frequency nor with 0.092c/d contrast sensitivity, between eyes injected at P3 with ShH10Y.h*CRB1* or ShH10Y.h*CRB2* compared to uninjected at 3M of age (Supplemental Figure 4B). Retinal function, measured by ERG, showed for all eyes a significantly decrease in retinal function at 3M (Supplemental Figure 4C, D). Moreover, when individual ERG responses were compared, a significantly decreased ERG response for both ShH10Y.h*CRB1* treated eyes (Supplemental Figure 4E) as well as ShH10Y.h*CRB2* treated compared to their other untreated eye was observed at 3M (Supplemental Figure 4F). AAV treated a-wave response (range 10-100 μ V) and b-wave responses (range 10-250 μ V) were lower in all animals compared to their uninjected eye. Indicating that the surgical technique at P3 could be damaging for the development of electrical activity in response to a light stimulus. To determine whether this is true, one eye was intravitreally injected with 1 μ l PBS while the other eye was left untreated. Even though no differences were observed in visual function response measured by OKT at 3M (Supplemental Figure 4B), a decreased retinal function measured by ERG was observed in the PBS injected eye in almost all individual animals at 3M of age (Supplemental Figure 4G). Altogether, these results indicate that at P3 the surgical technique might be damaging to the *Crb1* rat retina, which could be a reason why no improved visual response was observed during *CRB*-gene therapy at P3.

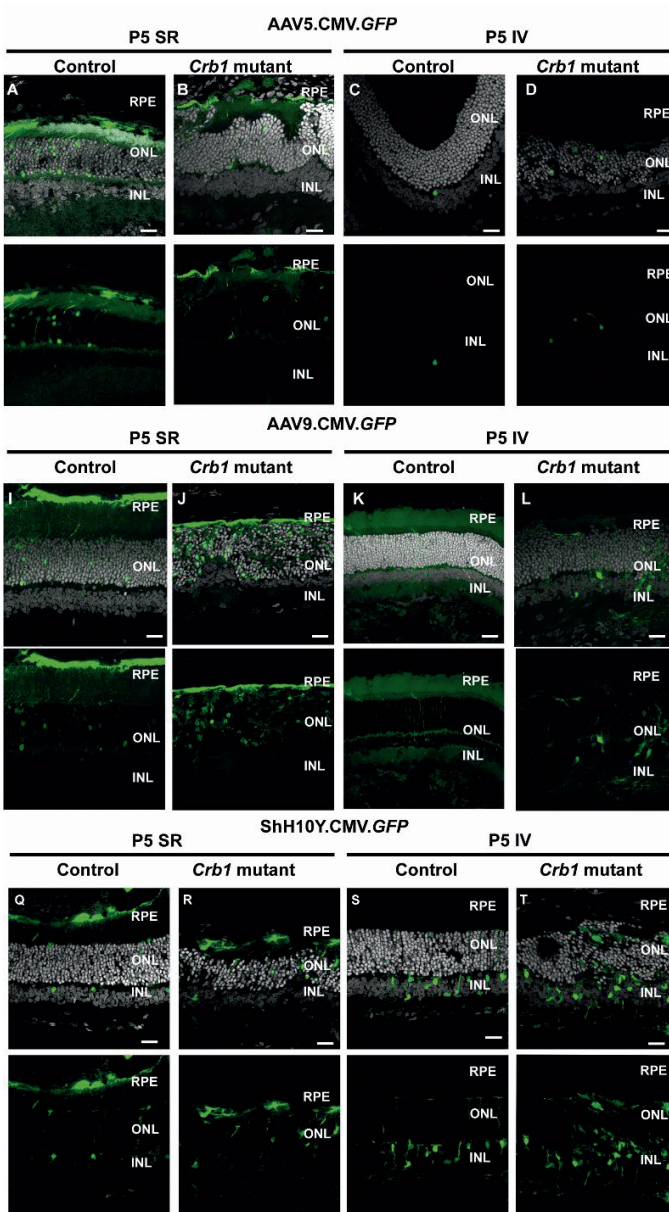


Figure 6 (A-D, I-L, Q-T). Retinal tropisms of AAV5, AAV9 and ShH0Y in new-born *Crb1* mutant and control rat retinas. P5 or P8 control and *Crb1* mutant rats were injected subretinally (SR) or intravitreally (IV) with either AAV5-, AAV9- or ShH10Y.CMV.GFP and analysed at 1 month of age. *Legend continues on the next page.*

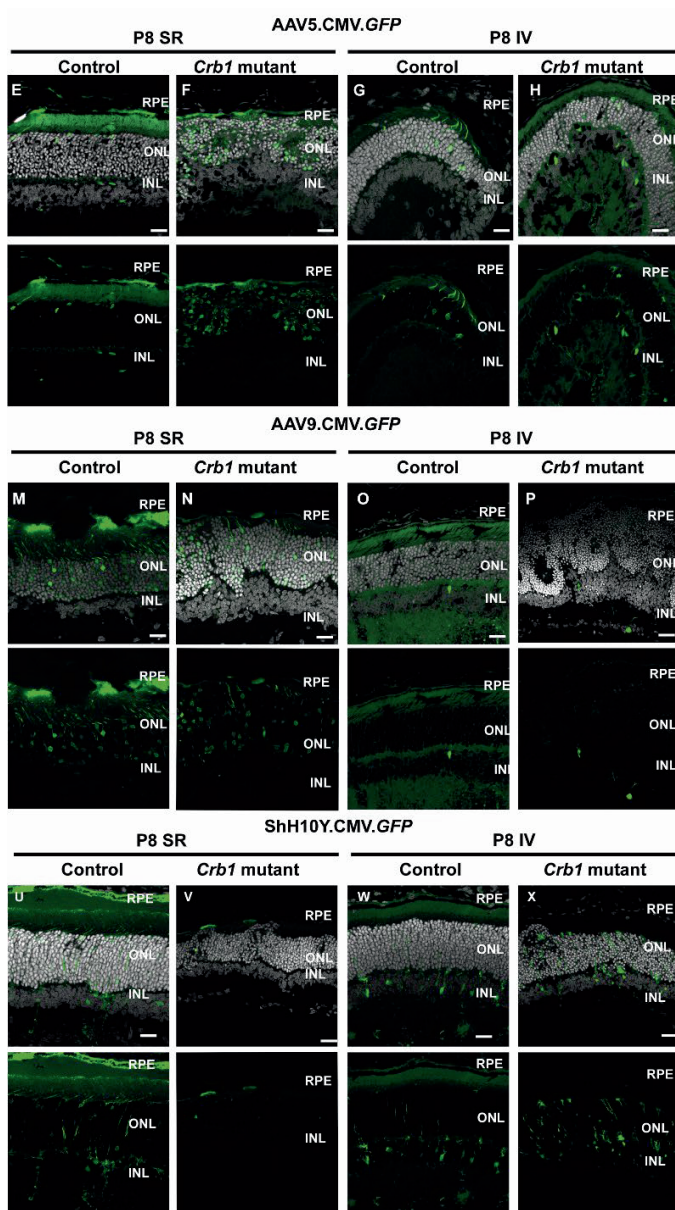


Figure 6 (E-H, M-P, U-X). Retinal tropisms of AAV5, AAV9 and ShH0Y in new-born *Crb1* mutant and control rat retinas. P5 or P8 control and *Crb1* mutant rats were injected subretinally (SR) or intravitreally (IV) with either AAV5-, AAV9- or ShH10Y.CMV.GFP and analysed at 1 month of age. *Legend continues on the next page.*

Figure 6. Retinal tropisms of AAV5, AAV9 and ShH10Y in new-born *Crb1* mutant and control rat retinas. Tropism studies show that SR injection of AAV5 and AAV9 mainly infect RPE and photoreceptors at P5 (A,B,I,J); similar results were obtained when injected at P8 (E,F,M,N). IV injection at P5 of AAV5 and AAV9 show mainly infection of sporadic photoreceptors and some INL cells (C,D,K,L); similar results were obtained when injected at P8 (G,H,O,P). SR injection of ShH10Y at both P5 and P8 in control and *Crb1* mutant retinas results in infection of RPE, photoreceptors and INL cells (Q,R,U,V); analysis of IV injection of ShH10Y at both P5 and P8 show transduction of INL cells (S,T,W,X). For each serotype and route of delivery, a dose of $\sim 1 \times 10^{13}$ gc/mL was injected in a volume of 1 μ L. Scale bar: 20 μ m. Number of animals analysed: AAV5 control P5 SR $n = 6$, P5 IV $n = 2$, P8 SR $n = 2$, P8 IV $n = 2$, AAV5 *Crb1* mutant P5 SR $n = 4$, P5 IV $n = 3$, P8 SR $n = 2$, P8 IV $n = 5$; AAV9 control P5 SR $n = 3$, P5 IV $n = 2$, P8 SR $n = 3$, P8 IV $n = 3$, AAV9 *Crb1* mutant P5 SR $n = 4$, P5 IV $n = 3$, P8 SR $n = 2$, P8 IV $n = 3$; ShH10Y control P5 SR $n = 2$, P5 IV $n = 6$, P8 SR $n = 2$, P8 IV $n = 5$, ShH10Y *Crb1* mutant P5 SR $n = 3$, P5 IV $n = 4$, P8 SR $n = 2$, P8 IV $n = 3$.

Discussion

In this study, we demonstrate (1) progressive retinal degeneration in *Crb1* mutant rats, causing loss of visual and retinal function; (2) ultrastructural localization of CRB1 at the subapical region of MGCs, and CRB2 at the subapical region of MGCs and photoreceptors in control rats; (3) a decrease in CRB1^{INDEL} at the subapical region of MGCs in *Crb1* mutant rats; (4) tropism by subretinal and intravitreal application of AAV5, AAV9, and ShH10Y in control and *Crb1* mutant rats; and (5) AAV-hCRB1 gene therapy at P5 for MGCs of *Crb1* mutant rats does not result in a functional rescue.

The *Crb1* mutant rats exhibit a significant decreased ERG response at 1 month of age in comparison with age-matched control rats, which is in accordance with previously published results comparing the *Crb1* mutant to BN-Harlan rats [10]. We further expand the characterization of the *Crb1* mutant rat strain by showing a reduced OKT spatial frequency response in 3-month-old *Crb1* mutant rats compared to age-matched control rats. Interestingly, although the control rats show a reduced ERG response from 1 month of age onwards, the OKT spatial frequency decline is minor. This discrepancy has been described before, where similar spatial frequencies only declined months after significant photoreceptor and ERG response loss [20].

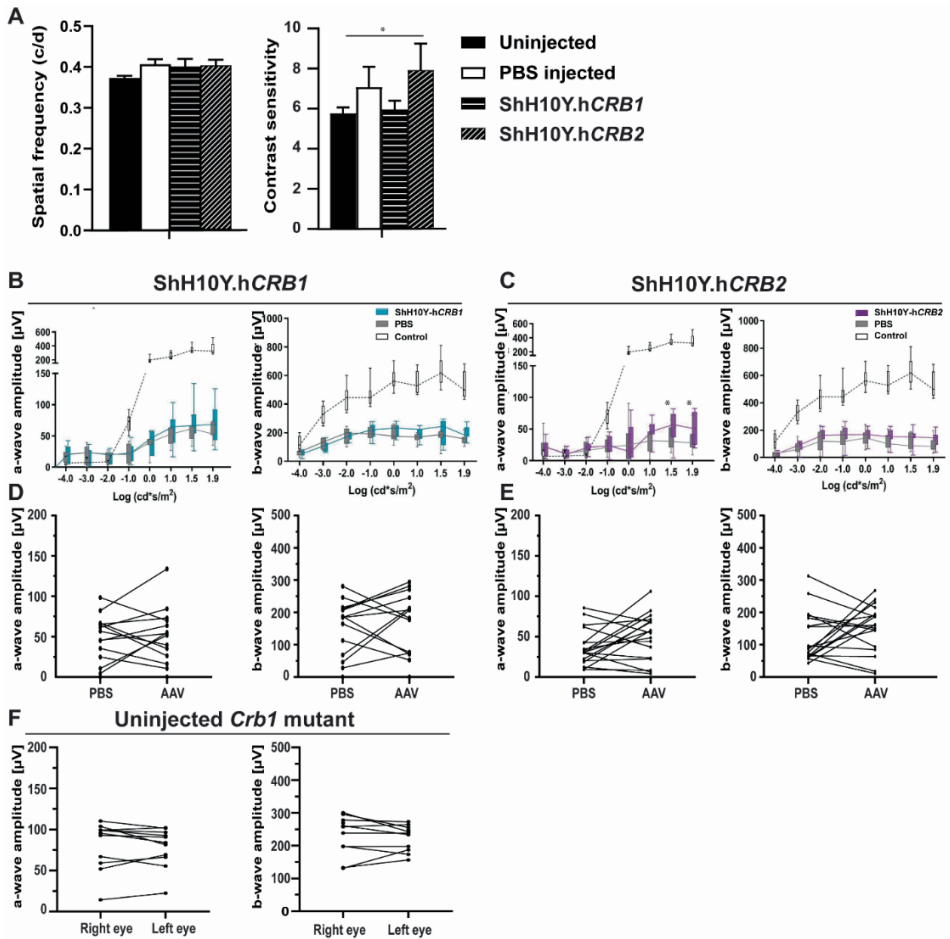


Figure 7. Retinal function in 3M rats after intravitreal injection at P5 of ShH10Y.hCRB1 or ShH10Y.hCRB2 is not restored. (A) OKT spatial frequency and 0.092 contrast sensitivity of 3M rats injected with PBS, ShH10Y.hCRB1, or ShH10Y.hCRB2. (B,C) Quantification of all scotopic a- and b-wave ERG at 3M of the group of rats injected with ShH10Y.hCRB1 (B) or ShH10Y.hCRB2 (C) with uninjected eye and a wild-type as the controls. (D,E) 1.5 stimulus intensity ERG at 3M comparison of individual rats injected with either ShH10Y.hCRB1 (D) or ShH10Y.hCRB2 (E) compared with PBS-injected eyes. (F) 1.5 stimulus intensity ERG at 3M comparison of the left and right eye of non-injected *Crb1* mutant rats. Boxes indicate the 25 and 75% quantile range and whiskers indicate the 5 and 95% quantiles, and the intersection of line and error bar indicates the median of the data (box-and-whisker plot). * $p < 0.05$. Number of animals used: ShH10Y.hCRB1 $n = 7$, 3M OKT and $n = 15$ 3M ERG; and for ShH10Y.hCRB2 injected $n = 15$ 3M OKT, and $n = 18$ 3M ERG. Mean \pm SEM.

Here, we observed the first signs of retinal degeneration from P10 in the *Crb1* mutant rat retina, including photoreceptor nuclei protrusions in the photoreceptor segment layers and OLM breaks at foci throughout the entire retina. These disruptions are ultimately resulting in large regions with a complete disorganized ONL and INL lamination in adult *Crb1* mutant rats. Interestingly, the phenotype at P10 in the *Crb1* mutant rats is comparable to previously described *Crb1* mouse models [3,17], but the retinal phenotype in these rats at 1 month of age is much more severe. In addition, in *Crb1* mouse models, the retinal degeneration is limited to the inferior quadrant [3,17], whereas in the *Crb1* mutant rats it is presented throughout the entire retina. These discrepancies could be because of (1) different genetic backgrounds, including species differences; (2) different types of mutations affecting different CRB isoforms [21,22], thereby expressing a distinct CRB1^{INDEL} protein in the *Crb1* mutant rats; or (3) the total expression levels of CRB2 might be significantly lower in new-born rats compared to new-born mice. Decreased levels of CRB2 or dysregulation of other CRB-interacting proteins could result in less stabilization of the adherens junction complex at the OLM, resulting in a more severe phenotype. In addition, transcriptomic analysis identified several dysregulated pathways in *Crb1* mutant rats, such as TGF- signaling, matrix metalloproteinases, type II interferon signaling, MAPK cascade, inflammatory pathways, regulation of actin cytoskeleton and many more [10]. More research is required to define which factors play a major role in the retinal degeneration in these *Crb1* mutant rats.

SD-OCT imaging allows to follow the retinal degeneration over time in *Crb1* mutant compared to age-matched control rat retinas. Previous research using SD-OCT with *Crb1* rd8 or *Crb1*^{lowMGC} mouse models show typical ocular lesions, such as pseudo-rosette formation [13,23,24]. Here, we observed a relatively healthy retinal lamination in P17 *Crb1* mutant rat retina with some sporadic disruptions at the OLM. At one month of age, the retinal lamination is disrupted throughout the retina, indicated by hyperreflective regions at the ONL. These hyperreflective disruptions are thought to begin in the OLM because of adhesion abnormalities between the photoreceptor and MGCs. Over time, in 2- and 3-month-old rats, an increased degeneration with larger hyperreflective regions, indicating a potential lack of retinal lamination, is observed.

Similar results were obtained using histological sections. Like human *CRB1*-RD patients [24], hyperreflective lesions of various sizes were observed in the *Crb1* mutant rat starting at 1 month of age. The hyperreflective ONL and INL in the *Crb1* mutant rats made automated as well as manual segmentation of the layers challenging, particularly at 2 and 3 months of age. Therefore, we quantified the length of the observed disruptions and compared it to the length of the retinal view, hereby distinguishing between the length of disrupted and normal laminated retinas. Quantification of the data showed a significant increase in OLM breaks and disruptions at the OPL in the *Crb1* mutant compared to age-matched control rats at 1, 2 and 3 months of age. Several researchers have shown that quantification of retinal layer size by SD-OCT, compared with histological sections, contain less variations, presumably due to artefacts from the post-mortem processing [25]. Altogether, these data are showing the importance of the SD-OCT imaging over time in *Crb1* mutant rats.

Immunohistochemical analysis reveal the localization of CRB2 at the subapical region (SAR) in control and *Crb1* mutant rats, while canonical CRB1 is only detected at the SAR of control rats. The CRB1 antibody used detects the carboxyl terminus of the CRB1 protein, and our data show that the *Crb1* mutant rats lack the full length CRB1 at the OLM. In control rats, subcellular localization of CRB1 and CRB2 by immunoelectron microscopy revealed the presence of CRB1 at the SAR adjacent to the adherens junctions in MGCs, and of CRB2 at the SAR in both MGCs and photoreceptors. These data correspond well to the localization previously found in mouse studies [26]. In postmortem human cadaver retinas, however, CRB1 localized at the subapical region in both MGCs and photoreceptor. In these studies, CRB2 localized at the SAR in MGCs, with CRB2 localized at vesicles in the photoreceptor inner segments [12,27]. Interestingly, recent data revealed the subcellular localization of both CRB1 and CRB2 at the SAR of MGCs as well as photoreceptors in human iPSC-derived retinal organoids, second trimester human fetal retina and non-human-primate retinas [8,19]. The cellular localization of CRB1 and CRB2 in Brown Norway rats are therefore only similar to mice.

The *Crb1* gene locus is complex with various *Crb1* splice forms and gene products from alternate promoters, such as *Crb1*-B [17,21,28]. Full-length canonical *Crb1* is encoded on 12 exons with the highly conserved CRB1 carboxyl terminus encoded on exon-12, whereas the *Crb1*-B lacks the conserved carboxyl terminus since encoded on 5'-alternate exon-5a, 6–11 alternate-3' [21]. The in-frame insertion-deletion mutation in exon 6 of the *Crb1* mutant rat also affects the *Crb1*-B gene, and it is to be tested whether the mutation specifically in *Crb1*-B contributes to the observed early-onset severe retinal phenotype. Interestingly, *Crb1* rd8 mice have an out-of-frame base-pair deletion in exon-9 that causes an alternate-3' and encodes, therefore, for two truncated transcripts (upstream promoter driving expression of *Crb1* exons 1–6 indel, 7–9 alternate-3'; and a promoter in intron-5 driving expression of *Crb1* exons 5a-6indel, 7–9 alternate-3') [17]. However, the mutation affecting these two gene products from *Crb1* rd8 do not result in a severe retinal degeneration as observed in the *Crb1* mutant rats, suggesting the existence of other modifying factors that play a role in the severity of the retinal phenotype. Reduced levels of CRB2 in MGCs and/or photoreceptors or retinal progenitors in mice lacking CRB1 result in a significant more severe retinitis pigmentosa or Leber congenital amaurosis retinal phenotype [8,27]. Altogether, these data suggest the existence of other modifying factors that play a role in the severity of the retinal phenotype observed in *Crb1* mutant rats. It remains of interest to test whether low levels of CRB2 contribute to the early-onset severe retinal phenotype observed in new-born *Crb1* mutant rats, whereas high levels of CRB2 might suppress the onset of retinal phenotype in *Crb1* mice.

For AAV-mediated gene therapy purposes, in new-born *Crb1* mutant rats, we determined the retinal tropism of three different AAV serotypes (AAV5, AAV9, ShH10Y) upon different routes of AAV delivery. The AAV capsids were injected at different time points (P5 or P8), either subretinal or intravitreal, in both control and *Crb1* mutant rats. Even though retinal injection efficiency can vary between animals, the transduced layers of cells with a specific capsid and type of injection was similar between animals injected at the two different time points. With subretinal delivery, the serotypes AAV5 and AAV9 successfully transduced the RPE and photoreceptors in new-born control and *Crb1* mutant rats, while subretinal delivery of ShH10Y was

transducing RPE, photoreceptors, MGCs and other cell types in the INL. Subretinal delivery of AAV9 at P5 and P8 in both control and *Crb1* mutant rats results in a similar transduction pattern as observed by others after subretinal injection in two-month old Sprague-Dawley rats [29]. In addition, AAV5 tropism at P5 and P8 in control and *Crb1* mutant rats is similar as described in 6- to 8-week-old C57/BL6 wild-type mice [30]. When AAV.CMV.*GFP* vectors were injected intravitreally in new-born control and *Crb1* mutant rats, serotypes AAV5 and AAV9 showed a relatively poor transduction efficiency of both photoreceptors and other cells in the INL. Other researchers showed a poor transduction of cells in the INL as well upon intravitreal delivery of AAV2, AAV6 and AAV8 in two-month-old Sprague-Dawley rats [29]. However, we observed efficient transduction of mainly MGCs in the INL after intravitreal injection in new-born control and *Crb1* mutant rats with ShH10Y, which is consistent with previously published data obtained in the adult rat [31].

Transduction efficiency in the degenerated retina might differ from that in the healthy control retina [30,32]. However, we did not observe a difference in cellular tropism nor in the transduction efficiency between control and *Crb1* mutant rats with all serotypes and the expression vector AAV.CMV.*GFP* tested. Moreover, no differences in tropism were observed when all AAV serotypes were injected either at P5, before the onset of retinal degeneration or at P8, closer to the first signs of degeneration. This might be explained by the correctly laminated retina in the new-born *Crb1* mutant rat retina, and it is well possible that AAV tropism might differ when injected at later time points where the degeneration is more advanced. In summary, we highlight the important differences of AAV capsids and types of delivery that could be considered with future gene therapy approaches.

Finally, we explored the possibility of AAV-mediated hCRB gene therapy in *Crb1* mutant new-born rats. Based on the tropism results, we used intravitreal injection of ShH10Y-hCRB1 and ShH10Y-hCRB2 at P5 in *Crb1* mutant rats for our gene therapy experiments. The efficacy of these ShH10Y-hCRB gene therapy vectors was shown previously [12,13]. When individual untreated *Crb1* mutant rat ERG responses were analyzed at different time points, no differences were detected between the left and

right eyes within the same animal. This suggests that both eyes show similar rates of loss of retinal function.

Lack of an improved visual function after AAV-*CRB* application could be caused by the time lag for AAV-mediated gene therapy; it might take several days to weeks before the h*CRB* transgene in *Crb1* mutant rats is expressed at full level in the target cells, in this case the target cells being the MGCs. In our tropism studies, we observed upon intravitreal injection of 1 μL 1×10^{13} gc/mL ShH10Y-h*CRB* at P5 and P3 a good but potentially incomplete transduction of *Crb1* mutant rat MGCs. In other studies, an increased b-wave was observed when 10-day-old Royal College of Surgeons rats were subretinally injected with a total of 8 μL containing 4×10^8 particles (4 μL superior hemisphere and 4 μL in the inferior hemisphere) of AAV2.CMV.*Merk* to target defective RPE [33]. Whereas, in our *Crb1* mutant rat studies, 1 μL of a dose of 1×10^{13} gc/mL was injected intravitreally at P5, which might be a too low dose of ShH10Y.h*CRB1* or ShH10Y.h*CRB2* to slow down the retinal degeneration observed in the *Crb1* mutant rats. In addition, 1 μL of our gene therapy vector might not spread well throughout the entire retina. In addition, the results obtained from AAV-mediated gene augmentation therapy in P3 rats indicate that the surgical technique might be damaging to the *Crb1* rat retina. Improving the surgical application technique and to enlarge the transduced area of the retina could be considered [34]. Moreover, we observed a wide variability in ERG response between different *Crb1* mutant rat litters, likely because of the Brown Norway genetic background. Backcrossing these rats into a more defined genetic background might decrease the observed variability in retinal phenotype. In *Crb1*^{rd8/rd8} mice on a C57BL/6 genetic background, considerable variation in retinal phenotype was observed as well [35]. In addition, the injection efficiency and thereby the number of AAV viral particles taken up by the retinal cells might vary between animals. Moreover, there might be differences in intracellular release of AAV-DNA from capsids inside the targeted cells. Finally, proof-of-concept studies showed functional and structural preservation in a *Crb1* mouse model by using AAV2/9.CMV.h*CRB2* [12] or AA2/ShH10Y.CMV.h*CRB2* [13]. However, the retinal phenotypes in these mice were less severe than the one observed at 1 and 3 months of age *Crb1* mutant rats. In previous studies, we showed that human CRB2 can

compensate for the loss of endogenous Crb proteins in the mouse retina [12,13]. Here, we tested human CRB1 or CRB2 in gene therapy studies to compensate for the loss of functional Crb1 protein in the rat retina. We showed expression of hCRB1 in *Crb1* mutant rats after intravitreally injected ShH10Y-hCRB1, but we did not observe an enhanced retinal function after gene therapy delivery. *In silico* analysis show that both CRB1 and CRB2 are highly conserved proteins between rat and human (Supplemental Figure 5). Despite the high sequence similarity, proteins may have distinct species-specific properties or activity that need to be taken into account when designing gene therapy studies. Here, we did not test the application of rat *Crb1* or *Crb2* gene therapy vectors to the rat retina due to ethical issues, as the expected outcome of such experiments on a large group of rats is presumed to be negative. Therefore, we cannot exclude the possibility that rat Crb1 or Crb2 proteins could alleviate the loss of endogenous rat *Crb1* in models with slower onset of retinal degeneration. All these differences could explain the lack of functional rescue observed here; thus, future experiments could focus on the development of novel gene therapy vectors that allow immediate early-onset expression of transgenes at P5 or low molecular weight drug therapy in new-born rats, or in utero gene therapy approaches.

In conclusion, we further characterized the early-onset morphological phenotype and the retinal function of *Crb1* mutant rats in comparison to age-matched control rats. In addition, we show that the ultrastructural localization of endogenous CRB1 and CRB2 in the rat retina is similar as observed in the mouse retina. In addition, as little is known about AAV tropism administered in new-born Brown Norway rats, we showed differences in cellular tropism when three different AAV capsids were injected in both *Crb1* mutant and control rats. Finally, no timely rescue of the retinal phenotype was observed using retinal function and visual acuity, suggesting the need for earlier onset of expression of recombinant hCRB proteins in Müller glial cells to rescue the severe retinal phenotype in *Crb1* mutant rats.

Experimental procedures

Animals

Procedures concerning animals were performed in accordance with the EU Directive 2010/63/EU for animal experiments and with permission of the Dutch Central Authority for Scientific Procedures on Animals (CCD), permit number 1160020172924, approved 18, January, 2018. The animals were maintained on a 12 h day–night cycle and were supplied ad libitum with food and water. Brown Norway rats from Janvier Labs with a spontaneous mutation in the *Crb1* gene were used in this study [10]; the *Crb1* mutant rat breeding was set up within the LUMC animal facility. Age-matched control Brown Norway rats lacking the mutation in the *Crb1* gene from Charles River Laboratories were used as controls. Animals were killed by carbon dioxide inhalation.

DNA isolation and genetic analysis

The presence of spontaneous in-frame insertion-deletion (indel) in exon 6 of the *Crb1* gene was validated using DNA extraction from rat's tails by proteinase K digestion overnight at 55 °C in lysis buffer (100 mM Tris-HCl, pH 8.5, 5 mM EDTA, 0.2% SDS, and 200 mM NaCl). Biopsies were centrifuged for 15 min, the supernatant was transferred and mixed vigorously with isopropanol, followed by a 10 min centrifuge at 14,000 rpm and removal of the supernatant. Then, the pellet was washed twice with 80% ethanol, air dried for 10 min at 55 °C and subsequently resuspended in 200 µL 10% TE (10 mM Tris-HCl, pH 8.0, 1mMEDTA). Finally, DNase was inactivated for 15 min at 65°C. For genotyping, PCR with primers targeting the location of the INDEL in the *Crb1* gene was performed and was subsequently sequenced using Sanger Sequencing, FW: 5'-TTCAGACTGTTCAGCCAAATGC-3', REV: 5'-TGTCGCCATTGGTAAGCCACC-3'.

Electroretinography (ERG)

Dark- and light-adapted ERGs were performed under dim red light using an Espion E2 (Diagnosys, LLC, MA). ERGs were performed on 1, 2 and 3-month-old control and

Crb1 mutant rats. Rats were anesthetized using 100 mg/kg ketamine and 10 mg/kg xylazine intraperitoneally and the pupils were dilated using tropicamide drops (5 mg/mL). Rats were placed on a heating pad, and reference and ground platinum electrodes were placed subcutaneously and in the base of the tail, respectively. ERGs were recorded from both eyes using gold wire electrodes. Hypromellose eye drops (3 mg/mL, Teva) were given between recordings to prevent eyes from drying. Single (scotopic and photopic ERG) or brief train (Flicker ERG) white (6500k) flashes were used. The band-pass filter frequencies were 0.3 and 300 Hz. Scotopic recordings were obtained from dark-adapted animals at the following light intensities: -4, -3, -2, -1, 0, 1, 1.5 and 1.9 log cd s/m² [36]. Flicker recordings were obtained under a fixed light intensity of 0.5 log cd s/m² with varying frequency (0.5, 1, 2, 3, 5, 7, 10, 12, 15, 18, 20 and 30 Hz) [37,38]. Photopic recordings were performed following 10 min light adaptation on a background light intensity of 30 cd*s/m² and the light intensity series used was: -2, -1, 0, 1, 1.5, 1.9 log cd*s/m² [36]. The numbers of rats used per time point are indicated under the designated figure. For the gene therapy studies, responses of the treated eye, either right or left eye, were compared with the other eye, mock injected (PBS), at each time point analyzed.

Optokinetic head tracking response (OKT)

Spatial frequency and contrast sensitivity thresholds were measured using an optomotor system (Cerebral Mechanics, Lethbridge, AB, Canada). Two and three month(s)-old rats were placed on a small platform in the center of four computer monitors that formed a virtual drum with a rotating vertical sine wave grating (12°/s (d/s)), as described previously [14]. Head movements in the same direction as the rotating gratings were considered as positive responses and no response was considered as negative response. Spatial frequency thresholds were determined with an increasing staircase paradigm, starting at 0.042 cycles/deg (c/d) with 100% contrast. Contrast sensitivity thresholds were measured across three spatial frequencies (0.092 c/d). The reciprocal of the contrast sensitivity threshold was used as the contrast sensitivity value at each spatial frequency.

Morphological analysis

Eyes were collected at a range of time points from P5 to 3-month-old control and *Crb1* mutant rats (n=2-4/age/group). For morphological analysis, eyes were enucleated and fixed with 4% paraformaldehyde in phosphate buffered saline (PBS) for 20 min at room temperature. After fixation, the eyes were dehydrated for 30 min in 30, 50, 70, 90 and 99% ethanol. Subsequently, the eyes were embedded in Technovit 7100 (Kulzer, Wehrheim, Germany) and sectioned (3 μ m) as previously described [39]. Slides were dried, counterstained with 0.5% toluidine blue and mounted under coverslips using Entellan (Merk, Darmstadt, Germany). Eye sections were scanned using a Panoramic 250 digital slide scanner (3DHISTECH Ltd., Budapest, Hungary) and images were processed with CaseViewer 2.1 (3DHISTECH Ltd., Budapest, Hungary).

3

Immunohistochemical analysis

Eyes were collected at a range of time points from P5 to 3-month-old control and *Crb1* mutant rats (n = 2-4/age/group). For immunohistochemical analysis, eyes were enucleated and fixed with 4% paraformaldehyde in PBS for 20 min at room temperature. Then, the eyes were cryo-protected with 15% and 30% sucrose in PBS, embedded in Tissue-Tek O.C.T Compound (Sakura, Finetek), and used for cryosectioning. Cryosections of 8 μ m were made with a Leica CM1900 cryostat (Leica Microsystems).

Sections for immunohistochemistry were blocked for 1 h at RT in 10% normal goat serum, 0.4% Triton X-100 and 1% bovine serum albumin (BSA) in PBS. The primary antibodies were diluted in 0.3% normal goat serum, 0.4% Triton X-100 and 1% BSA in PBS and incubated in a moist chamber overnight at 4°C. After rinsing in PBS, the sections were incubated for 1h at RT with the fluorescent-labelled secondary antibodies goat anti-mouse, goat anti-rabbit or goat anti-chicken IgGs conjugated to Alexa 488, Alexa 555 (1:1000; Abcam) or Cy3 (1:500), which were diluted in 0.1% goat serum in PBS. Nuclei were counterstained with DAPI and mounted in a Vectashield Hardset mounting medium (H1500 or H1800, Vector Laboratories, Burlingame, USA).

Sections were imaged on a Leica TCS SP8 confocal microscope. Confocal images were processed with Leica Application Suite X (v3.7.0.20979).

The following primary antibodies were used: P120-catenin (1:250; BD Biosciences Cat# 610134), CRB1 AK2 (1:200; homemade), CRB2 SK11 (1:200; [3]), glutamine synthetase (GS) (1:250; BD Biosciences Cat# 610518), PALS1 (1:200; homemade), recoverin (1:500; Millipore Cat# AB5585) and rhodopsin (1:500; Millipore Cat# MAB5356), SOX9 (1:250; Millipore Cat# AB5535).

Spectral domain optical coherence tomography (SD-OCT)

P17, 1, 2 and 3 month control and *Crb1* mutant rats were anesthetized using 60 mg/kg ketamine and 60 mg/kg xylazine (50 mg/kg ketamine and 5 mg/kg xylazine for P17 rats) intraperitoneally and the pupils were dilated using tropicamide drops (5 mg/mL). Anesthetized rats were placed in front of the SD-OCT imaging device (Envisu™ R2210 VHR, Leica, USA). Eyes were kept moisturized with Vidisic Carbogel and Systane ultraeyedrops during the whole procedure. Image acquisitions were performed using the following parameters: rectangular scans of 3.2 mm by 3.2 mm, A-scans/B-scans: 1000, B-scans: 100, Frames/B-scan: 6 (for high resolution B-scans); and A-scans/B-scans: 400, B-scans: 400, Frames/B-scan: 4 (also known as the isotropic scan for an enface projection image). Thickness of retinal layers were manually measured using BiopTigen InVivoVue Reader and Diver software in the individual layers at 0.3, 0.6, 0.9 and 1.3 mm both sides from the center of the optic nerve head in the nasal-temporal direction. In addition, the length of disrupted and healthy retinal lamination was measured using Fiji ImageJ software, where the frame with the optic nerve head and 800 μ m before and after the optic nerve head in nasal-temporal directions were used for quantification. Values of the three different frames in the left and right eye were averaged and plotted in the figure together; so, one value per animal.

Immuno-electron microscopy

Immuno-electron microscopy was performed as previously described [40]. In brief, 40 μ m sections were incubated with a primary antibody for 48h, it was then incubated

with a secondary peroxidase anti-peroxidase for 4 h. After that, sections were developed in a 2,2-diaminobenzidine solution for 4–8 min, and then the gold-substitute-silver-peroxidase method was applied. Sections were then prepared for electron microscopy and overlapping images were collected using a One View Camera (Gatan) as previously described [41].

Delivery of the AAV

For tropism experiments, five days old rats were anesthetized using hypothermia and eight days old rats were anesthetized using an intraperitoneally injected with 35 mg/kg ketamine and 35 mg/kg xylazine. Eyelids were opened and eyes were popped out using surgical tools, the pupils were dilated with 1% tropicamide drops (5 mg/mL) and kept moist with Hypromellose drops. Under visualization with an operating microscope intravitreal and subretinal injections were performed in control and *Crb1* mutant rats. We used AAV2/5, AAV2/9 or AAV2/ShH10^{Y445F}, with the full-length CMV promoter, *GFP*, and bovine growth hormone polyadenylation sequence for our tropism study. For each serotype and route of delivery, a dose of $\sim 1 \times 10^{13}$ gc/mL was injected in a volume of 1 μ L using a 33-gauge blunt-tipped Hamilton syringe (Hamilton Company, Reno, NV, USA). Eyes were closed and protected with “Hansaplast liquid protection” and treated with ointment containing chloramphenicol to prevent infections.

For the gene therapy experiments, similar procedures were followed as described above. Here, one eye was treated with an AAV vector and the other eye was mock-injected (PBS); this was randomized in the left and right eye. We used intravitreal injection of ShH10Y capsids to package the AAV2 inverted terminal repeats, the full length or minimal CMV promoter (CMV, or CMVmin), *hCRB1* or *hCRB2* cDNAs and synthetic poly-adenylation sequence for our gene therapy experiments. The AAVs were spiked with 1/10 dose ShH10Y, with the full-length CMV promoter, *GFP* cDNA and bovine growth hormone polyadenylation sequence. We carefully examined the quality of our AAV-*hCRB* vector preparations by qPCR and Western blots; we recently showed before that these batches of AAV vectors worked efficiently in *hCRB* gene therapy studies [13].

Tropism quantification

Immunohistochemical slides for tropism studies were imaged on a Leica TCS SP8 confocal microscope, and sections were scanned for AAV-*GFP*-positive areas to re-confirm the subretinal or intravitreal injection and define the tropism. For each condition, 4–8 confocal images spanning the area of transduction of each eye was acquired ($n \geq 2$ independently injected eyes for each condition). Each individual confocal image was acquired at 40X magnification. The number of eGFP-positive cells within each layer were manually counted. The total number of eGFP-positive cells per eye were divided by transduction diameter to determine the number of positive cells per 100 μm . Then eyes were averaged and coded as - = 0 GFP positive cells; +/- = 1 GFP positive cell, + = 2–5 GFP positive cells, ++ = 6–10 GFP positive cells, +++ = 11–15 GFP positive cells, and ++++ for >16 GFP positive cells.

Statistical analysis

We performed statistical analysis for group comparisons: comparing the untreated *Crb1* mutant and age-matched control rats by ERG using a two-way ANOVA; comparing all AAV-treated eyes with the other untreated or PBS-injected eyes using a two-way ANOVA (at 2 and 3 months of age); comparing the AAV-treated eye with the other untreated or PBS-injected eyes using a paired t-test; and, finally, statistical analysis on SD-OCT quantifications using a two-way ANOVA. These statistical analyses were performed using GraphPad Prism version 8 (GraphPad Software). All values are expressed as the mean \pm SEM if not otherwise indicated. Statistically significant values: * $p < 0.05$; ** $p < 0.01$; *** $p < 0.001$; **** $p < 0.0001$.

Article information

Patents: The LUMC is the holder of patent application PCT/NL2014/050549, which describes the potential clinical use of CRB2; J.W. is listed as an inventor on this patent, and J.W. is an employee of the LUMC.

Author contributions: Conceptualization, N.B., C.H.A. and J.W.; formal analysis, N.B., C.H.A., A.A.M., C.A.A., C.R.J. and J.W.; funding acquisition, J.W.; investigation,

N.B., C.H.A. and J.W.; methodology, N.B., C.H.A., A.A.M., C.A.A., T.M.B. and P.M.J.Q.; project administration, J.W.; resources, T.M.B., P.M.J.Q. and R.M.V.; supervision, J.W.; validation, N.B., C.H.A., A.A.M., C.A.A., C.R.J. and J.W.; visualization, N.B.; writing - original draft, N.B.; writing - review and editing, N.B., C.H.A., A.A.M., C.A.A., T.M.B., P.M.J.Q., A.J.K., C.R.J. and J.W. All authors have read and agreed to the published version of the manuscript.

Funding: This research was funded by Foundation Fighting Blindness (TA-GT-0715-0665-LUMC, to JW), the Netherlands Organization for Health Research and Development (ZonMw grant 43200004, to JW), Bontius Stichting (Bontius 23122019 to JW) and the Dutch blindness funds (Uitzicht 2013-13 to JW, Uitzicht 2018-6 to CHA and JW): Rotterdamse Stichting Blindenbelangen, MaculaFonds, Stichting Blindenhulp, Landelijke Stichting voor Blinden en Slechtzienden, Algemene Nederlandse Vereniging ter Voorkoming van Blindheid, Stichting Blinden-Penning.

Institutional review board statement: The study was conducted according to the guidelines of the EU Directive 2010/63/EU for animal experiments and with permission of the Dutch Central Authority for Scientific Procedures on Animals (CCD), permit number 1160020172924.

Data availability statement: The data that supports the finding of this study are available from the corresponding author upon reasonable request.

Acknowledgements: The authors thank Chelsey Linnenbank, Arend Boogaard, and Nynke van der Haar for technical assistance and all members of the Wijnholds lab for advice on the manuscript.

Conflicts of interest: The LUMC is the holder of patent application PCT/NL2014/050549, which describes the potential clinical use of CRB2; J.W. is listed as an inventor on this patent, and J.W. is an employee of the LUMC.

Abbreviations:

AAV	Adeno-associated viral vectors
CRB1	Crumbs homolog-1
CMV	Cytomegalovirus
ERG	Electroretinography
GS	Glutamine synthetase
INL	Inner nuclear layer
LCA	Leber congenital amaurosis
MGC	Müller glial cell
OKT	Optokinetic head tracking response
OLM	Outer limiting membrane
ONL	Outer nuclear layer
OPL	Outer plexiform layer
P5	Postnatal day 5
RP	Retinitis pigmentosa
RPE	Retinal pigment epithelium
SAR	Subapical region

References

1. Den Hollander, A.I.; Ten Brink, J.B.; De Kok, Y.J.M.; Van Soest, S.; Van Den Born, L.I.; Van Driel, M.A.; Van De Pol, D.J.R.; Payne, A.M.; Bhattacharya, S.S.; Kellner, U.; et al. Mutations in a human homologue of *Drosophila* crumbs cause retinitis pigmentosa (RP12). *Nat. Genet.* **1999**, *23*, 217–221.
2. Roh, M.H.; Makarova, O.; Liu, C.J.; Shin, K.; Lee, S.; Laurinec, S.; Goyal, M.; Wiggins, R.; Margolis, B. The Maguk protein, Pals1, functions as an adapter, linking mammalian homologues of crumbs and discs lost. *J. Cell Biol.* **2002**, *157*, 161–172.
3. van de Pavert, S.A.; Kantardzhieva, A.; Malysheva, A.; Meuleman, J.; Versteeg, I.; Levelt, C.; Klooster, J.; Geiger, S.; Seeliger, M.W.; Rashbass, P.; et al. Crumbs homologue 1 is required for maintenance of photoreceptor cell polarization and adhesion during light exposure. *J. Cell Sci.* **2004**, *117*, 4169–4177.
4. Margolis, B. The Crumbs3 polarity protein. *Cold Spring Harb. Perspect. Biol.* **2018**, *10*, 1–9.
5. van de Pavert, S.A.; Meuleman, J.; Malysheva, A.; Aartsen, W.M.; Versteeg, I.; Tonagel, F.; Kamphuis, W.; McCabe, C.J.; Seeliger, M.W.; Wijnholds, J. A single amino acid substitution (Cys249Trp) in *Crb1* causes retinal degeneration and deregulates expression of pituitary tumor transforming gene *Pttg1*. *J. Neurosci.* **2007**, *27*, 564–573.

6. Pellissier, L.P.; Alves, C.H.; Quinn, P.M.; Vos, R.M.; Tanimoto, N.; Lundvig, D.M.S.; Dudok, J.J.; Hooibrink, B.; Richard, F.; Beck, S.C.; et al. Targeted ablation of Crb1 and Crb2 in retinal progenitor cells mimics leber congenital amaurosis. *PLoS Genet.* **2013**, *9*.
7. Alves, C.H.; Pellissier, L.P.; Vos, R.M.; Garrido, M.G.; Sothilingam, V.; Seide, C.; Beck, S.C.; Klooster, J.; Furukawa, T.; Flannery, J.G.; et al. Targeted ablation of Crb2 in photoreceptor cells induces retinitis pigmentosa. *Hum. Mol. Genet.* **2014**, *23*, 3384–3401.
8. Quinn, P.M.; Mulder, A.A.; Henrique Alves, C.; Desrosiers, M.; de Vries, S.I.; Klooster, J.; Dalkara, D.; Koster, A.J.; Jost, C.R.; Wijnholds, J. Loss of CRB2 in Müller glial cells modifies a CRB1-associated retinitis pigmentosa phenotype into a Leber congenital amaurosis phenotype. *Hum. Mol. Genet.* **2019**, *28*, 105–123.
9. Quinn, P.M.; Alves, C.H.; Klooster, J.; Wijnholds, J. CRB2 in immature photoreceptors determines the superior-inferior symmetry of the developing retina to maintain retinal structure and function. *Hum. Mol. Genet.* **2018**, *27*, 3137–3153.
10. Zhao, M.; Andrieu-Soler, C.; Kowalczyk, L.; Paz Cortés, M.; Berdugo, M.; Dernigoghossian, M.; Halili, F.; Jeanny, J.-C.; Goldenberg, B.; Savoldelli, M.; et al. A new CRB1 rat mutation links müller glial cells to retinal telangiectasia. *J. Neurosci.* **2015**, *35*, 6093–6106.
11. Wang, D.; Tai, P.W.L.; Gao, G. Adeno-associated virus vector as a platform for gene therapy delivery. *Nat. Rev. Drug Discov.* **2019**, *18*, 358–378.
12. Pellissier, L.P.; Quinn, P.M.; Alves, C.H.; Vos, R.M.; Klooster, J.; Flannery, J.G.; Wijnholds, J. Gene therapy into photoreceptors and Müller glial cells restores retinal structure and function in CRB1 retinitis pigmentosa mouse models. *Hum. Mol. Genet.* **2015**, *24*, 1–15.
13. Buck, T.M.; Vos, R.M.; Alves, C.H.; Wijnholds, J. AAV-CRB2 protects against vision loss in an inducible CRB1 retinitis pigmentosa mouse model. *Mol. Ther. Methods Clin. Dev.* **2021**, *20*, 423–441.
14. Prusky, G.T.; Alam, N.M.; Beekman, S.; Douglas, R.M. Rapid quantification of adult and developing mouse spatial vision using a virtual optomotor system. *Investig. Ophthalmol. Vis. Sci.* **2004**, *45*, 4611.
15. Douglas, R.M.M.; Alam, N.M.M.; Silver, B.D.D.; MCGILL, T.J.J.; Tschetter, W.W.W.; Prusky, G.T.T. Independent visual threshold measurements in the two eyes of freely moving rats and mice using a virtual-reality optokinetic system. *Vis. Neurosci.* **2005**, *22*, 677–684.
16. Riepe, R.E.; Norenberg, M.D. Glutamine synthetase in the developing rat retina: An immunohistochemical study. *Exp. Eye Res.* **1978**, *27*, 435–444.
17. Mehalow, A.K.; Kameya, S.; Smith, R.S.; Hawes, N.L.; Denegre, J.M.; Young, J.A.; Bechtold, L.; Haider, N.B.; Tepass, U.; Heckenlively, J.R.; et al. CRB1 is

essential for external limiting membrane integrity and photoreceptor morphogenesis in the mammalian retina. *Hum. Mol. Genet.* **2003**, 12, 2179–2189.

18. van de Pavert, S.A.; Sanz sanz, A.; Aartsen, W.M.; Vos, R.M.; Versteeg, I.; Beck, S.C.; Klooster, J.; Seeliger, M.W.; Wijnholds, J. *Crb1* is a determinant of retinal apical muller glia cell features. *Glia* **2007**, 1486–1497.

19. Quinn, P.M.; Buck, T.M.; Mulder, A.A.; Ohonin, C.; Alves, C.H.; Vos, R.M.; Bialecka, M.; van Herwaarden, T.; van Dijk, E.H.C.; Talib, M.; et al. Human iPSC-derived retinas recapitulate the fetal CRB1 CRB2 complex formation and demonstrate that photoreceptors and müller glia are targets of AAV5. *Stem Cell Rep.* **2019**, 12, 906–919.

20. McGill, T.J.; Prusky, G.T.; Douglas, R.M.; Yasumura, D.; Matthes, M.T.; Lowe, R.J.; Duncan, J.L.; Yang, H.; Ahern, K.; Daniello, K.M.; et al. Discordant anatomical, electrophysiological, and visual behavioral profiles of retinal degeneration in rat models of retinal degenerative disease. *Investig. Ophthalmol. Vis. Sci.*, **2012**, 53, 6232–6244.

21. Ray, T.A.; Cochran, K.; Kozlowski, C.; Wang, J.; Alexander, G.; Cady, M.A.; Spencer, W.J.; Ruzyczki, P.A.; Clark, B.S.; Laeremans, A.; et al. Comprehensive identification of mRNA isoforms reveals the diversity of neural cell-surface molecules with roles in retinal development and disease. *Nat. Commun.* **2020**, 11, 1–20.

22. Boon, N.; Wijnholds, J.; Pellissier, L.P. Research models and gene augmentation therapy for CRB1 retinal dystrophies. *Front. Neurosci.* **2020**, 14, 1–13.

23. Berger, A.; Cavallero, S.; Dominguez, E.; Barbe, P.; Simonutti, M.; Sahel, J.A.; Sennlaub, F.; Raoul, W.; Paques, M.; Bemelmans, A.P. Spectral-domain optical coherence tomography of the rodent eye: Highlighting layers of the outer retina using signal averaging and comparison with histology. *PLoS ONE* **2014**, 9, e96494.

24. Aleman, T.S.; Cideciyan, A.V.; Aguirre, G.K.; Huang, W.C.; Mullins, C.L.; Roman, A.J.; Sumaroka, A.; Olivares, M.B.; Tsai, F.F.; Schwartz, S.B.; et al. Human CRB1-associated retinal degeneration: Comparison with the rd8 *Crb1*-mutant mouse model. *Investig. Ophthalmol. Vis. Sci.* **2011**, 52, 6898–6910.

25. Ryals, R.C.; Andrews, M.D.; Datta, S.; Coyner, A.S.; Fischer, C.M.; Wen, Y.; Pennesi, M.E.; McGill, T.J. Long-term characterization of retinal degeneration in royal college of surgeons rats using spectral-domain optical coherence tomography. *Investig. Ophthalmol. Vis. Sci.* **2017**, 58, 1378–1386.

26. van Rossum, A.G.S.H.; Aartsen, W.M.; Meuleman, J.; Klooster, J.; Malysheva, A.; Versteeg, I.; Arsanto, J.P.; Le Bivic, A.; Wijnholds, J. *Pals1/Mpp5* is required for correct localization of *Crb1* at the subapical region in polarized Müller glia cells. *Hum. Mol. Genet.* **2006**, 15, 2659–2672.

27. Pellissier, L.P.; Lundvig, D.M.S.; Tanimoto, N.; Klooster, J.; Vos, R.M.; Richard, F.; Sothilingam, V.; Garrido, M.G.; Bivic, A.L.; Seeliger, M.W.; et al. CRB2

acts as a modifying factor of CRB1-related retinal dystrophies in mice. *Hum. Mol. Genet.* **2014**, 23, 3759–3771.

28. Quinn, P.M.; Pellissier, L.P.; Wijnholds, J. The CRB1 complex: Following the trail of crumbs to a feasible gene therapy strategy. *Front. Neurosci.* **2017**, 11, 175.

29. Han, I.C.; Cheng, J.L.; Burnight, E.; Ralston, C.L.; Fick, J.L.; Thomsen, G.J.; Tovar, E.F.; Russell, S.; Sohn, E.H.; Mullins, R.F.; et al. Retinal tropism and transduction of adeno-associated virus (AAV) varies by serotype and route of delivery (intravitreal, subretinal or suprachoroidal) in rats. *Hum. Gene Ther.* **2020**, 1–29.

30. Charbel Issa, P.; de Silva, S.R.; Lipinski, D.M.; Singh, M.S.; Mouravlev, A.; You, Q.; Barnard, A.R.; Hankins, M.W.; During, M.J.; MacLaren, R.E. Assessment of tropism and effectiveness of new primate-derived hybrid recombinant AAV serotypes in the mouse and primate retina. *PLoS ONE* **2013**, 8, 1–12.

31. Klimczak, R.R.; Koerber, J.T.; Dalkara, D.; Flannery, J.G.; Schaffer, D.V. A novel adeno-associated viral variant for efficient and selective intravitreal transduction of rat Müller cells. *PLoS ONE* **2009**, 4, e7467.

32. Kolstad, K.D.; Dalkara, D.; Guerin, K.; Visel, M.; Hoffmann, N.; Schaffer, D.V.; Flannery, J.G. Changes in adeno-associated virus-mediated gene delivery in retinal degeneration. *Hum. Gene Ther.* **2010**, 21, 571–578.

33. Smith, A.J.; Schlichtenbrede, F.C.; Tschernutter, M.; Bainbridge, J.W.; Thrasher, A.J.; Ali, R.R. AAV-mediated gene transfer slows photoreceptor loss in the RCS rat model of retinitis pigmentosa. *Mol. Ther.* **2003**, 8, 188–195.

34. Da Costa, R.; Röger, C.; Segelken, J.; Barben, M.; Grimm, C.; Neidhardt, J. A novel method combining vitreous aspiration and intravitreal AAV2/8 injection results in retina-wide transduction in adult mice. *Investig. Ophthalmol. Vis. Sci.* **2016**, 57, 5326–5334.

35. Luhmann, U.F.O.; Carvalho, L.S.; Holthaus, S.M.; Cowing, J.A.; Greenaway, S.; Chu, C.J.; Herrmann, P.; Smith, A.J.; Munro, P.M.G.; Potter, P.; et al. The severity of retinal pathology in homozygous *Crb1rd8/rd8* mice is dependent on additional genetic factors. *Hum. Mol. Genet.* **2015**, 24, 128–141.

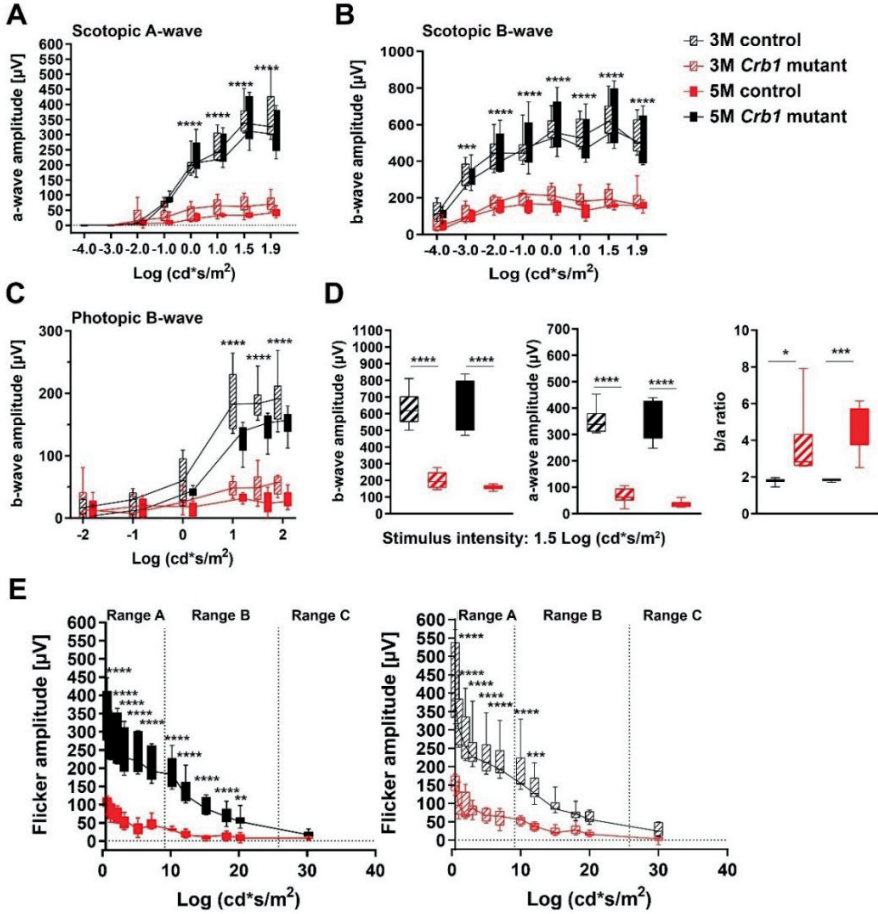
36. Nishiguchi, K.M.; Carvalho, L.S.; Rizzi, M.; Powell, K.; Holthaus, S.-M.; Azam, S.A.; Duran, Y.; Ribeiro, J.; Luhmann, U.F.O.; Bainbridge, J.W.B.; et al. Gene therapy restores vision in *rd1* mice after removal of a confounding mutation in *Gpr179*. *Nat. Commun.* **2015**, 6, 6006.

37. Tanimoto, N.; Sothilingam, V.; Kondo, M.; Biel, M.; Humphries, P.; Seeliger, M.W. Electroretinographic assessment of rod- and cone-mediated bipolar cell pathways using flicker stimuli in mice. *Sci. Rep.* **2015**, 5, 1–7.

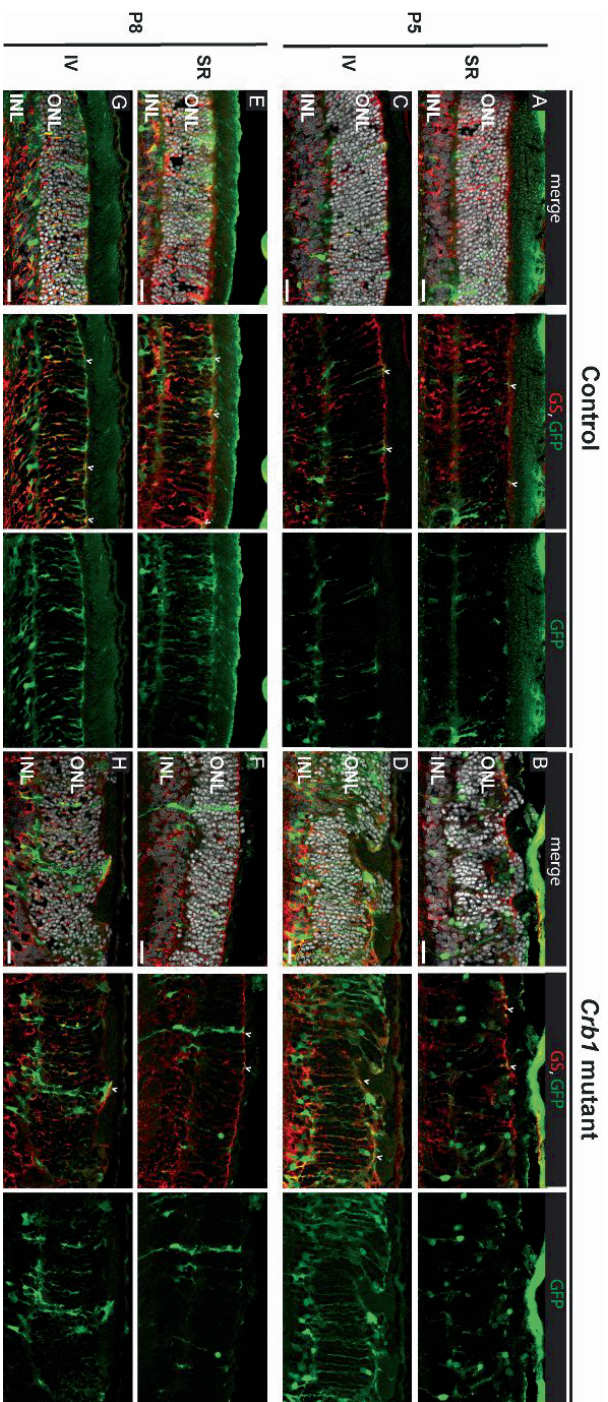
38. Tanimoto, N.; Akula, J.D.; Fulton, A.B.; Weber, B.H.F.; Seeliger, M.W. Differentiation of murine models of “negative ERG” by single and repetitive light stimuli. *Doc. Ophthalmol.* **2016**, 132, 101–109.

39. Alves, C.H.;Wijnholds, J. AAV gene augmentation therapy for CRB1-associated retinitis pigmentosa. In *Methods in Molecular Biology (Clifton, N.J.)*; Springer: Berlin/Heidelberg, Germany, **2018**; Volume 1715, pp. 135–151. ISBN 9781493975228.
40. Klooster, J.; Blokker, J.; ten Brink, J.B.; Unmehopa, U.; Fluiters, K.; Bergen, A.A.B.; Kamermans, M. Ultrastructural localization and expression of TRPM1 in the human retina. *Investig. Ophthalmol. Vis. Sci.* **2011**, 52, 8356–8362.
41. Faas, F.G.A.; Cristina Avramut, M.; van den Berg, B.M.; Mieke Mommaas, A.; Koster, A.J.; Ravelli, R.B.G. Virtual nanoscopy: Generation of ultra-large high resolution electron microscopy maps. *J. Cell Biol.* **2012**, 198, 457–469.
42. Marquardt, T. and Gruss, P. Generating neuronal diversity in the retina: one for nearly all. *TRENDS in Neurosciences.* **2002**, 25, 32-38.

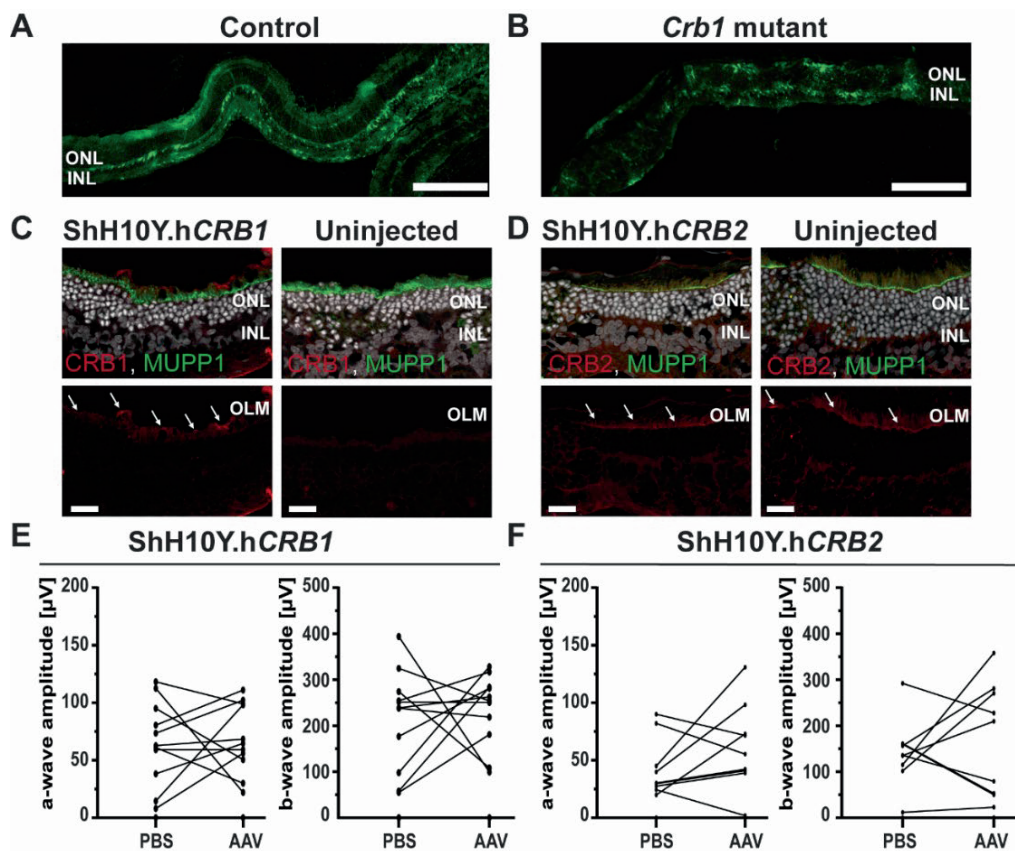
Supplemental data



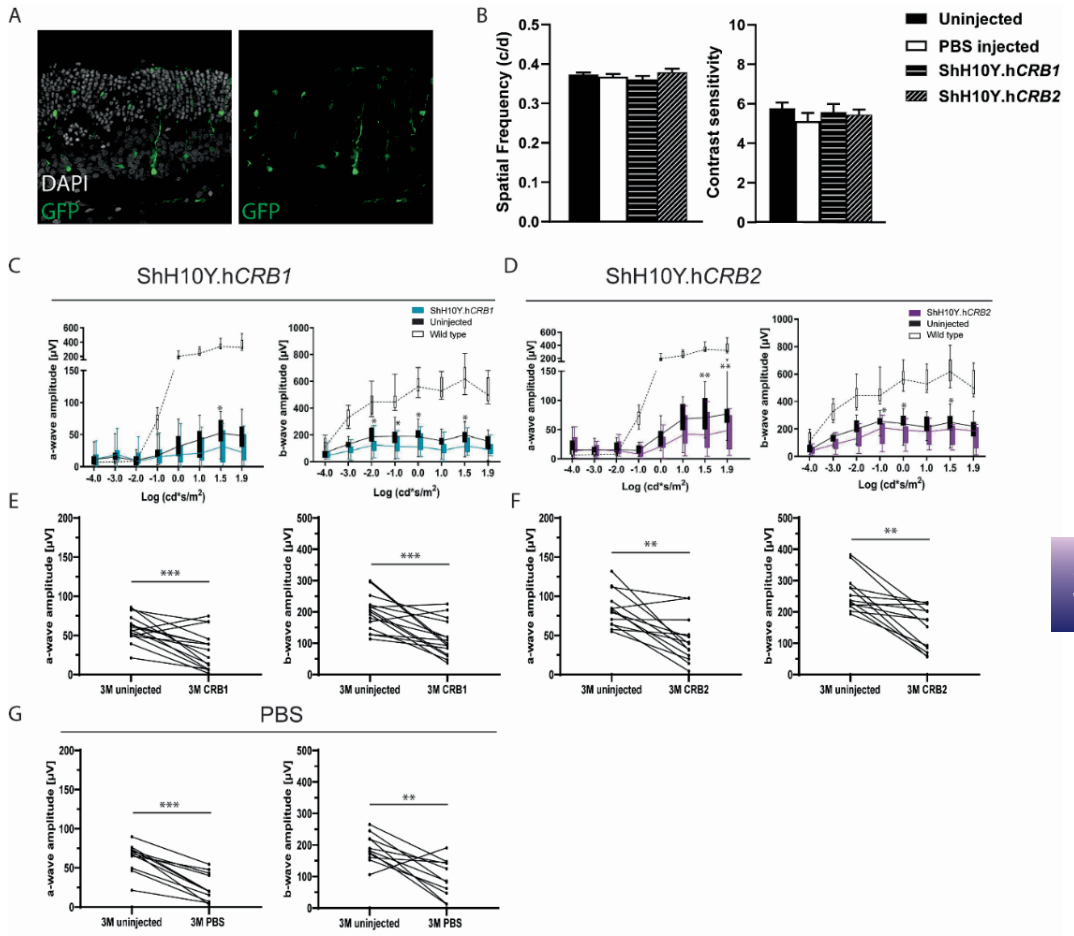
Supplemental Figure 1. Retinal function further decreases in 3 and 5 months of age *Crb1* mutant compared to control rats. Quantitative analysis of the scotopic a-wave (A) and b-wave (B), the photopic b-wave (C), the b-wave/a-wave amplitude and b/a-ratios (b/a) (D), and the flicker amplitude response (E) in 3 and 5 months of age *Crb1* mutant and control rats. Boxes indicate the 25 and 75% quantile range and whiskers indicate the 5 and 95% quantiles, and the intersection of line and error bar indicates the median of the data (box-and-whisker plot). Number of animals used for 3 months: control $n = 8$, *Crb1* mutant $n = 6$, and 5M: control $n = 6$, *Crb1* mutant $n = 6$. Mean \pm SEM. * $p < 0.05$; ** $p < 0.01$; *** $p < 0.001$; **** $P < 0.0001$



Supplemental Figure 2. Predominantly MGC transduction upon subretinal or intravitreal delivery of Shh10Y in both control and *Crb1* mutant rat retina. ShH10Y transduction at P5 subretinal (A-B), or intravitreal (C-D), and P8 subretinal (E-F), or intravitreal (G-H) in one month control (A, C, E, G) or *Crb1* mutant (B, D, F, H) rats retina. Co-stained with glutamine synthetase (GS; red), co-localization of GFP and GS indicated with arrowheads. At least $n = 2$ eyes used per time point. Note: INL = inner nuclear layer; ONL = outer nuclear layer; SR = subretinal injection; IV = intravitreal injection. Scale bar: 20 μ m.



Supplemental Figure 3. Gene therapy of ShH10Y.hCRB1 or ShH10Y.hCRB2 at P5 does not improve the severe retinal phenotype measured by ERG analysis at 2M of age. Overview of control (A) and *Crb1* mutant (B) rats intravitreally injected at P5 with ShH10Y.GFP, indicating the area of transduction. Immunohistochemical analysis of 3 months old *Crb1* mutant rats intravitreally injected at P3 with ShH10Y.hCRB1 (C) or with ShH10Y.hCRB2 (D) revealing the expression of hCRB1 and hCRB2. And 1.5 stimulus intensity ERG comparison of 2M individual rats injected with either ShH10Y.hCRB1 (E) or ShH10Y.hCRB2 (F) at P5 compared with PBS injected eyes. Number of animals used: P5 injection with ShH10Y.hCRB1 $n = 11$; ShH10Y.hCRB2 $n = 9$. Note: INL = inner nuclear layer; OLM = outer limiting membrane; ONL = outer nuclear layer. Scale bar: (A, B) 200 µm, (C, D) 20 µm.



Supplemental Figure 4. Gene therapy of ShH10Y.hCRB1 or ShH10Y.hCRB2 at P3 does not improve the severe retinal phenotype measured by OKT or ERG analysis. (A): IHC of GFP positive cells 1M after P3 intravitreal injection. (B): OKT spatial frequency and 0.092 contrast sensitivity of 3M *Crb1* rats injected with 1 µl PBS, ShH10Y.hCRB1, or ShH10.hCRB2. (C-D): Total a- and b-wave ERG response of rats treated with ShH10.hCRB1 (C) or ShH10.hCRB2 (D) compared to a wild-type control. (E-G): 1.5 stimulus intensity ERG comparison of 3M individual rats injected with either ShH10.hCRB1 (E), ShH10.hCRB2 (F), or (G) PBS compared with uninjected eyes. Boxes indicate the 25 and 75% quantile range and whiskers indicate the 5 and 95% quantiles, and the intersection of line and error bar indicates the median of the data (box-and-whisker plot). Number of animals used: ShH10.hCRB1 $n = 15$; for ShH10.hCRB2 $n = 13$; and for PBS $n = 15$. Mean \pm SEM. * $p < 0.05$; ** $p < 0.01$; *** $p < 0.001$; **** $p < 0.0001$.

A

```

CRB1_human
--MALRNIHTLLIIFLFSLLIYIKNSFCNKNNTRCLNSGQNNSTCRDFSKNDCCSCLD 58
Crb1_rat
MMNKLRKATLLALYLSSLLIIVNSFCNKNNTRCLNSGQNNSTCRDFSKNDCCSCLD 59
TANLNDKDNKEDPCFNFPQGSATVWIPGERSFLKCPPOYGSITCETITGSGQKNS 118
TANLNDKDNKEDPCFNFPQGSATVWIPGERSFLKCPPOYGSITCETITGSGQKNS 119
CQHGQICHQDPIYFVICPAGVAFRCIEDHDECASSPCQAGVQDQIDYSCFCVFGY 178
CQHGQICHQDPIYFVICPAGVAFRCIEDHDECASSPCQAGVQDQIDYSCFCVFGY 179
QQRHCLLEVDCAQPCPKNRAICLAEIGRYVICPHNTSIVNCELEIDECSQFCLNGAT 238
QQRHCLLEVDCAQPCPKNRAICLAEIGRYVICPHNTSIVNCELEIDECSQFCLNGAT 239
CQALGAYFDCAPGFLGDHCEINTECAQPCLAGLVCVGENRYSNCTYSQFTGTHC 298
CQALGAYFDCAPGFLGDHCEINTECAQPCLAGLVCVGENRYSNCTYSQFTGTHC 299
ETLMLCNSKPCNNNAICEVSNVNTVCHCQPGYTAQCEIDLEENSNPCQNSGCEVLS 358
ETLMLCNSKPCNNNAICEVSNVNTVCHCQPGYTAQCEIDLEENSNPCQNSGCEVLS 359
SEKYGRIITGLPSSFSVHEASGVVICOPQFTVHCEIDVNECSNFCQNGQTCENLKN 418
SEKYGRIITGLPSSFSVHEASGVVICOPQFTVHCEIDVNECSNFCQNGQTCENLKN 419
YTCPCFPNLSRTFYGGHDCSSILLACHTWQGLNNTGICPHFQDQHGHSCLPSSGYTGS 478
YTCPCFPNLSRTFYGGHDCSSILLACHTWQGLNNTGICPHFQDQHGHSCLPSSGYTGS 479
LCEIATLSEFGDFLAVKSGSVTVKGSVNCIALAFQVPMALLFNRSDVFPKLELL 538
LCEIATLSEFGDFLAVKSGSVTVKGSVNCIALAFQVPMALLFNRSDVFPKLELL 539
S0YIHLIQVNNQSKVLLFSIHTSDGQHWVFYFAVAFTVLLDSDCKEKCIKAKPTP 598
S0YIHLIQVNNQSKVLLFSIHTSDGQHWVFYFAVAFTVLLDSDCKEKCIKAKPTP 599
LSDQSIACAFNSFLQGLVQVMSISGVALINFTMSPSTFSPVQCLDQIKDNNHITLNI 658
LSDQSIACAFNSFLQGLVQVMSISGVALINFTMSPSTFSPVQCLDQIKDNNHITLNI 659
SGSLSNFKVAGKQKRWDCESQPCQGRGICNIMLSTQCCHRPEYQPCNLEIVAGRPQ 718
SGSLSNFKVAGKQKRWDCESQPCQGRGICNIMLSTQCCHRPEYQPCNLEIVAGRPQ 719
DSTQYARVYVWQGNFNLSHFTKRFQGITLITLGNSTYQVVCWIRKGLALTKTF 778
DSTQYARVYVWQGNFNLSHFTKRFQGITLITLGNSTYQVVCWIRKGLALTKTF 779
SPKLVVYFVNDQVHLISLKIYKPKYELYSQSGQGFISAPFKIKEDVYIIGLFDK 838
SPKLVVYFVNDQVHLISLKIYKPKYELYSQSGQGFISAPFKIKEDVYIIGLFDK 839
EKTAYLQGFKQICQDVRNLNANLEFFFNINMAALNIFLFDVQCAQDMSCKNPN 898
EKTAYLQGFKQICQDVRNLNANLEFFFNINMAALNIFLFDVQCAQDMSCKNPN 899
GOVCSRRDDFSCSPALTSGRACEVQWQGFSPCPHRAQQPVLQGFECIANAVFNQGS 958
GOVCSRRDDFSCSPALTSGRACEVQWQGFSPCPHRAQQPVLQGFECIANAVFNQGS 959
GQILFRNGANIITRELTNIITGRTKDAANVILHASKPEFLNLSIQDRLFFLQSGNSF 1018
GQILFRNGANIITRELTNIITGRTKDAANVILHASKPEFLNLSIQDRLFFLQSGNSF 1019
YMLSLITLQVNDQWHEVLSMTDPIQTSRQWQEVNNEFPVSTIATQSNLNFKNT 1078
YMLSLITLQVNDQWHEVLSMTDPIQTSRQWQEVNNEFPVSTIATQSNLNFKNT 1079
DIYVQDRAINDKIGLQCLSTIEIGIYLYSFENYVGFINKFQEQFKISTNSVVTGCL 1138
DIYVQDRAINDKIGLQCLSTIEIGIYLYSFENYVGFINKFQEQFKISTNSVVTGCL 1139
QLAVCNBNPLAGNCEIDFSSHYKCSPLMGKSKCEINLEDFSNPCINQNSDVAAY 1198
QLAVCNBNPLAGNCEIDFSSHYKCSPLMGKSKCEINLEDFSNPCINQNSDVAAY 1199
HRCFETQYFQNCEDVDNQCQHCANQARICSHNTGYSCLFNQTFKFRQKRLSFTV 1258
HRCFETQYFQNCEDVDNQCQHCANQARICSHNTGYSCLFNQTFKFRQKRLSFTV 1259
CQNKETLTCYNGQNTFQTEKLCMCRPQFQWKEDEIDECASQPCNNGGLCQDLAK 1318
CQNKETLTCYNGQNTFQTEKLCMCRPQFQWKEDEIDECASQPCNNGGLCQDLAK 1319
FQCLDVFAPGERCEVDLADLIIDIFITGTVFALLIILLIIVASVYVNSKRATQGT 1378
FQCLDVFAPGERCEVDLADLIIDIFITGTVFALLIILLIIVASVYVNSKRATQGT 1379
YSPSQEKEGSRVEMNMLPMPAMERLI 1406
YSPSQEKEGSRVEMNMLPMPAMERLI 1407

```

B

```

CRB2_human
--MALRNPPTDPPQ--ALASVLLIWLWAPALSLLAGTVPSFSPACASPCAPGTCQATE 59
Crb2_rat
MALLGVVWGFGRDVLVLLLLLLLLLPPVWVAGVLSFETMVCASDPCAPGTCQATE 60
GYTCQPMPEPRGATQPCNHGALCVQGGPDTGFCVYCVQPGQPRCLDEIDCASRPNH 119
GYTCQPMPEPRGATQPCNHGALCVQGGPDTGFCVYCVQPGQPRCLDEIDCASRPNH 120
GATCRNLADRYEHCPLGYAGVTCMEVDECAAPLHGSGCLDGVSFRCVCAPTGGT 179
GATCRNLADRYEHCPLGYAGVTCMEVDECAAPLHGSGCLDGVSFRCVCAPTGGT 180
RCQLDLEEQSPCAHQGTCHLVNCFRDCAGTYEGTHEREVLECASAPCEHNSACL 239
RCQLDLEEQSPCAHQGTCHLVNCFRDCAGTYEGTHEREVLECASAPCEHNSACL 240
EGLGSRFLCWFQYSGELCEVDEECSAPQHGRCQLQRSDPALGVQAAFGAFSFR 299
EGLGSRFLCWFQYSGELCEVDEECSAPQHGRCQLQRSDPALGVQAAFGAFSFR 300
HAAGFLCHCPQFEGADQVEVDECSARPCINGHGQCDLPMGFQHCPOYAGTCEEDV 359
HAAGFLCHCPQFEGADQVEVDECSARPCINGHGQCDLPMGFQHCPOYAGTCEEDV 360
DECLADPCLHGTCSDTVAGITCRPEFWGGRDSCVQLTQCGQITCLAAITCPIFESG 419
DECLADPCLHGTCSDTVAGITCRPEFWGGRDSCVQLTQCGQITCLAAITCPIFESG 420
HSYVCHCPQFTGPGQNTTFVWAGSPQASVPAAGPLALARFTLTPAGLATRND 479
HSYVCHCPQFTGPGQNTTFVWAGSPQASVPAAGPLALARFTLTPAGLATRND 480
TKESLELVAATLQATLMSYSTVLRLLPDIALMDHNNQVQVVLHLELALRHEHG 539
TKESLELVAATLQATLMSYSTVLRLLPDIALMDHNNQVQVVLHLELALRHEHG 540
CPARLCVAGPVALASATATPLAGISAGLQDAPFACIQDVRVGHILLPELDQEV 599
CPARLCVAGPVALASATATPLAGISAGLQDAPFACIQDVRVGHILLPELDQEV 600
LIGCERREQCRPLFCVHGGSCVDLWTFHRCDCARPHRGTCADEIIPATFLQAGPASP 659
LIGCERREQCRPLFCVHGGSCVDLWTFHRCDCARPHRGTCADEIIPATFLQAGPASP 660
FLIQELQGLVTLVSLNTRASAGLLQFQNDASAGLTVFSEQRARVFPSPVAVLQ 719
FLIQELQGLVTLVSLNTRASAGLLQFQNDASAGLTVFSEQRARVFPSPVAVLQ 720
RWDQRLHVMLEFQDFQDLQDQVQVHGRLLAADSQFWQGFQFQCLQLDQDCHLFF 779
RWDQRLHVMLEFQDFQDLQDQVQVHGRLLAADSQFWQGFQFQCLQLDQDCHLFF 778
FFLPLDSSQSEQLGGRQWMLTAGCSEDMCSDFQPCFNGGTLVWNSFHTCANFTQ 839
FFLPLDSSQSEQLGGRQWMLTAGCSEDMCSDFQPCFNGGTLVWNSFHTCANFTQ 840
FTCAQLNCPQGLPFPATCEVDFQVYVAFATFREGPFAVFTGYNKSSRLLQGLSLA 909
FTCAQLNCPQGLPFPATCEVDFQVYVAFATFREGPFAVFTGYNKSSRLLQGLSLA 900
FRTDSEAMLLRAA--AGALEGVWLVAVNGSLAGVGHGLPQAVLPIPGFRVADGWH 957
FRTDSEAMLLRAA--AGALEGVWLVAVNGSLAGVGHGLPQAVLPIPGFRVADGWH 954
RVRLAMERPAATSRMLLWDGATPVALRGLASDGLFQDQAVRILLAEFTQCLGRV 1017
RVRLAMERPAATSRMLLWDGATPVALRGLASDGLFQDQAVRILLAEFTQCLGRV 1014
ALGLLPLPLAFRFGAAGAREHFAENPQTA--PILCRGAPVCAPEFCLHGACRDLDF 1076
ALGLLPLPLAFRFGAAGAREHFAENPQTA--PILCRGAPVCAPEFCLHGACRDLDF 1074
AFACACQPMWGFRCARVDPCHSAPCARGCRHTHPDGRFCRCRPFQFGQPRCLVPRK 1136
AFACACQPMWGFRCARVDPCHSAPCARGCRHTHPDGRFCRCRPFQFGQPRCLVPRK 1134
ECSLAVTCLDSQSCFQGSBANCSCLEGLAQCVQFTLPCAMPCFLNQTFRAGQVSE 1196
ECSLAVTCLDSQSCFQGSBANCSCLEGLAQCVQFTLPCAMPCFLNQTFRAGQVSE 1194
CICNARFQGFCEVAKGLPLPLPFFLLEWVAFACACLILLLGLLGLSILAAKRRQSG 1256
CICNARFQGFCEVAKGLPLPLPFFLLEWVAFACACLILLLGLLGLSILAAKRRQSG 1254
TYSFSQGEVAGARLMDSVLVFPEERLI 1285
TYSFSQGEVAGARLMDSVLVFPEERLI 1283

```

3

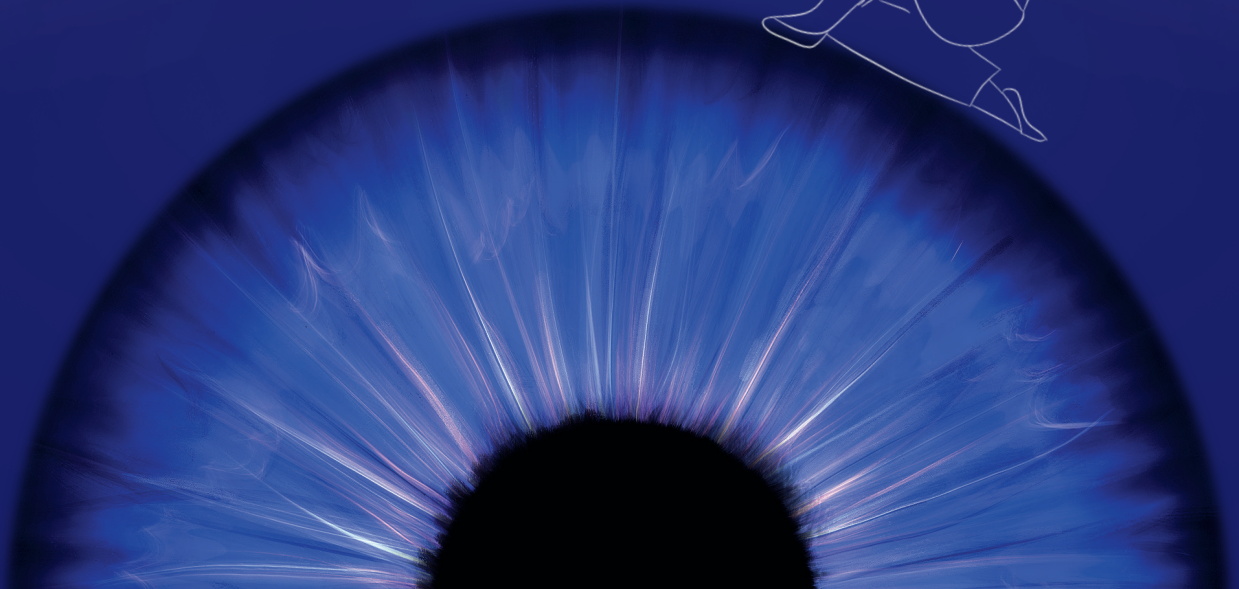
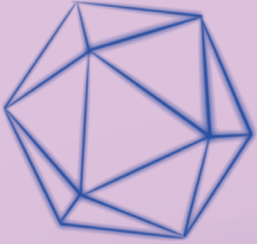
Supplemental Figure 5. Highly conserved CRB1 and CRB2 protein sequence between human and Brown Norway rats. Protein sequence alignment of human CRB1 with rat Crb1 (A) and human CRB2 with rat Crb2 (B). Protein sequence alignment reveals 75% identical matches and 84% conservative substitutions for human CRB1 compared with rat Crb1. And for human CRB2 compared with rat Crb2 there are 77% identical matches and 82% conservative substitutions shown. Upper and bold sequence is human, lower sequence is rat. Sequence alignment data from Uniprot and BLAST.

Chapter 4

AAV-Mediated Gene Augmentation Therapy of *CRB1*
Patient-Derived Retinal Organoids Restores the Histological
and Transcriptional Retinal Phenotype

N. Boon, X. Lu, C. A. Andriessen, I. Moustakas, T. M. Buck,
C. Freund, C. H. Arendzen, S. Böhringer, C.J.F. Boon, H. Mei, and
J. Wijnholds

Stem Cell Reports, 2023



Abstract

Retinitis pigmentosa (RP) and Leber congenital amaurosis are inherited retinal dystrophies which can be caused by mutations in the Crumbs homologue 1 (*CRB1*) gene. *CRB1* is required for organizing apical-basal polarity and adhesion between photoreceptors and Müller glial cells. *CRB1* patient-derived induced pluripotent stem cells were differentiated into *CRB1* retinal organoids that showed diminished expression of variant *CRB1* protein observed by immunohistochemical analysis. Single cell RNA-sequencing revealed impact on, among others, the endosomal pathway and cell adhesion and migration in *CRB1* patient-derived retinal organoids compared to isogenic controls. Adeno-associated viral (AAV) vector-mediated *hCRB2* or *hCRB1* gene augmentation in Müller glial and photoreceptor cells partially restored the histological phenotype and transcriptomic profile of *CRB1* patient-derived retinal organoids. Altogether, we show proof-of-concept that AAV.*hCRB1* or AAV.*hCRB2* treatment improved the phenotype of *CRB1* patient-derived retinal organoids, providing essential information for future gene therapy approaches for patients with mutations in the *CRB1* gene.

Introduction

Retinitis pigmentosa (RP) and Leber congenital amaurosis (LCA) are inherited retinal dystrophies caused by mutations in, among others, the Crumbs homologue 1 (*CRB1*) gene [1–3]. Canonical *CRB1* is a large transmembrane protein consisting of a short 37 amino acid intracellular domain containing a protein 4.1, ezrin, radixin, moesin (FERM) and a conserved glutamic acid-arginine-leucine-isoleucine (ERLI) PDZ binding motif, a single transmembrane domain, a large extracellular domain with multiple epidermal growth factor (EGF) and laminin-A globular like domains [1,4,5]. Recently, a short non-canonical alternatively spliced form of *CRB1*, *CRB1-B*, has been described containing substantial extracellular domain overlap but with distinct amino terminus and lacking the carboxyl terminal transmembrane and intracellular domains [6]. In mammals, canonical *CRB1* is a member of the Crumbs family together with *CRB2* and *CRB3A*. The canonical CRB complex is formed by interaction with protein

associated with Lin Seven 1 (PALS1), also known as membrane-associated guanylate kinase p55 subfamily member 5 (MPP5), which binds to the conserved C-terminal PDZ domain of CRB [7–9]. Binding of PALS1 can lead to the recruitment of Multiple PDZ domain protein 1 (MUPP1) or the InaD-like protein (INADL/PATJ) to the apical membrane [7]. This CRB complex is evolutionary conserved and is important for maintaining cell adhesion and regulating apical-basal polarity [10].

So far, no treatment possibilities are available for patients with RP or LCA caused by mutations in *CRB1*. Gene augmentation therapies using adeno-associated viral vectors (AAV) are of emerging interest for retinal dystrophies because of the recent FDA approval of an AAV-mediated gene therapy approach for RP and LCA patients with mutations in the *RPE65* gene [11]. AAVs are the leading platform for gene delivery because of their low toxicity, limited integration into the host genome, and because different AAV capsids display distinct cell tropisms. Their major disadvantage is the limited packaging capacity; inverted terminal repeats, cDNAs and regulatory sequences bigger than 4.9 kb often do not fit in a single AAV capsid. Unfortunately, the full-length cytomegalovirus (CMV) ubiquitous promoter and h*CRB1* cDNA exceeds this packaging limit. However, substantial expression levels of canonical hCRB1 protein in mouse mutant *Crb1* retina were observed using an AAV with codon optimized h*CRB1* cDNA linked to a minimal CMV promoter [12]. This AAV.CMVmin.h*CRB1* was deleterious upon intravitreal injection in *Crb1* mouse models [13]. As an alternative approach, *CRB* family member *CRB2* was used to restore retinal function and vision in *Crb* mice [13,14], showing the potential of AAV.h*CRB2* gene augmentation therapy for patients with mutations in the *CRB1* gene.

There are several mouse models described with mutations in the *Crb1* and/or *Crb2* gene mimicking the RP or LCA phenotype [8,15–21]. However, immuno-electron microscopy identified the subcellular localization of CRB1 and CRB2 proteins to be different in mouse and human models. In mice, *Crb2* is present in photoreceptor cells and Müller glial cells (MGC) at the subapical region (SAR) of the outer limiting membrane (OLM) while *Crb1* is solely present in MGC at the SAR [22]. In contrast, in human fetal retina and human induced pluripotent stem cell (hiPSC)-derived retinal

organoids both *CRB1* and *CRB2* are observed at the SAR in photoreceptors and MGC [23]. This discrepancy suggests the importance of using human-derived models for gene therapy approaches.

Here, we describe the phenotype of differentiation day 210 (DD210) and DD230 patient-derived retinal organoids harboring *CRB1* missense mutations compared to isogenic controls in more detail using immunohistochemical analysis and single-cell RNA sequencing. Next, the effect of AAV-mediated h*CRB1* or h*CRB2* gene augmentation therapy was analyzed on *CRB1* patient-derived and isogenic control retinal organoids. A partially improved retinal phenotype of *CRB1* patient-derived retinal organoids was observed, providing crucial data for future gene therapy approaches for patients with mutations in the *CRB1* gene.

Results

Reduced number of photoreceptor nuclei and thinner outer nuclear layer (ONL) in DD210 CRB1 patient-derived retinal organoids compared to isogenic controls

Retinal organoids were differentiated from hiPSC lines derived from three *CRB1* RP patients: (1) LUMC0116iCRB with c.3122T>C p.(Met1041Thr) homozygote missense mutations (here abbreviated as: P116), (2) LUMC0117iCRB with 2983G>T p.(Glu995*) and c.1892A>G, p.(Tyr631Cys) mutations (P117), and (3) LUMC0128iCRB with c.2843G>A p.(Cys948Tyr) and c.3122T>C p.(Met1041Thr) missense mutations (P128) [23]. Isogenic controls for P116 and P128 were generated by CRISPR/Cas9; (1) ISO-02 P116 with a homozygous correction, (2) ISO-03 P116 with a heterozygous correction, and (3) ISO-P128 a heterozygous correction of Cys948Tyr (Supplemental Table 1). Genomic stability of all iPSC lines was tested by a digital PCR test of the copy number variants (CNV) of 90% of the most recurrent abnormalities in hiPSC [24]. No aberrant CNV were observed in the hiPSC lines used in this study (Supplemental Figure 1A).

Previous research has shown that *CRB1* patient-derived retinal organoids at DD180 show disruptions at the OLM and photoreceptor nuclei protruding above the OLM [23]. Here, we analyzed the phenotype of the *CRB1* patient-derived retinal organoids at a later timepoint (DD210) and compared those to the isogenic controls. By light microscopy, no visible difference was observed in cultured retinal organoids comparing *CRB1* patient with the isogenic controls at DD210: all contained a translucent region at the outside of the organoid (the ONL) with inner and/or outer-segment-like structures around the retinal organoid (Figure 1A, Supplemental Figure 1B).

Immunohistochemistry of rod photoreceptor marker rhodopsin and MGC marker SOX9 at DD210 revealed the presence of rod photoreceptors and SOX9 positive MGCs for both patient and isogenic controls (Figure 1B, 1C, Supplemental Figure 1C, 1D).

When analyzing the phenotype in more detail, a moderate but statistically significant decrease in the number of photoreceptor nuclei and ONL thickness was observed in *CRB1* patient-derived retinal organoids compared to isogenic controls (Figure 1D). In contrast to *CRB1* patient-derived retinal organoids at DD180 [23], no statistically significant difference in the number of photoreceptor nuclei above the OLM was detected at DD210 (Figure 1D). In addition, no statistically significant differences were observed for the total retinal thickness and the inner nuclear layer (INL) thickness of the retinal organoids (Supplemental Figure 1F).

Missense mutations in CRB1 result in reduced levels of variant CRB1 protein in CRB1 patient-derived retinal organoids

Immunohistochemistry analysis of all three *CRB1* patient-derived retinal organoids at DD210 shows a diminished *CRB1* staining at the OLM compared to the isogenic control (Supplemental Figure 1E, 1E). Similar strongly diminished levels of variant *CRB1* in *CRB1* patient-derived retinal organoids compared to the isogenic control were observed at DD180 (Supplemental Figure 1G). While *CRB2* and *CRB* complex members *MUPP1* and *PALS1* remain at the OLM in both isogenic and *CRB1* patient-derived organoids (Figure 1E, 1F, Supplemental Figure 1F).

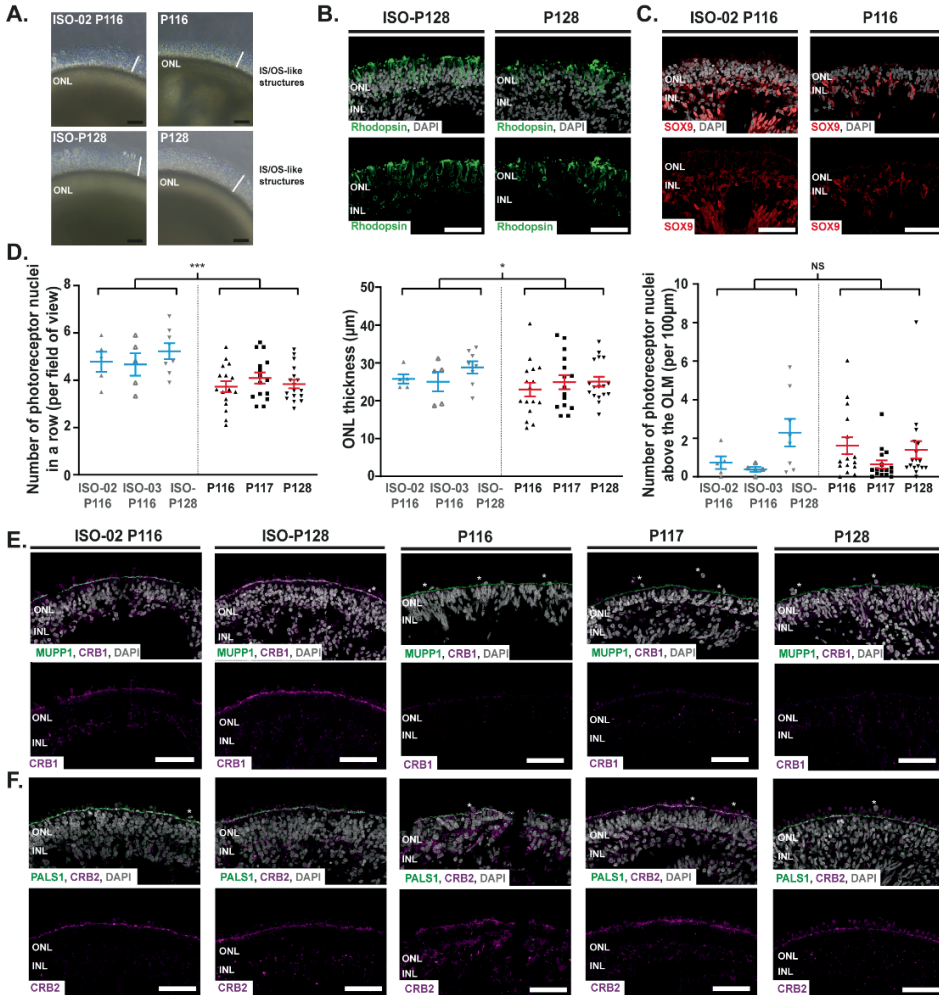


Figure 1. *CRB1* patient and isogenic control phenotypic analysis at DD210. (A) Representative brightfield images of ISO-02 P116, P116, ISO-P128, and P128 cultured organoids. (B) Representative immunohistochemical images of rhodopsin (green) in ISO-P128 and P128. (C) Representative immunohistochemical images of SOX9 (red) in ISO-P116 and P116. (D) Quantitative analysis of number of photoreceptor nuclei in a row per field of view ($p = 0.000$), ONL thickness per field of view ($p = 0.049$), and number of photoreceptor nuclei above the OLM per 100 μm ($p = 0.651$) in *CRB1* patient-derived and isogenic control retinal organoids. (E) Immunohistochemical images of CRB1 (red) and MUPP1 (green) in *CRB1* patient-derived retinal organoids with two appropriate isogenic controls. (F) Immunohistochemical images of CRB2 (red) and PALS1 (green) in *CRB1* patient-derived retinal organoids with two appropriate isogenic controls. Each datapoint in the graph represent individual organoids, of which an average has been taken of 3-6 representative images. The

standard error of mean (SEM) is derived from these averages. Number of individual organoids per condition and differentiation round: P116 $n = 16$, P117 $n = 15$, P128 $n = 17$ from four independent organoid batches, ISO-P128 $n = 8$ from three independent organoid batches, ISO-02 P116 $n = 5$ and ISO-03 P116 $n = 5$ from two independent organoid batches. Scalebar = 50 μ m, statistical analysis: generalized linear mixed models with $p < 0.05$ (*), $p < 0.01$ (**), and $p < 0.001$ (***) . Related to Supplemental Figure 1.

Missense mutations in CRB1 do not affect the levels of CRB1 or CRB2 RNA transcripts in CRB1 patient-derived retinal organoids

Next, we used single cell RNA sequencing (scRNA-seq) to identify differences in RNA transcripts and gene ontology pathways between DD230 *CRB1* patient-derived retinal organoids and isogenic controls. Transcriptionally similar cells were grouped and visualized (R package *Seurat*), revealing distinct clusters with differentially expressed marker genes (Supplemental Table 3). These identified expressed genes per cluster were compared to known retinal marker genes to classify clusters. Major retinal cell types could be visualized on a UMAP plot, such as MGC, photoreceptor cells (both rods and cones), bipolar cells, amacrine cells, horizontal cells, ganglion cells and retinal pigment epithelium (RPE) (Figure 2A). In addition, some of the clusters consisted of astrocytes and transitory cells (Figure 2A), and tissue that is generally attached to the retinal organoid was observed and classified as stromal cells (Figure 2A, Supplemental 2C). The expression of key cell-type specific markers of all clusters are shown in a feature plot and heatmap (Figure 2B, Supplemental Figure 2A). Interestingly, two rod photoreceptor cell subtypes can be distinguished. Upon further analysis, cluster rods I was identified to be composed of more mature cells with significantly higher transcript expression levels of *NR2E3*, *PDE6B* and *RHO* in comparison to cluster rods II (Supplemental Figure 2B) [25].

We confirmed that all the major retinal cell clusters were equally present in both P128 and ISO-P128 (Figure 2C) and P116 and ISO-P116 (Supplemental Figure 3A). Expression levels of both *CRB1* and *CRB2* were predominantly observed in MGC and photoreceptor cells. When analyzing *CRB1* expression levels in MGC and photoreceptor cells in more detail, no statistically significant differences were observed between P128 and ISO-P128 (Figure 2D) nor between P116 and ISO-P116

(Supplemental Figure 3B). Rods I and rods II were combined into a general “rods” cluster, since no statistically significant differences were observed in the individual clusters (data not shown). Moreover, the sequence of *CRBI-B*, an alternative transcript of *CRBI* containing distinct 5’ and 3’ ends, was added to the pre-built reference and was not detected in our DD230 retinal organoids (Supplemental Figure 2D). While *CRBI-B* transcripts were detected in adult human retina cDNA, the levels of *CRBI-B* transcripts were below detection level by reverse transcription quantitative real-time PCR (RT-qPCR) on DD210 retinal organoids (data not shown; Supplemental experimental procedures). In addition, no statistically significant difference was observed for the *CRB2* expression level (Figure 2E, Supplemental Figure 3C), nor for canonical CRB core complex members *PALSI*, *MUPPI*, *PATJ* (Figure 2F, Supplemental Figure 3D) or for FERM proteins *MSN*, *EZR*, or *EPB41L5* (Supplemental Figure 2E).

Gene profiling shows disruptions in the endosomal system in MGC and rods

Differential gene expression analysis followed by Gene Ontology (GO) term analysis comparing *CRBI* patient and isogenic control retinal organoids was performed. Analysis of P128 and ISO-P128 specifically in the MGCs, where most *CRBI* is expressed, revealed five groups of similar gene ontology terms containing differentially expressed genes deregulated in the patient-derived retinal organoids. The first gene ontology group is involved in the endosomal system, including extracellular exosomes, vesicles, endomembrane system, and early endosomes (Figure 2G). The second group is involved in the maintenance of location in the cell, cell motility, proliferation and cell-cell adhesion, the third group revealed differences in proteins containing various binding domains such as ferric iron and fatty acid, while the fourth group is involved in cell death (Figure 2G). Finally, the last one is a mixed group with pathways such as iron ion transport and post-translational protein phosphorylation (Figure 2G). In addition, as the *CRBI* transcript is also present in photoreceptor cells, differentially expressed markers and subsequent gene ontology terms were analyzed in rods (combination of rods I and rods II) and cones. In rods, gene ontology terms involved in the endosomal system were observed to be differentially expressed (Figure 2H). In

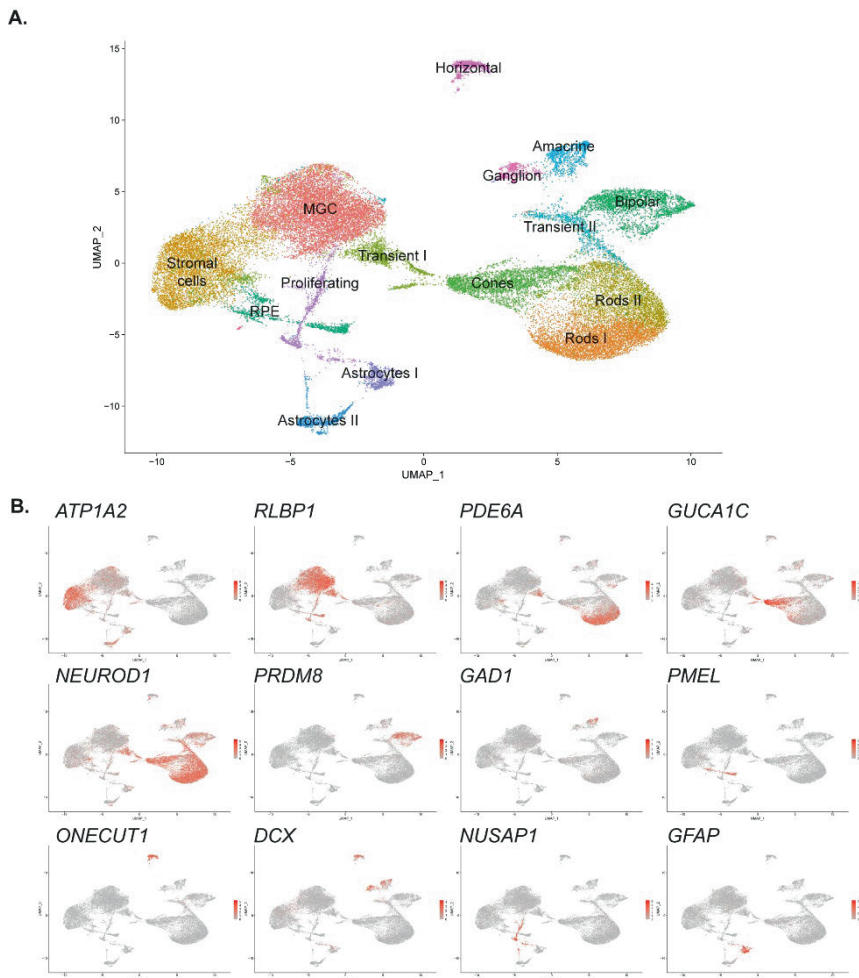


Figure 2 (A-B): scRNA-seq analysis comparing ISO-P128 with P128 shows disruptions in the endosomal system in Müller glial cells and rods. (A) UMAP plot of observed clusters and (B) expression plots of top markers indicating the distinct clusters. Number of independent organoids used: ISO-P128 $n = 6$, and P128 $n = 6$ from one differentiation round equally divided into three separate sequencing rounds. Related to Supplemental Figure 2 and 3.

addition, markers associated with the activation of the phototransduction cascade were detected (Figure 2H). No statistically significant differential expressed markers were observed in cone photoreceptor cells (data not shown).

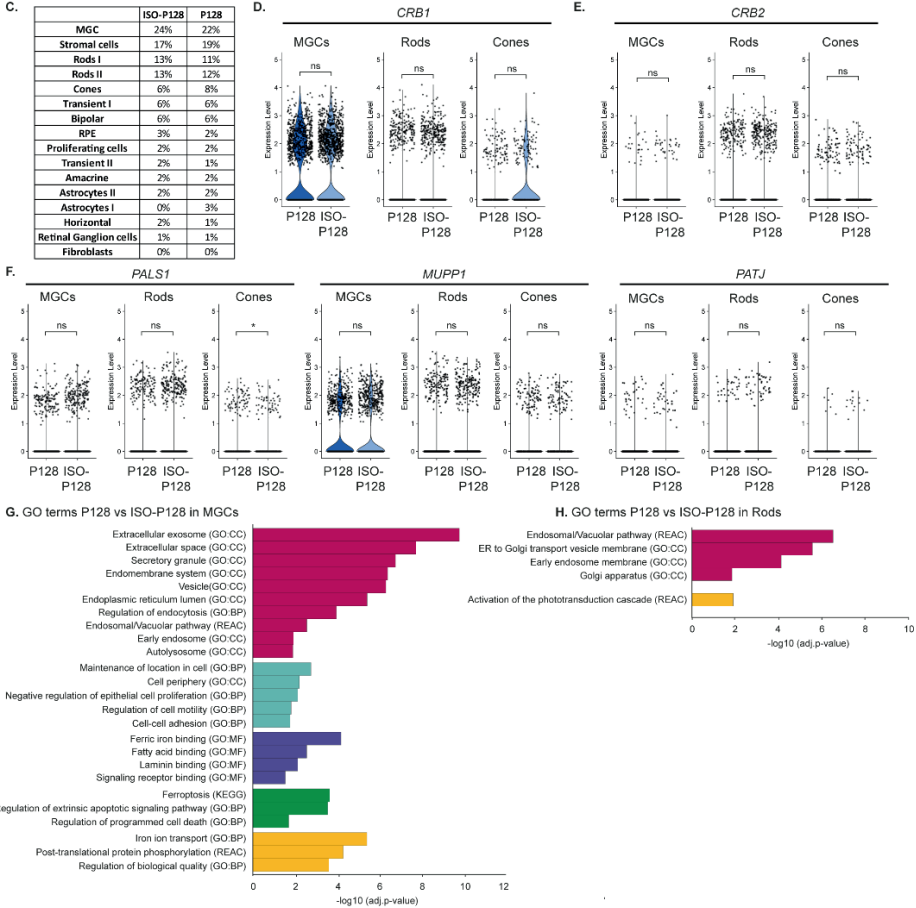


Figure 2 (C-H): scRNA-seq analysis comparing ISO-P128 with P128 shows disruptions in the endosomal system in Müller glial cells and rods (C) Table showing that all retinal cell types are present in both lines. (D) Violin plots of *CRB1* transcript levels specifically in MGCs ($p = 0.93$), rods ($p = 0.84$) and cones ($p = 0.72$). (E) Violin plots of *CRB2* transcript levels specifically in MGCs ($p = 0.43$), rods ($p = 0.18$) and cones ($p = 0.85$). (F) Violin plots of canonical core CRB complex members *PALS1*, *MUPP1*, and *PATJ* transcript levels in MGCs ($p = 0.32$; $p = 0.51$; $p = 0.73$, respectively), rods ($p = 0.97$; $p = 0.18$; $p = 0.63$), and cones ($p = 0.025$; $p = 0.25$; $p = 0.87$). (G, H) Gene ontology (GO) analysis of differentially expressed markers specifically in MGCs (G) and rods (H) clustered in groups with similar terms in the same colour. Number of independent organoids used: ISO-P128 $n = 6$, and P128 $n = 6$ from one differentiation round equally divided into three separate sequencing rounds. Related to Supplemental Figure 2 and 3.

Such an analysis was also performed comparing P116 with ISO-P116, where gene ontology terms associated with the endosomal system were differentially expressed in

rod photoreceptor cells (Supplemental Figure 3E). No statistically significant gene ontology terms were observed in MGC, explained by the low number of differentially expressed genes and the low number of cells sequenced in this cluster. Altogether, this data shows aberrations in the endosomal system between *CRB1* patient-derived retinal organoids compared to their isogenic controls.

Serotype AAV5.CMV.GFP is more efficient than AAV2.CMV.GFP in transducing Müller glial cells at DD120

CRB1 protein is localized at the OLM in human and non-human primate MGC and photoreceptors [17,23], and higher levels of *CRB1* transcript are found in MGC than in photoreceptors (Figure 2D). For AAV-mediated gene therapy approaches in *CRB1* patient-derived retinal organoids it is therefore essential to transduce sufficient number of MGC in addition to photoreceptors. Therefore, we identified which cells are transduced using specific viral capsids and titers at DD120. Control retinal organoids were transduced with 1×10^{10} gc, $6,6 \times 10^{10}$ gc or 10×10^{10} gc AAV2/5.CMV.GFP (AAV5.CMV.GFP) or AAV2/2.CMV.GFP (AAV2.CMV.GFP) and analyzed using immunohistochemistry after three weeks in culture.

A significant dose-dependent increase of GFP-positive cells was observed when control organoids were treated with AAV5.CMV.GFP or AAV2.CMV.GFP at DD120 (Supplemental Figure 3F, 3G). The AAV treated retinal organoids were quantified for number of GFP-positive cells in the ONL, the INL, and GFP-positive cells in the INL which were also SOX9 positive (marking MGCs). AAV2.CMV.GFP transduced more photoreceptor cells in the ONL than AAV5.CMV.GFP (Figure 3C). However, AAV5.CMV.GFP transduced more cells in the INL than AAV2.CMV.GFP (Figure 3D). More specifically, more SOX9-positive MGCs were transduced with AAV5.CMV.GFP than with AAV2.CMV.GFP (Figure 3E). Co-staining with photoreceptor markers (OTX2 and recoverin) and MGC markers (CRALBP and SOX9) confirmed the transduction of both cell types in AAV2.CMV.GFP as well as AAV5.CMV.GFP transduced organoids at DD120 (Figure 3F, G). Moreover, a 10x

magnification of a retinal organoid treated with 10×10^{10} gc AAV5.CMV.GFP at DD120 showed that most of the retinal organoid was transduced in our experiment (Figure 3H).

Because AAV5 transduced more MGCs than AAV2, treatment with AAV5 at DD120 was used for further AAV.hCRB gene augmentation therapy with an intermediate dose of $3,3 \times 10^{10}$ gc.

AAV-mediated hCRB gene augmentation therapy partially restores the histological phenotype of CRB1 patient-derived retinal organoids

After defining the AAV.GFP tropism, preclinical gene therapy approaches were performed on *CRB1* patient-derived retinal organoids using AAV5.CMVmin.hCRB1 or AAV5.CMV.hCRB2 (here abbreviated as: AAV.hCRB1 and AAV.hCRB2, respectively) at DD120 and analyzed at DD180 or DD210.

Immunohistochemical analysis and subsequent quantification of retinal organoids transduced with AAV.hCRB1 or AAV.hCRB2 and analyzed at DD180 show an increased number of photoreceptor nuclei in a row in AAV.CRB treated P117 compared to the control (Supplemental Figure 4B). In addition, fewer photoreceptor nuclei protruding above the OLM were observed after AAV.CRB treatment of P117 compared to the control organoids (Supplemental Figure 4C). No statistically significant difference was observed for the retinal nor the ONL thickness in both CRB1 patient and control organoids treated with AAV.hCRB1 or AAV.hCRB2 (Supplemental Figure 4D, 4E).

In addition, the long-term gene augmentation effect was examined for multiple *CRB1* patient-derived lines, where the organoids were collected and analyzed at DD210. One group of three different *CRB1* patient-derived retinal organoids was treated with solely AAV.hCRB1 or AAV.hCRB2 or left untreated, while in the following experiment the *CRB1* patient-derived retinal organoids were treated with AAV.hCRB1 with AAV.GFP, or AAV.hCRB2 with AAV.GFP, or AAV.GFP alone. Adding AAV.GFP facilitates in defining the regions where the AAV.hCRB most likely infected.

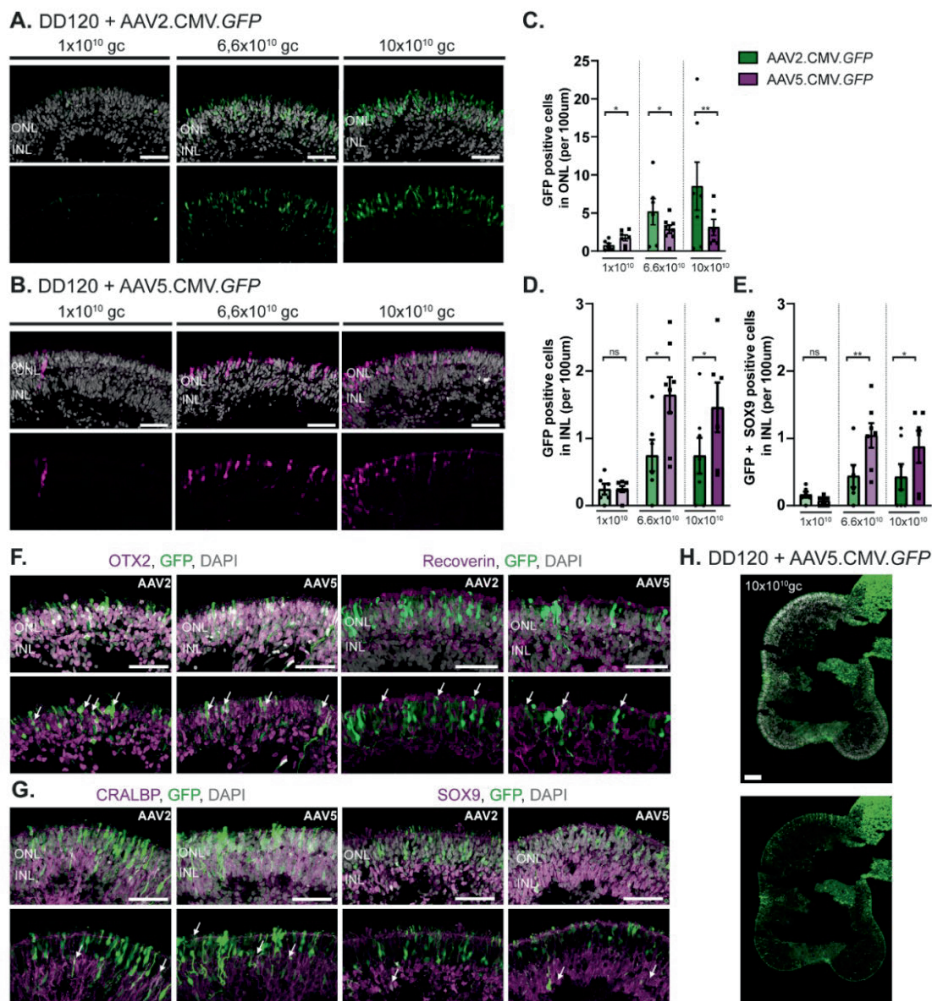


Figure 3: AAV2.CMV.GFP and AAV5.CMV.GFP transduction of DD120 control retinal organoids. (A,B) Representative immunohistochemical images of (A) AAV2.CMV.GFP and (B) AAV5.CMV.GFP treated control organoids at DD120 with three different titer concentrations: 1x10¹⁰, 6.6x10¹⁰, and 10x10¹⁰ gc (genome copies). (C, D, E) Quantification of AAV treated retinal organoids with AAV2.CMV.GFP or AAV5.CMV.GFP at the (C) ONL, (D) INL, or (E) GFP positive MGC in the INL. (F, G) Representative immunohistochemical images of photoreceptor cells marker (OTX2 and recoverin) and MGC markers (CRALBP and SOX9) showing colocalization with AAV.GFP for both AAV2.CMV.GFP and AAV5.CMV.GFP treated organoids. (H) Representative 10x magnification immunohistochemical analysis of DD120 control organoid transduced with 10x10¹⁰gc AAV5.CMV.GFP. Immunohistochemical images of (F, G, and H) are merged z-stack views, the others are single image views. Scalebar = 50µm. Each datapoint in the graph represent individual organoids, of which an average has been

taken of at least 3 representative images. The standard error of mean (SEM) is derived from these averages. Number of individual organoids per condition: for AAV2.CMV.GFP 1×10^{10} $n = 5$, 6.6×10^{10} $n = 6$, and 10×10^{10} $n = 7$, and for AAV5.CMV.GFP 1×10^{10} $n = 7$, 6.6×10^{10} $n = 8$, and 10×10^{10} $n = 6$ individual organoids from two independent differentiation rounds. Statical analysis: generalized linear mixed models with $p < 0.05$ (*), $p < 0.01$ (**), and $p < 0.001$ (***)). Related to Supplemental Figure 3.

Fluorescent images of organoids in culture co-treated with AAV.GFP and AAV.hCRB show the presence of GFP positive regions, while no visible differences were observed between treated and untreated organoids using bright field or fluorescent images (Figure 4A). Immunohistochemical staining of CRB1 in AAV.hCRB1 or CRB2 in AAV.hCRB2 treated retinal organoids showed proof of recombinant CRB protein localization at the OLM and in the RPE (Figure 4B, 4C, Supplemental Figure 4F, 4G, 4H, 4I). Further immunohistochemical analysis showed a partially improvement in the observed phenotype after AAV.hCRB1 or AAV.hCRB2 treatment (Figure 4D, E, F). For quantitative analysis, all three CRB1 patient-derived retinal organoids with and without concomitant treatment of AAV.GFP were pooled. No statistically significant difference was observed in fluorescence intensity of MUPP1 at the OLM in untreated compared to AAV.hCRB treated CRB1 patient-derived retinal organoids (Supplemental Figure 4J). In addition, the expression of another core CRB-complex member, PALS1, is not changed after AAV.hCRB treatment (Supplemental Figure 4K).

A statistically significant increased number of photoreceptor nuclei in a row was detected after AAV.hCRB1 and AAV.hCRB2 treatment at DD210, while this large difference was not observed in the treated isogenic controls (Figure 4G). Moreover, the ONL thickness (but not the retinal nor the INL thickness) was significantly increased after AAV.hCRB treatment of CRB1 patient-derived retinal organoids (Figure 4H, Supplemental Figure 4L, 4M). Finally, the number of photoreceptor nuclei above the OLM was significantly improved after AAV.hCRB2 treatment of CRB1 patient-derived retinal organoids at DD210 (Figure 4I). No statistically significant improvement in the number of photoreceptor nuclei above the OLM was observed after AAV.hCRB1 treatment of CRB1 patient-derived retinal organoids nor after AAV.hCRB1 or AAV.hCRB2 treatment in the control retinal organoids (Figure 4I).

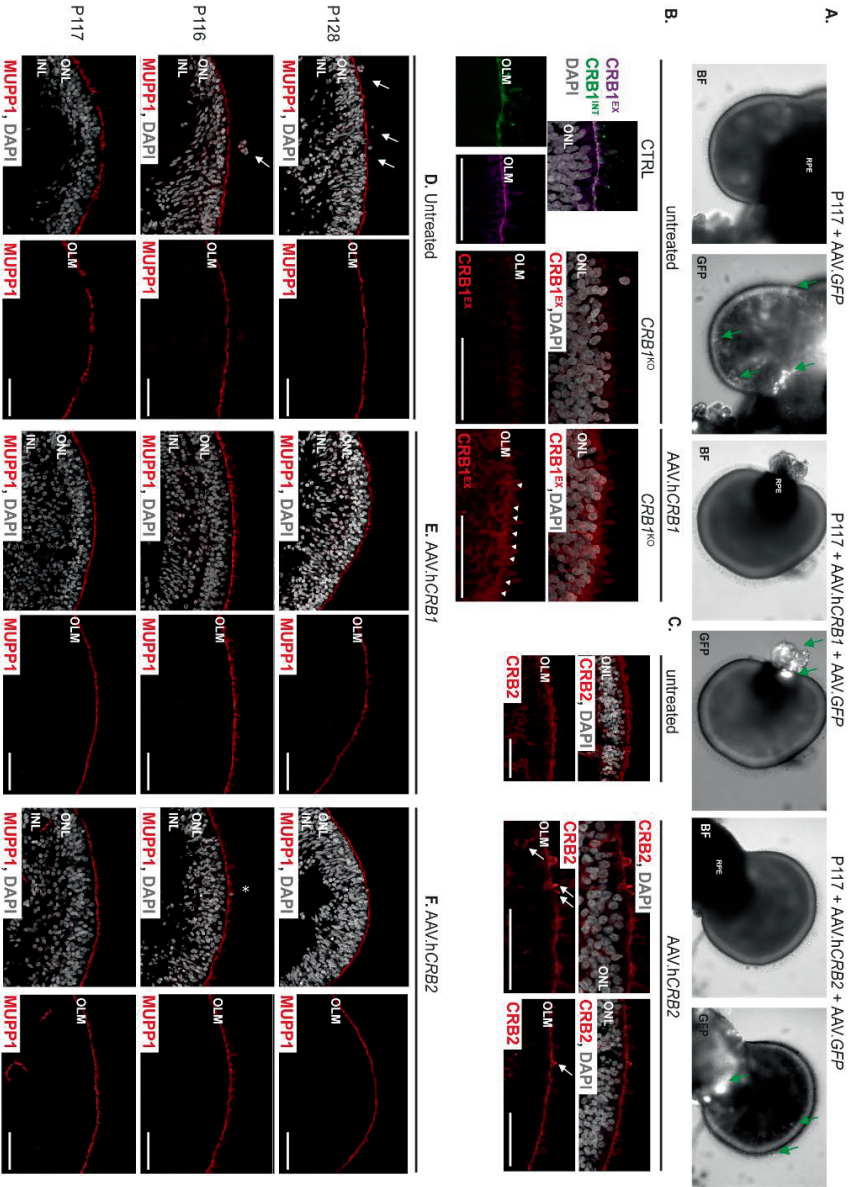


Figure 4 (A-F): AAV-mediated gene therapy treatment on *CRB1* patient-derived and isogenic control retinal organoids.

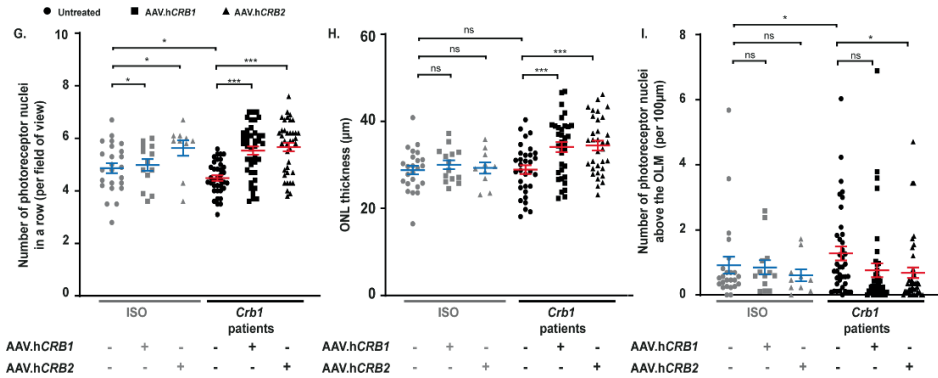


Figure 4 (G-I): AAV-mediated gene therapy treatment on *CRB1* patient-derived and isogenic control retinal organoids.

(A) Representative brightfield (BF) and fluorescent (GFP, GFP regions indicated with green arrow) images of DD210 cultured P117 retinal organoids treated with 3.3×10^{10} vg AAV.hCRB. (B) Immunohistochemical image of CRB1 in untreated control retinal organoid, untreated *CRB1*^{KO} retinal organoid, and AAV.hCRB1 treated *CRB1*^{KO} retinal organoid showing increased CRB1 localization at the OLM of AAV.hCRB1 treated *CRB1*^{KO} retinal organoids (arrowheads). (C) Immunohistochemical image of CRB2 in untreated and AAV.hCRB2 treated *CRB1* patient-derived retinal organoid at the OLM. Arrows indicate overexpression of CRB2 in photoreceptor cells in AAV.hCRB2 treated retinal organoids. (D, E, F): Representative immunohistochemical images of (D) untreated, (E) AAV.hCRB1, and (F) AAV.hCRB2 treated *CRB1* patient retinal organoids stained with MUPP1 (red) at DD210. (G) Quantification of the number of photoreceptor nuclei in a row (from left to right: $p = 0.000$, $p = 0.000$, $p = 0.039$, $p = 0.046$, $p = 0.046$), (H) ONL thickness ($p = 0.001$, $p = 0.001$, $p = 0.923$, $p = 0.757$, $p = 0.243$) and (I) the number of photoreceptor nuclei above the OLM ($p = 0.116$, $p = 0.034$, $p = 0.034$, $p = 0.717$, $p = 0.730$) in three *CRB1* patients and three isogenic control organoids with and without concomitant treatment of AAV.GFP pooled. Scalebar = 50µm. Each datapoint in the graph represent individual organoids, of which an average has been taken of at least 3 representative images. The standard error of mean (SEM) is derived from these averages. Number of individual organoids per condition: *CRB1* patients (P116, P117, P128 pooled) treated with AAV.hCRB1 $n = 34$, AAV.hCRB2 $n = 33$, untreated and GFP treated $n = 32$, and isogenic controls (ISO-02 P116, ISO-03 P116, ISO-P128 pooled) treated with AAV.hCRB1 $n = 14$, AAV.hCRB2 $n = 10$, and untreated and GFP treated $n = 24$ independent organoid from two different differentiation rounds. Statistical tests: generalized linear mixed models with $p < 0.05$ (*), $p < 0.01$ (**), and $p < 0.001$ (***) . Related to Supplemental Figure 4.

Altogether, this data show that the phenotype observed at DD180 and DD210 in *CRB1* patient-derived retinal organoids can be partially restored using AAV.hCRB1 or AAV.hCRB2 treatment.

Differentially expressed genes related to the endosomal system are partially restored in AAV.hCRB treated CRB1 patient-derived retinal organoids

To identify gene expression changes upon *CRB* gene augmentation therapy, all three *CRB1* patient-derived retinal organoids were treated with AAV.h*CRB1* and AAV.*GFP* or AAV.h*CRB2* and AAV.*GFP* and compared to the AAV.*GFP* treated control at DD230 using scRNA-seq. For all three patient-derived retinal organoids, we confirmed that the major retinal cell clusters were equally present in untreated and AAV treated conditions (data not shown). A custom reference with the AAV.*GFP*, codon optimized AAV.h*CRB1* and codon optimized AAV.h*CRB2* sequence were added to the dataset to detect which cell clusters were transduced. While analyzing all organoids and conditions together, we observed that AAV.*GFP* mainly transduces RPE, photoreceptor cells, transient I, and MGC (Supplemental Figure 5A). Specifically, 66% of the RPE, 35% of Rods, 36% of cones, 37% of transient I and 20% of MGC contained AAV.*GFP* expression. This is in line with what we previously observed in the immunohistochemical analysis (Figure 3E, F). Next, AAV.h*CRB1* and AAV.h*CRB2* expression was analyzed in AAV.h*CRB* treated retinal organoids. While being unable to fully distinguish exogenous and endogenous h*CRB* due to the high sequence similarity and the low levels of endogenous *CRB1* and *CRB2* in DD230 RPE, we observed a significant increase of AAV.h*CRB1* in AAV.h*CRB1* treated and AAV.h*CRB2* in AAV.h*CRB2* treated organoids in the RPE of the *CRB1* patient-derived retinal organoids (Supplemental Figure 5B, 5C).

Differential gene expression followed by GO term analysis of AAV.h*CRB1* treatment compared to untreated P128 retinal organoids in MGC revealed differences related to the endosomal system, cell-cell adhesion, and protein or receptor binding (Figure 5A). Also for AAV.h*CRB2* treatment similar terms were observed to be statistically significant in P128 (Figure 5C). Next, these GO terms and differentially expressed genes were compared to the ones observed when contrasting P128 with ISO-P128. Overlapping differentially expressed genes associated with the endosomal system show that after AAV.h*CRB1* treatment the expression levels from the patient retinal organoids are similar to levels of the isogenic control (Figure 5B). Moreover, after

AAV.h*CRB2* treatment the genes associated with the endosomal system appeared to be restored as well in MGC (Figure 5D).

Similar comparisons were performed for the other two *CRB1*^{-/-} patient-derived retinal organoids. For P116 and P117, statistically significant GO terms related to the endosomal system were also observed after AAV.h*CRB1* and AAV.h*CRB2* treatment (Supplemental Figure 5D, 5E, 5G, 5I, 5K). When analyzing in more detail the differentially expressed genes associated with the endosomal system in AAV.h*CRB1* treated P116 organoids, transcript levels seemed to be restored to isogenic control levels in MGC (Supplemental Figure 5J) as well as in rod photoreceptor cells (Supplemental Figure 5L). The genes for ISO-P116 indicated with a dashed line box around them were not statistically significant different from P116, but the genes after AAV.h*CRB* treatment are similarly expressed as the average expression in ISO-P116 (Supplemental Figure 5J). Similar results were observed for genes associated with the endosomal system in AAV.h*CRB2* treated organoids (Supplemental Figure 5I). Moreover, after both AAV.h*CRB1* and AAV.h*CRB2* treatment in MGC of P117, we observed that the expression levels changed in a similar direction (Supplemental Figure 5F).

In summary, AAV.h*CRB1* as well as AAV.h*CRB2* treatment on *CRB1* patient-derived retinal organoids restores gene expression related to the endosomal system back to isogenic control levels.

Discussion

In this manuscript we have (1) shown diminished levels of variant *CRB1* protein in *CRB1* retinitis pigmentosa patient retinal organoids that harbor missense mutations, (2) demonstrated moderate loss of photoreceptors in *CRB1* patient-derived retinal organoids at DD210, (3) detected transcriptional differences suggesting changes within the endosomal system in *CRB1* patient compared to isogenic control organoids, (4) shown that AAV5.CMV.*GFP* efficiently transduced MGCs in addition to photoreceptors and RPE at DD120, and (5) observed a partially restored phenotype after AAV.h*CRB1* or AAV.h*CRB2* mediated gene therapy in *CRB1* patient-derived retinal organoids.

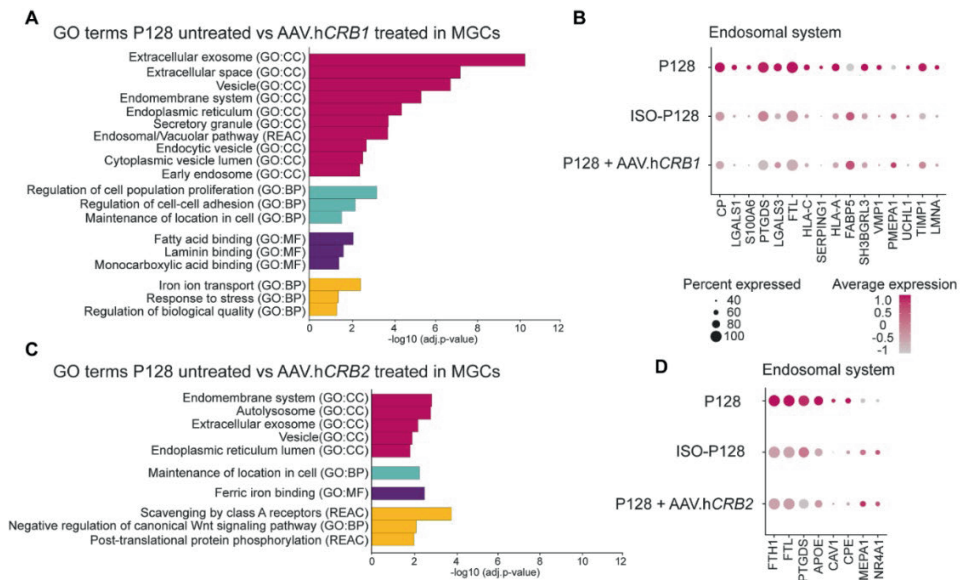


Figure 5: Single cell RNA-sequencing of *CRB1* patient-derived retinal organoid treated with AAV.hCRB1 or AAV.hCRB2 restores transcriptional effect on the endosomal system. (A,C) Gene ontology (GO) analysis of differentially expressed markers contrasting untreated with (A) AAV.hCRB1 or (C) AAV.hCRB2 treated P128 in MGCs clustered in groups with similar terms in the same colour. (B, D) All significantly differentially expressed markers in terms related to the endosomal system after treatment with (B) AAV.hCRB1 or (D) AAV.hCRB2. All markers present in (B, D) are also statistically significant for P128 compared to ISO-P128. Number of independent organoids used: P128 $n = 6$, P128 with AAV.hCRB1 $n = 5$, P128 with AAV.hCRB2 $n = 5$ from one differentiation round equally divided into three separate sequencing rounds. Related to Supplemental Figure 5.

CRB1 patient's clinical and genetic characteristics were described previously in detail in a prospective natural history study on 22 patients [3]. The P116 retinal organoids were derived from skin fibroblasts from a patient with at first diagnosis retinitis pigmentosa and discontinuous outer limiting membrane (OLM) and ellipsoid zone (EZ) in parafovea and perifovea on spectral domain optical coherence tomography (SD-OCT), see supplemental tables 1 and 2 in Nguyen et al 2022. The P117 retinal organoids were derived from a patient that experienced mild retinitis pigmentosa with at first diagnosis loss of visual acuity and continuous OLM and EZ in parafovea and perifovea. The P128 retinal organoids were derived from a patient with at first diagnosis retinitis pigmentosa, nyctalopia, and discontinuous OLM and EZ in parafovea and perifovea.

Here, the *CRB1* patient-derived retinal organoids were compared to corresponding isogenic controls at DD210. We show a decreased number of photoreceptor nuclei in a row and a reduced ONL thickness in the *CRB1* patient-derived retinal organoids compared to the isogenic controls. Decreased levels of variant CRB1 at the OLM of *CRB1* patient-derived retinal organoids might be associated with increased protrusion of photoreceptor cell bodies into the cell culture medium at DD180 [23] and thinning of the photoreceptor outer nuclear layer at DD210 (current manuscript). This process is similar to the complete loss of CRB1 at the OLM in *Crb1* mouse retina which results in protrusion of photoreceptor cell bodies into the subretinal space [8,16] or the loss of CRB2 at the OLM in *Crb2* mouse retina [20].

Moreover, it was shown that CRB1 and CRB2 are present at the OLM of both photoreceptor and MGCs in iPSC-derived retinal organoids [23]. Our scRNA-seq data confirms on the transcriptome, with more *CRB1* expression in MGCs than in photoreceptor cells and more *CRB2* expression in photoreceptor cells than in MGCs. The rather high expression levels of *CRB1* and low levels of *CRB2* in MGCs might be related to the phenotype variation, since mutations in *CRB1* may cause either early onset RP or LCA. Variable low levels of *CRB2* transcripts in MGCs of *CRB1* patients may be involved in the severity of the phenotype. Such a hypothesis would be in strong correlation with our previous studies in mice, that suggests a modifying role for *CRB2* in *CRB1*-related dystrophies [13,14,17,21,26].

CRB1 variant protein at the OLM was strongly diminished in *CRB1* patient-derived retinal organoids, while *CRB1* expression levels remained similar. In contrast, CRB core complex members as well as the FERM proteins remained at the OLM and similar expression levels were observed. This indicates that a variant CRB1 protein is produced but it does not localize to or maintain its expected location at the OLM. The endolysosomal system is required for transport of CRB1 to the OLM but also for recycling of endocytosed CRB1 from the early endosome to the OLM and the transport into degradative vesicles. *Drosophila* studies show that Crb trafficking is mediated by transport along microtubules by Rab11- and retromer-containing endosomes [27,28]. In addition, in *Drosophila* salivary gland cells Crumbs maintains the active pool of Rab

proteins at the apical domain, which is essential for maintaining the organization of the apical membrane and efficient apical secretion [29]. The scRNA-seq gene ontology data shown here suggests an aberrant endosomal pathway specifically in MGCs and rods of *CRB1* patient-derived retinal organoids. Dysregulation of CRB1 at the OLM can thus cause changes in the endosomal system. Endosomal recycling is pivotal for maintenance of neuronal health, and defects in its function results in human neurodegenerative disorders [30,31]. We hypothesize that the reduced levels of variant CRB1 at the OLM are caused by disturbed variant CRB1 protein transport to the OLM, or disturbed endosomal recycling of variant CRB1 between OLM and the early endosome, or increased variant CRB1 degradation in the retinal organoids. Preliminary studies suggest changes in the recycling endosome and in degradative vesicles (Buck TM et al Wijnholds J, unpublished results). In analogy to the roles of the Crumbs protein in *Drosophila* salivary glands [29], in future studies we will examine the putative role for CRB1 in the maintenance of an active pool of RAB11 and VPS35 (retromer) recycling endosome proteins at the OLM.

Previously, we described an improved phenotype after AAV.h*CRB2* treatment in *Crb* mutant mouse models [13,14]. Here, we investigated whether we could observe an improved CRB1-RP phenotype after AAV-mediated gene augmentation therapy in *CRB1* patient-derived retinal organoids. Proof-of-concept for developing gene therapy in retinal organoids for CRX-LCA has been described, where AAVs were used to alleviate the phenotype observed in CRX mutant retinal organoids [32]. In addition, AAV-mediated gene augmentation of RP2 knock-out retinal organoids prevents ONL thinning and restored rhodopsin expression [33]. In this manuscript, using AAV.h*CRB1* and AAV.h*CRB2* gene augmentation therapy, a partially restored phenotype was observed in *CRB1* patient-derived retinal organoids. The number of photoreceptor nuclei in a row and ONL thickness were significantly improved after AAV.h*CRB* treatment when analyzed at DD210, showing the long-term effects of the gene augmentation therapy. Moreover, neither positive nor negative effects were observed when treating isogenic controls with AAV.h*CRB1* or AAV.h*CRB2*. Furthermore, the infection of AAV.h*CRB1* on the *CRB1*^{KO} retinal organoids show localization of recombinant CRB1 protein at the OLM. Whereas the recombinant CRB1 protein

localizes merely at the OLM, we also detected CRB1 protein around the OLM as previously detected in first trimester human fetal retina and DD120 immature wild type retinal organoids [23]. The imprecise localization of recombinant CRB1 is potentially related to a partial restoration of CRB1-positive recycling endosomal vesicles at the OLM and is subject of future studies. To our knowledge, this is the first time that an improved phenotype after AAV.hCRB gene augmentation in *CRB1* patient-derived retinal organoids is observed.

In conclusion, we demonstrate in *CRB1* patient-derived retinal organoids a moderate loss of photoreceptor nuclei in a row, strongly reduced levels of CRB1 variant protein with unaffected *CRB1* transcript levels, and a dysregulated molecular gene profiling phenotype of MGC and rod photoreceptor cells, suggesting an aberrant endosomal system. Moreover, using AAV-mediated gene augmentation therapy approaches we have improved the histological and transcriptional retinal phenotype in *CRB1* patient-derived retinal organoids. These data provide essential information for future gene therapy approaches for patients with mutations in the *CRB1* gene.

Experimental procedures

Cell culture and retinal organoid differentiation

The following hiPSC lines were used for organoid differentiation: three *CRB1* RP patient-derived lines and one control (LUMC0116iCRB09, LUMC0117iCRB01, LUMC0128iCRB01, LUMC0004iCTRL10; [23]), and three isogenic controls of the *CRB1* patient-derived lines (LUMC0116iCRB-ISO02, LUMC0116iCRB-ISO03, LUMC0128iCRB-ISO01) (Supplemental Figure 1, Supplemental Table 1). hiPSC lines were derived from skin fibroblast using polycistronic Lentiviral vectors [34].

hiPSC were maintained on Matrigel coated plates in mTeSR plus medium and passaged mechanically using gentle cell dissociation reagent (STEMCELL Technologies). Retinal organoid differentiation was carried out as previously reported with some modifications (Supplemental experimental procedures) [23,35]. Retinal organoids were collected at DD180 or DD210 for immunohistochemical analysis; a list of all primary

antibodies used for immunofluorescent staining is provided in (Supplemental Table 2). At least three different differentiation batches were analyzed to verify disease phenotypes.

AAV transduction of hiPSC-derived retinal organoids

Two to three retinal organoids were plated in a 96-well agarose coated plate and were infected with AAV in 50 μ L RLM2 and incubated for 8h at 5% CO₂ at 37°C. After this, the wells were topped up to 200 μ L with RLM2. The next morning, treated organoids were transferred to a 24 well plate and cultured for at least 3 weeks or until the desired differentiation day. AAV5.CMV.*GFP* and AAV2.CMV.*GFP* (105530; Addgene) were used at a titer of 1×10^{10} , 3.3×10^{10} , 6.6×10^{10} , or 10×10^{10} gc. AAV5.CMVmin.h*CRB1* and AAV5.CMV.h*CRB2* (HORAMA) were used with a titer of 3.3×10^{10} gc.

Quantification and statistical analysis

40x magnification images were manually quantified using Fiji ImageJ (ImageJ 1.53f51). At least 4 organoids per condition with 3-6 representative images of each organoid were used for quantification. Three regions in each image were manually analyzed for the number of photoreceptor nuclei in a row in the ONL, the number of photoreceptor nuclei above the OLM, retinal thickness, INL thickness, and ONL thickness. Quantifications were performed independently by at least two researchers without the knowledge of genotype or treatment. For the MUPP1 quantifications, a ROI was drawn at the OLM and the average intensity was measured using ImageJ. All datapoints measured were averaged per organoid and plotted in the graph; so that each point is one organoid. No normalization of the values was performed. Data were either presented per 100 μ m retinal length or per field of view. Data presentation and statistical analysis were performed using GraphPad Prism version 8 (GraphPad Software) and IBM SPSS statistics (version 25), respectively. For statistical analysis, all individual values per image were used. A generalized linear mixed models with treatment (and patient) as a fixed effect was performed on all quantification parameters; the statistical test took into account that multiple *CRB1* patients were merged by introducing a

random intercept per patient. Data is presented as mean per organoid \pm standard error of the mean (SEM). Significance is indicated in graphs as $p < 0.05$ (*), $p < 0.01$ (**), and $p < 0.001$ (***)).

Single cell RNA sequencing

Retinal organoids were dissociated using an adapted protocol from the Papain Dissociation kit (Worthington, I-LK 03150). Analysis and processing of single-cell transcriptomics using Seurat is detailed in supplemental experimental procedures.

Article information

Data and code availability: Accession number for the scRNA-seq data reported in this paper GSE212582.

Funding: This work was funded by The Netherlands Organization for Health Research and Development (ZonMw grant 43200004, to JW), research grant MDBR-19-131-CRB1 from the University of Pennsylvania Orphan Disease Center in partnership with the Curing Retinal Blindness Foundation (to JW), Bontius Stichting 32072-8231, and HORAMA 41400-8231.

Author contributions: Conceptualization, N.B. and J.W.; Software, N.B., I.M., S.B. and H.M; Formal analysis, N.B.; Investigation, N.B., X.L., C.A.A, and T.M.B.; Resources, C.J.F.B., C.F., and C.H.A.; Data curation, N.B. and I.M.; Writing – original draft, N.B.; Writing – review & editing, N.B., and J.W.; Visualization, N.B.; Supervision, J.W.; Project administration, J.W.; Funding acquisition, J.W.

Acknowledgements: The authors would like to thank the LUMC light and electron microscope facility for help during image acquisition, Susan Kloet and Roberta Menafra from the Leiden Genome Technology Center for building the custom references for the single cell dataset, Gaëlle Lefevre from Coave Therapeutics, and all the members of the Wijnholds lab for advice on experiments and the manuscript.

Abbreviations

AAV	Adeno-associated viral vectors
CRB1	Crumbs homolog-1
CNV	Copy number variation
CMV	Cytomegalovirus
CRALBP	Cellular retinaldehyde-binding protein
DD210	Differentiation day 210
EGF	Epidermal growth factor
ERLI	Glutamic acid-arginine-leucine-isoleucine
FERM	Protein 4.1, Ezrin, Radixin, Moesin
GFP	Green Fluorescent Protein
GO	Gene ontology
hiPSC	Human-induced pluripotent stem cell
INL	Inner nuclear layer
LCA	Leber congenital amaurosis
MGC	Müller glial cell
MPP5	Membrane-associated guanylate kinase p55 subfamily member 5
MUPP1	Multiple PDZ domain protein 1
NGS	Next Generation Sequencing
OLM	Outer limiting membrane
ONL	Outer nuclear layer
OPL	Outer plexiform layer
OTX2	Orthodenticle Homebox2
PALS1	Protein associated with Lin Seven 1
RHO	Rhodopsin
RP	Retinitis pigmentosa
RPE	Retinal pigment epithelium
RT	Room temperature
RT-qPCR	Reverse transcription quantitative real-time PCR
SAR	Subapical region
scRNA-seq	Single cell RNA-sequencing
SEM	Standard error of mean
SOX9	SRY-Box Transcription Factor 9

References

1. Den Hollander, A.I.; Ten Brink, J.B.; De Kok, Y.J.M.; Van Soest, S.; Van Den Born, L.I.; Van Driel, M.A.; Van De Pol, D.J.R.; Payne, A.M.; Bhattacharya, S.S.; Kellner, U.; et al. Mutations in a human homologue of *Drosophila* crumbs cause retinitis pigmentosa (RP12). *Nat. Genet.* **1999**, *23*, 217–221, doi:10.1038/13848.
2. Talib, M.; van Schooneveld, M.J.; van Genderen, M.M.; Wijnholds, J.; Florijn, R.J.; ten Brink, J.B.; Schalijs-Delfos, N.E.; Dagnelie, G.; Cremers, F.P.M.; Wolterbeek, R.; et al. Genotypic and Phenotypic Characteristics of CRB1-Associated

Retinal Dystrophies: A Long-Term Follow-up Study. *Ophthalmology* **2017**, *124*, 884–895, doi:10.1016/j.ophtha.2017.01.047.

3. Nguyen, X.T.A.; Talib, M.; van Schooneveld, M.J.; Wijnholds, J.; van Genderen, M.M.; Schalij-Delfos, N.E.; Klaver, C.C.W.; Talsma, H.E.; Fiocco, M.; Florijn, R.J.; et al. CRB1-Associated Retinal Dystrophies: A Prospective Natural History Study in Anticipation of Future Clinical Trials. *Am. J. Ophthalmol.* **2022**, *234*, 37–48, doi:10.1016/j.ajo.2021.07.021.

4. Boon, N.; Wijnholds, J.; Pellissier, L.P. Research Models and Gene Augmentation Therapy for CRB1 Retinal Dystrophies. *Front. Neurosci.* **2020**, *14*, 1–13, doi:10.3389/fnins.2020.00860.

5. Quinn, P.M.; Pellissier, L.P.; Wijnholds, J. The CRB1 complex: Following the trail of crumbs to a feasible gene therapy strategy. *Front. Neurosci.* **2017**, *11*, doi:10.3389/fnins.2017.00175.

6. Ray, T.A.; Cochran, K.; Kozlowski, C.; Wang, J.; Alexander, G.; Cady, M.A.; Spencer, W.J.; Ruzycki, P.A.; Clark, B.S.; Laeremans, A.; et al. Comprehensive identification of mRNA isoforms reveals the diversity of neural cell-surface molecules with roles in retinal development and disease. *Nat. Commun.* **2020**, *11*, doi:10.1038/s41467-020-17009-7.

7. Roh, M.H.; Makarova, O.; Liu, C.J.; Shin, K.; Lee, S.; Laurinec, S.; Goyal, M.; Wiggins, R.; Margolis, B. The Maguk protein, Pals1, functions as an adapter, linking mammalian homologues of crumbs and discs lost. *J. Cell Biol.* **2002**, *157*, 161–172, doi:10.1083/jcb.200109010.

8. van de Pavert, S.A.; Kantardzhieva, A.; Malysheva, A.; Meuleman, J.; Versteeg, I.; Levelt, C.; Klooster, J.; Geiger, S.; Seeliger, M.W.; Rashbass, P.; et al. Crumbs homologue 1 is required for maintenance of photoreceptor cell polarization and adhesion during light exposure. *J. Cell Sci.* **2004**, *117*, 4169–4177, doi:10.1242/jcs.01301.

9. Margolis, B. The Crumbs3 polarity protein. *Cold Spring Harb. Perspect. Biol.* **2018**, *10*, 1–9, doi:10.1101/cshperspect.a027961.

10. Bulgakova, N.A.; Knust, E. The Crumbs complex: From epithelial-cell polarity to retinal degeneration. *J. Cell Sci.* **2009**, *122*, 2587–2596, doi:10.1242/jcs.023648.

11. Maguire, A.M.; Russell, S.; Wellman, J.A.; Chung, D.C.; Yu, Z.F.; Tillman, A.; Wittes, J.; Pappas, J.; Elci, O.; Marshall, K.A.; et al. Efficacy, Safety, and Durability of Voretigene Neparvovec-rzyl in RPE65 Mutation-Associated Inherited Retinal Dystrophy: Results of Phase 1 and 3 Trials. *Ophthalmology* **2019**, *126*, 1273–1285, doi:10.1016/j.ophtha.2019.06.017.

12. Pellissier, L.P.; Hoek, R.M.; Vos, R.M.; Aartsen, W.M.; Klimczak, R.R.; Hoyng, S.A.; Flannery, J.G.; Wijnholds, J. Specific tools for targeting and expression

in Müller glial cells. *Mol. Ther. - Methods Clin. Dev.* **2014**, *1*, 14009, doi:10.1038/mtm.2014.9.

13. Pellissier, L.P.; Quinn, P.M.; Henrique Alves, C.; Vos, R.M.; Klooster, J.; Flannery, J.G.; Alexander Heimel, J.; Wijnholds, J. Gene therapy into photoreceptors and Müller glial cells restores retinal structure and function in *CRB1* retinitis pigmentosa mouse models. *Hum. Mol. Genet.* **2015**, *24*, 3104–3118, doi:10.1093/hmg/ddv062.

14. Buck, T.M.; Vos, R.M.; Alves, C.H.; Wijnholds, J. AAV-*CRB2* protects against vision loss in an inducible *CRB1* retinitis pigmentosa mouse model. *Mol. Ther. Methods Clin. Dev.* **2021**, *20*, 423–441, doi:10.1016/j.omtm.2020.12.012.

15. Pellissier, L.P.; Alves, C.H.; Quinn, P.M.; Vos, R.M.; Tanimoto, N.; Lundvig, D.M.S.; Dudok, J.J.; Hooibrink, B.; Richard, F.; Beck, S.C.; et al. Targeted Ablation of *Crb1* and *Crb2* in Retinal Progenitor Cells Mimics Leber Congenital Amaurosis. *PLoS Genet.* **2013**, *9*, doi:10.1371/journal.pgen.1003976.

16. van de Pavert, S.A.; Meuleman, J.; Malysheva, A.; Aartsen, W.M.; Versteeg, I.; Tonagel, F.; Kamphuis, W.; McCabe, C.J.; Seeliger, M.W.; Wijnholds, J. A single amino acid substitution (Cys249Trp) in *Crb1* causes retinal degeneration and deregulates expression of pituitary tumor transforming gene *Pttg1*. *J. Neurosci.* **2007**, *27*, 564–573, doi:10.1523/JNEUROSCI.3496-06.2007.

17. Quinn, P.M.; Mulder, A.A.; Henrique Alves, C.; Desrosiers, M.; de Vries, S.I.; Klooster, J.; Dalkara, D.; Koster, A.J.; Jost, C.R.; Wijnholds, J. Loss of *CRB2* in Müller glial cells modifies a *CRB1*-associated retinitis pigmentosa phenotype into a Leber congenital amaurosis phenotype. *Hum. Mol. Genet.* **2019**, *28*, 105–123, doi:10.1093/hmg/ddy337.

18. Alves, C.H.; Boon, N.; Mulder, A.A.; Koster, A.J.; Jost, C.R.; Wijnholds, J. *CRB2* Loss in Rod Photoreceptors Is Associated with Progressive Loss of Retinal Contrast Sensitivity. *Int. J. Mol. Sci.* **2019**, *20*, 4069, doi:10.3390/ijms20174069.

19. Mehalow, A.K.; Kameya, S.; Smith, R.S.; Hawes, N.L.; Denegre, J.M.; Young, J.A.; Bechtold, L.; Haider, N.B.; Tepass, U.; Heckenlively, J.R.; et al. *CRB1* is essential for external limiting membrane integrity and photoreceptor morphogenesis in the mammalian retina. *Hum. Mol. Genet.* **2003**, *12*, 2179–2189, doi:10.1093/hmg/ddg232.

20. Alves, C.H.; Bossers, K.; Vos, R.M.; Essing, A.H.W.; Swagemakers, S.; Van Der Spek, P.J.; Verhaagen, J.; Wijnholds, J. Microarray and morphological analysis of early postnatal *CRB2* mutant retinas on a pure C57BL/6J genetic background. *PLoS One* **2013**, *8*, 1–17, doi:10.1371/journal.pone.0082532.

21. Quinn, P.M.; Alves, C.H.; Klooster, J.; Wijnholds, J. *CRB2* in immature photoreceptors determines the superior-inferior symmetry of the developing retina to

maintain retinal structure and function. *Hum. Mol. Genet.* **2018**, *27*, 3137–3153, doi:10.1093/hmg/ddy194.

22. van Rossum, A.G.S.H.; Aartsen, W.M.; Meuleman, J.; Klooster, J.; Malysheva, A.; Versteeg, I.; Arsanto, J.P.; Le Bivic, A.; Wijnholds, J. Pals1/Mpp5 is required for correct localization of Crb1 at the subapical region in polarized Müller glia cells. *Hum. Mol. Genet.* **2006**, *15*, 2659–2672, doi:10.1093/hmg/ddl194.

23. Quinn, P.M.; Buck, T.M.; Mulder, A.A.; Ohonin, C.; Alves, C.H.; Vos, R.M.; Bialecka, M.; van Herwaarden, T.; van Dijk, E.H.C.; Talib, M.; et al. Human iPSC-Derived Retinas Recapitulate the Fetal CRB1 CRB2 Complex Formation and Demonstrate that Photoreceptors and Müller Glia Are Targets of AAV5. *Stem Cell Reports* **2019**, *12*, 906–919, doi:10.1016/j.stemcr.2019.03.002.

24. Assou, S.; Girault, N.; Plinet, M.; Bouckenheimer, J.; Sansac, C.; Combe, M.; Mianné, J.; Bourguignon, C.; Fieldes, M.; Ahmed, E.; et al. Recurrent Genetic Abnormalities in Human Pluripotent Stem Cells: Definition and Routine Detection in Culture Supernatant by Targeted Droplet Digital PCR. *Stem Cell Reports* **2020**, *14*, 1–8, doi:10.1016/j.stemcr.2019.12.004.

25. Swaroop, A.; Kim, D.; Forrest, D. Transcriptional regulation of photoreceptor development and homeostasis in the mammalian retina. *Nat. Rev. Neurosci.* **2010**, *11*, 563–576, doi:10.1038/nrn2880.

26. Pellissier, L.P.; Lundvig, D.M.S.; Tanimoto, N.; Klooster, J.; Vos, R.M.; Richard, F.; Sothilingam, V.; Garrido, M.G.; Bivic, A. Le; Seeliger, M.W.; et al. CRB2 acts as a modifying factor of CRB1-related retinal dystrophies in mice. *Hum. Mol. Genet.* **2014**, *23*, 3759–3771, doi:10.1093/hmg/ddu089.

27. Aguilar-Aragon, M.; Fletcher, G.; Thompson, B.J. The cytoskeletal motor proteins Dynein and MyoV direct apical transport of Crumbs. *Dev. Biol.* **2020**, *459*, 126–137, doi:10.1016/j.ydbio.2019.12.009.

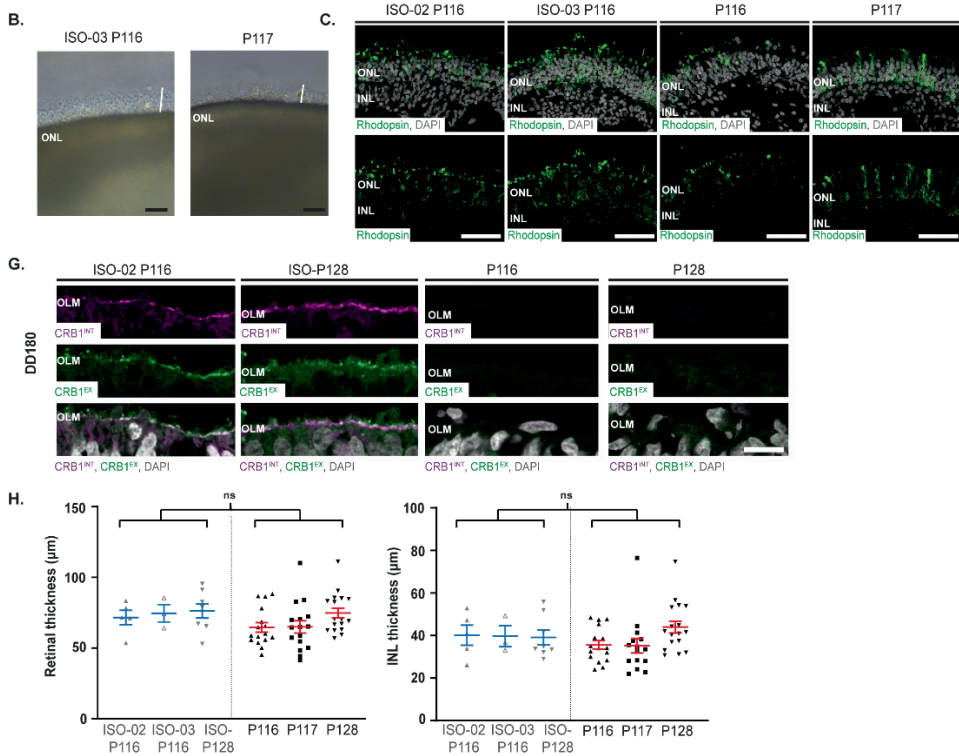
28. Pocha, S.M.; Wassmer, T.; Niehage, C.; Hoflack, B.; Knust, E. Retromer controls epithelial cell polarity by trafficking the apical determinant crumbs. *Curr. Biol.* **2011**, *21*, 1111–1117, doi:10.1016/j.cub.2011.05.007.

29. Lattner, J.; Leng, W.; Knust, E.; Brankatschk, M.; Flores-Benitez, D. Crumbs organizes the transport machinery by regulating apical levels of pi (4,5)p2 in drosophila. *Elife* **2019**, *8*, 1–45, doi:10.7554/eLife.50900.

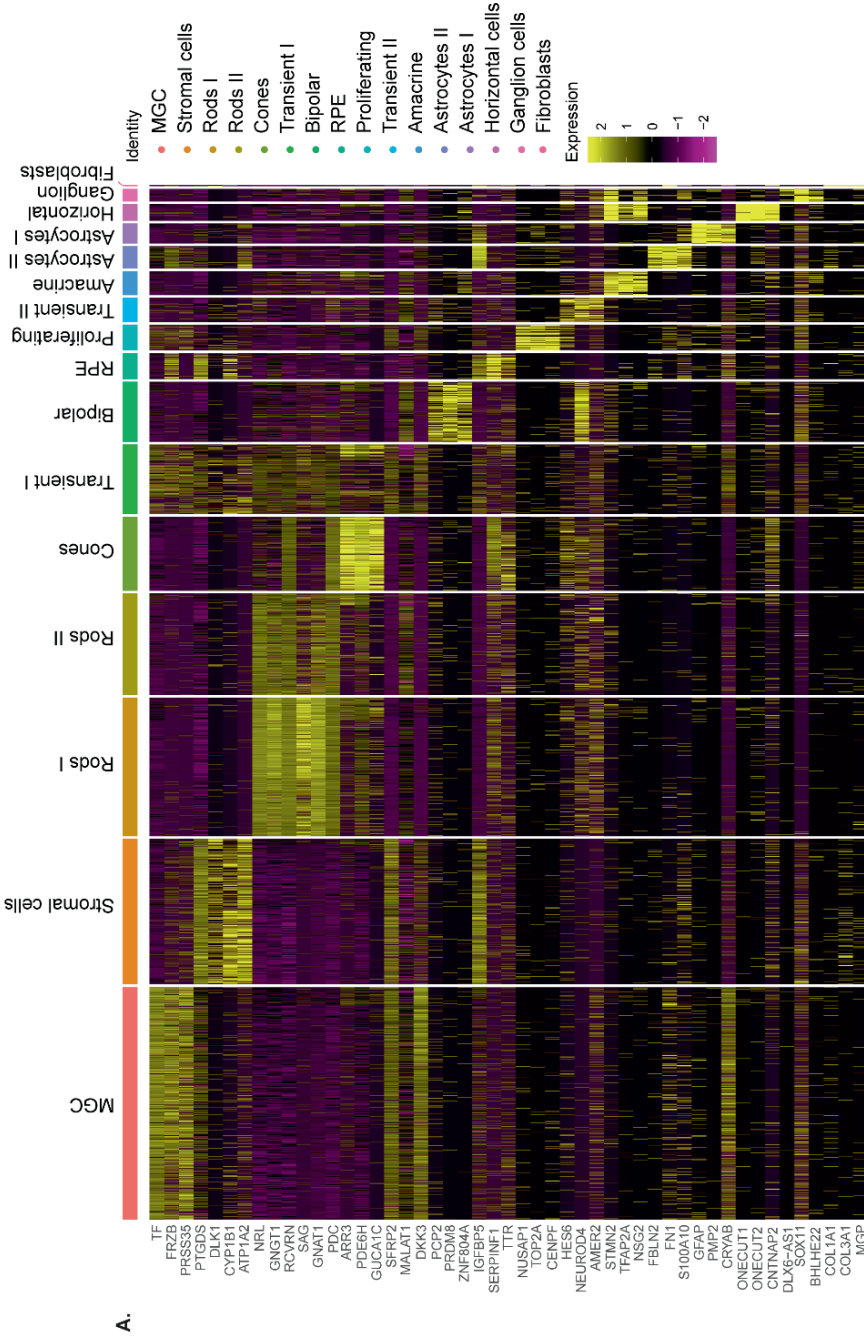
30. Saitoh, S. Endosomal Recycling Defects and Neurodevelopmental Disorders. *Cells* **2022**, *11*, doi:10.3390/cells11010148.

31. Tang, F.L.; Erion, J.R.; Tian, Y.; Liu, W.; Yin, D.M.; Ye, J.; Tang, B.; Mei, L.; Xiong, W.C. VPS35 in dopamine neurons is required for endosome-to- golgi retrieval of Lamp2a, a receptor of chaperone-mediated autophagy that is critical for α -synuclein degradation and prevention of pathogenesis of Parkinson's disease. *J. Neurosci.* **2015**, *35*, 10613–10628, doi:10.1523/JNEUROSCI.0042-15.2015.

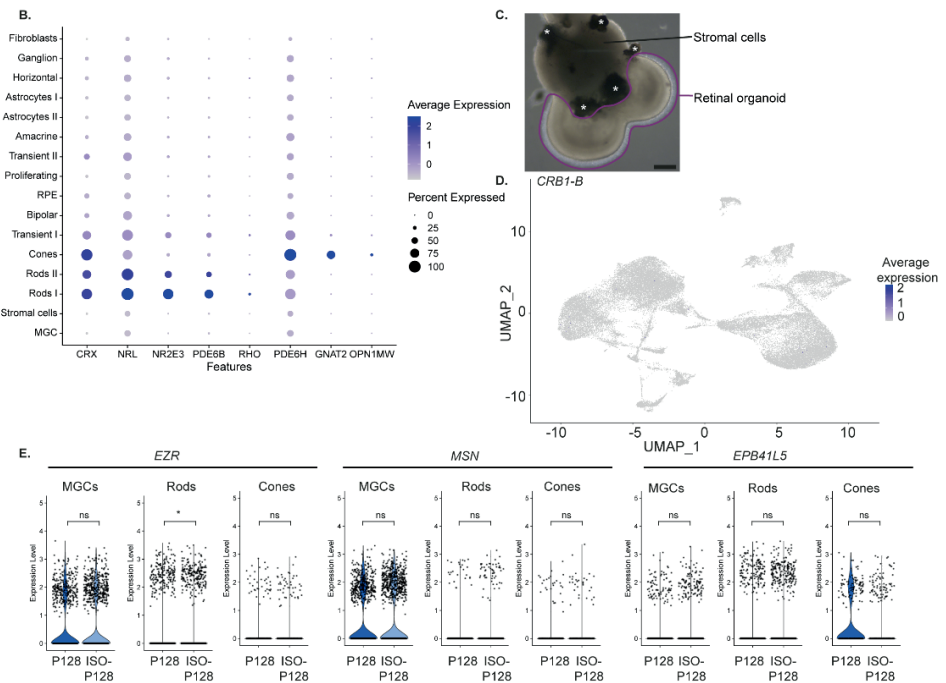
32. Kruczek, K.; Qu, Z.; Gentry, J.; Fadl, B.R.; Gieser, L.; Hiriyan, S.; Batz, Z.; Samant, M.; Samanta, A.; Chu, C.J.; et al. Gene Therapy of Dominant CRX-Leber Congenital Amaurosis using Patient Stem Cell-Derived Retinal Organoids. *Stem Cell Reports* **2021**, *16*, 252–263, doi:10.1016/j.stemcr.2020.12.018.
33. Lane, A.; Jovanovic, K.; Shortall, C.; Ottaviani, D.; Panes, A.B.; Schwarz, N.; Guarascio, R.; Hayes, M.J.; Palfi, A.; Chadderton, N.; et al. Modeling and Rescue of RP2 Retinitis Pigmentosa Using iPSC-Derived Retinal Organoids. *Stem Cell Reports* **2020**, *15*, 67–79, doi:10.1016/j.stemcr.2020.05.007.
34. Warlich, E.; Kuehle, J.; Cantz, T.; Brugman, M.H.; Maetzig, T.; Galla, M.; Filipczyk, A.A.; Halle, S.; Klump, H.; Schöler, H.R.; et al. Lentiviral vector design and imaging approaches to visualize the early stages of cellular reprogramming. *Mol. Ther.* **2011**, *19*, 782–789, doi:10.1038/mt.2010.314.
35. Zhong, X.; Gutierrez, C.; Xue, T.; Hampton, C.; Vergara, M.N.; Cao, L.H.; Peters, A.; Park, T.S.; Zambidis, E.T.; Meyer, J.S.; et al. Generation of three-dimensional retinal tissue with functional photoreceptors from human iPSCs. *Nat. Commun.* **2014**, *5*, doi:10.1038/ncomms5047.



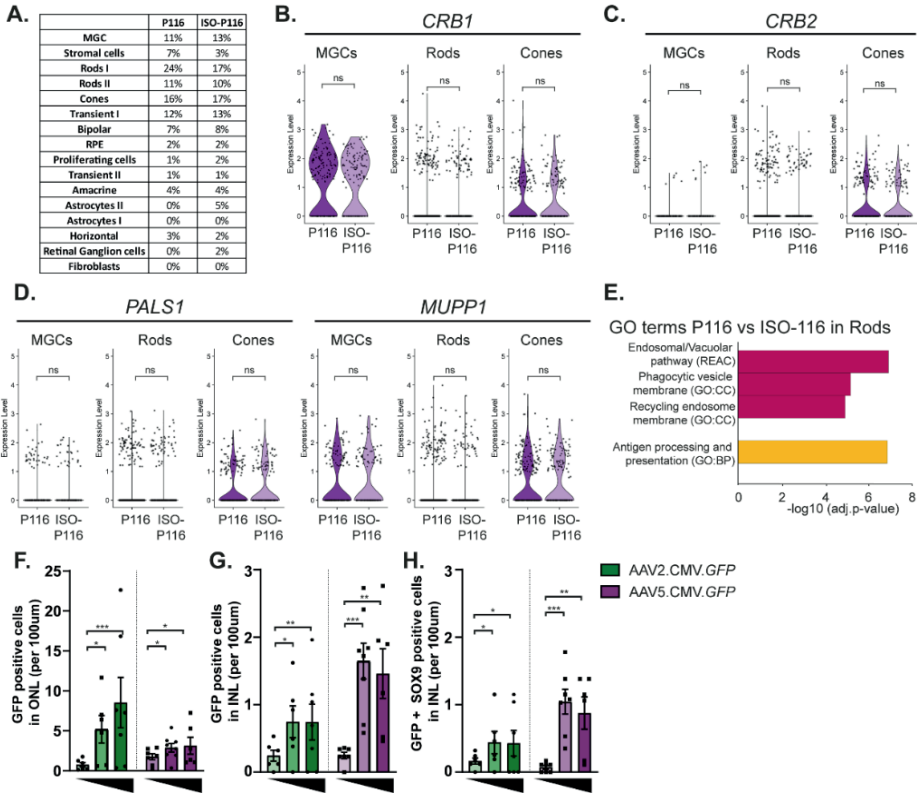
Supplemental Figure 1 (B, C, G, H): *CRB1* patient derived and isogenic control retinal organoids phenotypic analysis at DD210. (B) Representative brightfield images of ISO-03 P116 and P117 cultured organoids. (C) Representative immunohistochemical images of rhodopsin (green) in ISO-02 P116, ISO-03 P116, P116, and P117. (D) Representative immunohistochemical images of SOX9 (red) in ISO-P128, P128, P117, and ISO-03 P116. (E, F) Representative immunohistochemical images of (E) CRB1 (magenta) co-localized with MUPP1 (green) and of (F) CRB2 (magenta) co-localized with PALS1 (green) in ISO-03 P116. (G) Representative immunohistochemical images of CRB1^{EX} (green) and CRB1^{INT} (magenta) in *CRB1* patient-derived retinal organoids compared to isogenic controls at DD180. (H) Quantitative analysis of the total retinal thickness ($p = 0.158$) and INL thickness ($p = 0.696$) per field of view in *CRB1* patient derived and isogenic control retinal organoids. Each datapoint in the graph represent individual organoids, of which an average has been taken of at least 3 representative images. The standard error of mean (SEM) is derived from these averages. Number of individual organoids per condition and differentiation round: P116 $n = 16$, P117 $n = 15$, P128 $n = 17$ from four independent organoid batches, ISO-P128 $n = 8$ from three independent organoid batches, ISO-02 P116 $n = 5$ and ISO-03 P116 $n = 5$ from two independent organoid batches. Scalebar = (C-F) 50 μ m, (G) 10 μ m.



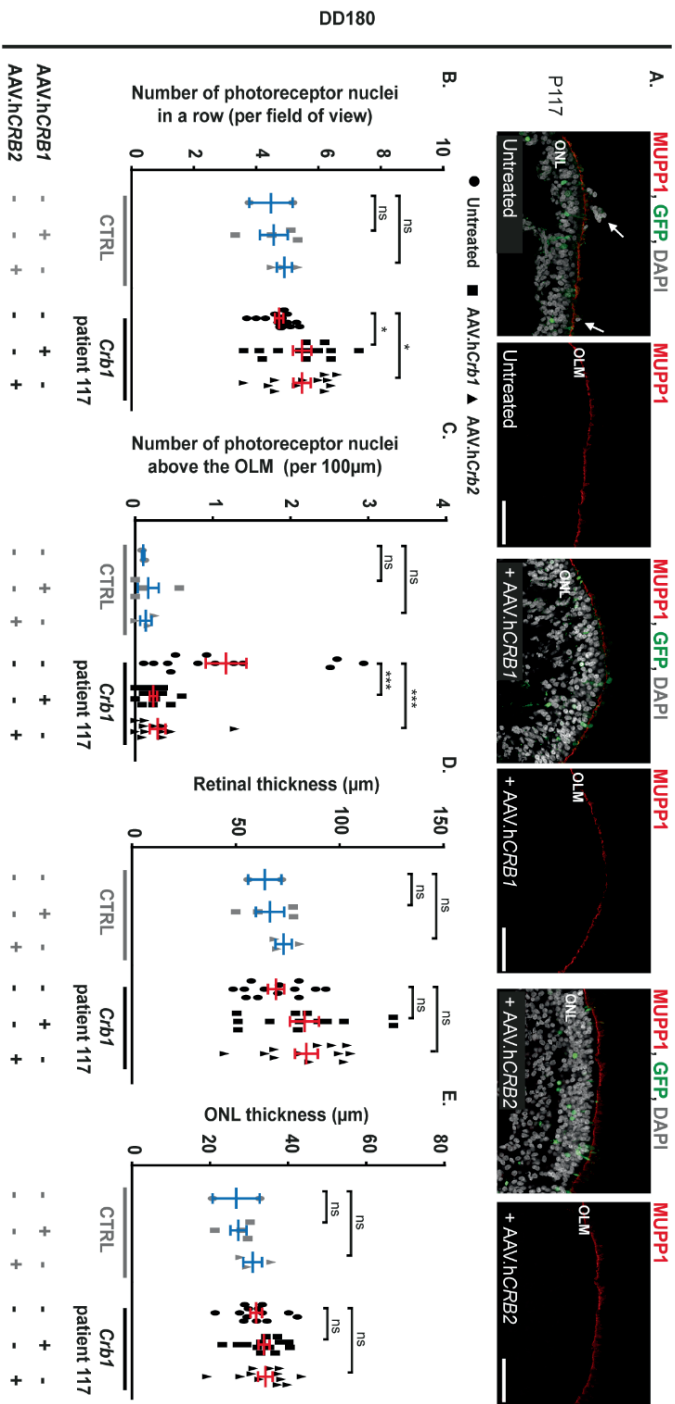
Supplemental Figure 2 (A): scRNA-seq analysis comparing ISO-P128 with P128. (A) Heatmap of top markers indicating the distinct clusters.



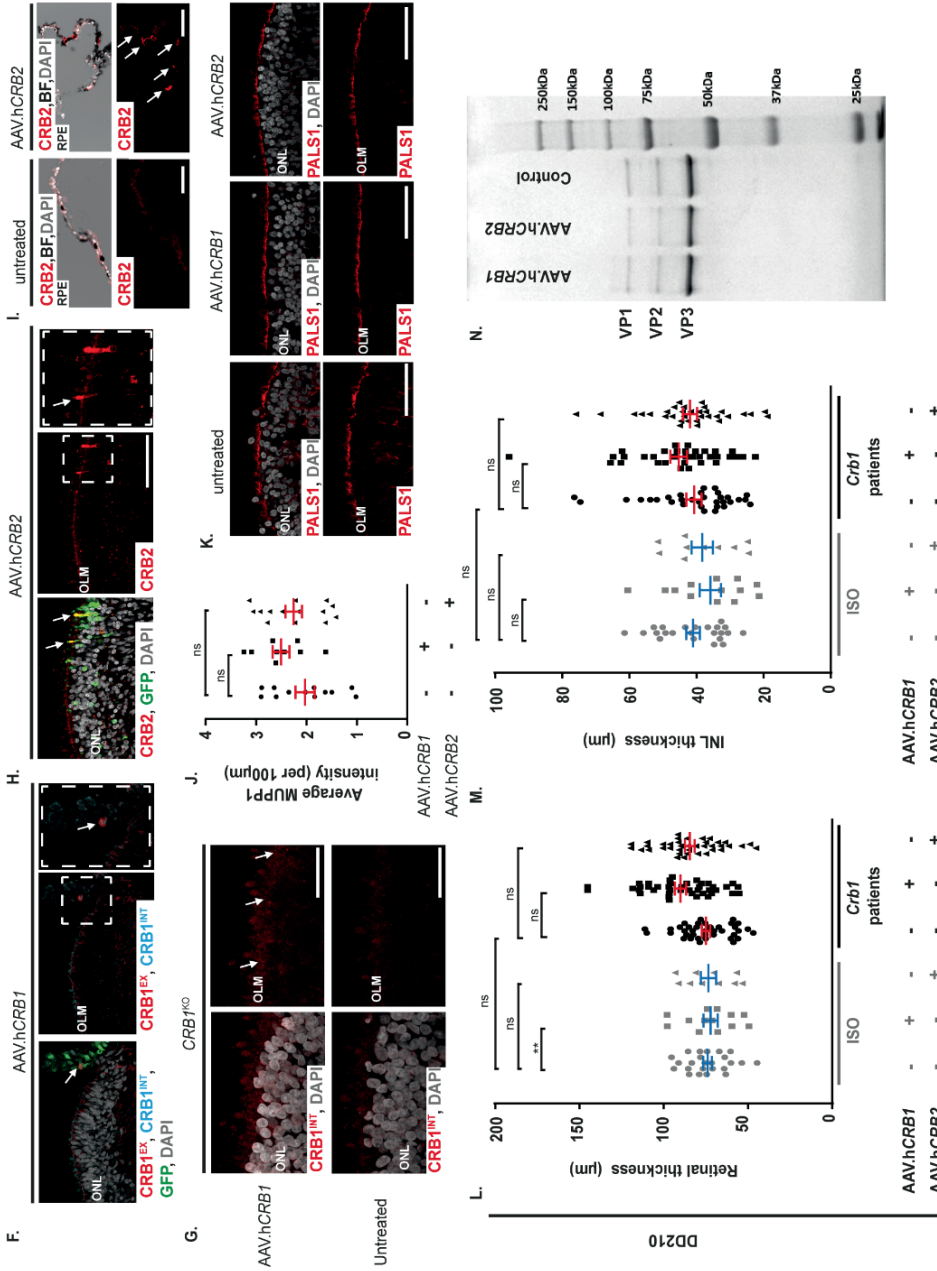
Supplemental Figure 2: scRNA-seq analysis comparing ISO-P128 with P128. Related to Figure 2. (B) Dot-plot showing higher expression of mature rod photoreceptor cell features in rods I then in rods II cluster. (C) Overview of a retinal organoid in culture with RPE (asterisks) and stromal cells attached to it. When using the organoid for single cell sequencing, the stromal cells and RPE were cut off as much as possible. Scalebar 200 μ m. (D) Feature plot showing the absence of *CRB1* alternative transcript *CRB1-B* in these retinal organoids. (E) Violin plots of *Ezrin* (*EZR*), *Moesin* (*MSN*), and *EPB41L5* specifically in MGCs (from left to right: $p = 0.41$, $p = 0.17$, $p = 0.59$), rods ($p = 0.018$, $p = 0.89$, $p = 0.53$) and cones ($p = 0.77$, $p = 0.79$, $p = 0.24$) in P128 vs ISO-P128. Number of independent organoids used: ISO-P128 $n = 6$, and P128 $n = 6$ from one differentiation round equally divided into three separate sequencing rounds.



Supplemental Figure 3: scRNA-seq analysis comparing ISO-P116 and P116 retinal organoids. Related to Figure 2. (A) Table showing all retinal cell types equally present in the retinal organoids. (B) Violin plots of *CRB1* and (C) *CRB2* expression levels specifically in MGCs ($p = 0.78, p = 0.28$), rods ($p = 0.37, p = 0.88$), and cones ($p = 0.51, p = 0.96$). (D) Violin plots of canonical core CRB complex members *PALSI*, and *MUPP1* transcripts in MGCs ($p = 0.49, p = 0.98$), rods ($p = 0.36, p = 0.61$), and cones ($p = 0.41, p = 0.86$). (E) Gene ontology (GO) analysis of differentially expressed markers specifically in rods clustered with similar terms in the same colour. Number of independent organoids used: ISO-P116 $n = 4$, and P116 $n = 4$ from one differentiation and sequencing round. (F, G, H) Quantification of AAV2.CMV.GFP and AAV5.CMV.GFP retinal organoids at DD120 with three different titre concentrations: 1×10^{10} , 6.6×10^{10} , and 10×10^{10} gc (genome copies) in the (F) ONL, (G) INL, and (H)) GFP positive MGC in the INL per $100 \mu\text{m}$. Each datapoint in the graph represent individual organoids, of which an average has been taken of at least 3 representative images. The standard error of mean (SEM) is derived from these averages. Number of organoids per condition: for AAV2.CMV.GFP $1 \times 10^{10} n = 5$, $6.6 \times 10^{10} n = 6$, and $10 \times 10^{10} n = 7$, and for AAV5.CMV.GFP $1 \times 10^{10} n = 7$, $6.6 \times 10^{10} n = 8$, and $10 \times 10^{10} n = 6$ individual organoids from two independent differentiation rounds. Statistical analysis: generalized linear mixed models with $p < 0.05$ (*), $p < 0.01$ (**), and $p < 0.001$ (***)



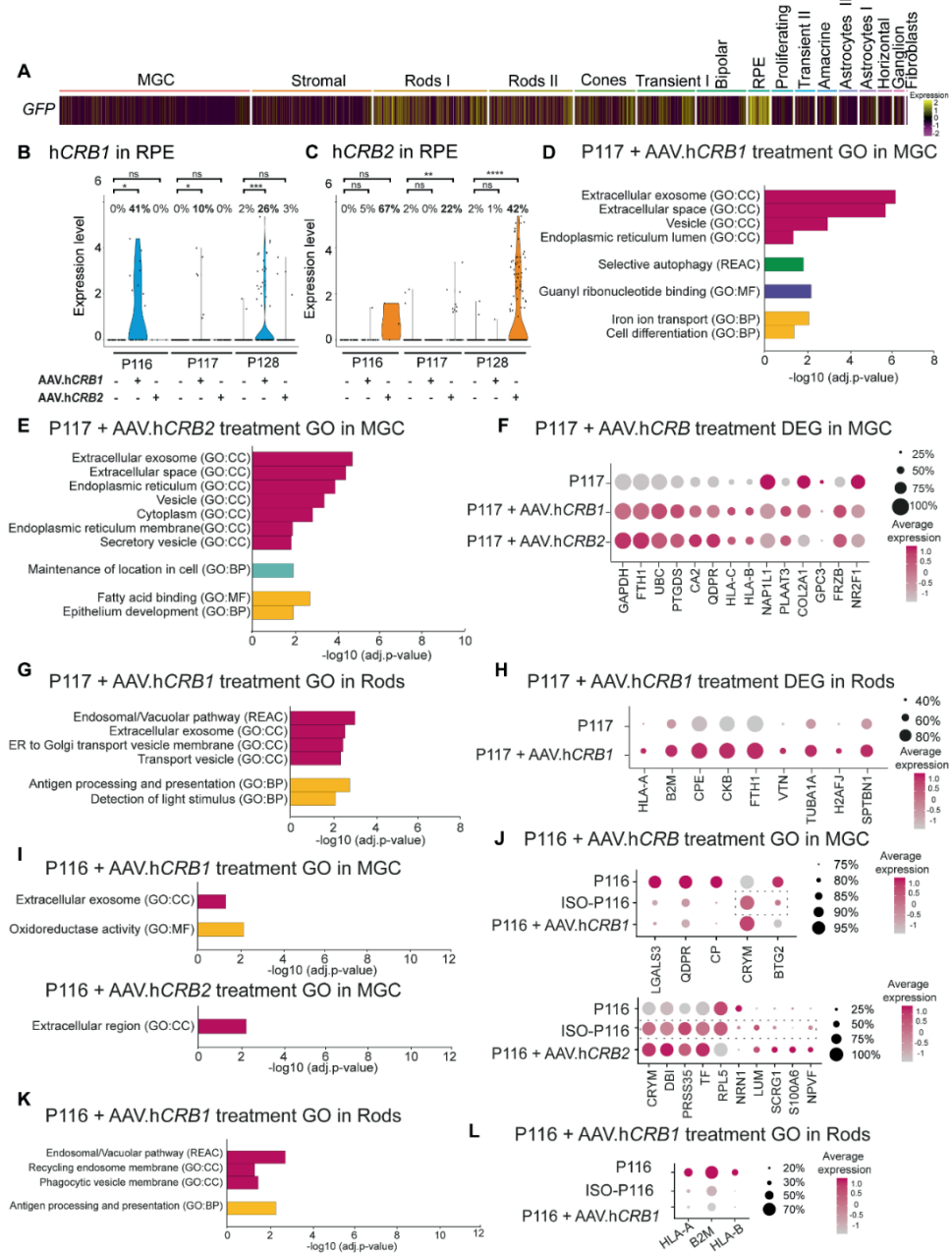
Supplemental Figure 4: AAV-mediated gene therapy treatment on *CRB1* patient-derived and isogenic control retinal organoids (A-E). Related to Figure 4. (A) Representative immunohistochemical images of untreated, AAV.h*CRB1*, and AAV.h*CRB2* treated P117 and control retinal organoids stained with MUPP1 (red) and AAV.GFP (green) at DD180. (B) Quantification at DD180 of the number of photoreceptor nuclei in a row per field of view (from left to right: $p = 0.042$, $p = 0.041$, $p = 0.925$, $p = 0.548$), (C) the number of photoreceptor nuclei above the OLM per 100 µm ($p = 0.000$, $p = 0.001$, $p = 0.676$, $p = 0.865$), (D) retinal thickness per field of view ($p = 0.104$, $p = 0.078$, $p = 0.819$, $p = 0.389$), and (E) ONL thickness per field of view ($p = 0.438$, $p = 0.355$, $p = 0.933$, $p = 0.378$).



Supplemental Figure 4 (F-N): AAV-mediated gene therapy treatment on *CRB1* patient-derived and isogenic control retinal organoids.

Legend continues on the next page

Supplemental Figure 4: AAV-mediated gene therapy treatment on *CRB1* patient-derived and isogenic control retinal organoids. Related to Figure 4. (F) Representative immunohistochemical images of anti-*CRB1*^{EX} and anti-*CRB1*^{INT} showing localization in the RPE after AAV.h*CRB1* treatment in *CRB1* patient-derived retinal organoid. (G) Immunohistochemical image of anti-*CRB1*^{INT} showing localization at the OLM after AAV.h*CRB1* treatment in *CRB1*^{KO} retinal organoid. (H, I) Representative immunohistochemical images of *CRB2* at the (H) OLM and (I) RPE after AAV.h*CRB2* treatment in *CRB1* patient-derived retinal organoids. (J) Quantification of the average MUPP1 fluorescence intensity at the OLM of DD210 *CRB1* patient derived retinal organoids (P116, P117, P128 pooled) treated with AAV.h*CRB*. (K) Representative immunohistochemical images of PALS1 at the OLM with and without AAV.h*CRB* treatment in a *CRB1* patient-derived retinal organoid. (L) Quantification of the retinal thickness ($p = 0.008$, $p = 0.082$, $p = 0.993$, $p = 0.981$, $p = 0.981$) and (M) the INL thickness ($p = 0.139$, $p = 0.632$, $p = 0.958$, $p = 0.195$, $p = 0.707$) per field of view of *CRB1* patient and isogenic control retinal organoids at DD210. (N) SDS-PAGE gel of AAV.h*CRB1* and AAV.h*CRB2* showing no contamination in the AAV preparation. Scalebar = 50 μ m. Each datapoint in the graph represent individual organoids, of which an average has been taken of at least 3 representative images. The standard error of mean (SEM) is derived from these averages. Number of individual organoids per condition at DD180 P117 treated with AAV.h*CRB1* $n = 13$, AAV.h*CRB2* $n = 12$, untreated $n = 14$ from two different differentiation rounds, control organoids treated with AAV.h*CRB1* $n = 4$, AAV.h*CRB2* $n = 3$, and untreated $n = 2$ from one differentiation round. And at DD210 *CRB1* patient-derived retinal organoids (P116, P117, P128 pooled) treated with AAV.h*CRB1* $n = 34$, AAV.h*CRB2* $n = 33$, untreated $n = 32$, and isogenic controls (ISO-02 P116, ISO-03 P116, ISO-P128 pooled) treated with AAV.h*CRB1* $n = 14$, AAV.h*CRB2* $n = 10$, and untreated $n = 24$ independent organoid from two different differentiation rounds. Statistical tests: generalized linear mixed models with $p < 0.05$ (*), $p < 0.01$ (**), and $p < 0.001$ (***)



Supplemental Figure 5: Single cell RNA-sequencing of *CRB1* patient-derived retinal organoid treated with AAV.hCRB1 or AAV.hCRB2 restores transcriptional effect on the endosomal system. Related to Figure 5. (A) Heatmap showing AAV.GFP expression in the clusters, mainly transducing MGC, photoreceptor cells, and RPE. (B, C) Violin plot of transcript

expression of (B) AAV.h*CRB1* (from left to right: $p = 0.018$, $p = 0.41$, $p = 0.041$, $p = 0.078$, $p < 0.001$, $p = 0.54$) or (C) AAV.h*CRB2* ($p = 0.5$, $p = 0.1$, $p = 0.38$, $p = 0.0037$, $p = 0.53$, $p < 0.00001$) in the RPE of AAV.h*CRB* treated retinal organoids. (D, E) Gene ontology (GO) analysis of differentially expressed markers contrasting untreated with (D) AAV.h*CRB1* or (E) AAV.h*CRB2* treated P117 in MGCs clustered in groups with similar terms in the same colour. (F) All significantly differentially expressed markers in terms related to the endosomal system after treatment with AAV.h*CRB1* or AAV.h*CRB2* in MGC. (G, H) P117 treated with AAV.h*CRB1* in rods showing gene ontology (G) and all terms related to the endosomal system (H). (I) GO of P116 treatment with AAV.h*CRB* in MGC and (J) dot plot of terms related to the endosomal system after treatment. The data in the box with a dashed line are not statistically significant different from P116, all the other data points (in F, H, J, and L) are statistically significant different from untreated patient derived retinal organoids. Number of independent organoids used: P116 $n = 4$, P116 with AAV.h*CRB1* $n = 3$, P116 with AAV.h*CRB2* $n = 3$ from one differentiation and sequencing round, and P117 $n = 5$, P117 with AAV.h*CRB1* $n = 5$, P117 with AAV.h*CRB2* $n = 5$ from one differentiation round equally divided into three separate sequencing rounds.

Supplemental Table 1. hiPSC line information. Related to all figures.

Line name [published]	Description	Gender
LUMC04iCTRL10 [1]	Control iPSC line	Male
CRB1 ^{KO} LUMC04iCTRL10	<i>CRB1</i> ^{KO} line was derived from LUMC04iCTRL10; it has a stop codon in the second exon of <i>CRB1</i> . Only used here for proof of recombinant CRB1 protein expression after AAV.h <i>CRB1</i> treatment.	Male
LUMC0116iCRB09 [1]	<u>P116</u> = Allele 1 and 2: homozygous c.3122T>C--> p.(Met1041Thr)	Male
iso02LUMC0116iCRB09	<u>ISO-02 P116</u> = Allele 1: c.3122T>C gene corrected to c.3120C>G. Allele 2: c.3122T>C. p.(Met1041Thr)	Male
iso03LUMC0116iCRB09	<u>ISO-03 P116</u> = Homozygous c.3122T>C gene corrected to c.3120C>G	Male
LUMC0117iCRB01 [1]	<u>P117</u> = Allele 1: c.1892A>G (p.Tyr631Cys). Allele 2: c.2911G>T (p.(Glu995*))	Male
LUMC0128iCRB01 [1]	<u>P128</u> = Allele 1: c.2843G>A --> p.(Cys948Tyr). Allele 2: c.3122T>C --> p.(Met1041Thr)	Male
iso02LUMC0128iCRB01	<u>ISO-P128</u> = Allele 1: c.2843G>A. p.(Cys948Tyr). Allele 2: c.3122T>C gene corrected to c.3120C>G	Male

Supplemental Table 2. List of primary antibodies used in the study. Related to all figures.

Antigen	Dilution	Source	Identifier
CRB1 (intracellular domain – used if not otherwise specified)	1:200	Homemade	NA
CRB1 (extracellular domain)	1:200	Abnova	H00023418-A01
CRB2	1:200	Homemade	NA
CRALBP	1:200	Abcam	Ab15051
MUPP1	1:200	BD Biosciences	M98820
PALS1	1:200	Homemade	NA
OTX2	1:200	Proteintech	13497-1-AP
Rhodopsin	1:200	Sigma	SAB4502636
Glutamine synthetase (GS)	1:250	BD Bioscience	610518
SOX9	1:250	Millipore	AB5535

Supplemental Table 3. Top 10 DEG differentially expressed genes per cluster. Related to Figure 2. Statistically significant log₂ fold changes of the expression level of differentially expressed genes in the cluster (pct1) comparing with the remaining clusters (pct2). With the defined cell type per cluster. This table is not included in this thesis, due to the large size, and can be found online [6].

4

Supplemental Table 4. Differentially expressed genes EG markers and gene ontology terms contrasting P128 and ISO-P128, and P116 and ISO-P116. Related to Figure 2, S3A-E. Log₂ fold changes of the expression level of statistically significant expressed genes in CRB1 patient-derived retinal organoids comparing with the isogenic control in MGCs or in rod photoreceptor cells and the associated gene ontology terms. This table is not included in this thesis, due to the large size, and can be found online [6].

Supplemental Table 5. DEG markers and gene ontology terms comparing untreated and AAV.hCRB treated CRB1 patient derived retinal organoids. Related to Figure 5, S5. Log₂ fold changes of the expression level of statistically significant expressed genes in AAV.hCRB treated CRB1 patient-derived retinal organoids comparing with the untreated and the associated gene ontology terms. This table is not included in this thesis, due to the large size, and can be found online [6].

Supplemental experimental procedures

Cell culture and retinal organoid differentiation

Human induced pluripotent stem cells (hiPSC) were maintained on Matrigel coated plates in mTeSR plus medium (STEMCELL Technologies) and passaged mechanically. Retinal organoid differentiation was carried out as previously reported

with some modifications [1,2]. Confluent hiPSCs were collected and incubated with (\pm)blebbistatin in mTeSR medium in micro-mold spheroids (Z764000-6EA, Merck) over night. Then, medium was transitioned to Neural Induction Medium 1 (NIM1) using mTeSR/NIM1 (3:1), then (1:1), and finally (0:1) over three days to form embryoid bodies (EBs). After 1 week, EBs were plated onto Matrigel-coated wells with daily NIM-1 medium change till DD15 and daily change of NIM-2 starting at DD16. Between DD20 and latest DD28, neuroepithelial structures were selected and flushed from the Matrigel plates using a P1000 pipet and kept in floating culture in agarose coated plates from this point onwards. After selecting the best-looking structures, all structures were flushed from the Matrigel plates and kept in floating culture to increase the yield of obtained organoids. Then, typically from DD40 until DD100, good retinal organoid structures were selected and placed individually in a 48 well plate. Brain and other non-retinal structures were removed as well between this time period. Daily medium change of NIM-2 is used till DD34, then typically three times a week Retinal Lamination Medium 1 (RLM-1) was used from DD35 to DD63. Then, RLM-1 + 1 μ M retinoic acid until DD84, followed by RLM-2 + 0.5 μ M retinoic acid, and RLM-2 from DD120 was used for the rest of the culture.

Immunohistochemical analysis

Organoids were collected at DD180 or DD210 for immunohistochemical analysis. Organoids were fixed with 4% paraformaldehyde in PBS for 20 minutes at RT, briefly washed with PBS and subsequently cryo-protected with 15% and 30% sucrose in PBS until organoids sunk to the bottom of the well. Organoids were embedded in Tissue-Tek O.C.T. Compound (Sakura, Finetek), thereafter 8 μ M cryosections were made with a Leica CM1900 cryostat (Leica Microsystems) and stored in the freezer.

For immunohistochemistry, the sections were blocked for 1h at RT in 10% normal goat serum, 0.4% Triton X-100, and 1% bovine serum albumin in PBS. Primary antibodies were incubated overnight at 4°C or for at least 3h at RT with 0.3% normal goat serum, 0.4% Triton X-100, 1% BSA and appropriate primary antibody concentration (Supplemental Table 2). Then, slides were washed for two times 15 minutes in PBS and subsequently incubated for 1h at RT with fluorescent-labelled secondary antibody

in 0.1% goat serum in PBS. Nuclei were counterstained with DAPI and mounted in Vectashield Hardset mounting medium (H1800, Vector laboratories, Burlingame, USA). Sections were imaged on a Leica TCS SP8 confocal microscope and images were processed with Leica Application suite X (v3.7.0.20979).

RNA isolation, cDNA synthesis, and qPCR analysis

RNA was isolated from DD210 retinal organoids of P116, P117, P128, ISO-P128, and ISO-02 P116 using TRIZOL reagent (Gibco Life Technologies) according to the manufacturer manual. The isolated RNA was dissolved in 20 μ l RNase-free water. 0.5 μ g of total RNA was reverse transcribed into first-strand cDNA using QuantiTect Reverse Transcription Kit (205311, QIAGEN) in a total reaction volume of 20 μ l. From all cDNA samples, a 1 in 20 dilution was made and used for qPCR analysis.

Two different exon-spanning primer pairs were designed at the 5' end of the CRB1-B gene giving rise to an amplicon of 70 to 120bp (FW1: TGTTTGGAGCCAGGACACAT, REV1: ACGTCTTCTTCGCAGTGGAT and FW2: GAGCCAGGACACATGGTTTTTC, REV2: TTCCCAGGCAAGTTCTCAC). Real-time qPCR was based on the monitoring of SYBR Green I dye fluorescence on a CFX Connect Real-Time System (BioRad). The qPCR conditions were as follows: 5 μ l SYBR green PCR 2x master mix (4913914001, Merck), 0.2 μ l of 10 μ M FW and REV primers, and 5 μ l of the diluted cDNA. qPCR machine started with a melting step at 95°C for 10min, followed by 40 cycles of 95°C for 15 seconds and an annealing at 60°C for one minute. At the end of the PCR run, a dissociation curve was determined by ramping the temperature of the sample from 60 to 95°C while continuously collecting fluorescence data. MQ water controls were included for each primer pair to check for any significant levels of contaminants. The following two reference genes were used: glyceraldehyde 3-phosphate dehydrogenase (GAPDH) and elongation factor 1a (EF1A), previously described by [3].

qPCR was performed on both primer pairs with at least three individual DD210 retinal organoids of P116, P117, P128, ISO-P128, and ISO-02 P116 cDNA and human adult retina cDNA (Marathon-ready; Clontech). CRB1-B was detected in adult human retina

cDNA but was below detection level in the patient-derived and isogenic control retinal organoids at DD210.

Single cell RNA sequencing – Retinal organoid dissociation

Retinal organoids were dissociated using an adapted protocol from the Papain Dissociation kit (Worthington, I-LK 03150). In short, single retinal organoids were selected and cut into small pieces to remove excess RPE or non-neural tissue as much as possible and placed on a 48 well plate with 500µl dissociation solution (20 units/ml papain and 0.005% DNase). These were incubated for 30 minutes on a shaker in the incubator, then the organoids were triturated using a 1mL pipettor to dissociate the tissue. The plate was placed back for 15-20 minutes on the shaker in the incubator, then again triturated, this was repeated until a single cell suspension was obtained. 500µl albumin ovomucoid protease inhibitor solution was added to the single cell suspension, centrifuged at 300x g for 5min. Supernatant was removed, pellet resuspend in PBS and filtered through a 40um cell strainer (Pluristrainer; SKU 43-10040-50).

Filtered single cell suspension was centrifuged at 300x g for 5min at 4°C and resuspend in 100µl staining buffer (2%BSA/0.01%Tween, PBS) with 10µl Fc Blocking reagent (FcX, BioLegend) for 10 minutes on ice. 0.5µg of unique Cell Hashing antibodies were added and incubated for 20 minutes on ice. Stained cells were washed 3 times with 1mL staining buffer, spun at 4 °C for 5 minutes at 350g. Stained single cell suspensions were counted for cell concentration and cell viability (TC20, Bio-rad). Typically, all single cell suspensions had a 70% or higher cell viability. Stained cells were pooled and re-counted until desired concentration for single cell sequencing (cell viability of at least 80%). Every sequencing round contained 14 hashed retinal organoid samples; the goal was to capture a total of approximately 30.000 cells per pool.

Single cell RNA sequencing – Droplet-based single-cell RNA sequencing

ScRNA-seq data was generated using the Chromium 10x 3'UTR-sequencing. Single cell suspensions were loaded onto the Chromium Single Cell system using the v3 chemistry. Subsequent steps were performed according to manufacturer's instructions.

Single cell RNA sequencing – Computational analysis of single cell data

Raw sequencing output were processed using the Cell Ranger (v6.0.1) pipeline (10X Genomics) with default settings and the pre-built human genome reference (GRCh38). Custom references of codon optimized AAV.hCRB1, codon optimized AAV.hCRB2, AAV.GFP and CRB1-B were added using the known FASTA sequence.

Filtered expression matrices were further processed with a Seurat (v4.1.0) based workflow in R (v4.1.0) [4]. In short, cells were demultiplexed based on their HTO enrichment using HTODemux function of Seurat, and singlets were selected for downstream analysis. Quality control followed, keeping cells with nFeature_RNA > 800 and <6000, nCount_RNA <30000, and percent.mt <12. The raw counts were normalized with NormalizedData function (scale.factor = 30000). The top 2000 most variable genes were selected using FindVariableFeatures. Principal component analysis (PCA) was then performed using these 2000 genes. The first 15 PCs were used to calculate cell clusters and project the cells on a two-dimensional plot using Uniform Manifold Approximation and Projection (UMAP) algorithm. Top markers from FindAllMarkers function were analysed and compared to well-known cell type-specific markers to classify the clusters. For downstream analysis, data was subset per cluster, per patient derived retinal organoids, and/or per treatment. Then, differentially expressed genes were retrieved from the FindMarkers function. Genes with $p_val_adj \leq 0,05$ were used for GO (Gene Ontology) term analysis, GO analysis was performed using g:Profiler (version e106_eg53_p16_65fcd97) with g:SCS multiple testing correction method applying significance threshold of 0.05 [5]. Relevant terms and associated genes were included for visualization in this manuscript. For the violin plots comparing genes in CRB1 patient-derived and isogenic control retinal organoids, the function `stat_compare_means` with a Wilcoxon t-test was used to determine statistically significant differences.

Number of cells used for downstream analysis per condition: (1) coming from one sequencing round, ISO-P116 with AAV.GFP: $n=993$ cells from 4 organoids, P116 with AAV.GFP: $n=1497$ cells from 4 organoids, P116 with AAV.hCRB1 and AAV.GFP: $n=1225$ cells from 3 organoids, P116 with AAV.hCRB2 and AAV.GFP: $n = 884$ cells

from 3 organoids, and (2) equally divided in three separate sequencing rounds, ISO-P128 with AAV.*GFP*: $n = 5786$ cells from 6 organoids, P128 with AAV.*GFP*: $n = 4908$ cells from 6 organoids, P128 with AAV.h*CRB1* and AAV.*GFP*: $n = 4386$ cells from 5 organoids, P128 with AAV.h*CRB2* and AAV.*GFP*: $n = 3870$ cells from 5 organoids, P117 with AAV.*GFP*: $n = 3552$ cells from 5 organoids, P117 with AAV.h*CRB1* and AAV.*GFP*: $n = 3108$ cells from 5 organoids, P117 with AAV.h*CRB2* and AAV.*GFP*: $n = 2868$ cells from 5 organoids.

Supplemental references

1. Quinn, P.M.; Buck, T.M.; Mulder, A.A.; Ohonin, C.; Alves, C.H.; Vos, R.M.; Bialecka, M.; van Herwaarden, T.; van Dijk, E.H.C.; Talib, M.; et al. Human iPSC-Derived Retinas Recapitulate the Fetal CRB1 CRB2 Complex Formation and Demonstrate that Photoreceptors and Müller Glia Are Targets of AAV5. *Stem Cell Reports* **2019**, *12*, 906–919, doi:10.1016/j.stemcr.2019.03.002.
2. Zhong, X.; Gutierrez, C.; Xue, T.; Hampton, C.; Vergara, M.N.; Cao, L.H.; Peters, A.; Park, T.S.; Zambidis, E.T.; Meyer, J.S.; et al. Generation of three-dimensional retinal tissue with functional photoreceptors from human iPSCs. *Nat. Commun.* **2014**, *5*, doi:10.1038/ncomms5047.
3. Pellissier, L.P.; Lundvig, D.M.S.; Tanimoto, N.; Klooster, J.; Vos, R.M.; Richard, F.; Sothilingam, V.; Garrido, M.G.; Bivic, A. Le; Seeliger, M.W.; et al. CRB2 acts as a modifying factor of CRB1-related retinal dystrophies in mice. *Hum. Mol. Genet.* **2014**, *23*, 3759–3771, doi:10.1093/hmg/ddu089.
4. Hao, Y.; Hao, S.; Andersen-Nissen, E.; Mauck, W.M.; Zheng, S.; Butler, A.; Lee, M.J.; Wilk, A.J.; Darby, C.; Zager, M.; et al. Integrated analysis of multimodal single-cell data. *Cell* **2021**, *184*, 3573–3587.e29, doi:10.1016/j.cell.2021.04.048.
5. Raudvere, U.; Kolberg, L.; Kuzmin, I.; Arak, T.; Adler, P.; Peterson, H.; Vilo, J. G:Profiler: A web server for functional enrichment analysis and conversions of gene lists (2019 update). *Nucleic Acids Res.* **2019**, *47*, W191–W198, doi:10.1093/nar/gkz369.
6. Boon, N.; X. Lu, C. A. Andriessen, I. Moustakas, T. M. Buck, C. Freund, C. H. Arendzen, S. Böhringer, H. Mei, J. Wijnholds. AAV-mediated gene augmentation therapy of *CRB1* patient-derived retinal organoids restores the histological and transcriptional retinal phenotype. *Stem Cell Reports* **2023**

Chapter 5

Characterization and AAV-Mediated Gene Therapy in Human
Derived $CRB1^{KO}$ and $CRB1^{KO}CRB2^{+/-}$ Retinal Organoids

N. Boon, X. Lu, C. A. Andriessen, M. Orlova, P. M. J.
Quinn, C. J. F. Boon, and J. Wijnholds

Manuscript Submitted



Abstract

Using human induced pluripotent stem cell (hiPSC)-derived models for ophthalmology research is an emerging strategy to explore patient phenotypes *in vitro*, which allows access to previously limited or inaccessible material. The majority of patients with mutations in *CRB1* develop either early-onset retinitis pigmentosa as young children or Leber congenital amaurosis as newborns. The cause for the phenotypic variance exhibited in *CRB1*-associated inherited retinal diseases is unknown, but might be linked to differences in CRB1 and CRB2 protein levels in Müller glial and photoreceptor cells. Here, *CRB1*^{KO} and *CRB1*^{KO}*CRB2*^{+/-} hiPSC were generated by CRISPR/Cas9 and differentiated into retinal organoids. Differentiation day 210 retinal organoids showed a significant decrease in the number of photoreceptor nuclei in a row and a significant increase in the number of photoreceptor cell nuclei above the outer limiting membrane. This phenotype with outer retinal abnormalities is similar to previously observed in *CRB1* retinitis pigmentosa patient-derived retinal organoids and *Crb1* or *Crb2* mutant mouse retinal disease models. The *CRB1*^{KO} and *CRB1*^{KO}*CRB2*^{+/-} retinal organoids develop an additional inner retinal phenotype due to the complete loss of CRB1 from Müller glial cells, suggesting an essential role for CRB1 in proper localization of neuronal cell types in the inner and outer retina. AAV transduction was explored at early and late stages of organoid development. Moreover, AAV-mediated gene augmentation therapy with AAV.h*CRB2* improved the outer retinal phenotype in *CRB1*^{KO} retinal organoids partially. Altogether, these data provide essential information for future gene therapy approaches for patients with *CRB1*-associated retinal dystrophies.

Introduction

Crumbs homologue 1 (CRB1) is a large transmembrane protein initially discovered at the apical membrane of *Drosophila* epithelial cells [1]. The human *CRB1* gene is mapped to chromosome 1q31.3, has 12 identified mRNA transcripts, over 210 kb genomic DNA, and three CRB family members [2]. Canonical human CRB1 consists of multiple epidermal growth factor (EGF) and laminin-globular like domains in its

large extracellular domain. The short intracellular domain contains a FERM domain juxtaposed to the single transmembrane domain and at the carboxyl-terminus a conserved glutamic acid-arginine-leucine-isoleucine (ERLI) PDZ binding motive [2–4]. A short alternative transcript of *CRB1*, *CRB1-B*, was described encoding a protein with significant extracellular domain overlap with canonical CRB1 while bearing unique amino-terminal and carboxy-terminal protein domains [5]. The function of *CRB1-B* in the human retina is not known. In mammals, the CRB family members are CRB1, CRB2 and CRB3A. CRB2 displays a similar protein structure to CRB1, except for a depletion of four EGF domains. The canonical CRB complex is formed by interaction with protein associated with Lin Seven 1 (PALS1), which binds to the conserved carboxy-terminal PDZ domain of CRB [6–8]. The CRB complex is evolutionary conserved and is important for regulating apical-basal polarity and maintaining cell adhesion [9].

Inherited retinal dystrophies such as retinitis pigmentosa (RP) or Leber congenital amaurosis (LCA) can be caused by mutations in the *CRB1* gene. Approximately 7-17% of LCA and 3-9% of RP patients are reported with mutations in *CRB1* [10–13]. RP is a clinically and genetically heterogeneous disease where children or aged patients experience night blindness which progresses to complete loss of vision [14–16], while LCA causes visual impairment in newborns [13]. There are over 200 different mutations along the *CRB1* gene described to be causing early onset RP in children or LCA without a clear genotype-phenotype correlation [14,17]. No treatment possibilities are available for patients with a mutation in the *CRB1* gene. Multiple animal-derived models have been described that mimic the phenotype of *CRB1* patients [5,18–22]. However, recent immuno-electron microscopy studies have shown that the subcellular localization of CRB1 and CRB2 is different between rodents and humans [23]. In mice, CRB1 is located at the subapical region just above the outer limiting membrane (OLM) of Müller glial cells (MGC) while CRB2 is located at the subapical region of MGC and photoreceptor cells [24]. In adult non-human-primate retina, human-derived retinal organoids and human fetal retina, both CRB1 and CRB2 are located at the subapical region of MGC and photoreceptor cells [23]. In addition, a reappraisal of the phenotype-genotype correlation of 50 patients with regards to canonical CRB1 and the

photoreceptor-specific CRB1-B has shown that the retinal phenotype is mainly driven by canonical *CRB1* isoform impairment [25]. These data indicate thus the importance of using human-derived models to study the retinal dystrophy caused by mutations in *CRB1*.

The use of human-induced pluripotent stem cells (hiPSC)-derived models for research is an emerging strategy to explore patient organoid or cell phenotypes *in vitro*. This is specifically of interest for patients with mutations in *CRB1*, because the subcellular localization of the protein is different between rodents and humans. hiPSC can be differentiated into well-defined retinal organoids, which recapitulate the development of the fetal retina [23]. Previously, we have shown that *CRB1*-patient derived retinal organoids frequently show ectopic photoreceptor cells above the OLM and detected less variant CRB1 protein at the OLM of patient-derived retinal organoids at differentiation day 180 (DD180) and DD210 [23,26]. In a large clinical cohort, it is shown previously that there is no clear genotype-phenotype correlation for patients with a mutation in the *CRB1* gene and the mutations are distributed along the *CRB1* gene [14]. Here, we describe the use of hiPSC-derived *CRB1*^{KO} retinal organoids as a candidate model for Leber congenital amaurosis, where a single nucleotide was deleted by CRISPR/Cas9 in exon 2 resulting in a frameshift with a premature stop codon and thus a knockout of the gene of interest. In addition, *CRB1*^{KO}*CRB2*^{+/-} hiPSC were used, since previous research has shown that concomitant decreased levels of *CRB2* can exacerbate the phenotype in *CRB1* mutant mice [27–29]. Homozygous mutations were introduced by CRISPR/Cas9 in exon 2 of *CRB1* and a heterozygous mutation in exon 3 of *CRB2*, generating *CRB1*^{KO}*CRB2*^{+/-} hiPSC. *CRB* retinal organoids completely lacking CRB1 protein showed an outer and inner retina phenotype mimicking a mild form of LCA. *CRB1*^{KO} retinal organoids were used for adeno-associated viral vector (AAV)-mediated h*CRB1* or h*CRB2* gene augmentation therapy.

Results

Generation of $CRB1^{KO}$ and $CRB1^{KO}CRB2^{+/-}$ hiPSC from the isogenic control

From the control iPSC line LUMC4iCTRL10 (now called: ISO-4.10), three $CRB1^{KO}$ and three $CRB1^{KO}CRB2^{+/-}$ clones were generated using CRISPR-Cas9 technology (Applied StemCell). In short, guide RNAs were designed to target exon 2 of $CRB1$ and exon 3 of $CRB2$. For the $CRB1^{KO}$, three independent homozygous subclones (CL19, CL26, and CL72) carried a homozygous deletion (c.500del), resulting in a frameshift with premature stop p.(Ser44Serfs*) for the $CRB1$ gene (Supplemental Figure 1A). For $CRB1^{KO}CRB2^{+/-}$, two clones (CL4 and CL9) carried the same homozygous c.500del mutation and the CL17 iPSC clone carried a homozygous c.498_507delinsTGCC mutation in the $CRB1$ gene, both mutations result in a frameshift with premature translation stop of CRB1 (Supplemental Figure 1A).

For the $CRB2$ gene, the $CRB1^{KO}CRB2^{+/-}$ clones showed heterozygous mutations targeting exon 3 (Supplemental Figure 1B). Next Generation Sequencing (NGS) of the $CRB2$ gene showed for $CRB1^{KO}CRB2^{+/-}$ clones 4 and 9 a 23bp deletion in exon 3 of the $CRB2$ gene (Supplemental Figure 1B), resulting in a frameshift with an alternative translation of CRB2. $CRB1^{KO}CRB2^{+/-}$ clone 17 show a 2bp deletion in exon 3 of the $CRB2$ gene (Supplemental Figure 1B), resulting in a frameshift with an alternative translation of CRB2 and the normal protein translation. Karyotyping of all clones showed a normal karyotype (Supplemental Figure 1C, D), but the $CRB1^{KO}$ and $CRB1^{KO}CRB2^{+/-}$ showed a commonly observed gain in copy number variation on chromosome 20q (Supplemental Figure 1E). The biological significance of such recurrent abnormalities is still discussed [30], and further research is required to define this. These CRB and isogenic (ISO-4.10) hiPSC lines were differentiated into $CRB1^{KO}$, $CRB1^{KO}CRB2^{+/-}$, and isogenic control retinal organoids.

CRB1^{KO} and CRB1^{KO}CRB2^{+/-} retinal organoids show an inner retinal phenotype at DD210

The *CRB1^{KO}*, *CRB1^{KO}CRB2^{+/-}*, and isogenic control iPSC lines were differentiated into defined retinal organoids with outer segment like structures up to, at least, DD210 based on bright field images of the retinal organoids in culture (Figure 1A-C'). In addition, a laminated retina with a clear outer nuclear layer (ONL) marked by rhodopsin positive photoreceptor cells (Figure 1D) and an inner nuclear layer (INL) indicated with SOX9 positive MGCs and ISLET1-2 positive rod and ON-cone bipolar cells (Figure 1E) were observed in all retinal organoids at DD210. However, we observed a less defined alignment of SOX9 and ISLET1-2 positive cells in the inner retina of *CRB1^{KO}* and *CRB1^{KO}CRB2^{+/-}* compared with isogenic control retinal organoids, possibly due to the complete loss of canonical CRB1 in MGC (and photoreceptors). This was previously not observed in *CRB1* patient-derived retinal organoids that expressed strongly decreased but existing basic levels of variant CRB1 [23,26]. The data on the *CRB1^{KO}* and *CRB1^{KO}CRB2^{+/-}* retinal organoids at DD210 suggests the disrupted localization of rod and ON-cone bipolar cells. In summary, whereas in previous studies on *CRB1* patient-derived retinal organoids with missense mutations we observed disruptions of the photoreceptor layer, the *CRB1^{KO}* and *CRB1^{KO}CRB2^{+/-}* retinal organoids show at DD210 an extended retinal phenotype that includes disruptions of the inner retina.

CRB1^{KO} and CRB1^{KO}CRB2^{+/-} retinal organoids show an outer retinal phenotype at DD180 and DD210

To verify that the *CRB1^{KO}* mutation caused a complete loss of CRB1 protein expression, immunohistochemical staining of CRB1 on DD180 and DD210 isogenic control, *CRB1^{KO}*, and *CRB1^{KO}CRB2^{+/-}* retinal organoids was performed. CRB1 and MUPP1 staining at the OLM were observed in the isogenic control at DD180 (Figure 2A). No CRB1 staining was detected in *CRB1^{KO}* and *CRB1^{KO}CRB2^{+/-}* retinal organoids, whereas MUPP1 was detected at the OLM (Figure 2A). Both extracellular and intracellular CRB1 antibodies detected no CRB1 staining at the OLM of *CRB1^{KO}* and

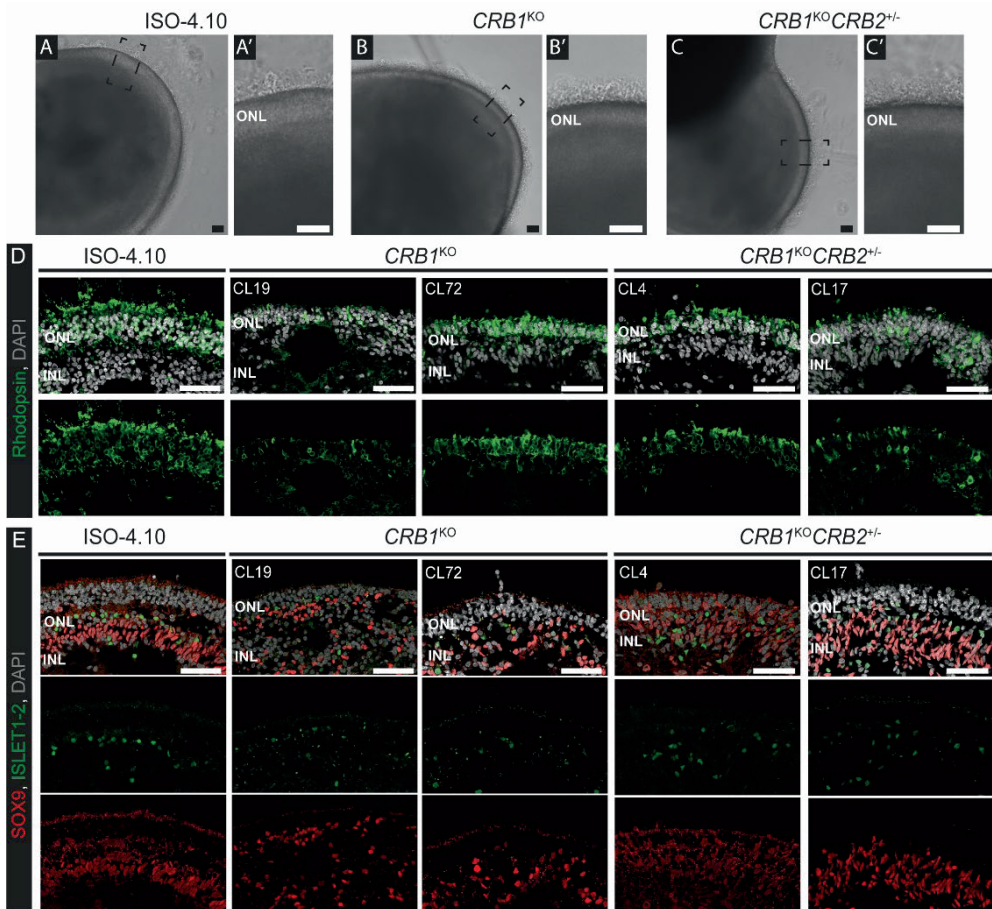


Figure 1: *CRB1*^{KO} and *CRB1*^{KO}*CRB2*^{+/-} retinal organoids at DD210. (A, B, C) Representative brightfield images of the (A) isogenic control and (B) *CRB1*^{KO} and (C) *CRB1*^{KO}*CRB2*^{+/-} retinal organoids at DD210, with a zoom-in of the outer segment-like structures in the boxed areas (A', B', C'). (D, E) Representative immunohistochemistry images of DD210 isogenic control and two *CRB1*^{KO} and *CRB1*^{KO}*CRB2*^{+/-} retinal organoids stained with (D) rhodopsin and (E) SOX9 (red) and ISLET1-2 (green). Note: INL = Inner Nuclear Layer, ONL = Outer Nuclear Layer. Scalebar = 50 μm.

CRB1^{KO}*CRB2*^{+/-} DD180 retinal organoids (Supplemental Figure 2A). Also, at DD210, no CRB1 was detected in *CRB1*^{KO} and *CRB1*^{KO}*CRB2*^{+/-} retinal organoids, whereas PALS1 was detected at the OLM (Supplemental Figure 2B). Moreover, CRB2 protein was detected at the OLM in DD180 and DD210 isogenic control, *CRB1*^{KO}, and

$CRB1^{KO}CRB2^{+/-}$ retinal organoids (Figure 2B, Supplemental Figure 2C). Localization of CRB2 was also detected at the OLM of $CRB1^{KO}CRB2^{+/-}$ retinal organoids that harbor one wild type and one knockout allele of $CRB2$.

When analyzing the $CRB1^{KO}$ and $CRB1^{KO}CRB2^{+/-}$ retinal organoids in more detail, a significantly increased number of photoreceptor nuclei above the OLM was observed compared to the isogenic control at DD180 (Figure 2C). Moreover, a statistically significant decrease in the number of photoreceptor nuclei in a row and ONL thickness was observed in DD180 $CRB1^{KO}$ and $CRB1^{KO}CRB2^{+/-}$ retinal organoids compared to the isogenic control (Figure 2D, Supplemental Figure 3A). No difference was observed for the INL thickness nor the retinal thickness in $CRB1^{KO}$ and $CRB1^{KO}CRB2^{+/-}$ retinal organoids (Supplemental Figure 3B, C). At DD210, the number of photoreceptor nuclei in a row was still significantly decreased in $CRB1^{KO}$ and $CRB1^{KO}CRB2^{+/-}$ retinal organoids (Figure 2E). However, there were fewer photoreceptor nuclei above the OLM in $CRB1^{KO}$ and $CRB1^{KO}CRB2^{+/-}$ retinal organoids, though still statistically significant for $CRB1^{KO}CRB2^{+/-}$ retinal organoids compared to the isogenic control (Figure 2F). Again, no statistically significant difference in INL thickness and retinal thickness was observed at DD210 (Supplemental Figure 3E, F). The data indicate that an outer retinal phenotype was observed at DD180 and DD210 retinal organoids, which is comparable to previously observed outer retinal phenotype in $CRB1$ patient-derived retinal organoids and in $Crb1$ mutant mouse models. Together these data define outcome measures for assessing therapeutic efficacy in $CRB1^{KO}$ and $CRB1^{KO}CRB2^{+/-}$ retinal organoids.

AAV5.CMV.GFP and AAV2.CMV.GFP transduce control retinal organoids more efficiently at DD135 than at DD200

Previously, we have shown that serotype AAV2/5.CMV.GFP (from now: AAV5.CMV.GFP) was more efficient than AAV2/2.CMV.GFP (from now: AAV2.CMV.GFP) in transducing MGC at DD120 [26]. Here, the tropism of these two serotypes were investigated in control retinal organoids transduced at later timepoints: DD135 or DD200.

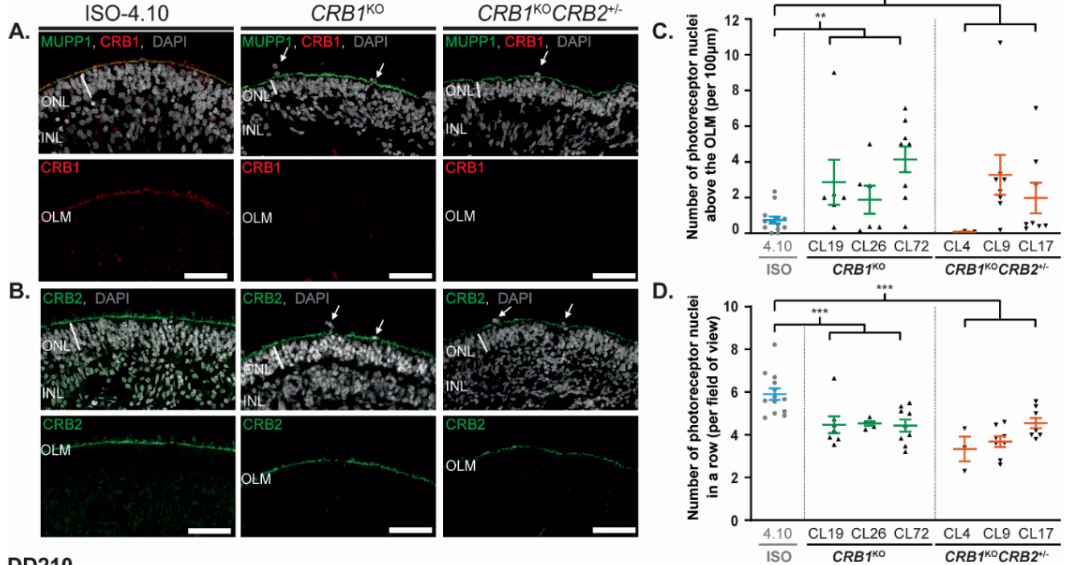
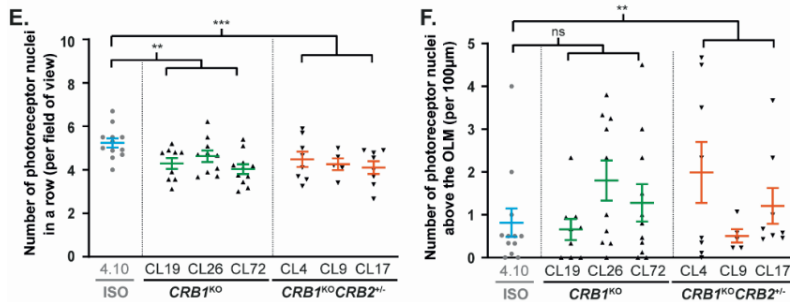
DD180

DD210


Figure 2: $CRB1^{KO}$ and $CRB1^{KO}CRB2^{+/-}$ retinal organoids show more photoreceptor nuclei above the OLM compared to the isogenic control at DD180 and DD210. Representative immunohistochemical images of (A) CRB1 (red) co-stained with MUPP1 (green) and (B) CRB2 (green) at the OLM of DD180 control, $CRB1^{KO}$, and $CRB1^{KO}CRB2^{+/-}$ retinal organoids. (C) Quantification of the number of photoreceptor nuclei above the OLM and (D) number of photoreceptor nuclei in a row of DD180 control, $CRB1^{KO}$, $CRB1^{KO}CRB2^{+/-}$ retinal organoids. (E) Quantification of the number of photoreceptor nuclei above the OLM and (F) number of photoreceptor nuclei in a row of DD210 control, $CRB1^{KO}$, $CRB1^{KO}CRB2^{+/-}$ retinal organoids. Each datapoint in the graph represents individual organoids, of which an average has been taken of at least three representative images. The standard error of mean (SEM) is derived from these averages. Number of individual organoids used for the quantification per condition at DD180: 4.10 $n=14$, $CRB1^{KO}$ CL19 $n=7$, CL26 $n=5$, CL72 $n=9$, $CRB1^{KO}CRB2^{+/-}$ CL4 $n=3$, CL9 $n=8$, CL17 $n=8$; and DD210: 4.10 $n=12$, $CRB1^{KO}$ CL19 $n=9$, CL26 $n=10$, CL72 $n=11$, $CRB1^{KO}CRB2^{+/-}$ CL4 $n=8$, CL17 $n=8$ from at least two independent differentiation batches and $CRB1^{KO}CRB2^{+/-}$ CL9 $n=5$ from one differentiation batch. Note: INL = Inner Nuclear Layer,

ONL = Outer Nuclear Layer, OLM = Outer Limiting Membrane. Scalebar = 50 μ m, statistical analysis: generalized linear mixed models with $p < 0.05$ (*), $p < 0.01$ (**), and $p < 0.001$ (***)

At DD135, control retinal organoids were transduced with 1×10^{10} gc, 6.6×10^{10} gc or 10×10^{10} gc of AAV2.CMV.*GFP* or AAV5.CMV.*GFP* and analyzed using immunohistochemistry after three weeks in culture. A dose-dependent increase of GFP positive cells was observed when control organoids were treated with AAV5.CMV.*GFP* or AAV2.CMV.*GFP* at DD135 (Figure 3A-C). The AAV-treated retinal organoids were quantified for the number of GFP positive cells in the ONL and INL. AAV2.CMV.*GFP* significantly transduced more cells in the ONL at the two highest titers (Figure 3D), whereas AAV5.CMV.*GFP* transduced significantly more cells in the INL at 6.6×10^{10} gc (Figure 3E). Co-staining with photoreceptor marker (OTX2) and MGC markers (CRALBP) confirmed the transduction of both cell types in AAV2.CMV.*GFP* as well as AAV5.CMV.*GFP* transduced organoids (Figure 3F, G). These data is in accordance with what was observed when control retinal organoids were transduced at DD120.

5
Next, we investigated whether transduction with the same AAV capsids at a later timepoint would influence the tropism. Here, control retinal organoids were transduced with 1×10^{10} gc or 10×10^{10} gc at DD200 with AAV2.CMV.*GFP* or AAV5.CMV.*GFP*. Again, a dose-dependent increase in GFP positive cells transduced in the ONL was observed for AAV2.CMV.*GFP* and AAV5.CMV.*GFP* treated retinal organoids (Supplemental Figure 4A, B). This dose-dependent increase was statistically significant for both capsids in the ONL (Supplemental Figure 4C) and only for AAV5.CMV.*GFP* in the INL (Supplemental Figure 4D). Moreover, AAV5.CMV.*GFP* infected significantly more cells in the ONL than AAV2.CMV.*GFP* at both titers (Supplemental Figure 4C). A small but statistically significant increase in GFP positive cells in the INL was observed at the dose of 10×10^{10} gc AAV5.CMV.*GFP* (Supplemental Figure 4D). However, the number of GFP positive cells co-localizing with SOX9-marked MGC cells showed no significant increase at the dose of 10×10^{10} gc AAV5.CMV.*GFP* (Supplemental Figure 4E). Both AAV serotypes showed co-localization with SOX9 positive MGCs (Supplemental Figure 4F). Interestingly, within relatively large retinal

organoids only a few cells were transduced with AAV2.CMV.GFP or with AAV5.CMV.GFP at DD200 (Supplemental Figure 4G), especially when compared with previous efficient transductions at DD120 [26] and DD135.

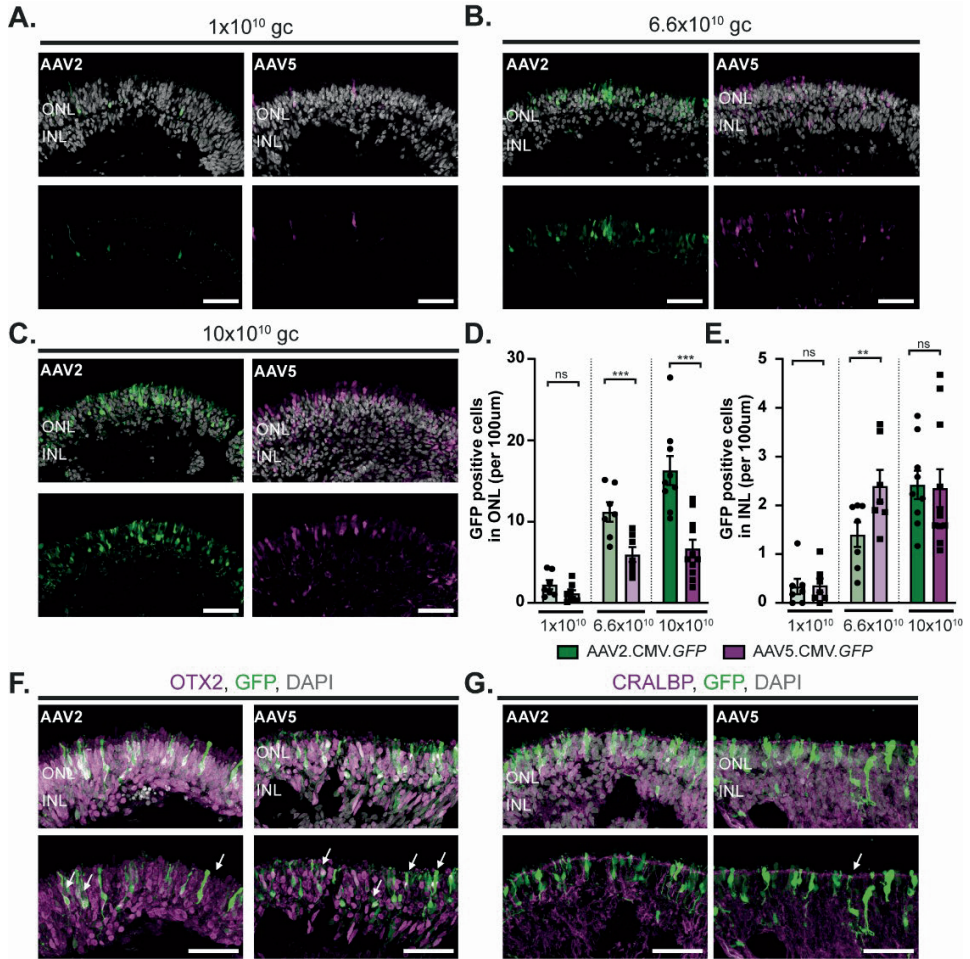


Figure 3: AAV transduction study of control retinal organoids transduced at DD135 with AAV2.CMV.GFP or AAV5.CMV.GFP (A, B, C) Representative immunohistochemical images of control retinal organoids transduced with (A) 1x10¹⁰gc, (B) 6.6x10¹⁰gc, or (C) 10x10¹⁰gc AAV2.CMV.GFP or AAV5.CMV.GFP. (D, E) Quantification of the number of GFP positive cells in the (D) ONL and (E) INL. (F, G) Immunohistochemical images of co-localization of AAV.GFP with photoreceptor marker OTX2 (F) or MGC marker CRALBP (G). Each datapoint in the graph represents individual organoids, of which an average has been taken of 3-6 representative images. The SEM is derived from these averages. Number of individual

organoids used for quantification per condition for AAV2.CMV.GFP: 1×10^{10} gc $n = 7$, 6.6×10^{10} gc $n = 7$, 10×10^{10} gc $n = 10$; and for AAV5.CMV.GFP: 1×10^{10} gc $n = 9$, 6.6×10^{10} gc $n = 7$, 10×10^{10} gc $n = 11$ from at least two independent differentiations. Note: INL = Inner Nuclear Layer, ONL = Outer Nuclear Layer. Scalebar = $50 \mu\text{m}$, statistical analysis: generalized linear mixed models with $p < 0.05$ (*), $p < 0.01$ (**), and $p < 0.001$ (***)

AAV-mediated CRB2 gene augmentation therapy improves the outer retinal phenotype in CRB1^{KO} retinal organoids

For gene therapy purposes, CRB1^{KO} retinal organoids were treated at DD120 with 3.3×10^{10} genome copies (gc) AAV5.CMV.hCRB1 or AAV5.CMV.hCRB2 (from now: AAV.hCRB1 and AAV.hCRB2, respectively) and subsequently analyzed at DD210 using immunohistochemistry. First, the isogenic control was treated with AAV.hCRB to determine whether there is a positive or negative effect of the gene therapy on control retinal organoids. No difference in retinal lamination or localization of MUPP1 at the OLM was observed after AAV.hCRB treatment of the isogenic control (Figure 4A, B, C). Also no statistically significant difference was observed after AAV.hCRB1 nor with AAV.hCRB2 treatment of the isogenic control for the number of photoreceptor nuclei in a row and the photoreceptor nuclei above the OLM (Figure 4D, E).

5

Next, AAV-mediated gene augmentation therapy was performed on three CRB1^{KO} iPSC lines differentiated into retinal organoids. AAV transduction was performed on two independent differentiation batches, one batch with and one without additional co-infection of 3.3×10^{10} gc AAV5.CMV.GFP. The results of both experiments were pooled. Immunohistochemical analysis at DD210 showed proper lamination and MUPP1 localization at the OLM after AAV.hCRB treatment (Figure 4A, B, C). AAV.hCRB1 and AAV.hCRB2 expression has been confirmed using immunohistochemistry at the OLM after AAV.hCRB treatment in CRB1^{KO} (Supplemental Figure 5A, B) and in CRB1 patient-derived retinal organoids [26]. A statistically significant increase in the number of photoreceptor nuclei in a row after AAV.hCRB2 treatment was observed for CRB1^{KO} CL19 and CL26 compared to the untreated CRB1^{KO} (Figure 4D). This improvement was more pronounced when the three CRB1^{KO} clones were combined (Figure 4E). In addition, a small, but not statistically significant, decrease in number of photoreceptor nuclei above the OLM

was observed after AAV.h*CRB2* treatment of the combined *CRB1*^{KO} retinal organoids (Figure 4G). No statistically significant improvement was observed after AAV.h*CRB1* treatment of *CRB1*^{KO} retinal organoids (Figure 4D-G, Supplemental Figure 5C-H). For the ONL thickness, retinal thickness, and INL thickness no statistically significant differences were observed with AAV.h*CRB* treatment of *CRB1*^{KO} retinal organoids (Supplemental Figure 5C-H). Altogether, the data show a partial improvement of the outer retinal phenotype of *CRB1*^{KO} retinal organoids after treatment with AAV.h*CRB2* in DD210 retinal organoids.

Discussion

In this study, we have shown that the complete loss of CRB1 in human *CRB1*^{KO} and *CRB1*^{KO}*CRB2*^{+/-} retinal organoids results in degeneration of the inner and outer retina, whereas *CRB1* retinitis pigmentosa patient-derived retinal organoids carrying a missense mutation showed strongly reduced levels of variant CRB1 and degeneration of the outer retina [23,26]. We also show that AAV transduction efficiency of retinal organoids depends on the time point of retinal organoid development. In addition, a partially improved outer retina phenotype of *CRB1*^{KO} retinal organoids was observed after AAV.h*CRB2* transduction.

Here, in order to generate a model for a mild form of LCA, CRISPR/Cas9 was used to generate *CRB1*^{KO} iPSC with a nucleotide deletion in exon 2 of the *CRB1* gene. The nucleotide deletion caused a frameshift resulting in a premature protein translation stop codon. Immunohistochemical analysis confirmed the complete loss of CRB1 in *CRB1*^{KO} retinal organoids at DD180 and DD210. A decreased number of photoreceptor nuclei in a row in the ONL and an increased number of photoreceptor cell nuclei above the OLM were observed at DD180 and DD210 in *CRB1*^{KO} retinal organoids compared to the isogenic control. The data are similar to what was previously observed in *CRB1* retinitis pigmentosa patient-derived retinal organoids carrying missense mutations that allow the expression of a variant CRB1 protein [26]. Moreover, the complete loss of

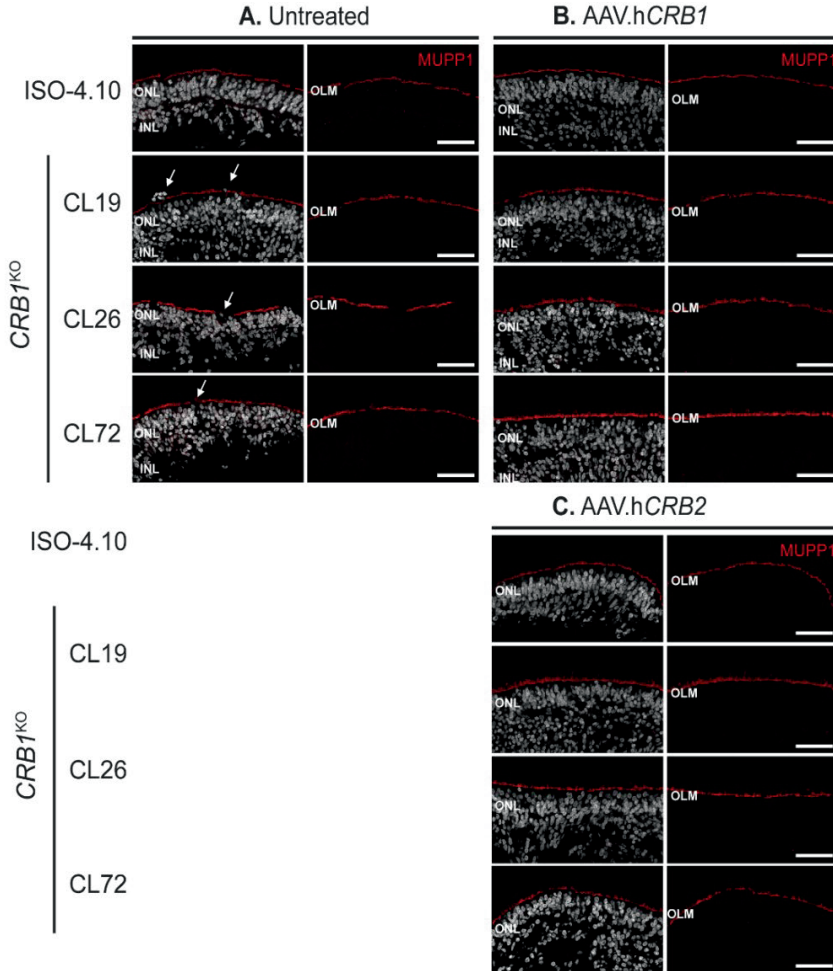


Figure 4 (A-C): AAV-mediated gene therapy on $CRB1^{KO}$ organoids shows an improved number of photoreceptor nuclei in a row. (A, B, C) Representative immunohistochemical images of (A) untreated, (B) AAV.hCRB1, or (C) AAV.hCRB2 treated control and $CRB1^{KO}$ retinal organoids at DD120 and analysed at DD210. Stained with MUPP1 (red) at the OLM.

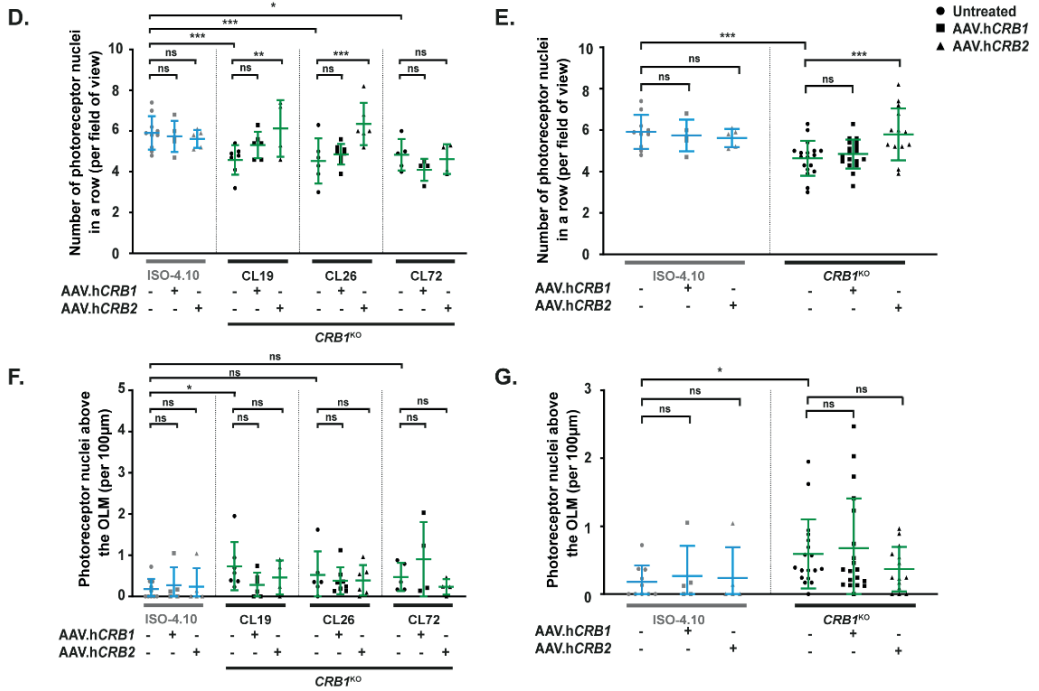


Figure 4 (D-G): AAV-mediated gene therapy on $CRB1^{KO}$ organoids shows an improved number of photoreceptor nuclei in a row. (D, E, F, G) Quantification of the number of photoreceptor nuclei in a row (D, E) and above the OLM (F, G) per $CRB1^{KO}$ clone (D, F) or all $CRB1^{KO}$ clones combined (E, G). Each datapoint in the graph represent an individual organoid, of which an average has been taken of at least three representative images. The SEM is derived from these averages. Number of individual organoids used for quantification per condition for untreated: 4.10 $n = 10$, $CRB1^{KO}$ CL19 $n = 7$, CL26 $n = 7$, CL72 $n = 5$; AAV.hCRB1 treated: 4.10 $n = 5$, $CRB1^{KO}$ CL19 $n = 6$, CL26 $n = 8$, CL72 $n = 4$ from two independent differentiation batches; and AAV.hCRB2 treated: 4.10 $n = 5$, $CRB1^{KO}$ CL19 $n = 4$, CL26 $n = 6$, CL72 $n = 3$ from one differentiation batch. Note: INL = Inner Nuclear Layer, ONL = Outer Nuclear Layer, OLM = Outer Limiting Membrane. Scalebar = 50µm, statistical analysis: generalized linear mixed models with $p < 0.05$ (*), $p < 0.01$ (**), and $p < 0.001$ (***)

CRB1 in MGC of *Crb1* mouse retina also results in the protrusion of photoreceptor cell bodies into the subretinal space [7,31]. A more severe retinal phenotype in $CRB1^{KO}$ mice was observed with concomitant loss of *Crb2* in MGC [22,32], so this was investigated as well in the $CRB1^{KO}CRB2^{+/-}$ human retinal organoid model. A heterozygous mutation in *CRB2* targeting exon 3 was introduced in combination with a mutation targeting exon 2 of the *CRB1* gene, resulting in $CRB1^{KO}CRB2^{+/-}$ retinal organoids. These retinal

organoids show a similar outer retina phenotype as the *CRB1*^{KO} and *CRB1* patient-derived retinal organoids [26]. Interestingly, the *CRB1*^{KO} and *CRB1*^{KO}*CRB2*^{+/-} outer retina phenotypes studied here seem to be not much more severe than the outer retina phenotype previously observed in *CRB1* retinitis pigmentosa patient-derived retinal organoids [23,26]. The retinal organoids can show a variability in phenotype which can be caused by differences in genetic background, developmental age of the organoid or practical handling differences between researchers during the organoid culture. To exclude differences in genetic background, the *CRB1* and *CRB1*^{KO}*CRB2*^{+/-} knockout mutations needs to be introduced into the isogenic *CRB1* RP patient hiPSC. This will allow for a direct comparison between *CRB1* RP patient and *CRB1*^{KO} and *CRB1*^{KO}*CRB2*^{+/-} retinal organoids with their isogenic controls all on the same genetic background. Furthermore, then the retinal organoids need to be cultured at the same time under the same culturing conditions in multiple batches of differentiation.

5 Interestingly, an inner and outer retinal phenotype was observed in *CRB1*^{KO} and *CRB1*^{KO}*CRB2*^{+/-} retinal organoids compared to the isogenic control. This inner retinal phenotype was previously not observed in three independent *CRB1* retinitis pigmentosa patient-derived retinal organoids compared to their isogenic controls [23,26]. Staining for ISLET1/2-positive rods and ON-cone bipolar cells and SOX9-positive MGCs showed abnormal localization of these cell types in the INL of *CRB1*^{KO} and *CRB1*^{KO}*CRB2*^{+/-} retinal organoids. The data suggest that a complete lack of CRB1 in MGC and photoreceptors can result in a more advanced LCA-like phenotype affecting inner and outer retina. Interestingly, scRNA-seq analysis on DD230 *CRB1* patient-derived retinal organoids showed differences in gene expression profiles of MGC and photoreceptors, but changes were not detected in inner retinal cell types [26]. Future scRNA-seq studies on *CRB1*^{KO} and *CRB1*^{KO}*CRB2*^{+/-} retinal organoids with their isogenic controls might provide insight in changes in the inner and outer retina. Moreover, the *CRB1* retinitis pigmentosa patient-derived retinal organoids had missense mutations and surprisingly showed a strong reduction in levels of variant CRB1 protein, whereas the *CRB1* mRNA transcript levels were not changed [26]. The *CRB1*^{KO} and *CRB1*^{KO}*CRB2*^{+/-} retinal organoids showed complete loss of CRB1 leading to an inner and outer retina phenotype. scRNA-seq revealed that human MGC and

photoreceptors express relatively high levels of *CRB1* transcripts, and that photoreceptors express relatively high levels of *CRB2* while the MGCs express relatively low levels of *CRB2* [26]. We hypothesize that relatively low levels of human *CRB2* in MGC are the cause for the phenotype in the inner retina of *CRB1*^{KO} retinal organoids. But, interestingly, mouse retinas that solely lack either *CRB1* or *CRB2* in MGC show very mild RP outer retinal phenotypes [7,29,31] whereas a severe LCA-like retinal phenotype affecting inner and outer retina occurs in mouse retinas that lack both *CRB1* and *CRB2* in MGC [18]. Patients with missense variations in the *CRB1* gene can develop either early-onset RP or LCA or macular dystrophy [14,17]. Future studies need to show whether these differences in retinal phenotypes are due to relatively low levels of *CRB2* and variant *CRB1* in MGC.

All of the *CRB1*^{KO} and *CRB1*^{KO}*CRB2*^{+/-} iPSC, but not the isogenic control iPSC from which the *CRB* mutant lines were derived, contained a copy number variation (CNV) gain in chromosome 20q. This gain in chromosome 20q is one of the most common recurrent abnormalities in iPSCs and the biological significance of such recurrent abnormalities is still discussed [27]. Novel insights of CNV gains at 20q11.21 show that the differential gene expression pattern had a negative effect on the differentiation potential [33]. Genes associated with PI3K/AKT signaling pathway were significantly downregulated in the iPSC with a CNV gain at chromosome 20q, this pathway has an essential role in the survival of human pluripotent stem cells [33]. In our case, differentiating the *CRB1*^{KO} and *CRB1*^{KO}*CRB2*^{+/-} hiPSC into retinal organoids was more challenging than for the isogenic control. However, this could also be due to the quality of medium compounds (for example Matrigel), or other culture conditions, since we experienced this as well with other iPSC lines. Other groups also described the variability in the efficiency of differentiating certain iPSC lines efficiently into retinal organoids [34]. Therefore, more research is needed if this CNV can have a negative effect on the differentiation potential into retinal organoids.

AAV tropism at two differentiation days was compared. Mainly photoreceptor cells and MGC were transduced on DD135 and DD200 retinal organoids with either AAV2.CMV.*GFP* or AAV5.CMV.*GFP*. Similar transduction was previously observed

at DD120 and DD220 [23,26]. In conclusion, we have shown that AAV2/2 and AAV2/5 are capable of infecting MGC and photoreceptor cells in hiPSC-derived control retinal organoids.

Using AAV-mediated gene augmentation therapy we have partially improved the outer retinal phenotype in $CRB1^{KO}$ retinal organoids after AAV.h*CRB2* treatment. However, we did not observe a statistically significant improved number of photoreceptor nuclei in a row after AAV.h*CRB1* treatment of $CRB1^{KO}$ retinal organoids. The AAV.h*CRB1* vector contains a minimal CMV promoter, whereas the AAV.h*CRB2* vector contains a full-length CMV promoter. The short CMV promoter worked efficiently in mouse retina [35], but the promoter activities might differ in human MGCs and photoreceptors. In patient *CRB1* retinal organoids a statistically significant improved number of photoreceptor nuclei in a row in the ONL was observed after treatment with AAV.h*CRB1* and with AAV.h*CRB2* [26]. This could potentially be explained by the difference in low expression of a variant CRB1 protein in *CRB1* patient-derived retinal organoids and the complete absence of CRB1 protein expression in the $CRB1^{KO}$ retinal organoids. We hypothesize that the $CRB1^{KO}$ retinal organoids might need higher levels of AAV.h*CRB1* in MGCs to improve the outer retinal phenotype. Another possibility, as described above, could be because of modifying factors and differences in the genetic background. $CRB1^{KO}$ retinal organoids showed a partially improved retinal phenotype after AAV.h*CRB2* treatment. Using anti-CRB2 immunohistochemical staining recombinant h*CRB2* protein was detected at the OLM.

In conclusion, we generated and differentiated $CRB1^{KO}$ and $CRB1^{KO}CRB2^{+/-}$ hiPSC into retinal organoids and observed an extended phenotype compared to the phenotype observed in *CRB1*-patient derived retinal organoids and in *Crb* mutant mouse studies. The $CRB1^{KO}$ and $CRB1^{KO}CRB2^{+/-}$ retinal organoids showed an inner and outer retinal phenotype, whereas the *CRB1* patient-derived retinal organoids showed only an outer retinal phenotype. Using AAV-mediated gene augmentation therapy we have partially improved the outer retinal phenotype in $CRB1^{KO}$ retinal organoids. These data provide essential information for future gene therapy approaches for patients with mutations in the *CRB1* gene.

Experimental procedures

Generation of $CRB1^{KO}$ and $CRB1^{KO}CRB2^{+/-}$ hiPSC

Three $CRB1^{KO}$ (CL19, CL26, and CL72) and three $CRB1^{KO}CRB2^{+/-}$ (CL4, CL9, and CL17) were generated from the isogenic control (LUMC04iCTRL10) using CRISPR/Cas9 technology (Supplemental Table 1) (Applied Stem Cell, California, USA). In short, two guide RNAs (gRNA) per gene of interest were designed, targeting exon 2 of $CRB1$ and exon 3 of $CRB2$. These gRNAs were individually cloned into a gRNA/Cas9 expression vector by inserting double-stranded oligo cassettes of each gRNA between the two BbsI sites in the pBT-U6-Cas9-2A-GFP vector. Each oligo cassette consists of a 20bp gRNA sequence with a guanosine at the 5'-end for optimal expression, and adherent ends for cloning at BbsI sites. Following construct delivery into the target cells, the abilities of these gRNAs to promote double stranded breaks were evaluated using Sanger sequencing. gRNAs with the best targeting and repairing efficiency per gene of interest were selected for transfection of iPSC, gRNA for $CRB1$ = GAAACTACCATTGGTTCCTG and for $CRB2$ = AGAGCCAGCCGTGCG CACAT. After transfecting gRNA and Cas9 into the target cells, single cell-derived clones were screened and three correct clones per gene of interest were selected and expanded for further use. Confirmation of the mutation was done by PCR and subsequent sanger sequencing.

Confirmation of the mutation was done by PCR and subsequent sanger sequencing for $CRB1$ and NGS for $CRB2$ (Supplemental Table 2).

Next generation sequencing sample preparation and data analysis

Genomic DNA of hiPSC LUMC0004iCTRL10, and three $CRB1^{KO}CRB2^{+/-}$ (CL4, CL9, and CL17) were extracted using the DNeasy Blood & Tissue Kit protocol (Qiagen; 69506). The NGS first round PCR for $CRB2$ (Supplemental Table 2), to amplify a target region with Illumina adapter overhang, was performed using a GoTaq® G2 DNA Polymerase kit (Promega; M7845). After this, amplicons were purified by the AMPure XP kit (Beckman Coulter; A63881). Then the barcode PCR was performed to generate

a library of amplicons using Illumina tag-specific primer pairs with unique sequence combinations for demultiplexing and sample identification (Supplemental Table 3) using Kapa HiFi 2x Ready Mix (Roche; KK2602) and subsequently the purification using AMPure XP kit was carried out. The concentration was determined using Qubit2.0 fluorometer (Invitrogen) and Qubit dsDNA HS assay kit (Invitrogen; Q32854). The sample quality control was performed using capillary electrophoresis with a 2100 BioAnalyzer (Agilent). The amplicons from each sample were pooled at equivalent DNA quantities. Finally, this library of pooled barcoded amplicons was subjected to Illumina MiSeq sequencing with 100k reads. The data were analyzed using CRISPResso2 [38,39].

Cell culture and retinal organoid differentiation

The following hiPSC lines were used for organoid differentiation: three *CRB1*^{KO} (CL19, CL26, and CL72) and three *CRB1*^{KO}*CRB2*^{+/-} (CL4, CL9, and CL17) derived from the isogenic control (LUMC04iCTRL10) (Supplemental Table 1). hiPSC lines were derived from skin fibroblasts using polycistronic Lentiviral vectors [36]. hiPSC were cultured on Matrigel coated plates in mTeSR plus medium (STEMCELL Technologies) and passaged mechanically using gentle cell dissociation reagent. Retinal organoid differentiation was carried out as previously reported [26,37].

AAV transduction of hiPSC-derived retinal organoids

Two to three retinal organoids were plated in a single 96-well agarose coated plate, multiple 96-wells were used per experiment, and were infected at DD120, DD135 or DD200 with the appropriate AAV concentration in 50 μ L RLM2. Treated organoids were incubated at 5% CO₂ at 37°C and 8h later the organoids were topped up to 200 μ L. The next day, the treated organoids were transferred to a 24 well plate and cultured until the desired differentiation day (for AAV.*CRB* treatment) or for three weeks (for AAV.*GFP* tropism). The following viral vectors were used: AAV2/2.CMV.*GFP* (105530-AAV2; Addgene), AAV2/5.CMV.*GFP* (105530-AAV5; Addgene), AAV5.CMVmin.h*CRB1* and AAV5.CMV.h*CRB2* (HORAMA) with a titer of 1×10^{10} , 3.3×10^{10} , 6.6×10^{10} , or 10×10^{10} genome copies (gc) per well.

Immunohistochemical analysis

Organoids were collected and fixed with 4% paraformaldehyde in PBS for 20 minutes at room temperature (RT). Then briefly washed in PBS and subsequently cryo-protected in 15% and 30% sucrose for at least 30 minutes. The samples were embedded in Tissue-Tek O.C.T. Compound (Sakura, Finetek) and stored at -20°C for future use. Then cryosections of 8 μM were made with a Leica CM1900 cryostat (Leica Microsystems). Slides with cryosections were stored at -20°C for future use.

For the immunohistochemical analysis, the slides were blocked in 10% normal goat serum, 0.4% Triton X-100, and 1% bovine serum albumin in PBS for 1h at RT. Primary antibodies were incubated for least 3h at RT or overnight at 4°C with 0.3% normal goat serum, 0.4% Triton X-100, 1% BSA and appropriate primary antibody concentration. Slides were washed twice in PBS, and incubated with a secondary antibody in 0.1% goat serum in PBS for 1h at RT. Slides were then washed twice again in PBS, and mounted using Vectashield Hardset with DAPI mounting medium (H1800, Vector Laboratories, Burlingame, USA). The slides were imaged on a Leica TCS SP8 confocal microscope and images were processed using Leica Application Suite X (v3.7.0.20979).

The following primary antibodies were used: CRB1 AK2 (1:200; homemade = CRB1^{INT}, used for CRB1 if not otherwise specified), CRB1^{EX} (1:200, Abnova H00023418-A01), CRB2 SK11 (1:200; homemade), PALS1 (1:200; homemade), rhodopsin (1:500; Millipore Cat# MAB5356), SOX9 (1:250; Millipore Cat# AB5535), ISLET1-2 (1:200, DSHB Developmental Studies Hybridoma Bank 39.4D5-c Islet-1 & Islet-2 homeobox), MUPP1 (1:200, BD Biosciences M98820), OTX2 (1:200, Proteintech 13497-1-AP), CRALBP (1:200, Abcam Ab15051).

The following secondary antibodies were used; goat anti-mouse, goat anti-rabbit, or goat anti-chicken IgGs conjugated to Alexa 488, Alexa555, Alexa647 (1:1000, Abcam).

Quantification and statistical analysis

40x magnification images were manually quantified using Fiji ImageJ (ImageJ 1.53f51). At least 4 organoids from at least two differentiation batches per condition with 3-6 representative images of each organoid were used for quantification. The exact number of organoids used per experiment is mentioned in the figure legends. In each image, three regions were quantified for the number of photoreceptor nuclei in a row, the number of protruding cells above the OLM, the retinal thickness, INL thickness, and ONL thickness. All measured datapoints were averaged per organoid and plotted in the graph; so that each dot is one organoid. Data was either presented per 100 μ m retinal length or per field of view. Data presentation was performed using GraphPad Prism version 8 (GraphPad Software).

Statistical analysis was performed using IBM SPSS statistics (version 25). A generalized mixed model with treatment as a fixed effect was performed on all quantification parameters; all individual data points per image were used for statistical analysis. Each datapoint in the graph represents individual organoids, of which an average has been taken of 3-6 representative images. The standard error of the mean (SEM) is derived from these averages. Significance is indicated in graphs as $p < 0.05$ (*), $p < 0.01$ (**), and $p < 0.001$ (***)

5

Article information

Author contributions: Conceptualization, N.B. and J.W.; Formal analysis, N.B.; Investigation, N.B., X.L., C.A.A, M.O, and P.M.J.Q.; Data curation, N.B.; Writing - original draft, N.B.; Writing - review & editing, N.B, C.J.F.B, and J.W.; Visualization, N.B.; Supervision, J.W.; Project administration, J.W.; Funding acquisition, J.W.

Funding: This work was funded by The Netherlands Organization for Health Research and Development (ZonMw grant 43200004, to JW), research grant MDBR-19-131-CRB1 from the University of Pennsylvania Orphan Disease Center in partnership with the Curing Retinal Blindness Foundation (to JW), Bontius Stichting 32072-8231, and HORAMA 41400-8231.

Acknowledgements: The authors would like to thank Chelsey Linnenbank for technical assistance, the LUMC light and electron microscope facility for help during image acquisition, and all the previous and current members of the Wijnholds lab for advice on experiments and the manuscript.

Abbreviations:

AAV	Adeno-associated viral vectors
CRB1	Crumbs homolog-1
CNV	Copy number variation
CMV	Cytomegalovirus
DD210	Differentiation day 210
EGF	Epidermal growth factor
ERLI	Glutamic acid-arginine-leucine-isoleucine
GFP	Green Fluorescent Protein
gRNA	Guide RNA
hiPSC	Human-induced pluripotent stem cell
INL	Inner nuclear layer
LCA	Leber congenital amaurosis
MGC	Müller glial cell
MUPP1	Multiple PDZ domain protein 1
NGS	Next Generation Sequencing
OLM	Outer limiting membrane
ONL	Outer nuclear layer
PALS1	Protein associated with Lin Seven 1
RP	Retinitis pigmentosa
RT	Room temperature
SEM	Standard error of mean
SOX9	SRY-Box Transcription Factor 9

References

1. Tepass, U.; Theres, C.; Knust, E. crumbs encodes an EGF-like protein expressed on apical membranes of Drosophila epithelial cells and required for organization of epithelia. *Cell* **1990**, 61, 787–799, doi:10.1016/0092-8674(90)90189-L.
2. Den Hollander, A.I.; Ten Brink, J.B.; De Kok, Y.J.M.; Van Soest, S.; Van Den Born, L.I.; Van Driel, M.A.; Van De Pol, D.J.R.; Payne, A.M.; Bhattacharya, S.S.;

Kellner, U.; et al. Mutations in a human homologue of *Drosophila* crumbs cause retinitis pigmentosa (RP12). *Nat. Genet.* **1999**, *23*, 217–221, doi:10.1038/13848.

3. Boon, N.; Wijnholds, J.; Pellissier, L.P. Research Models and Gene Augmentation Therapy for CRB1 Retinal Dystrophies. *Front. Neurosci.* **2020**, *14*, 1–13, doi:10.3389/fnins.2020.00860.

4. Quinn, P.M.; Pellissier, L.P.; Wijnholds, J. The CRB1 complex: Following the trail of crumbs to a feasible gene therapy strategy. *Front. Neurosci.* **2017**, *11*, doi:10.3389/fnins.2017.00175.

5. Ray, T.A.; Cochran, K.; Kozlowski, C.; Wang, J.; Alexander, G.; Cady, M.A.; Spencer, W.J.; Ruzycki, P.A.; Clark, B.S.; Laeremans, A.; et al. Comprehensive identification of mRNA isoforms reveals the diversity of neural cell-surface molecules with roles in retinal development and disease. *Nat. Commun.* **2020**, *11*, doi:10.1038/s41467-020-17009-7.

6. Margolis, B. The Crumbs3 polarity protein. *Cold Spring Harb. Perspect. Biol.* **2018**, *10*, 1–9, doi:10.1101/cshperspect.a027961.

7. van de Pavert, S.A.; Kantardzhieva, A.; Malysheva, A.; Meuleman, J.; Versteeg, I.; Levelt, C.; Klooster, J.; Geiger, S.; Seeliger, M.W.; Rashbass, P.; et al. Crumbs homologue 1 is required for maintenance of photoreceptor cell polarization and adhesion during light exposure. *J. Cell Sci.* **2004**, *117*, 4169–4177, doi:10.1242/jcs.01301.

8. Roh, M.H.; Makarova, O.; Liu, C.J.; Shin, K.; Lee, S.; Laurinec, S.; Goyal, M.; Wiggins, R.; Margolis, B. The Maguk protein, Pals1, functions as an adapter, linking mammalian homologues of crumbs and discs lost. *J. Cell Biol.* **2002**, *157*, 161–172, doi:10.1083/jcb.200109010.

9. Bulgakova, N.A.; Knust, E. The Crumbs complex: From epithelial-cell polarity to retinal degeneration. *J. Cell Sci.* **2009**, *122*, 2587–2596, doi:10.1242/jcs.023648.

10. Vallespin, E.; Cantalapiedra, D.; Riveiro-Alvarez, R.; Wilke, R.; Aguirre-Lamban, J.; Avila-Fernandez, A.; Lopez-Martinez, M.A.; Gimenez, A.; Trujillo-Tiebas, M.J.; Ramos, C.; et al. Mutation screening of 299 Spanish families with retinal dystrophies by leber congenital amaurosis genotyping microarray. *Investig. Ophthalmol. Vis. Sci.* **2007**, *48*, 5653–5661, doi:10.1167/iovs.07-0007.

11. Bujakowska, K.; Audo, I.; Mohand-Säid, S.; Lancelot, M.E.; Antonio, A.; Germain, A.; eveillard, T.Ł.; Letexier, Melanie; Saraiva, J.P.; Lonjou, C.; et al. CRB1 mutations in inherited retinal dystrophies. *Hum. Mutat.* **2012**, *33*, 306–315, doi:10.1002/humu.21653.

12. Corton, M.; Tatu, S.D.; Avila-Fernandez, A.; Vallespín, E.; Tapias, I.; Cantalapiedra, D.; Blanco-Kelly, F.; Riveiro-Alvarez, R.; Bernal, S.; García-Sandoval, B.; et al. High frequency of CRB1 mutations as cause of Early-Onset Retinal

Dystrophies in the Spanish population. *Orphanet J. Rare Dis.* **2013**, 8, doi:10.1186/1750-1172-8-20.

13. Den Hollander, A.I.; Davis, J.; Van Der Velde-Visser, S.D.; Zonneveld, M.N.; Pierrottet, C.O.; Koenekoop, R.K.; Kellner, U.; Van Den Born, L.I.; Heckenlively, J.R.; Hoyng, C.B.; et al. *CRB1* mutation spectrum in inherited retinal dystrophies. *Hum. Mutat.* **2004**, 24, 355–369, doi:10.1002/humu.20093.

14. Talib, M.; van Schooneveld, M.J.; van Genderen, M.M.; Wijnholds, J.; Florijn, R.J.; ten Brink, J.B.; Schalijs-Delfos, N.E.; Dagnelie, G.; Cremers, F.P.M.; Wolterbeek, R.; et al. Genotypic and Phenotypic Characteristics of *CRB1*-Associated Retinal Dystrophies: A Long-Term Follow-up Study. *Ophthalmology* **2017**, 124, 884–895, doi:10.1016/j.ophtha.2017.01.047.

15. Verbakel, S.K.; van Huet, R.A.C.; Boon, C.J.F.; den Hollander, A.I.; Collin, R.W.J.; Klaver, C.C.W.; Hoyng, C.B.; Roepman, R.; Klevering, B.J. Non-syndromic retinitis pigmentosa. *Prog. Retin. Eye Res.* **2018**, 66, 157–186, doi:10.1016/j.preteyeres.2018.03.005.

16. Nguyen, X.; Moekotte, L.; Plomp, A.S.; Bergen, A.A.; Genderen, M.M. Van; Boon, C.J.F. Retinitis Pigmentosa: Current Clinical Management and Emerging Therapies. *Int. J. Mol. Sci.* **2023**, 24.

17. Talib, M.; Van Cauwenbergh, C.; De Zaeytijd, J.; Van Wynsberghe, D.; De Baere, E.; Boon, C.J.F.; Leroy, B.P. *CRB1*-Associated retinal dystrophies in a Belgian cohort: Genetic characteristics and long-Term clinical follow-up. *Br. J. Ophthalmol.* **2022**, 106, 696–704, doi:10.1136/bjophthalmol-2020-316781.

18. Quinn, P.M.; Mulder, A.A.; Henrique Alves, C.; Desrosiers, M.; de Vries, S.I.; Klooster, J.; Dalkara, D.; Koster, A.J.; Jost, C.R.; Wijnholds, J. Loss of *CRB2* in Müller glial cells modifies a *CRB1*-associated retinitis pigmentosa phenotype into a Leber congenital amaurosis phenotype. *Hum. Mol. Genet.* **2019**, 28, 105–123, doi:10.1093/hmg/ddy337.

19. Mehalow, A.K.; Kameya, S.; Smith, R.S.; Hawes, N.L.; Denegre, J.M.; Young, J.A.; Bechtold, L.; Haider, N.B.; Tepass, U.; Heckenlively, J.R.; et al. *CRB1* is essential for external limiting membrane integrity and photoreceptor morphogenesis in the mammalian retina. *Hum. Mol. Genet.* **2003**, 12, 2179–2189, doi:10.1093/hmg/ddg232.

20. van de Pavert, S.A.; Sanz sanz, A.; Aartsen, W.M.; Vos, R.M.; Versteeg, I.; Beck, S.C.; Klooster, J.; Seeliger, M.W.; Wijnholds, J. *Crb1* is a Determinant of Retinal Apical Muller Glia Cell Features. *Glia* **2007**, 1486–1497, doi:10.1002/glia.

21. Alves, C.H.; Sanz sanz, A.; Park, B.; Pellissier, L.P.; Tanimoto, N.; Beck, S.C.; Huber, G.; Murtaza, M.; Richard, F.; Sridevi gurubaran, I.; et al. Loss of *CRB2* in the mouse retina mimics human retinitis pigmentosa due to mutations in the *CRB1* gene. *Hum. Mol. Genet.* **2013**, 22, 35–50, doi:10.1093/hmg/dds398.

22. Pellissier, L.P.; Alves, C.H.; Quinn, P.M.; Vos, R.M.; Tanimoto, N.; Lundvig, D.M.S.; Dudok, J.J.; Hooibrink, B.; Richard, F.; Beck, S.C.; et al. Targeted Ablation of Crb1 and Crb2 in Retinal Progenitor Cells Mimics Leber Congenital Amaurosis. *PLoS Genet.* **2013**, *9*, doi:10.1371/journal.pgen.1003976.
23. Quinn, P.M.; Buck, T.M.; Mulder, A.A.; Ohonin, C.; Alves, C.H.; Vos, R.M.; Bialecka, M.; van Herwaarden, T.; van Dijk, E.H.C.; Talib, M.; et al. Human iPSC-Derived Retinas Recapitulate the Fetal CRB1 CRB2 Complex Formation and Demonstrate that Photoreceptors and Müller Glia Are Targets of AAV5. *Stem Cell Reports* **2019**, *12*, 906–919, doi:10.1016/j.stemcr.2019.03.002.
24. van Rossum, A.G.S.H.; Aartsen, W.M.; Meuleman, J.; Klooster, J.; Malysheva, A.; Versteeg, I.; Arsanto, J.P.; Le Bivic, A.; Wijnholds, J. Pals1/Mpp5 is required for correct localization of Crb1 at the subapical region in polarized Müller glia cells. *Hum. Mol. Genet.* **2006**, *15*, 2659–2672, doi:10.1093/hmg/ddl194.
25. Mairot, K.; Smirnov, V.; Bocquet, B.; Labesse, G.; Arndt, C.; Defoort-dhellemmes, S.; Zanlonghi, X.; Hamroun, D.; Denis, D.; Picot, M.C.; et al. Crb1-related retinal dystrophies in a cohort of 50 patients: A reappraisal in the light of specific müller cell and photoreceptor crb1 isoforms. *Int. J. Mol. Sci.* **2021**, *22*, doi:10.3390/ijms222312642.
26. Boon, N.; Lu, X.; Andriessen, C.A.; Moustakas, I.; Buck, T.M.; Freund, C.; Arendzen, C.H.; Böhringer, S.; Boon, C.J.F.; Mei, H.; Wijnholds, J. AAV-mediated gene augmentation therapy of CRB1 patient-derived retinal organoids restores the histological and transcriptional retinal phenotype. *Stem Cell Reports* **2023**, doi:https://doi.org/10.1016/j.stemcr.2023.03.014.
27. Alves, C.H.; Boon, N.; Mulder, A.A.; Koster, A.J.; Jost, C.R.; Wijnholds, J. CRB2 Loss in Rod Photoreceptors Is Associated with Progressive Loss of Retinal Contrast Sensitivity. *Int. J. Mol. Sci.* **2019**, *20*, 4069, doi:10.3390/ijms20174069.
28. Quinn, P.M.; Alves, C.H.; Klooster, J.; Wijnholds, J. CRB2 in immature photoreceptors determines the superior-inferior symmetry of the developing retina to maintain retinal structure and function. *Hum. Mol. Genet.* **2018**, *27*, 3137–3153, doi:10.1093/hmg/ddy194.
29. Alves, C.H.; Pellissier, L.P.; Vos, R.M.; Garrido, M.G.; Sothilingam, V.; Seide, C.; Beck, S.C.; Klooster, J.; Furukawa, T.; Flannery, J.G.; et al. Targeted ablation of Crb2 in photoreceptor cells induces retinitis pigmentosa. *Hum. Mol. Genet.* **2014**, *23*, 3384–3401, doi:10.1093/hmg/ddu048.
30. Assou, S.; Girault, N.; Plinet, M.; Bouckenheimer, J.; Sansac, C.; Combe, M.; Mianné, J.; Bourguignon, C.; Fieldes, M.; Ahmed, E.; et al. Recurrent Genetic Abnormalities in Human Pluripotent Stem Cells: Definition and Routine Detection in Culture Supernatant by Targeted Droplet Digital PCR. *Stem Cell Reports* **2020**, *14*, 1–8, doi:10.1016/j.stemcr.2019.12.004.

31. van de Pavert, S.A.; Meuleman, J.; Malysheva, A.; Aartsen, W.M.; Versteeg, I.; Tonagel, F.; Kamphuis, W.; McCabe, C.J.; Seeliger, M.W.; Wijnholds, J. A single amino acid substitution (Cys249Trp) in *Crb1* causes retinal degeneration and deregulates expression of pituitary tumor transforming gene *Pttg1*. *J. Neurosci.* **2007**, *27*, 564–573, doi:10.1523/JNEUROSCI.3496-06.2007.
32. Buck, T.M.; Vos, R.M.; Alves, C.H.; Wijnholds, J. AAV-CRB2 protects against vision loss in an inducible CRB1 retinitis pigmentosa mouse model. *Mol. Ther. Methods Clin. Dev.* **2021**, *20*, 423–441, doi:10.1016/j.omtm.2020.12.012.
33. Jo, H.Y.; Lee, Y.; Ahn, H.; Han, H.J.; Kwon, A.; Kim, B.Y.; Ha, H.Y.; Kim, S.C.; Kim, J.H.; Kim, Y.O.; et al. Functional in vivo and in vitro effects of 20q11.21 genetic aberrations on hPSC differentiation. *Sci. Rep.* **2020**, *10*, 1–14, doi:10.1038/s41598-020-75657-7.
34. Hallam, D.; Hilgen, G.; Dorgau, B.; Zhu, L.; Yu, M.; Bojic, S.; Hewitt, P.; Schmitt, M.; Uteng, M.; Kustermann, S.; et al. Human-Induced Pluripotent Stem Cells Generate Light Responsive Retinal Organoids with Variable and Nutrient-Dependent Efficiency. *Stem Cells* **2018**, *36*, 1535–1551, doi:10.1002/stem.2883.
35. Pellissier, L.P.; Hoek, R.M.; Vos, R.M.; Aartsen, W.M.; Klimczak, R.R.; Hoyng, S.A.; Flannery, J.G.; Wijnholds, J. Specific tools for targeting and expression in Müller glial cells. *Mol. Ther. - Methods Clin. Dev.* **2014**, *1*, 14009, doi:10.1038/mtm.2014.9.
36. Warlich, E.; Kuehle, J.; Cantz, T.; Brugman, M.H.; Maetzig, T.; Galla, M.; Filipczyk, A.A.; Halle, S.; Klump, H.; Schöler, H.R.; et al. Lentiviral vector design and imaging approaches to visualize the early stages of cellular reprogramming. *Mol. Ther.* **2011**, *19*, 782–789, doi:10.1038/mt.2010.314.
37. Zhong, X.; Gutierrez, C.; Xue, T.; Hampton, C.; Vergara, M.N.; Cao, L.H.; Peters, A.; Park, T.S.; Zambidis, E.T.; Meyer, J.S.; et al. Generation of three-dimensional retinal tissue with functional photoreceptors from human iPSCs. *Nat. Commun.* **2014**, *5*, doi:10.1038/ncomms5047.
38. Wang, Q.; Liu, J.; Janssen, J.M.; Le Boutejller, M.; Frock, R.L.; Gonçalves, M.A.F.V. Precise and broad scope genome editing based on high-specificity Cas9 nickases. *Nucleic Acids Res* **2021** *49*, 1173-1198.
39. Clement, K.; Rees, H.; Canver, M.C.; Gehrke, J.M.; Farouni, R.; Hsu, J.Y.; Cole, M.A.; Liu, D.R.; Joung, J.K.; Bauer, D.E.; Pinello, L. CRISPResso2 provides accurate and rapid genome editing sequence analysis. *Nat Biotechnol* **2019** *37*, 224-226.

Supplemental information

Supplemental Table 1. hiPSC line information (Applied Stem Cell, California, USA), related to Supplemental Figure 1.

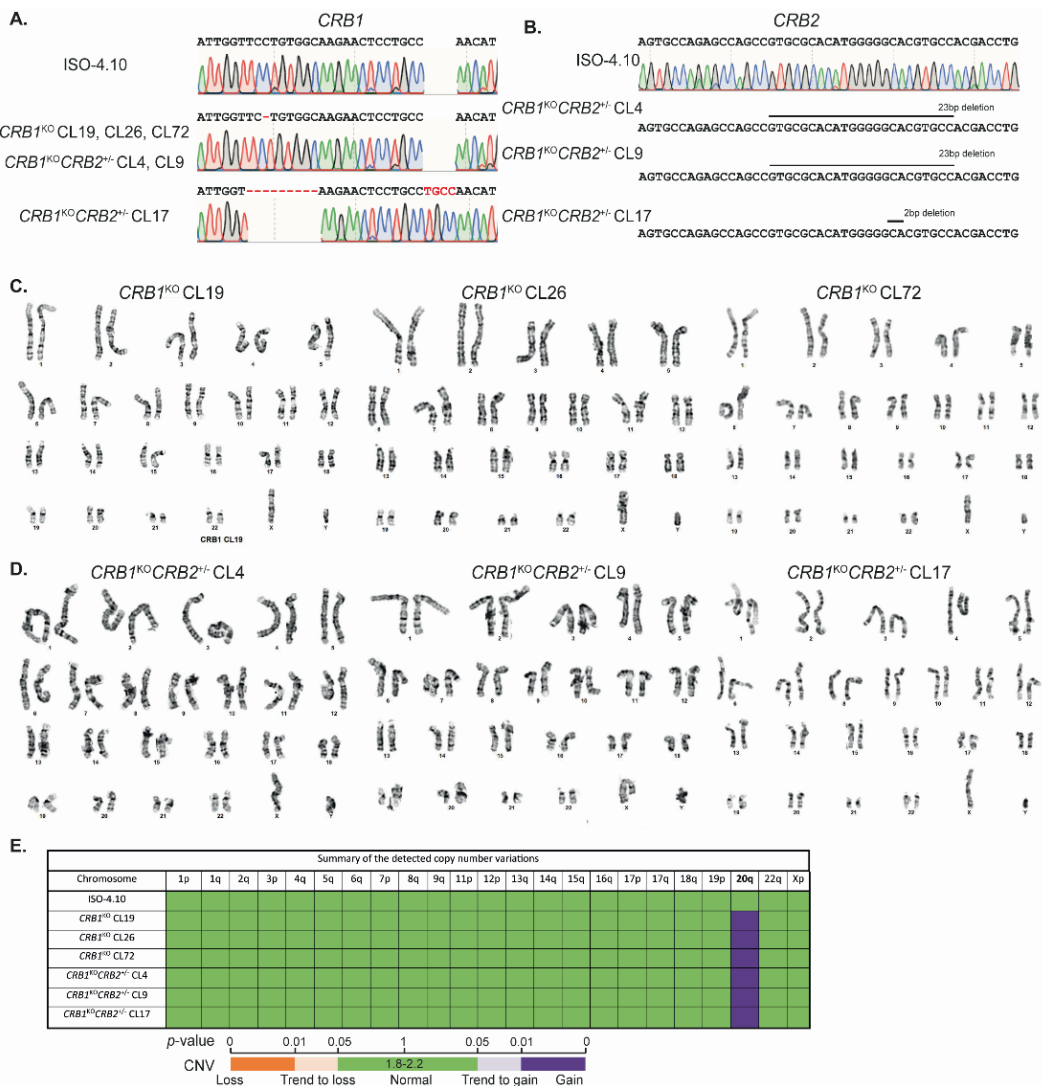
Previously published	Description	Gender
LUMC04iCTRL10 [23]	<u>ISO-4.10</u> = Isogenic control	Male
NA	<u>CRB1^{KO} CL19</u> = homozygous c.500del; p.(Ser44Serfs*)	Male
NA	<u>CRB1^{KO} CL26</u> = homozygous c.500del; p.(Ser44Serfs*)	Male
NA	<u>CRB1^{KO} CL72</u> = homozygous c.500del ; p.(Ser44Serfs*)	Male
NA	<u>CRB1^{KO}CRB2^{+/-} CL4</u> = CRB1: homozygous c.500del ; p.(Ser44Serfs*), CRB2: heterozygous mutation targeting exon3.	Male
NA	<u>CRB1^{KO}CRB2^{+/-} CL9</u> = CRB1: homozygous c.500del ; p.(Ser44Serfs*), CRB2: heterozygous mutation targeting exon3.	Male
NA	<u>CRB1^{KO}CRB2^{+/-} CL17</u> = CRB1: homozygous c.498_507delinsTGCC; p.(Ser44Lysfs*), CRB2: heterozygous mutation targeting exon3.	Male

Supplemental Table 2. PCR primer sequences for confirmation of mutations.

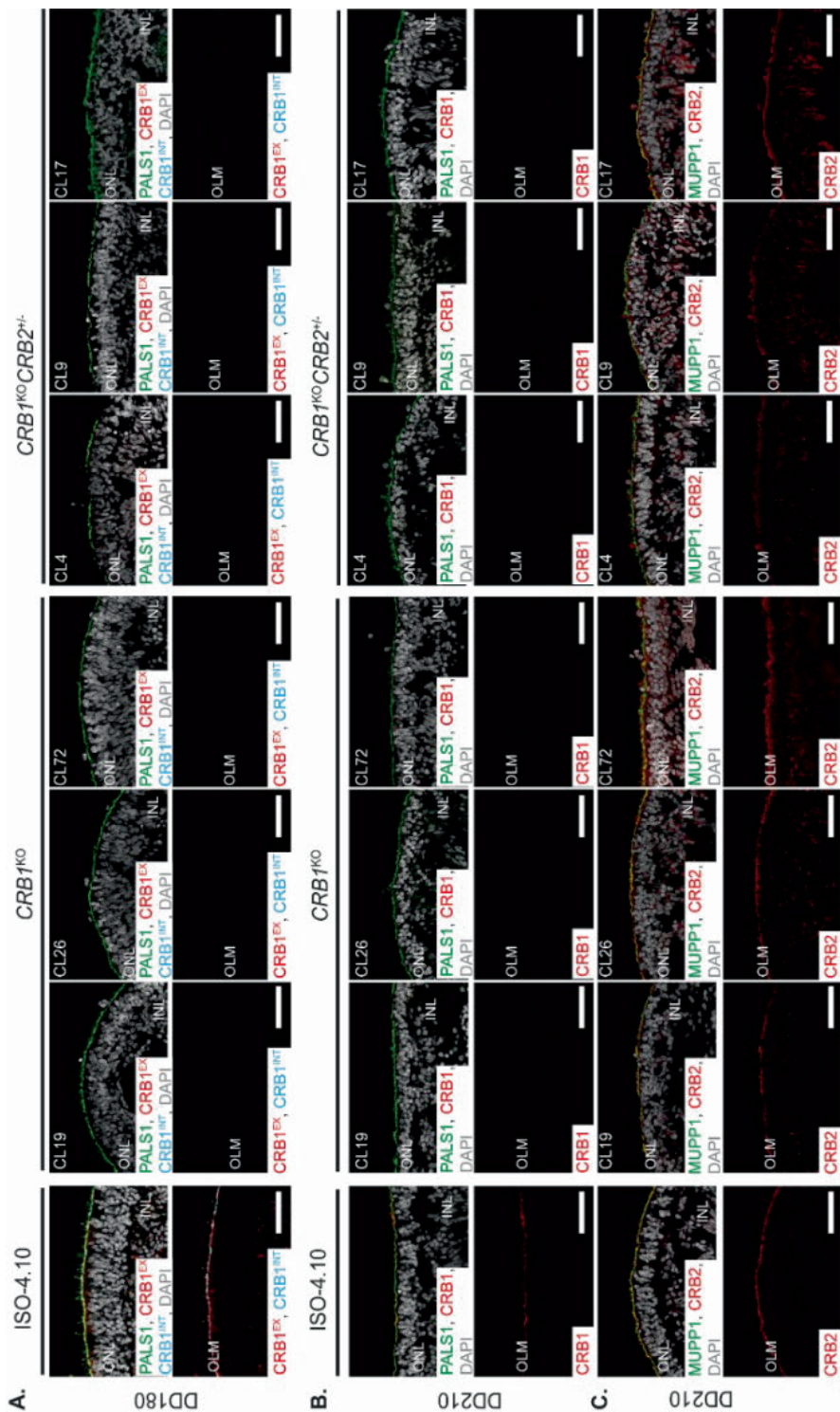
Target	PCR primers	
<i>CRB1</i>	FW	GACAATGATTGTTCTTGTTTCAGACACAGCC
	REV	CATCCACTTCCAAGTCGCAGTGTC
Sanger sequencing primers		
<i>CRB1</i>	FW	GGACAAAGACTGTGACAACATGAAAGACC
	REV	GGACACAGAAGCAGGAGTAACCATC
Target	NGS primers (5' to 3') (Illumina adapter overhang)	
<i>CRB2</i>	FW	GATGTGTATAAGAGACAGGTGCCATCCTGCACCCTGTG
	REV	CGTGTGCTCTCCGATCTTCGCTACCCGTTGACCAGGT

Supplemental Table 3. Barcode PCR primers used in the NGS amplicon sequence analysis.

Barcode name	Primer Sequence (5' to 3')	Barcode in primer	Read in Miseq
719	CAAGCAGAAGACGGCATAACGAGAT TACTACGC GTGACTGGAGTTCAGACGTGT GCTCTTCCGATCT	TACTACGC	TACTACGC
720	CAAGCAGAAGACGGCATAACGAGAT AGGCTCCG GTGACTGGAGTTCAGACGTGT GCTCTTCCGATCT	AGGCTCCG	AGGCTCCG
721	CAAGCAGAAGACGGCATAACGAGAT GCAGCGTA GTGACTGGAGTTCAGACGTGT GCTCTTCCGATCT	GCAGCGTA	GCAGCGTA
722	CAAGCAGAAGACGGCATAACGAGAT GAGCGCTA GTGACTGGAGTTCAGACGTGT GCTCTTCCGATCT	GAGCGCTA	GAGCGCTA
508	AATGATACGGCGACCACCGAGATCTACAC GTACTGAC TCGTCGGCAGCGTCAGATGTG TATAAGAGACAG	GTACTGAC	GTACTGAC



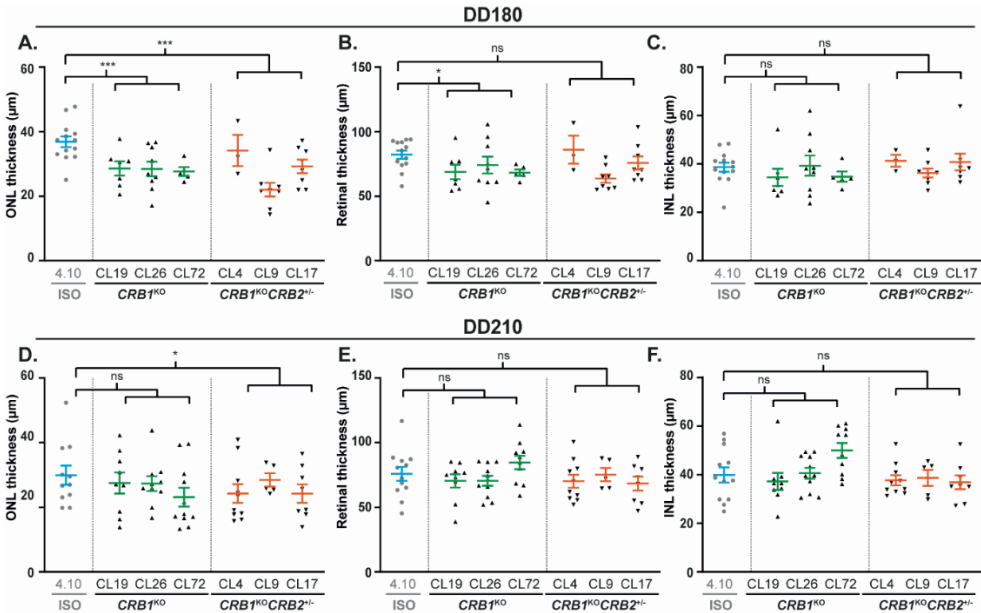
Supplemental Figure 1: Confirmation of mutations and condition of *CRB1*^{KO} and *CRB1*^{KO}*CRB2*^{+/-} hiPSC. Related to all figures. (A) Confirmation of the homozygous *CRB1* mutation in *CRB1*^{KO} and *CRB1*^{KO}*CRB2*^{+/-} hiPSC using Sanger sequencing, with *CRB1*^{KO}*CRB2*^{+/-} CL17 containing a distinct mutation. (B) Confirmation of the heterozygous *CRB2* mutation in *CRB1*^{KO}*CRB2*^{+/-} hiPSC using Sanger Sequencing and Next Generation Sequencing (C, D) Karyotyping results of (C) *CRB1*^{KO} and (D) *CRB1*^{KO}*CRB2*^{+/-} hiPSC. (E) Meta-analysis of 90% most recurrent abnormalities in hiPSCs showing a gain in copy number variation (CNV) in chromosome 20q for hiPSC used in this study.



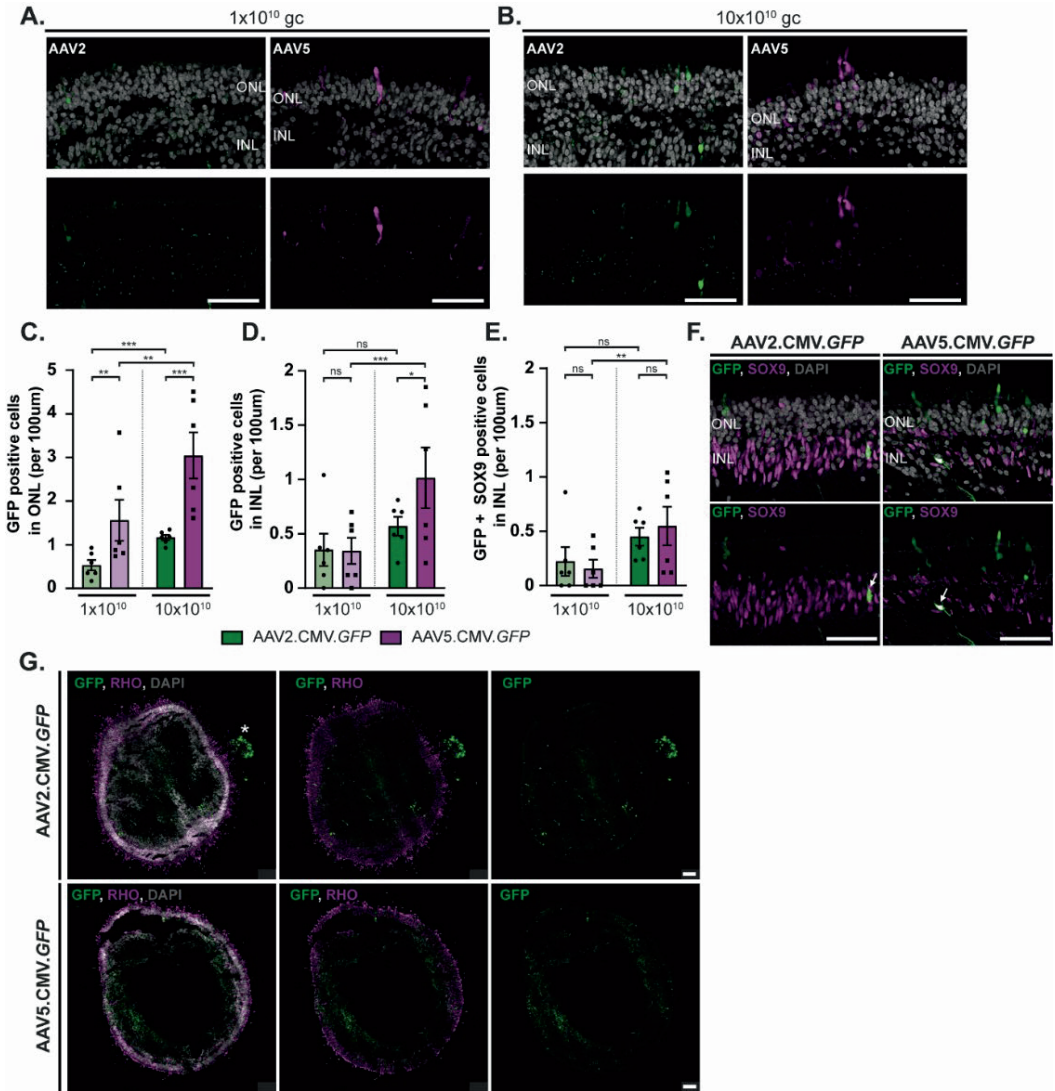
Supplemental Figure 2: CRB1 is absent in DD180 and DD210 $CRB1^{KO}$ and $CRB1^{KO}CRB2^{+/-}$ retinal organoids. Related to Figure 2.

Legend continues on the next page.

Representative immunohistochemical images of three *CRB1*^{KO} and three *CRB1*^{KO}*CRB2*^{+/-} retinal organoids compared to the isogenic control at DD180 and DD210. (A) DD180 organoids expressing PALS1 (green) in all retinal organoids at the OLM and *CRB1*^{EX} (red), and *CRB1*^{INT} (cyan) was only detected in the isogenic control. (B) DD210 retinal organoids stained with PALS1 (green) and *CRB1* (red), similar as observed in DD180. (C) MUPP1 (green) and *CRB2* (red) is expressed at the OLM in control, *CRB1*^{KO}, and *CRB1*^{KO}*CRB2*^{+/-} retinal organoids at DD210. Note: INL = Inner Nuclear Layer, ONL = Outer Nuclear Layer, OLM = Outer Limiting Membrane. Scalebar = 50µm.

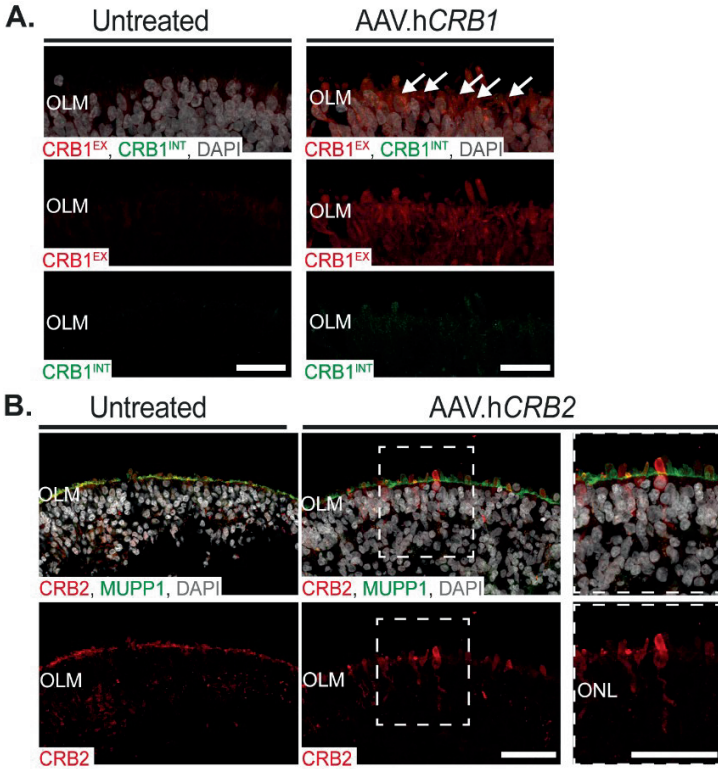


Supplemental Figure 3: Additional phenotype quantifications of DD180 and DD210 *CRB1*^{KO} and *CRB1*^{KO}*CRB2*^{+/-} retinal organoids. (A, B, C) Quantification of the (A) ONL, (B) retinal, and (C) INL thickness of DD180 retinal organoids. (D, E, F) Quantification of the (D) ONL, (E) retinal, and (F) INL thickness of DD210 retinal organoids. Each datapoint in the graph represents an individual organoid, of which an average has been taken of 3-6 representative images. The SEM is derived from these averages. Number of individual organoids used for the quantification per condition at DD180: 4.10 $n=14$, *CRB1*^{KO} CL19 $n=7$, CL26 $n=5$, CL72 $n=9$, *CRB1*^{KO}*CRB2*^{+/-} CL4 $n=3$, CL9 $n=8$, CL17 $n=8$; and DD210: 4.10 $n=12$, *CRB1*^{KO} CL19 $n=9$, CL26 $n=10$, CL72 $n=11$, *CRB1*^{KO}*CRB2*^{+/-} CL4 $n=8$, CL17 $n=8$ from at least two independent differentiation batches and *CRB1*^{KO}*CRB2*^{+/-} CL9 $n=5$ from one differentiation batch. Statistical analysis: generalized linear mixed models with $p < 0.05$ (*), $p < 0.01$ (**), and $p < 0.001$ (***)

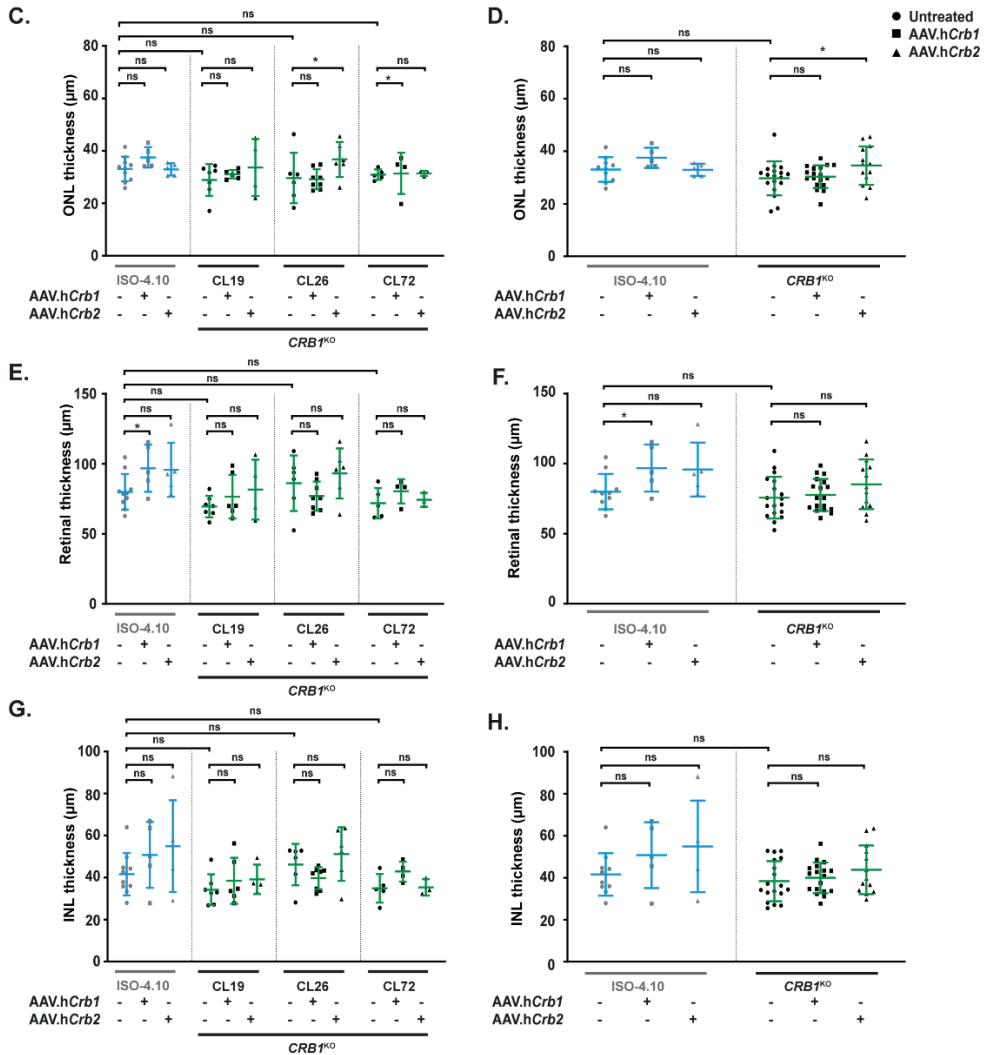


Supplemental Figure 4: AAV transduction study of control retinal organoids transduced at DD200 with AAV2.CMV.GFP or AAV5.CMV.GFP (A, B) Representative immunohistochemical images of control retinal organoids transduced with (A) 1x10¹⁰gc, or (B) 10x10¹⁰gc AAV2.CMV.GFP or AAV5.CMV.GFP. (C,D, E) Quantification of the number of GFP positive cells in the (D) ONL, (E) INL, and (F) GFP positive and co-localized with SOX9 in the INL (marking MGCs). Statistical analysis was performed within the same AAV capsid (dose-dependent) or within the same AAV titer (comparing AAV2 with AAV5 transduction efficiency). (F, G) Immunohistochemical images of co-localization of AAV.GFP with MGC marker SOX9 (F) and photoreceptor cell marker Rhodopsin (RHO) (G). Arrows indicate

colocalization of SOX9 with GFP (F), and the asterisk indicates the retinal pigment epithelium (G). Each datapoint in the graph represents individual organoids, of which an average has been taken of 3-6 representative images. The SEM is derived from these averages. Number of individual organoids used for quantification per condition for AAV2.CMV.GFP: 1×10^{10} gc $n = 6$, 10×10^{10} gc $n = 6$; and for AAV5.CMV.GFP: 1×10^{10} gc $n = 6$, 10×10^{10} gc $n = 6$ from one differentiation bath. Note: INL = Inner Nuclear Layer, ONL = Outer Nuclear Layer. Scalebar = $50 \mu\text{m}$, statistical analysis: generalized linear mixed models with $p < 0.05$ (*), $p < 0.01$ (**), and $p < 0.001$ (***)



Supplemental Figure 5 (A-B): AAV-mediated gene therapy on *CRB1*^{KO} organoids. (A, B) representative immunohistochemical image of (A) CRB1 in untreated and AAV.hCRB1 and (B) CRB2 in untreated and AAV.hCRB2 treated *CRB1*^{KO} retinal organoids.

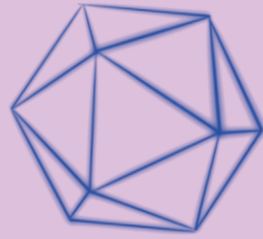


Supplemental Figure 5 (C-H): AAV-mediated gene therapy on $CRB1^{KO}$ organoids. (C, D, E, F, G, H) Quantification of the (C, D) ONL thickness, (E, F) the retinal thickness, and (G, H) INL thickness per $CRB1^{KO}$ clone (C, E, G) or all $CRB1^{KO}$ clones combined (D, F, H). Each datapoint in the graph represents individual organoids, of which an average has been taken of at least three representative images. The SEM is derived from these averages. Number of individual organoids used for quantification per condition for untreated: 4.10 $n = 10$, $CRB1^{KO}$ CL19 $n = 7$, CL26 $n = 7$, CL72 $n = 5$; AAV.hCrb1 treated: 4.10 $n = 5$, $CRB1^{KO}$ CL19 $n = 6$, CL26 $n = 8$, CL72 $n = 4$ from two independent differentiation batches; and AAV.hCrb2 treated: 4.10 $n = 5$, $CRB1^{KO}$ CL19 $n = 4$, CL26 $n = 6$, CL72 $n = 3$ from one differentiation batch. Note: ONL = Outer Nuclear Layer, OLM = Outer Limiting Membrane. Scalebar = $50\mu\text{m}$, statistical analysis: generalized linear mixed models with $p < 0.05$ (*), $p < 0.01$ (**), and $p < 0.001$ (***)

Chapter 6

General Discussion

N. Boon and J. Wijnholds



Abstract

Mutations in the *CRB1* gene can cause inherited retinal diseases such as retinitis pigmentosa (RP) and Leber congenital amaurosis (LCA). So far there are no treatment options for patients with a mutation in the *CRB1* gene. In this last chapter of the thesis we will describe (1) CRB1 in retinal disease, (2) CRB protein localization and function, (3) different models to study *CRB1* related retinal dystrophies, (4) AAV-mediated gene augmentation therapy for *CRB1* related retinal dystrophies, and (5) the future perspectives.

CRB1 in retinal disease

Inherited retinal dystrophies affect about 2 million people worldwide and share progressive degeneration of photoreceptors and/or retinal pigment epithelium (RPE) cells. Examples of retinal degeneration include Retinitis Pigmentosa (RP) or Leber congenital amaurosis (LCA), RP affects at least 1 in 3500 to 4000 people and LCA affecting at least 1 in 32000 to 80000 people worldwide [1,2]. RP patients typically experience night blindness followed by progressive visual field loss and complete loss of vision in early or middle-life [3–5], whereas LCA patients experience more severe retinal dystrophy causing serious visual impairment or immediate blindness at birth [6]. Approximately 10% of all LCA cases and 3-9% of all RP cases are caused by mutations in the *Crumbs homologue 1 (CRB1)* gene. There are over 200 different mutations described along the *CRB1* gene resulting in these retinal dystrophies, but so far there is no clear genotype-phenotype correlation [3,7]. The observed clinical variability of disease onset and severity, even within a patient cohort with the same homozygous mutations, supports the hypothesis that the phenotype is potentially modulated by other factors [8]. So far, there are no treatment possibilities for patients with mutations in the *CRB1* gene.

CRB protein localization and function

The human *CRB1* gene is mapped to chromosome 1q31.3 and contains 12 exons consisting of 210 kb of genomic DNA [9]. Canonical CRB1 protein is, like its

Drosophila homologue, a transmembrane protein consisting of a large extracellular domain with multiple epidermal growth factor (EGF) and laminin-globular like domains and a short intracellular domain with a conserved PDZ binding motif [10]. Multiple transcripts of *CRB1* have been described [9,11], including an alternative shorter transcript of *CRB1*, *CRB1-B*, lacking exons 1 to 5 and exon 12 but with substantial overlap encoding the extracellular domain [12]. CRB1 together with CRB2 and CRB3A are members of the Crumbs family. CRB2 displays similar protein structure as CRB1, with a depletion of four epidermal growth factor domains in the extracellular domain, while CRB3 lacks the entire typical extracellular domain but contains the transmembrane domain and the conserved intracellular domain [11,13]. Various research has shown that CRB1 and CRB2 are apical polarity factors, essential for the formation and function of epithelial tissues [14]. The evolutionary conserved CRB complex regulates the apical-basal polarity and maintains cell adhesion [15]. The CRB complex is formed by interaction of CRB with protein associated with Lin Seven 1 (PALS1), also known as membrane-associated guanylate kinase p55 subfamily member 5 (MPP5). The multiple PDZ proteins PATJ and multiple PDZ domain 1, MUPP1, recruit PALS1 to the apical membrane [16,17]. PALS1 can interact with MPP3 or MPP4 at the subapical region in the mouse retina [18–20].

In mammalian tissue, retinal CRB1 and CRB2 are predominantly expressed at the outer limiting membrane (OLM) at the subapical region adjacent to adherence junctions in the inner segments of photoreceptors or at the apical villi of Müller glial cells. Immuno-electron microscopy allows the identification of the subcellular localization of CRB1 and CRB2 in the retina of different species. In mouse [21] and brown Norway rats retina (**Chapter 3**), *Crb1* was present at the subapical region above the adherence junctions of solely Müller glial cells (MGC) whereas *Crb2* was present at the subapical region above the adherence junctions of MGC as well as photoreceptor cells (Figure 1A) [21,22]. However, in adult non-human primates CRB1 and CRB2 are localized at the subapical region of MGC and photoreceptors (Figure 1B) [21]. In accordance, data of human fetal retina and human-induced pluripotent stem cell-derived retinal organoids show that both CRB1 and CRB2 are located at the subapical region above the adherence junctions of both MGC and photoreceptor cells (Figure 1B)

[23]. Single cell RNA-sequencing of late-stage human-derived retinal organoids confirmed that *CRB1* and *CRB2* transcripts are present in MGC and photoreceptor cells (Chapter 4) [24]. Knowledge of this discrepancy in CRB localization is pivotal for future research and understanding of the observed phenotype in the research models.

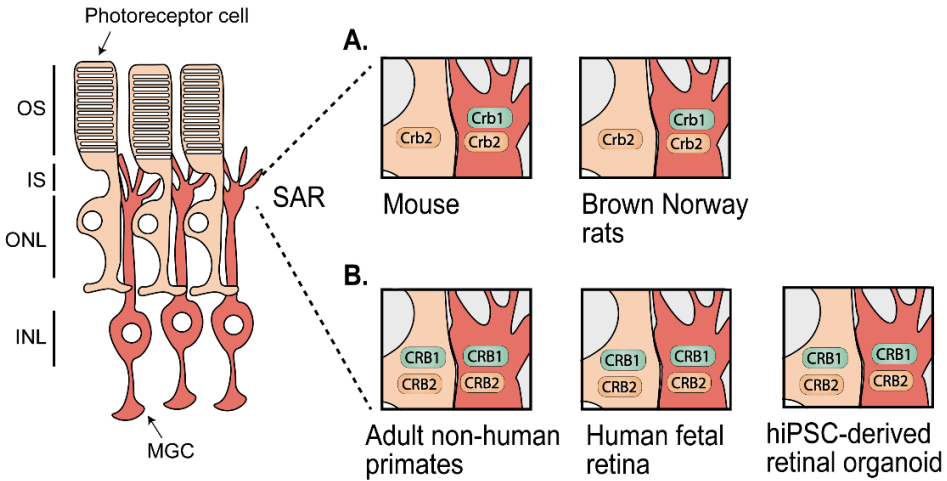


Figure 1. Schematic representation of subcellular localization of CRB1 and CRB2. (A, B) Subcellular localization of CRB1 and CRB2 in (A) mouse and brown Norway rats and (B) hiPSC-derived retinal organoids, human fetal retina, and adult non-human primates at the SAR of MGC (dark orange) or photoreceptor cells (light orange). Note: INL = inner nuclear layer; IS = inner segments; MGC = Müller glial cell; ONL = outer nuclear layer; OS = outer segments; SAR = subapical region.

6

Models to study the *CRB1*-related retinal dystrophies

Multiple rodent-derived models are described which mimic parts of the heterogeneous disease phenotype observed in *CRB1* patients. This is visualized by the tremendous number of distinct animal models previously characterized over the years: four LCA and ten RP-like mouse models and one *Crb1* rat model [25–33]. These models show the effect of loss of CRB1 or CRB2 proteins in cell types such as retinal progenitors, photoreceptor progenitors, rod photoreceptors or Müller glial cells.

In Chapter 2, two more RP-like mouse models were characterized: *Crb2*^{ΔRods} and *Crb1*^{KO}*Crb2*^{ΔRods} mice [34]. In these mice *Crb2* was specifically ablated from rod photoreceptor cells (*Crb2*^{ΔRods}) or had concomitant loss of *Crb1* from MGC

(*Crb1*^{KO}*Crb2*^{ΔRods}). While measuring retinal function using electroretinography (ERG), similar ERG responses were observed in one month *Crb2*^{ΔRods} and *Crb1*^{KO}*Crb2*^{ΔRods} mice compared to age-matched controls. At 3 months of age, a slightly reduced a-wave response, indicating alterations in rod photoreceptor function, was observed in *Crb1*^{KO}*Crb2*^{ΔRods} mice whereas the ERG response of *Crb2*^{ΔRods} mice was still similar to age-matched controls. The ERG response reduced further over time, and in 9 and 12 months mice both *Crb1*^{KO}*Crb2*^{ΔRods} and *Crb2*^{ΔRods} mice had a statistically significant reduced a-wave response compared to age-matched controls. Next, visual function was measured using optokinetic head tracking response (OKT) that showed a significant decrease in contrast sensitivity in 3, 7, and 9M *Crb1*^{KO}*Crb2*^{ΔRods} mice. Interestingly, no difference in OKT contrast sensitivity was observed in *Crb2*^{ΔRods} mice, indicating that the visual function impairment is due to cumulative loss of *Crb1* and *Crb2*. Histological analysis confirmed the degenerative phenotype. Normal retinal lamination was observed in 1 month old *Crb1*^{KO}*Crb2*^{ΔRods} and *Crb2*^{ΔRods} mice. When the mice age the number of photoreceptor nuclei mainly at the peripheral superior retina were lost. A statistically significant decrease of number of photoreceptor nuclei in a row was observed in *Crb1*^{KO}*Crb2*^{ΔRods} at 6M of age mainly in the peripheral superior retina. Moreover, disruptions at the OLM in *Crb1*^{KO}*Crb2*^{ΔRods} mice was observed throughout the retina. Transmission electron microscopy (TEM) showed disrupted adherens junctions in *Crb1*^{KO}*Crb2*^{ΔRods} and also observed collapsed MGC apical villi in the peripheral retina due to lack of structural support from neighbouring photoreceptor inner segments. Using immunohistochemistry the disturbed radial alignment of MGCs was shown [34].

In comparison to the other *Crb* mouse models, the phenotype of these *Crb1*^{KO}*Crb2*^{ΔRods} mice is relatively mild. Mouse models with ablation of *Crb2* from immature photoreceptor cells or from retinal progenitor cells show the morphological phenotype onset from embryonic day 15 (E15) to postnatal day 10 (P10) [26,28,35,36], whereas ablation of *Crb2* from rod photoreceptor cells show at foci first signs of degeneration at 1 month of age. Mice with ablation of *Crb2* from MGC show similarly as mice with loss of *Crb1* from MGC a very mild morphological phenotype with no functional consequence measured by ERG [27,28,30]. Concomitant ablation of *Crb1*

and *Crb2* in MGC enhanced the observed phenotype, making some of the RP phenotypes to a more severe LCA-like phenotype [25,28]. An ablation of *Crb1* with reduced levels of *Crb2* in MGC results in a RP-like phenotype [37]. Interestingly, ablation of exclusively *Crb1* or *Crb2* from MGC results in no functional phenotype, whereas ablation of both *Crb1* and *Crb2* from MGC results in a severe LCA-like phenotype [38]. This phenotype is comparable to when *Crb1* is ablated from MGCs and *Crb2* is ablated from immature photoreceptor cells or retinal progenitor cells [25,28]. Suggesting that, either CRB1 or CRB2 in MGC and CRB2 in photoreceptor cells are essential for proper retinal lamination and function in mice.

Not only *Crb1* mutant mouse models have been characterized, in **Chapter 3** the phenotype of a Brown Norway rat (BN/OrlRj) with a spontaneous mutation in the *Crb1* gene is described in more detail. Using immunohistochemistry, the first signs of retinal degeneration were observed at P10 indicated by OLM breaks and protrusions of photoreceptor cell nuclei into the photoreceptor segment layers. Using spectral domain optical coherence tomography (SD-OCT), the retina of control and *Crb1* mutant Brown Norway rats were followed over time. Retinal lamination appeared to be similar in control and *Crb1* mutant rats at P17 but degenerated over time, degeneration was indicated by an increasing number of hyperreflective regions in the INL and ONL of *Crb1* mutant rats. Quantification of the SD-OCT B-scans revealed a statistically significant decrease of laminated retina in *Crb1* mutant rats compared to controls starting at 1 month of age and continuing to degenerate up to at least 3 months of age. This degenerative phenotype was observed using immunohistochemistry in more detail. Displaced SOX9 positive MGCs and loss of rhodopsin-positive and recoverin-positive photoreceptor inner and outer segments were observed in 1 month of age *Crb1* mutant rats. Moreover, measurements by ERG showed a statistically significant decreased retinal function in 1 month of age *Crb1* mutant rats compared to control Brown Norway rats. Visual function as measured by OKT spatial frequency was statistically significant decreased at 3 months of age in *Crb1* mutant rats [22].

Interestingly, the observed phenotype in the *Crb1* mutant rats is more severe than the ones observed in *Crb1* mouse models. These discrepancies could be because of (1) species differences with different genetic backgrounds; (2) different types of

mutations affecting different CRB isoforms, thereby expressing a distinct CRB1^{INDEL} protein in the *Crb1* mutant rats; or (3) the total expression levels of CRB2 might be lower in new-born rats compared to new-born mice. Decreased levels of CRB2 or dysregulation of other CRB-interacting proteins could result in less stabilization of the adherens junction complex at the OLM, resulting in a more severe phenotype. These discrepancies between distinct animal models highlight the importance of using human derived models as well.

In **Chapter 4 and 5** the use of human induced pluripotent cells (hiPSC) derived retinal organoids are described. Differentiating hiPSC into retinal organoids allows access to previously limited or inaccessible human-derived materials. Numerous research groups use or try to improve the differentiation method to generate well laminated retinal organoids [39–43]. RNA sequencing profiling demonstrated that *in vivo* retinogenesis was recapitulated in the retinal organoids in terms of temporal expression of cell differentiation markers, mRNA alternative splicing, and retinal disease genes [44]. In addition, single-cell RNA sequencing (scRNA-seq) revealed that retinal organoids and fetal retina have similar cellular composition at equivalent ages [45]. Moreover, CRB1 and CRB2 expression in retinal organoids also recapitulates those observed in human fetal retina [23]. Therefore, retinal organoids are of great interest for investigating mechanisms of retinal degeneration, developing therapeutic strategies, and many more.

In **Chapter 4**, three *CRB1* RP patient-derived hiPSC were differentiated into retinal organoids up to differentiation day 230 (DD230) [24]. The phenotype was analysed at DD210, where a significantly reduced number of photoreceptor nuclei in a row and a significantly thinner ONL was observed in the *CRB1* RP patient-derived retinal organoids in comparison to the isogenic controls. scRNA-seq data analysis has shown that all the major retinal cell types were equally present in DD230 *CRB1* patient-derived and isogenic control retinal organoids. Interestingly, levels of *CRB1* transcript was similar in *CRB1* patient-derived retinal organoid and the isogenic control, whereas variant patient CRB1 protein was strongly diminished in *CRB1* patient-derived retinal organoids [24]. The data indicate that a variant CRB1 protein is most likely produced, but it potentially has an increased turnover because it does not localize to its expected

location at the OLM. Alternatively, the trafficking machinery or endolysosomal system of CRB1 might be affected in the *CRB1* patient-derived retinal organoids. In *Drosophila* studies it is shown that the Crb trafficking is mediated by transport along microtubules by Rab11- and retromer containing endosomes [46,47]. Here, our gene ontology analysis on *CRB1* patient-derived retinal organoids suggests an aberrant endosomal vesicular system in Müller glial cells and rod photoreceptor cells. The reduced level of variant CRB1 protein in *CRB1* patient-derived retinal organoids is being studied by putative changes in RAB11- and retromer-mediated receptor cycling and the lysosomal compartment [48].

In **Chapter 5**, *CRB1*^{KO} and *CRB1*^{KO}*CRB2*^{+/-} hiPSC were generated from a control hiPSC line and subsequently differentiated into retinal organoids. In the *CRB1*^{KO} hiPSC, a single nucleotide deletion was introduced in *CRB1* exon 2, resulting in a frameshift with premature stop and thus a knockout of the gene of interest. Since concomitant loss of *Crb2* can enhance the phenotype in *Crb1* mutant mice [25,28], *CRB1*^{KO}*CRB2*^{+/-} hiPSC were used as well. Here, mutations were introduced in exon 2 of *CRB1* and in exon 3 of *CRB2*, resulting in a frameshift mutation with a premature termination codon and a homozygous knockout of CRB1 and a heterozygous knockout of CRB2. Three clones of each were used for differentiation into retinal organoids. The *CRB1*^{KO} and *CRB1*^{KO}*CRB2*^{+/-} retinal organoids show a statistically significant decrease in number of photoreceptor nuclei in a row compared to the isogenic control at DD180 and DD210, and a statistically significant increase of number of photoreceptor nuclei above the OLM at DD180 for *CRB1*^{KO} and at DD180 and DD210 for *CRB1*^{KO}*CRB2*^{+/-} retinal organoids. The *CRB1*^{KO} and *CRB1*^{KO}*CRB2*^{+/-} retinal organoids develop an extended phenotype that includes disruptions at the inner retina, indicated by misaligned SOX9 positive MGC and ISLET1-2 positive rod and ON-cone bipolar cells at DD210.

The outer retina phenotype observed in the retinal organoids from **Chapter 4** is similar to the ones observed in *Crb1* RP mutant mouse models [30], an extended phenotype affecting the inner and outer retina was described in **Chapter 5** retinal organoids which was more similar to LCA mouse models [38]. Making the retinal

organoids described in this thesis a suitable model to study RP or LCA treatment possibilities.

AAV-mediated gene augmentation therapy for *CRB1*-related retinal dystrophies

In December 2017, the FDA approved gene augmentation therapy using adeno-associated viral (AAV) vectors for young RP and LCA patients with biallelic mutations in the *RPE65* gene, using AAV2 to deliver by subretinal injection a functional copy of the *RPE65* gene into the RPE (voretigene neparvec, Luxturna) [49]. Nowadays, there are numerous clinical studies exploring the potential of gene augmentation therapies for retinal dystrophies using AAV vectors [50–52]. AAVs are the leading platform for gene therapy approaches because of their capability to transduce both non-dividing and dividing cells, they show limited integration into the host genome, AAVs show low toxicity and immune response, and AAV capsid variants display distinct cell tropism [50,52]. However, despite these advantages, there were recently a subset of patients observed with progressive atrophy after subretinal AAV treatment. A study by the University Eye Hospital in Tübingen confirmed that subretinal injection of voretigene neparvec (VN, Luxturna, Novartis, Basel, CH) can potentially lead to RPE atrophy with consequent photoreceptor loss in and outside of the bleb area [53]. These atrophic regions can progress over a period of over 1.5 years. However, stable visual function improvement was observed in all patients in the observation period [53]. Longer follow up of these patients and studying the cause of RPE atrophy in more detail is important to understand and prevent this phenomenon. Further studies will reveal whether the toxicity is due to the overexpression of RPE65, the subretinal injection technique, impurities in the AAV preparation, or cellular response to the naked AAV or contaminating DNA. Studies showed that some but not all naked DNA can induce an innate immune response mediated by Toll-like-receptor 9 (TLR-9). The TLR-9 response can potentially be reduced by reducing the number of non-methylated CpG in the gene therapy vector construct. Alternatively, the TLR-9 response could potentially be reduced by incorporation of specific TTAGGG repeat DNA sequences into the AAV vector [54–57]. One could consider an alternative method of gene therapy application

in the retina such as intravitreal injection. Intravitreal injection is a more commonly performed ocular procedure and enables exposure of the vector to the entire retina. However, the intravitreal injection might transduce more off-target cells [58]. In addition, intravitreal injection of AAV raised sustained cellular inflammation in the vitreous of non-human primate eyes [59]. Therefore, continuing improving research applications and detection techniques is important for the future of gene therapy for patients.

AAV.GFP transduction comparison of distinct animal and human-derived models

Different AAV capsids display distinct cell tropisms, and therefore it is essential to define the AAV tropism in multiple models such as in mouse, rats (**Chapter 3**), and human-derived retinal organoids (**Chapter 4 and 5**).

Intravitreal injection of AAV2/5 and AAV2/9 showed relatively poor transduction efficiency of both photoreceptors and other cells in the inner nuclear layer (INL) in new-born rats [22]. Other researchers also showed a poor transduction of cells in the INL upon intravitreal delivery of all serotypes tested in this study (including AAV2/9) in two-month-old Sprague-Dawley rats [60]. However, an efficient transduction of mainly MGCs was observed after intravitreal injection of AAV6/ShH10^{Y445F} in new-born rats [22]. Efficient transduction of mainly MGCs in the INL after intravitreal injection of ShH10^{Y445F} was also observed in other models [61–63]. For subretinal injection of AAV2/5 and AAV2/9 in new-born rats, the RPE and photoreceptor cells were successfully transduced, whereas subretinal injection of AAV6 variant ShH10^{Y445F} was transducing the RPE, photoreceptor cells, MGCs, and other cell types in the INL [22]. Interestingly, subretinal injection of AAV2/9 or ShH10^{Y445F} in mice were the most powerful capsids to target RPE, MGCs and photoreceptor cells [61]. So subretinal injection of AAV2/9 seem to be different between these mice and rats. However, in adult Sprague-Dawley rats subretinal injection of AAV9 mainly transduced cells in the ONL, but also some (1-5 GFP positive cells per 100µm) cells in the INL [60]. Indicating that not only the species, but also the age of rodents could cause differences in AAV tropism.

Moreover, tropism differences between healthy and degenerated retina has also been described for specific serotypes. A significantly enhanced cellular transduction after intravitreal injection of AAV2 or AAV9 was observed in two-month old diabetic retinopathy mice treated with streptozotocin (STZ) compared to nondiabetic mice [64]. However, short duration STZ treatment (two weeks) did not have a significant effect on the transduction patterns of AAV vectors in the retina. Moreover, in both two weeks and two months STZ treatment diabetic mice, intravitreal injection of AAV5 did not show a statistically significant enhancement compared to nondiabetic control mice [64]. This suggests that certain retinal structural changes are needed to enhance some of the AAV capsids transduction in diabetic retinas. In **Chapter 3** healthy and *Crb1* mutant brown Norway rats showed similar AAV transduction for both subretinal as well as intravitreal injection at P5 or at P8. However, it might be possible that when control and *Crb1* mutant rats are injected at one month of age or older, when the retinal degeneration is further advanced, that AAV transduction of certain serotypes might be different.

Next, AAV tropism of certain serotypes (packed with *GFP*) was defined in human-derived models such as retinal organoids. Transduction of AAV2/5 and ShH10^{Y445F} significantly outperformed AAV2/9 at transducing MGCs of DD220 retinal organoids [23]. Moreover, Achberger *et al.* showed that retinal organoids transduced with self-complementary AAV2/2 (scAAV2/2) have a relatively low eGFP fluorescence intensity expression after 7 days of treatment at DD80 or DD300, whereas the scAAV2/7m8 capsid variant show significantly higher eGFP expression [63]. In **Chapter 4** we show that both single-stranded AAV2/2 and AAV2/5 with the CMV promoter and Woodchuck hepatitis virus post-transcriptional regulatory element (WPRE) sequence transduce very efficiently photoreceptor cells and, to a lesser extent, MGCs at DD120 retinal organoids [24]. In **Chapter 5** a similar transduction efficiency and tropism was observed when control retinal organoids were transduced with AAV2/2 and AAV2/5 at DD135 and DD200. In accordance with this, transduction of AAV2/5 with the CAG promoter at DD150 retinal organoids also showed efficient photoreceptor cell transduction [65]. In addition, efficient photoreceptor cell and MGC

transduction was previously shown with transduction at DD220 [23]. Differences in transduction efficiency might be caused by the maturity of the retinal organoids; it might very well be that certain receptors responsible for taking up the AAVs are less accessible at certain differentiation days. In conclusion, we have shown that AAV2/2 and AAV2/5 are capable of infecting Müller glial cells and photoreceptor cells in hiPSC-derived retinal organoids at DD120 (**Chapter 4**), DD135 (**Chapter 5**), DD200 (**Chapter 5**), and DD220 [23,24].

Another alternative is using human retinal explants which are derived from (cadaveric) human donor eyes. Wiley *et al.* showed a variable tropism of seven AAV serotypes (AAV2/1, AAV2/2, AAV2/4, AAV2/5, AAV2/6, AAV2/8, and AAV2/9) in three human donor eyes [66]. This intra-donor variability was least apparent in AAV2/8, which consistently inefficiently transduced cells in the ONL. Which is interesting, since AAV8 is used in many *in vivo* transductions. Whereas AAV2/1 and AAV2/5 were particularly efficient at solely transducing photoreceptor cells, and AAV2/4 and AAV2/6 efficiently transduced cells in the ONL and the INL [66]. Quinn *et al.* showed that AAV2/5 and ShH10^{Y445F} have a higher potency in transducing photoreceptor cells in the ONL than AAV2/9. No intra-donor variability was observed here; AAV transduction of a serotype was similar in the three independent cadaveric human donor retinal explants investigated [23]. However, they observed that the photoreceptors of cadaveric human retinal explants were only efficiently infected in the presence of intact photoreceptor segments, indicating a role for the segments in the photoreceptor uptake of AAV particles [23]. The intra-donor variability on transduction efficiency of distinct AAV capsids need to be investigated in more detail.

AAV.hCRB treatment of animal and human-derived models

For AAV-CRB mediated gene augmentation studies the correct cell type needs to be targeted. For *Crb1* mutant rats mainly MGC with loss of CRB1 should be targeted, for this reason AAV6 variant ShH10^{Y445F} was used for AAV-mediated gene augmentation therapy in **Chapter 3**. In **Chapter 4 and 5**, both photoreceptor cells and MGCs with loss of CRB1 should be targeted in the *CRB1* patient or knockout retinal organoids and therefore AAV2/5.hCRB was used.

However, the main disadvantage of AAVs is the limiting package capacity of ~4.7 kb: larger gene expression cassettes than 4.5 kb do not fit in a single stranded AAV vector containing two inverted terminal repeats. Because of this limiting packaging capacity, the development of AAV-mediated gene therapy is challenging. *CRB1* cDNA plus the full length cytomegalovirus (CMV) ubiquitous promoter exceeds the package limit. However, this problem can be circumvented by using a minimal CMV promoter. Intravitreal injection of ShH10^{Y445F} with a CMV minimal promoter showed significant levels of GFP expression in MGCs of *Crb1* knockout mice [61]. Subretinal injection of AAV9 with minimal CMV promoter or hGRK1 promoter mediated substantial levels of Crb1 protein expression at the OLM [61]. Pre-clinical studies have shown that full length or short form of CRB1 were potentially deleterious or causing subretinal toxicity in *Crb1* mutant mouse models [37,58,61]. However, both mouse models have shown that Crb2 can compensate for the loss of Crb1 in *Crb1* mutant mice [37,58]. An improved photoreceptor layer morphology and ERG response was detected in a *Crb1* mutant mouse after AAV9.*CRB2* delivery targeting both photoreceptor and MGC [58]. However, no rescue was observed when either only photoreceptors or only MGCs were targeted with *CRB2* [58], indicating again the importance of targeting the correct cells. Here, both AAV.CMVmin.h*CRB1* and AAV.CMV.h*CRB2* were used for gene augmentation strategies in **Chapters 3, 4, and 5**.

In **Chapter 3**, AAV-mediated gene augmentation therapy using 1 µl of a dose of 1×10^{13} gc/mL ShH10^{Y445F}.CMVmin.h*CRB1* (ShH10Y.h*CRB1*) or ShH10^{Y445F}.CMV.h*CRB2* (ShH10Y.h*CRB2*) was explored in new-born *Crb1* mutant rats. Retinal function or visual function of individual *Crb1* mutant rats analysed at 3-months-old were not significantly different between ShH10Y.h*CRB1* and PBS injected, nor when treated with ShH10Y.h*CRB2*. Due to the absence of an enhanced retinal function after AAV treatment, we hypothesized that (1) the intravitreally injected 1 µl of a dose of 1×10^{13} gc/mL AAV might not been a high enough dose to spread well through the retina, (2) the injection efficiency and thereby number of AAV particles taken up by the retinal cells might not have been optimal, or (3) the injection at postnatal day 5 (P5) does not allow timely expression of the h*CRB1* or h*CRB2* transgenes to

diminish the severe retinal degeneration. Therefore, intravitreal delivery of ShH10Y.h*CRB1* or ShH10Y.h*CRB2* at P3 was explored as well. No difference was observed in visual function response measured by OKT at 3M. However, a statistically significant decrease in retinal function measured by ERG was observed in rats treated with ShH10Y.h*CRB1*, ShH10Y.h*CRB2*, or PBS in comparison with non-injected eyes. Since the PBS injection already resulted in a statistical significant decrease in ERG response, the surgical technique at P3 might be damaging to the *Crb1* rat retina. In addition, because of the variability between untreated Brown Norway litters, backcrossing these rats into a more defined genetic background might decrease the observed variability. To conclude, no timely rescue of the severe retinal degeneration was observed after AAV-mediated gene augmentation therapy in *Crb1* mutant rats. Future experiments could focus on treatment with immediate expression of transgenes or *in utero* gene therapy approaches.

Previously, proof-of-concept studies of AAV-mediated gene therapy for *CRX*-LCA and *RP2* knockout retinal organoids have been described [65,67]. Here, AAV-mediated gene augmentation therapy was performed on hiPSC-derived *CRB1* RP patient-derived as well as *CRB1*^{KO} LCA retinal organoids (**Chapter 4, 5**). The retinal organoids were transduced with a dose of $3,3 \times 10^{10}$ gc at DD120 and were collected and analyzed at DD210. For the *CRB1* RP patient-derived retinal organoids in **Chapter 4**, AAV.h*CRB1* as well as AAV.h*CRB2* transduction resulted in a significant increase in the number of photoreceptor nuclei in a row as well as the ONL thickness [24]. Moreover, AAV.h*CRB2* treatment resulted in a significantly decreased number of photoreceptor nuclei above the OLM in the *CRB1* patient-derived retinal organoids. In addition, scRNA-sequencing revealed a partial restoration of transcriptional effect on the endosomal system after AAV.h*CRB1* or AAV.h*CRB2* treatment in *CRB1* patient-derived retinal organoids [24]. In **Chapter 5** a statistically significant increase in number of photoreceptor nuclei in a row was observed at DD210 after AAV.h*CRB2* treatment in *CRB1*^{KO} LCA retinal organoids. To our knowledge this is the first time that an improved phenotype after AAV.h*CRB* gene augmentation in *CRB1* RP patient-derived and *CRB1*^{KO} LCA retinal organoids is observed, providing essential

information for future gene therapy possibilities in patients with a mutation in the *CRB1* gene.

Future perspectives

Even though for some studies *in vivo* animal models are far from being completely replaced by human-derived models, it is pivotal for future studies to understand and use the knowledge of differences between rodents and humans. For instance, the subcellular localization of CRB1 and CRB2 are different in human-derived tissue in comparison to rodents [21–23]. In addition, mouse mRNA isoforms revealed that the *Crbl-b* isoform could potentially be associated with photoreceptor death [12], whereas reassessment of the phenotype-genotype correlation of 50 *CRB1* patients has shown that variations in the canonical full length form of CRB1 is mainly causative for retinal degeneration [68]. Therefore, showing that the AAV-mediated gene augmentation therapy was successful in mouse [37,58] as well as in retinal organoids (**Chapter 4 and 5**) [24] provides the essential information needed to continue with future gene therapy applications for patients with mutations in *CRB1*.

Nevertheless, current human-derived models can be improved to better mimic the human situation. First, improving the differentiation efficiency of retinal organoids is of interest. Currently, multiple groups describe a wide variability in differentiation efficiency between distinct iPSC lines [69–72]. In our studies, we also observe a wide variability in differentiation efficiency, even within the same line using the same differentiation protocol (unpublished data). Eliminating the factors causing this variability would be crucial for future studies. Moreover, the use of a bioreactor has shown to be efficient in scaling up the manufacture of retinal organoids in combination with an increased yield of photoreceptor cells bearing cilia and nascent outer-segment like structures [42]. Moreover, one could use a retina on a chip to further mimic the human situation. iPSC can be differentiated into RPE using for example small molecules [73] or using a mix of growth factors [74–76]. If iPSC-RPE and retinal organoids are combined on a chip (RoC), they can interact with each other and thereby better mimic the human situation. These RoC are able to form a physiological interaction of the iPSC-RPE and photoreceptor outer segments of the retinal organoids,

which is essential for the visual cycle in humans [77]. In addition, the microfluidic concept through a bottom channel and constant nutrient supply adds a vascular-like perfusion to the RoC [77]. In addition, a choroid on a chip (CoC) model is available which mimics the tissue vascularization, pigmentation, and immune response in the presence of circulating immune cells [78]. Combination of these RoC with CoC further mimic the human situation in a human-derived model system.

Conclusion

In conclusion, this thesis provides novel information on AAV.hCRB gene augmentation therapy in multiple *CRB1* mutant animal and human-derived models. We show the phenotype of (1) a novel mouse model with *CRB2* ablation specifically in rod photoreceptor cells with loss of retinal function (**Chapter 2**), (2) a *Crb1* mutant brown Norway rat with severe and early onset progressive vision loss (**Chapter 3**), (3) *CRB1* RP patient-derived retinal organoids (**Chapter 4**), and (4) *CRB1*^{KO} and *CRB1*^{KO}*CRB2*^{+/-} LCA-like retinal organoids (**Chapter 5**). Next, AAV-mediated gene augmentation strategies were explored in *Crb1* mutant rats (**Chapter 3**) and *CRB1* RP patient-derived and *CRB1*^{KO} LCA retinal organoids (**Chapter 4 and 5**). Finally, single-cell RNA-sequencing was performed on AAV.hCRB treated and untreated *CRB1* RP patient-derived retinal organoids (**Chapter 4**). To our knowledge this is the first time that an improved phenotype after AAV.hCRB gene augmentation in *CRB1* RP patient-derived and *CRB1*^{KO} LCA retinal organoids is observed, providing essential information for future gene therapy possibilities in patients with a mutation in the *CRB1* gene.

Article information

Author contributions: Writing - original draft, N.B.; Writing - review & editing, N.B., and J.W.

Abbreviations:

AAV	Adeno-associated viral vectors
CRB1	Crumbs homolog-1
cKO	Conditional knockout
CNV	Copy number variation
CMV	Cytomegalovirus
CoC	Choroid on a chip
DD210	Differentiation day 210
E15	Embryonic day 15
EGF	Epidermal growth factor
ERG	Electroretinography
GFP	Green Fluorescent Protein
hiPSC	Human-induced pluripotent stem cell
INL	Inner nuclear layer
LCA	Leber congenital amaurosis
MGC	Müller glial cell
OKT	Optokinetic head tracking response
OLM	Outer limiting membrane
ONL	Outer nuclear layer
OPL	Outer plexiform layer
P5	Postnatal day 5
PALS1	Protein associated with Lin Seven 1
RoC	Retinal organoids on a chip
RP	Retinitis pigmentosa
RPE	Retinal pigment epithelium
SAR	Subapical region
scRNA-seq	Single cell RNA-sequencing
SD-OCT	Spectral domain optical coherence tomography
SOX9	SRY-Box Transcription Factor 9
WPRE	Woodchuck hepatitis virus post-transcriptional regulatory element

References

1. Hartong, D.; Berson, E.; Dryja, T. Retinitis pigmentosa Prevalence and inheritance patterns. *Lancet* **2006**, 368, 1795–1809.
2. Daiger, S.P.; Sullivan, L.S.; Bowne, S.J. Genes and mutations causing retinitis pigmentosa. *Clin Genet.* **2013**, 84, 1–16, doi:10.1111/cge.12203.Genes.
3. Talib, M.; van Schooneveld, M.J.; van Genderen, M.M.; Wijnholds, J.; Florijn, R.J.; ten Brink, J.B.; Schalijs-Delfos, N.E.; Dagnelie, G.; Cremers, F.P.M.; Wolterbeek, R.; et al. Genotypic and Phenotypic Characteristics of CRB1-Associated Retinal Dystrophies: A Long-Term Follow-up Study. *Ophthalmology* **2017**, 124, 884–895, doi:10.1016/j.ophtha.2017.01.047.
4. Verbakel, S.K.; van Huet, R.A.C.; Boon, C.J.F.; den Hollander, A.I.; Collin, R.W.J.; Klaver, C.C.W.; Hoyng, C.B.; Roepman, R.; Klevering, B.J. Non-syndromic retinitis pigmentosa. *Prog. Retin. Eye Res.* **2018**, 66, 157–186, doi:10.1016/j.preteyeres.2018.03.005.
5. Nguyen, X.T.A.; Talib, M.; van Schooneveld, M.J.; Wijnholds, J.; van Genderen, M.M.; Schalijs-Delfos, N.E.; Klaver, C.C.W.; Talsma, H.E.; Fiocco, M.; Florijn, R.J.; et al. CRB1-Associated Retinal Dystrophies: A Prospective Natural History Study in Anticipation of Future Clinical Trials. *Am. J. Ophthalmol.* **2022**, 234, 37–48, doi:10.1016/j.ajo.2021.07.021.
6. Den Hollander, A.I.; Davis, J.; Van Der Velde-Visser, S.D.; Zonneveld, M.N.; Pierrotet, C.O.; Koenekoop, R.K.; Kellner, U.; Van Den Born, L.I.; Heckenlively, J.R.; Hoyng, C.B.; et al. CRB1 mutation spectrum in inherited retinal dystrophies. *Hum. Mutat.* **2004**, 24, 355–369, doi:10.1002/humu.20093.
7. Talib, M.; Van Cauwenbergh, C.; De Zaeytijd, J.; Van Wynsberghe, D.; De Baere, E.; Boon, C.J.F.; Leroy, B.P. CRB1-Associated retinal dystrophies in a Belgian cohort: Genetic characteristics and long-Term clinical follow-up. *Br. J. Ophthalmol.* **2022**, 106, 696–704, doi:10.1136/bjophthalmol-2020-316781.
8. Mathijssen, I.B.; Florijn, R.J.; Van Den Born, L.I.; Zekveld-Vroon, R.C.; Ten Brink, J.B.; Plomp, A.S.; Baas, F.; Meijers-Heijboer, H.; Bergen, A.A.B.; Van Schooneveld, M.J. Long-term follow-up of patients with retinitis pigmentosa type 12 caused by CRB1 mutations: A severe phenotype with considerable interindividual variability. *Retina* **2017**, 37, 161–172, doi:10.1097/IAE.0000000000001127.
9. Den Hollander, A.I.; Johnson, K.; De Kok, Y.J.M.; Klebes, A.; Brunner, H.G.; Knust, E.; Cremers, F.P.M. CRB1 has a cytoplasmic domain that is functionally conserved between human and *Drosophila*. *Hum. Mol. Genet.* **2001**, 10, 2767–2773, doi:10.1093/hmg/10.24.2767.
10. Tepass, U.; Theres, C.; Knust, E. crumbs encodes an EGF-like protein expressed on apical membranes of *Drosophila* epithelial cells and required for

organization of epithelia. *Cell* **1990**, 61, 787–799, doi:10.1016/0092-8674(90)90189-L.

11. Quinn, P.M.; Pellissier, L.P.; Wijnholds, J. The CRB1 complex: Following the trail of crumbs to a feasible gene therapy strategy. *Front. Neurosci.* **2017**, 11, doi:10.3389/fnins.2017.00175.

12. Ray, T.A.; Cochran, K.; Kozlowski, C.; Wang, J.; Alexander, G.; Cady, M.A.; Spencer, W.J.; Ruzycski, P.A.; Clark, B.S.; Laeremans, A.; et al. Comprehensive identification of mRNA isoforms reveals the diversity of neural cell-surface molecules with roles in retinal development and disease. *Nat. Commun.* **2020**, 11, doi:10.1038/s41467-020-17009-7.

13. Boon, N.; Wijnholds, J.; Pellissier, L.P. Research Models and Gene Augmentation Therapy for CRB1 Retinal Dystrophies. *Front. Neurosci.* **2020**, 14, 1–13, doi:10.3389/fnins.2020.00860.

14. Bazellières, E.; Aksenova, V.; Barthélémy-Requin, M.; Massey-Harroche, D.; Le Bivic, A. Role of the Crumbs proteins in ciliogenesis, cell migration and actin organization. *Semin. Cell Dev. Biol.* **2018**, 81, 13–20, doi:10.1016/j.semdb.2017.10.018.

15. Bulgakova, N.A.; Knust, E. The Crumbs complex: From epithelial-cell polarity to retinal degeneration. *J. Cell Sci.* **2009**, 122, 2587–2596, doi:10.1242/jcs.023648.

16. Michel, D.; Arsanto, J.P.; Massey-Harroche, D.; Béclin, C.; Wijnholds, J.; Le Bivic, A. PATJ connects and stabilizes apical and lateral components of tight junctions in human intestinal cells. *J. Cell Sci.* **2005**, 118, 4049–4057, doi:10.1242/jcs.02528.

17. Assémat, E.; Crost, E.; Ponsere, M.; Wijnholds, J.; Le Bivic, A.; Massey-Harroche, D. The multi-PDZ domain protein-1 (MUPP-1) expression regulates cellular levels of the PALS-1/PATJ polarity complex. *Exp. Cell Res.* **2013**, 319, 2514–2525, doi:10.1016/j.yexcr.2013.07.011.

18. Kantardzhieva, A.; Alexeeva, S.; Versteeg, I.; Wijnholds, J. MPP3 is recruited to the MPP5 protein scaffold at the retinal outer limiting membrane. *FEBS J.* **2006**, 273, 1152–1165, doi:10.1111/j.1742-4658.2006.05140.x.

19. Kantardzhieva, A.; Gosens, I.; Alexeeva, S.; Punte, I.M.; Versteeg, I.; Krieger, E.; Neeffjes-Mol, C.A.; Den Hollander, A.I.; Letteboer, S.J.F.; Klooster, J.; et al. MPP5 recruits MPP4 to the CRB1 complex in photoreceptors. *Investig. Ophthalmol. Vis. Sci.* **2005**, 46, 2192–2201, doi:10.1167/iops.04-1417.

20. Dudok, J.J.; Sanz, A.S.; Lundvig, D.M.S.; Sothilingam, V.; Garrido, M.G.; Klooster, J.; Seeliger, M.W.; Wijnholds, J. MPP3 regulates levels of PALS1 and adhesion between photoreceptors and Müller cells. *Glia* **2013**, 61, 1629–1644, doi:10.1002/glia.22545.

21. van Rossum, A.G.S.H.; Aartsen, W.M.; Meuleman, J.; Klooster, J.; Malysheva, A.; Versteeg, I.; Arsanto, J.P.; Le Bivic, A.; Wijnholds, J. Pals1/Mpp5 is required for correct localization of Crb1 at the subapical region in polarized Müller glia cells. *Hum. Mol. Genet.* **2006**, *15*, 2659–2672, doi:10.1093/hmg/ddl194.
22. Boon, N.; Henrique Alves, C.; Mulder, A.A.; Andriessen, C.A.; Buck, T.M.; Quinn, P.M.J.; Vos, R.M.; Koster, A.J.; Jost, C.R.; Wijnholds, J. Defining phenotype, tropism, and retinal gene therapy using adeno-associated viral vectors (AAVs) in newborn brown norway rats with a spontaneous mutation in CRB1. *Int. J. Mol. Sci.* **2021**, *22*, doi:10.3390/ijms22073563.
23. Quinn, P.M.; Buck, T.M.; Mulder, A.A.; Ohonin, C.; Alves, C.H.; Vos, R.M.; Bialecka, M.; van Herwaarden, T.; van Dijk, E.H.C.; Talib, M.; et al. Human iPSC-Derived Retinas Recapitulate the Fetal CRB1 CRB2 Complex Formation and Demonstrate that Photoreceptors and Müller Glia Are Targets of AAV5. *Stem Cell Reports* **2019**, *12*, 906–919, doi:10.1016/j.stemcr.2019.03.002.
24. Boon, N.; Lu, X.; Andriessen, C.A.; Moustakas, I.; Buck, T.M.; Freund, C.; Arendzen, C.H.; Böhringer, S.; Mei, H.; Wijnholds, J. AAV-mediated gene augmentation therapy of CRB1 patient-derived retinal organoids restores the histological and transcriptional retinal phenotype. *Stem Cell Reports* **2023**, doi:https://doi.org/10.1016/j.stemcr.2023.03.014.
25. Pellissier, L.P.; Alves, C.H.; Quinn, P.M.; Vos, R.M.; Tanimoto, N.; Lundvig, D.M.S.; Dudok, J.J.; Hooibrink, B.; Richard, F.; Beck, S.C.; et al. Targeted Ablation of Crb1 and Crb2 in Retinal Progenitor Cells Mimics Leber Congenital Amaurosis. *PLoS Genet.* **2013**, *9*, doi:10.1371/journal.pgen.1003976.
26. Quinn, P.M.; Alves, C.H.; Klooster, J.; Wijnholds, J. CRB2 in immature photoreceptors determines the superior-inferior symmetry of the developing retina to maintain retinal structure and function. *Hum. Mol. Genet.* **2018**, *27*, 3137–3153, doi:10.1093/hmg/ddy194.
27. van de Pavert, S.A.; Sanz sanz, A.; Aartsen, W.M.; Vos, R.M.; Versteeg, I.; Beck, S.C.; Klooster, J.; Seeliger, M.W.; Wijnholds, J. Crb1 is a Determinant of Retinal Apical Muller Glia Cell Features. *Glia* **2007**, 1486–1497, doi:10.1002/glia.
28. Alves, C.H.; Pellissier, L.P.; Vos, R.M.; Garrido, M.G.; Sothilingam, V.; Seide, C.; Beck, S.C.; Klooster, J.; Furukawa, T.; Flannery, J.G.; et al. Targeted ablation of Crb2 in photoreceptor cells induces retinitis pigmentosa. *Hum. Mol. Genet.* **2014**, *23*, 3384–3401, doi:10.1093/hmg/ddu048.
29. Mehalow, A.K.; Kameya, S.; Smith, R.S.; Hawes, N.L.; Denegre, J.M.; Young, J.A.; Bechtold, L.; Haider, N.B.; Tepass, U.; Heckenlively, J.R.; et al. CRB1 is essential for external limiting membrane integrity and photoreceptor morphogenesis in the mammalian retina. *Hum. Mol. Genet.* **2003**, *12*, 2179–2189, doi:10.1093/hmg/ddg232.

30. van de Pavert, S.A.; Kantardzhieva, A.; Malysheva, A.; Meuleman, J.; Versteeg, I.; Levelt, C.; Klooster, J.; Geiger, S.; Seeliger, M.W.; Rashbass, P.; et al. Crumbs homologue 1 is required for maintenance of photoreceptor cell polarization and adhesion during light exposure. *J. Cell Sci.* **2004**, *117*, 4169–4177, doi:10.1242/jcs.01301.
31. Quinn, P.M.J.; Wijnholds, J. Retinogenesis of the human fetal retina: An apical polarity perspective. *Genes* **2019**, *10*, doi:10.3390/genes10120987.
32. Zhao, M.; Andrieu-Soler, C.; Kowalczyk, L.; Paz Cortés, M.; Berdugo, M.; Dernigoghossian, M.; Halili, F.; Jeanny, J.-C.; Goldenberg, B.; Savoldelli, M.; et al. A New CRB1 Rat Mutation Links Müller Glial Cells to Retinal Telangiectasia. *J. Neurosci.* **2015**, *35*, 6093–6106, doi:10.1523/jneurosci.3412-14.2015.
33. Cho, S.H.; Nahar, A.; Kim, J.H.; Lee, M.; Kozmik, Z.; Kim, S. Targeted deletion of Crb1/Crb2 in the optic vesicle models key features of leber congenital amaurosis 8. *Dev. Biol.* **2019**, *453*, 141–154, doi:10.1016/j.ydbio.2019.05.008.
34. Alves, C.H.; Boon, N.; Mulder, A.A.; Koster, A.J.; Jost, C.R.; Wijnholds, J. CRB2 Loss in Rod Photoreceptors Is Associated with Progressive Loss of Retinal Contrast Sensitivity. *Int. J. Mol. Sci.* **2019**, *20*, 4069, doi:10.3390/ijms20174069.
35. Pellissier, L.P.; Lundvig, D.M.S.; Tanimoto, N.; Klooster, J.; Vos, R.M.; Richard, F.; Sothilingam, V.; Garrido, M.G.; Bivic, A. Le; Seeliger, M.W.; et al. CRB2 acts as a modifying factor of CRB1-related retinal dystrophies in mice. *Hum. Mol. Genet.* **2014**, *23*, 3759–3771, doi:10.1093/hmg/ddu089.
36. Alves, C.H.; Sanz sanz, A.; Park, B.; Pellissier, L.P.; Tanimoto, N.; Beck, S.C.; Huber, G.; Murtaza, M.; Richard, F.; Sridevi gurubaran, I.; et al. Loss of CRB2 in the mouse retina mimics human retinitis pigmentosa due to mutations in the CRB1 gene. *Hum. Mol. Genet.* **2013**, *22*, 35–50, doi:10.1093/hmg/dds398.
37. Buck, T.M.; Vos, R.M.; Alves, C.H.; Wijnholds, J. AAV-CRB2 protects against vision loss in an inducible CRB1 retinitis pigmentosa mouse model. *Mol. Ther. Methods Clin. Dev.* **2021**, *20*, 423–441, doi:10.1016/j.omtm.2020.12.012.
38. Quinn, P.M.; Mulder, A.A.; Henrique Alves, C.; Desrosiers, M.; de Vries, S.I.; Klooster, J.; Dalkara, D.; Koster, A.J.; Jost, C.R.; Wijnholds, J. Loss of CRB2 in Müller glial cells modifies a CRB1-associated retinitis pigmentosa phenotype into a Leber congenital amaurosis phenotype. *Hum. Mol. Genet.* **2019**, *28*, 105–123, doi:10.1093/hmg/ddy337.
39. Zhong, X.; Gutierrez, C.; Xue, T.; Hampton, C.; Vergara, M.N.; Cao, L.H.; Peters, A.; Park, T.S.; Zambidis, E.T.; Meyer, J.S.; et al. Generation of three-dimensional retinal tissue with functional photoreceptors from human iPSCs. *Nat. Commun.* **2014**, *5*, doi:10.1038/ncomms5047.
40. Meyer, J.S.; Howden, S.E.; Wallace, K. a; Verhoeven, A.D.; Wright, L.S.; Capowski, E.E.; Pinilla, I.; Martin, J.M.; Tian, S.; Stewart, R.; et al. Optic Vesicle-like

Structures Derived from Human Pluripotent Stem Cells Facilitate a Customized Approach to Retinal Disease Treatment. *Stem Cells* **2011**, 29, 1206–1218.

41. Nakano, T.; Ando, S.; Takata, N.; Kawada, M.; MUGURUMA, K.; Sekiguchi, K.; Saito, K.; Yonemura, S.; Eiraku, M.; Sasai, Y. Self-formation of optic cups and storable stratified neural retina from human ESCs. *Cell Stem Cell* **2012**, 10, 771–785, doi:10.1016/j.stem.2012.05.009.

42. Ovando-Roche, P.; West, E.L.; Branch, M.J.; Sampson, R.D.; Fernando, M.; Munro, P.; Georgiadis, A.; Rizzi, M.; Kloc, M.; Naeem, A.; et al. Use of bioreactors for culturing human retinal organoids improves photoreceptor yields. *Stem Cell Res. Ther.* **2018**, 9, 1–14, doi:10.1186/s13287-018-0907-0.

43. Luo, Z.; Zhong, X.; Li, K.; Xie, B.; Liu, Y.; Ye, M.; Li, K.; Xu, C.; Ge, J. An Optimized System for Effective Derivation of Three-Dimensional Retinal Tissue via Wnt Signaling Regulation. *Stem Cells* **2018**, 36, 1709–1722, doi:10.1002/stem.2890.

44. Kim, S.; Lowe, A.; Dharmat, R.; Lee, S.; Owen, L.A.; Wang, J.; Shakoor, A.; Li, Y.; Morgan, D.J.; Hejazi, A.A.; et al. Generation, transcriptome profiling, and functional validation of cone-rich human retinal organoids. *Proc. Natl. Acad. Sci. U. S. A.* **2019**, 166, 10824–10833, doi:10.1073/pnas.1901572116.

45. Sridhar, A.; Hoshino, A.; Finkbeiner, C.R.; Chitsazan, A.; Haugan, A.K.; Eschenbacher, K.M.; Jackson, D.L.; Trapnell, C.; Bermingham-mcdonogh, O.; Glass, I.; et al. Single-cell transcriptomic comparison of human fetal retina, hPSC-derived retinal organoids, and long-term retinal cultures. *Cell Rep.* **2021**, 30, 1644–1659, doi:10.1016/j.celrep.2020.01.007.Single-Cell.

46. Aguilar-Aragon, M.; Fletcher, G.; Thompson, B.J. The cytoskeletal motor proteins Dynein and MyoV direct apical transport of Crumbs. *Dev. Biol.* **2020**, 459, 126–137, doi:10.1016/j.ydbio.2019.12.009.

47. Pocha, S.M.; Wassmer, T.; Niehage, C.; Hoflack, B.; Knust, E. Retromer controls epithelial cell polarity by trafficking the apical determinant crumbs. *Curr. Biol.* **2011**, 21, 1111–1117, doi:10.1016/j.cub.2011.05.007.

48. Buck, T.M.; Quinn, P.M.J.; Pellissier, L.P.; Mulder, A.A.; Jongejan, A.; Koot, D.; Almushattat, H.; Arendzen, C.H.; Vos, R.M.; Bradley, E.J.; et al. CRB1 is required for NOTCH1 interaction and RAB11A sorting vesicles in human retinal organoids. *In Thesis: CRB1 gene therapy coming of age: mechanistic insight and rAAV assays on mouse & human retinal organoid models*; **2022**; pp. 192-240 (CH5).

49. Maguire, A.M.; Russell, S.; Wellman, J.A.; Chung, D.C.; Yu, Z.F.; Tillman, A.; Wittes, J.; Pappas, J.; Elci, O.; Marshall, K.A.; et al. Efficacy, Safety, and Durability of Voretigene Neparvovec-rzyl in RPE65 Mutation-Associated Inherited Retinal Dystrophy: Results of Phase 1 and 3 Trials. *Ophthalmology* **2019**, 126, 1273–1285, doi:10.1016/j.ophtha.2019.06.017.

50. Wang, D.; Tai, P.W.L.; Gao, G. Adeno-associated virus vector as a platform for gene therapy delivery. *Nat. Rev. Drug Discov.* 2019, 18, 358–378, doi:10.1038/s41573-019-0012-9.
51. Lipinski, D.M.; Thake, M.; MacLaren, R.E. Clinical applications of retinal gene therapy. *Prog. Retin. Eye Res.* 2013, 32, 22–47, doi:10.1016/j.preteyeres.2012.09.001.
52. Buck, T.M.; Wijnholds, J. Recombinant adeno-associated viral vectors (RAAV)-vector elements in ocular gene therapy clinical trials and transgene expression and bioactivity assays. *Int. J. Mol. Sci.* 2020, 21, 1–52, doi:10.3390/ijms21124197.
53. Reichel, F.F.; Seitz, I.; Wozar, F.; Dimopoulos, S.; Jung, R.; Kempf, M.; Kohl, S.; Kortüm, F.C.; Ott, S.; Pohl, L.; et al. Development of retinal atrophy after subretinal gene therapy with voretigene neparvovec. *Br. J. Ophthalmol.* 2022, 1–5, doi:10.1136/bjophthalmol-2021-321023.
54. Faust, S.M.; Bell, P.; Cutler, B.J.; Ashley, S.N.; Zhu, Y.; Rabinowitz, J.E.; Wilson, J.M. CpG-depleted adeno-associated virus vectors evade immune detection. *J. Clin. Invest.* 2013, 123, 2994–3001, doi:10.1172/JCI68205.
55. Gursel, I.; Gursel, M.; Yamada, H.; Ishii, K.J.; Takeshita, F.; Klinman, D.M. Repetitive Elements in Mammalian Telomeres Suppress Bacterial DNA-Induced Immune Activation. *J. Immunol.* 2003, 171, 1393–1400, doi:10.4049/jimmunol.171.3.1393.
56. Chan, Y.K.; Wang, S.K.; Chu, C.J.; Copland, A.; Alexander, J.; Verdera, H.C.; Chiang, J.J.; Sethi, M.; Wang, M.K.; Jr, W.J.N.; et al. Engineering adeno-associated viral vectors to evade innate immune and inflammatory responses. *Sci Transl Med.* 2021, 13, 1–34, doi:10.1126/scitranslmed.abd3438.Engineering.
57. Xiang, Z.Q.; Kurupati, R.K.; Li, Y.; Kuranda, K.; Zhou, X.; Mingozzi, F.; High, K.A.; Ertl, H.C.J. The Effect of CpG Sequences on Capsid-Specific CD8+ T Cell Responses to AAV Vector Gene Transfer. *Mol. Ther.* 2020, 28, 771–783, doi:10.1016/j.ymthe.2019.11.014.
58. Pellissier, L.P.; Quinn, P.M.; Henrique Alves, C.; Vos, R.M.; Klooster, J.; Flannery, J.G.; Alexander Heimel, J.; Wijnholds, J. Gene therapy into photoreceptors and Muller glial cells restores retinal structure and function in CRB1 retinitis pigmentosa mouse models. *Hum. Mol. Genet.* 2015, 24, 3104–3118, doi:10.1093/hmg/ddv062.
59. Timmers, A.M.; Newmark, J.A.; Turunen, H.T.; Farivar, T.; Liu, J.; Song, C.; Ye, G.J.; Pennock, S.; Gaskin, C.; Knop, D.R.; et al. Ocular Inflammatory Response to Intravitreal Injection of Adeno-Associated Virus Vector: Relative Contribution of Genome and Capsid. *Hum. Gene Ther.* 2020, 31, 80–89, doi:10.1089/hum.2019.144.
60. Han, I.C.; Cheng, J.L.; Burnight, E.; Ralston, C.L.; Fick, J.L.; Thomsen, G.J.; Tovar, E.F.; Russell, S.; Sohn, E.H.; Mullins, R.F.; et al. Retinal Tropism and

Transduction of Adeno-Associated Virus (AAV) Varies by Serotype and Route of Delivery (Intravitreal, Subretinal or Suprachoroidal) in Rats. *Hum. Gene Ther.* **2020**, 1–29, doi:10.1089/hum.2020.043.

61. Pellissier, L.P.; Hoek, R.M.; Vos, R.M.; Aartsen, W.M.; Klimczak, R.R.; Hoyng, S.A.; Flannery, J.G.; Wijnholds, J. Specific tools for targeting and expression in Müller glial cells. *Mol. Ther. - Methods Clin. Dev.* **2014**, 1, 14009, doi:10.1038/mtm.2014.9.

62. Klimczak, R.R.; Koerber, J.T.; Dalkara, D.; Flannery, J.G.; Schaffer, D. V. A novel adeno-associated viral variant for efficient and selective intravitreal transduction of rat Müller cells. *PLoS One* **2009**, 4, doi:10.1371/journal.pone.0007467.

63. Achberger, K.; Cipriano, M.; Düchs, M.J.; Schön, C.; Michelfelder, S.; Stierstorfer, B.; Lamla, T.; Kauschke, S.G.; Chuchuy, J.; Roosz, J.; et al. Human stem cell-based retina on chip as new translational model for validation of AAV retinal gene therapy vectors. *Stem Cell Reports* **2021**, 16, 2242–2256, doi:10.1016/j.stemcr.2021.08.008.

64. Lee, S.H.; Yang, J.Y.; Madrakhimov, S.; Park, H.Y.; Park, K.; Park, T.K. Adeno-Associated Viral Vector 2 and 9 Transduction Is Enhanced in Streptozotocin-Induced Diabetic Mouse Retina. *Mol. Ther. - Methods Clin. Dev.* **2019**, 13, 55–66, doi:10.1016/j.omtm.2018.11.008.

65. Lane, A.; Jovanovic, K.; Shortall, C.; Ottaviani, D.; Panes, A.B.; Schwarz, N.; Guarascio, R.; Hayes, M.J.; Palfi, A.; Chadderton, N.; et al. Modeling and Rescue of RP2 Retinitis Pigmentosa Using iPSC-Derived Retinal Organoids. *Stem Cell Reports* **2020**, 15, 67–79, doi:10.1016/j.stemcr.2020.05.007.

66. Wiley, L.A.; Burnight, E.R.; Kaalberg, E.E.; Jiao, C.; Riker, M.J.; Halder, J.A.; Luse, M.A.; Han, I.C.; Russell, S.R.; Sohn, E.H.; et al. Assessment of Adeno-Associated Virus Serotype Tropism in Human Retinal Explants. *Hum. Gene Ther.* **2018**, 29, 424–436, doi:10.1089/hum.2017.179.

67. Kruczek, K.; Qu, Z.; Gentry, J.; Fadl, B.R.; Gieser, L.; Hiriyanna, S.; Batz, Z.; Samant, M.; Samanta, A.; Chu, C.J.; et al. Gene Therapy of Dominant CRX-Leber Congenital Amaurosis using Patient Stem Cell-Derived Retinal Organoids. *Stem Cell Reports* **2021**, 16, 252–263, doi:10.1016/j.stemcr.2020.12.018.

68. Mairot, K.; Smirnov, V.; Bocquet, B.; Labesse, G.; Arndt, C.; Defoort-dhellemmes, S.; Zanlonghi, X.; Hamroun, D.; Denis, D.; Picot, M.C.; et al. Crb1-related retinal dystrophies in a cohort of 50 patients: A reappraisal in the light of specific müller cell and photoreceptor crb1 isoforms. *Int. J. Mol. Sci.* **2021**, 22, doi:10.3390/ijms222312642.

69. Capowski, E.E.; Samimi, K.; Mayerl, S.J.; Phillips, M.J.; Pinilla, I.; Howden, S.E.; Saha, J.; Jansen, A.D.; Edwards, K.L.; Jager, L.D.; et al. Reproducibility and

- staging of 3D human retinal organoids across multiple pluripotent stem cell lines. *Hum. Dev.* **2019**, 146, dev171686, doi:10.1242/dev.171686.
70. Cora, V.; Haderspeck, J.; Antkowiak, L.; Mattheus, U.; Neckel, P.H.; Mack, A.F.; Bolz, S.; Ueffing, M.; Pashkovskaia, N.; Achberger, K.; et al. A Cleared View on Retinal Organoids. *Cells* **2019**, 8, 391, doi:10.3390/cells8050391.
71. Mellough, C.B.; Collin, J.; Queen, R.; Hilgen, G.; Dorgau, B.; Zerti, D.; Felemban, M.; White, K.; Sernagor, E.; Lako, M. Systematic Comparison of Retinal Organoid Differentiation from Human Pluripotent Stem Cells Reveals Stage Specific, Cell Line, and Methodological Differences. *Stem Cells Transl. Med.* **2019**, 8, 694–706, doi:10.1002/sctm.18-0267.
72. Chichagova, V.; Hilgen, G.; Ghareeb, A.; Georgiou, M.; Carter, M.; Sernagor, E.; Lako, M.; Armstrong, L. Human iPSC differentiation to retinal organoids in response to IGF1 and BMP4 activation is line- and method-dependent. *Stem Cells* **2020**, 38, 195–201.
73. Maruotti, J.; Sripathi, S.R.; Bharti, K.; Fuller, J.; Wahlin, K.J.; Ranganathan, V.; Sluch, V.M.; Berlinicke, C.A.; Davis, J.; Kim, C.; et al. Small-molecule-directed, efficient generation of retinal pigment epithelium from human pluripotent stem cells. *Proc. Natl. Acad. Sci. U. S. A.* **2015**, 112, 10950–10955, doi:10.1073/pnas.1422818112.
74. Zahabi, A.; Shahbazi, E.; Ahmadi, H.; Hassani, S.N.; Totonchi, M.; Taei, A.; Masoudi, N.; Ebrahimi, M.; Aghdami, N.; Seifinejad, A.; et al. A new efficient protocol for directed differentiation of retinal pigmented epithelial cells from normal and retinal disease induced pluripotent stem cells. *Stem Cells Dev.* **2012**, 21, 2262–2272, doi:10.1089/scd.2011.0599.
75. Buchholz, D.E.; Pennington, B.O.; Croze, R.H.; Hinman, C.R.; Coffey, P.J.; Clegg, D.O. Rapid and Efficient Directed Differentiation of Human Pluripotent Stem Cells Into Retinal Pigmented Epithelium. *Stem Cells Transl. Med.* **2013**, 2, 384–393, doi:10.5966/sctm.2012-0163.
76. Shutova, M. V.; Surdina, A. V.; Ischenko, D.S.; Naumov, V.A.; Bogomazova, A.N.; Vassina, E.M.; Alekseev, D.G.; Lagarkova, M.A.; Kiselev, S.L. An integrative analysis of reprogramming in human isogenic system identified a clone selection criterion. *Cell Cycle* **2016**, 15, 986–997, doi:10.1080/15384101.2016.1152425.
77. Achberger, K.; Probst, C.; Haderspeck, J.C.; Bolz, S.; Rogal, J.; Chuchuy, J.; Nikolova, M.; Cora, V.; Antkowiak, L.; Haq, W.; et al. Merging organoid and organ-on-a-chip technology to generate complex multi-layer tissue models in a human retina-on-a-chip platform. *Elife* **2019**, 8, 1–26, doi:10.7554/eLife.46188.
78. Cipriano, M.; Schlünder, K.; Probst, C.; Linke, K.; Weiss, M.; Fischer, M.J.; Mesch, L.; Achberger, K.; Liebau, S.; Mesquida, M.; et al. Human immunocompetent choroid-on-chip: a novel tool for studying ocular effects of biological drugs. *Commun. Biol.* **2022**, 5, 1–13, doi:10.1038/s42003-021-02977-3.

Chapter 7

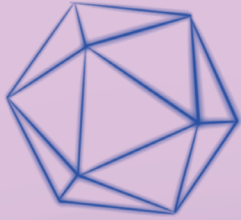
Summary

Nederlandse Samenvatting

List of publications

Curriculum Vitae

Acknowledgements



Summary

Crumbs homologue 1 (CRB1) is a large transmembrane protein located in the retina. It consists of a large extracellular domain with multiple epidermal growth factor (EGF) and laminin-globular like domains, as well as a short intracellular domain with a conserved PDZ binding motif. CRB1, CRB2, and CRB3 are all members of the Crumbs family, with CRB1 and CRB2 being specifically localized in the retina. The *CRB1* gene has been associated with more than 200 different mutations, leading to retinal dystrophies such as retinitis pigmentosa (RP) and Leber congenital amaurosis (LCA), with no clear genotype-phenotype correlation. The clinical variability of disease onset and severity, even among patients with the same homozygous mutations, supports the hypothesis that other factors may modulate the phenotype. Currently, there are no treatment options available for patients with mutations in the *CRB1* gene.

Since *CRB1*-related RP and LCA are heterogeneous diseases, various animal-derived models have been described to mimic different aspects of the heterogeneous disease phenotype. This diversity is represented by numerous distinct animal models previously generated by us and other researchers, including four LCA and ten RP-like mouse models. **Chapter 2** introduces two additional RP-like mouse models: *Crb2*^{ΔRods} and *Crb1*^{KO}*Crb2*^{ΔRods} mice. In this chapter, we demonstrate that the specific loss of CRB2 from rod photoreceptors leads to retinitis pigmentosa, and that concomitant loss of CRB1 exacerbates the retinitis pigmentosa phenotype. The impaired contrast sensitivity observed might serve as an outcome parameter to measure functional vision gain or maintenance following adeno-associated viral vector (AAV)-mediated gene augmentation therapy. Furthermore, in **Chapter 3**, we provide a more detailed description of the phenotype observed in a rat with a spontaneous mutation in the *Crb1* gene. The initial signs of retinal degeneration were observed at postnatal day 10 (p10), and a significant decrease in retinal function was already evident at 1 month of age in these *Crb1* mutant rats. Additionally, spectral domain optical coherence tomography (SD-OCT) was employed to monitor the retinal degeneration in a single rat over time.

To understand differences between rodent and humans, we determined the subcellular localization of CRB1 and CRB2 using immuno-electron microscopy in **Chapter 3**. We observed that the endogenous expression of CRB1 and CRB2 in rats is similar to what has been observed in the mouse retina. However, recent studies on non-human primates, human fetal retina, and human derived retinal organoids have shown a distinct localization of CRB1 and CRB2. This highlights the importance of utilizing human-derived models for gene augmentation therapies. In **Chapter 4 and 5**, we described the use of human induced pluripotent cells (hiPSC) derived retinal organoids. In **Chapter 4**, we presented *CRB1* RP patient-derived, and in **Chapter 5**, we described *CRB1*^{KO} and *CRB1*^{KO}*CRB2*^{+/-} LCA retinal organoids. Both the *CRB1* patient-derived and the *CRB1*^{KO} and *CRB1*^{KO}*CRB2*^{+/-} retinal organoids exhibit a significant reduction in the number of photoreceptor nuclei in a row and a significant increase in the number of photoreceptor cells above the OLM in compared to the isogenic controls. Single cell RNA sequencing in **Chapter 4** revealed similar *CRB1* transcript levels in patient-derived and isogenic control retinal organoids, while the CRB1 protein was clearly diminished. Additionally, in **Chapter 5**, the KO organoids showed less CRB1 protein at the OLM compared to the isogenic control. Collectively, the *CRB1* patient-derived and *CRB1*^{KO} and *CRB1*^{KO}*CRB2*^{+/-} retinal organoids accurately mimic the phenotype observed in patients and are, therefore, a suitable model for studying gene augmentation therapy possibilities.

Before studying the possibility of gene augmentation therapy using AAVs, it is crucial to determine the tropism of different capsids in rats (**Chapter 3**) and in retinal organoids (**Chapter 4 and 5**). In rats, subretinal injection of AAV2/5 and AAV2/9 successfully transduced the RPE and photoreceptor cells, whereas AAV6 variant ShH10^{Y445F} was transducing the RPE, photoreceptor cells, MGCs, and other cell types in the INL. Intravitreal injection of AAV2/5 and AAV2/9 showed relatively poor transduction efficiency of both photoreceptors and other cells in the INL. However, an efficient transduction of mainly MGCs was observed after intravitreal injection of ShH10^{Y445F}. Due to these observations, ShH10^{Y445F}.hCRB was used for AAV-mediated gene augmentation therapy in rats (**Chapter 3**). In **Chapter 4**, AAV2/2 and AAV2/5 were used to define tropism of early organoids, while **Chapter 5** used AAV2/2 and AAV2/5

to define tropism of older retinal organoids. Both AAV2/2 and AAV2/5 efficiently transduced mainly photoreceptor cells and also some MGC and other cells in the INL, with AAV2/5 slightly more efficiently transducing cells in the INL. To target both the photoreceptor cells and MGC in the retinal organoids, AAV2/5.hCRB was used in **Chapter 4 and 5**.

Previous research demonstrated the successful preservation of retinal morphology and function in *Crb1* RP mouse models through AAV-mediated *CRB2* gene augmentation therapy. Based on these promising results, AAV-mediated gene augmentation therapy was initially explored in an animal model with a severe and early-onset phenotype: the *Crb1* mutant rat (**Chapter 3**). Unfortunately, timely rescue of the retinal phenotype using retinal function and visual acuity was not observed, likely due to the severity and early onset of the phenotype. This suggests the need for an earlier onset of recombinant hCRB protein expression to efficiently rescue the severe retinal phenotype in *Crb1* mutant rats. Next, AAV-mediated gene augmentation therapy was conducted on human derived induced pluripotent stem cells (hiPSC) derived retinal organoids (**Chapter 4 and 5**). In these chapters, the RP phenotype showed partial improved after treatment with AAV.hCRB2, as evidenced by a restored number of photoreceptor nuclei in a row. For the *CRB1* RP patient-derived retinal organoids (**Chapter 4**), a partial improvement was observed following treatment with AAV.hCRB1. Single cell RNA sequencing analysis of AAV treated *CRB1* patient-derived retinal organoids demonstrated a partial restoration of transcript expression levels of genes related to the endosomal system back to isogenic control levels. These findings indicate the potential efficacy of AAV-mediated gene augmentation therapy for treating CRB1-related retinal dystrophies.

7

In conclusion, in this thesis has provided valuable insights into several aspects of *CRB1* related retinal dystrophies. Specifically, we have demonstrated (1) the phenotypic characteristics of *CRB1* mutant mice, rats, and human-derived retinal organoids, shedding light of the disease progression in various models. (2) We have investigated the distinct tropism of AAV capsids in different species, which is crucial for developing targeted gene therapy approaches. (3) And we have achieved successful AAV-mediated gene augmentation therapy in *CRB1* patient-derived as well as *CRB1*^{KO} and

CRB1^{KO}*CRB2*^{+/-} retinal organoids, suggesting the potential therapeutic relevance of this approach. Altogether, these findings represent a significant advancement in understanding the pathogenesis and potential treatment options for patients with mutations in the *CRB1* gene.

Nederlandse Samenvatting

Crumbs-homoloog-1 (CRB1) is een groot transmembraan eiwit dat zich in het netvlies bevindt. Het bevat een extracellulair domain met meerdere epidermale groei factor (EGF) en laminin-A globulaire domeinen, evenals een intracellulair domein met een geconserveerd PDZ bindingsmotief. CRB1, CRB2, en CRB3 behoren tot de Crumbs familie, waarvan CRB1 en CRB2 zich in het netvlies bevinden. Er zijn meer dan 200 verschillende *CRB1* mutaties beschreven die zich over het gehele *CRB1* gen verspreiden. Deze mutaties kunnen erfelijke degeneratieve aandoeningen van het netvlies veroorzaken zonder een duidelijke genotype-fenotype correlatie; voorbeelden zijn retinitis pigmentosa (RP) en Leber congenitale amaurosis (LCA). De klinische variabiliteit van de start en de ernst van een netvlies degeneratie, zelfs in een familie met dezelfde homozygote mutatie, suggereert dat er modifierende factoren betrokken kunnen zijn bij het tot uiting komen van het fenotype. Tot op heden is er nog geen behandelbaarheid voor patiënten met mutaties in het *CRB1* gen.

Aangezien *CRB1*-gerelateerde RP en LCA een divers ziektebeeld vertonen, zijn er meerdere diermodellen ontwikkeld die elk verschillende fenotypen van patiënten nabootsen: vier LCA en tien RP-achtige muismodellen. In **Hoofdstuk 2**, worden nog twee RP-achtige muis modellen beschreven: *Crb2*^{ARods} en *Crb1*^{KO}*Crb2*^{ARods} muizen. In dit hoofdstuk tonen we aan dat muizen met een tekort aan het CRB2 eiwit in staafjes fotoreceptoren RP ontwikkelen, en dat er een verergerd fenotype optreedt wanneer in deze muizen ook het CRB1 eiwit in Müller Glial cellen (MGC) afwezig is. Het verminderde zicht werd gemeten door middel van OKT contrast gevoeligheid metingen bij deze muizen. Deze meting kan waardevol zijn voor latere experimenten met adeno-geassocieerde virale vector (AAV)-gemedieerde gentherapie om verbeteringen in het functionele zicht te beoordelen. In **Hoofdstuk 3** hebben we het fenotype van ratten met een spontane mutatie in het *Crb1* gen beschreven. De eerste tekenen van retinale degeneratie werden waargenomen vanaf postnatale dag 10 (p10) in het netvlies van deze ratten. Op de leeftijd van 1 maand werd al een statistisch significante verslechtering van de netvliesfunctie gemeten met een electroretinogram (ERG) bij deze *Crb1* mutant ratten. Bovendien konden we de netvliesdegeneratie bij individuele

ratten op verschillende tijdstippen visualiseren met behulp van spectraal-domein Optical Coherence Tomography (SD-OCT).

In dit onderzoek was het essentieel om de verschillen tussen knaagdieren en mensen goed te bestuderen. Daarom werd de sub-cellulaire lokalisatie van het CRB1 en CRB2 eiwit bepaald met behulp van immuno-elektronen microscopie. In **Hoofdstuk 3** wordt aangetoond dat de endogene expressie van het CRB1- en CRB2-eiwit in Brown Norway ratten overeenkomt met eerdere bevindingen in de muis retina. Echter, recente studies op niet-humane primaten, humaan foetaal retina, en humaan-afgeleide netvlies organoïden tonen een andere lokalisatie van het CRB1- en CRB2-eiwit. Dit benadrukt opnieuw het belang van het gebruik van humaan-afgeleide modellen voor gentherapie, waar mogelijk.

In **Hoofdstuk 4 en 5** werd gebruik gemaakt van humaan geïnduceerde pluripotente stamcel (hiPSC) afgeleide netvlies organoïden. **Hoofdstuk 4** beschrijft netvlies organoïden afkomstig van *CRB1*-patiënten, terwijl **Hoofdstuk 5** zich richt op *CRB1*^{KO} en *CRB1*^{KO}*CRB2*^{+/-} netvlies organoïden. Zowel de netvlies organoïden afkomstig van *CRB1*-patiënten als de *CRB1*^{KO} en *CRB1*^{KO}*CRB2*^{+/-} netvlies organoïden tonen een significante afname van fotoreceptor kernen in een rij, en meer fotoreceptoren boven de buitenste limiterende membraan (OLM), in vergelijking met de isogene controles. Single-cel RNA-sequensen in **Hoofdstuk 4** toont aan dat de expressieniveaus van het *CRB1* transcript vergelijkbaar zijn tussen de *CRB1* patiënt-afgeleide netvlies organoïden en de isogene controles, terwijl het CRB1 eiwit duidelijk verminderd is in *CRB1* patiënt-afgeleide netvlies organoïden. Dit geldt ook voor de *CRB1*^{KO} en *CRB1*^{KO}*CRB2*^{+/-} netvlies organoïden in vergelijking met de isogene controle, waarbij ook een verminderd CRB1 eiwit op de OLM wordt waargenomen (**Hoofdstuk 5**). Samengevat vertonen zowel de *CRB1* patiënt-afgeleide netvlies organoïden als de *CRB1*^{KO} en *CRB1*^{KO}*CRB2*^{+/-} netvlies organoïden een vergelijkbaar fenotype als wat wordt waargenomen bij patiënten. Dit maakt beide modellen bruikbaar voor verdere AAV-gemedieerde gentherapie studies.

Voordat de mogelijkheid van gentherapie met behulp van AAV kan worden bestudeerd, is het belangrijk om de AAV-tropisme in ratten (**Hoofdstuk 3**) en in netvlies organoïden (**Hoofdstuk 4 en 5**) te onderzoeken. Subretinale injectie van AAV2/5 en AAV2/9 in ratten resulteerde in transductie van het retinaal pigmentepitheel (RPE) en fotoreceptoren, terwijl de AAV6 variant ShH10^{Y445F} zowel de RPE, fotoreceptoren, MGC, als andere cel types in de INL transduceerden. Intravitreale injectie van AAV2/5 en AAV2/9 toonde een relatief lage transductie efficiëntie van zowel fotoreceptoren als cellen in de INL, maar na intravitreale injectie van ShH10^{Y445F} werd een efficiënte transductie van voornamelijk MGC waargenomen. Om deze reden is in **Hoofdstuk 3** gebruik gemaakt van ShH10^{Y445F}.hCRB voor verdere AAV-gemedieerde gentherapie toepassingen bij de *Crb1* mutant ratten. AAV2/5 en AAV2/2 zijn onderzocht in **Hoofdstuk 4** voor de transductie van jonge controle organoïden, terwijl in **Hoofdstuk 5** oudere controle organoïden werden gebruikt. Zowel AAV2/2 als AAV2/5 transduceerden fotoreceptoren, MGC, en andere cellen in de INL op een efficiënte wijze, waarbij AAV2/5 net iets efficiënter was in de transductie van cellen in de INL (inclusief MGC). Om de doelcellen (fotoreceptoren en MGC) in de netvlies organoïden te transduceren, is AAV2/5.hCRB gebruikt in **Hoofdstuk 4 en 5** voor verdere mogelijkheden van gentherapie.

Voorafgaand onderzoek heeft aangetoond dat AAV-gemedieerde *CRB2* gentherapie succesvol was in het beschermen van netvlies degeneratie in *Crb1* RP muis modellen. Daarom werd in **Hoofdstuk 3** de toepasbaarheid van gentherapie onderzocht in de *Crb1* mutant ratten met ernstige en vroeg beginnende netvliesdegeneratie. Helaas werd er geen verbetering waargenomen in het degeneratieve fenotype, vanwege de ernstige degeneratie die al op jonge leeftijd aanwezig was bij deze ratten. Dit suggereerde dat vroegtijdige expressie van recombinant CRB-eiwitten nodig is om de degeneratie in deze *Crb1* mutant ratten tegen te gaan. Daarnaast werd AAV-gemedieerde *CRB* gentherapie onderzocht op humaan-afgeleide netvlies organoïden (**Hoofdstuk 4 en 5**). In **Hoofdstuk 4 en 5** werd het RP fenotype gedeeltelijk verbeterd na behandeling met AAV.hCRB2, wat resulteerde in een herstel van de hoeveelheid fotoreceptor kernen in een rij. Bij de *CRB1* patiënt-afgeleide netvlies organoïden (**Hoofdstuk 4**) werd ook een gedeeltelijke verbetering van het fenotype waargenomen na AAV.hCRB1 behandeling.

Single cel-RNA sequentie analyse van AAV behandelde *CRB1* patiënt-afgeleiden netvlies organoïden toonde ook een gedeeltelijk herstel van de transcript expressie van genen die gerelateerd zijn aan het endosomale systeem.

In conclusie, in dit proefschrift hebben we (1) het fenotype van *CRB1* mutant muizen, ratten, en humaan-afgeleide netvlies organoïden getoond, (2) de verschillen in AAV-tropisme in diverse modellen weergegeven, en (3) we hebben AAV.h*CRB* gemedieerde gentherapie succesvol toegepast in *CRB1* patiënt, *CRB1*^{KO}, en *CRB1*^{KO}*CRB2*^{+/-} netvlies organoïden. De data die in dit proefschrift wordt beschreven, is van belang voor toekomstige gentherapie studies in patiënten met een mutatie in het *CRB1* gen.

List of publications

Boon N., Lu, X., Andriessen, C.A., Orlova, M., Quinn, P.M.J., C.J.F. Boon, and Wijnholds, J. Characterization and AAV-mediated Gene Therapy in Human Derived *CRB1*^{KO} and *CRB1*^{KO}*CRB2*^{+/-} Retinal Organoids. *Manuscript Submitted*

Boon N., Lu, X., Andriessen, C.A., Moustakas, I., Freund, C., Arendzen, C.H., Böhringer, C.J.F., Boon, S., Mei, H., and Wijnholds, J. AAV-Mediated Gene Augmentation Therapy of *CRB1*-Patient Derived Retinal Organoids Restores the Histological and Transcriptional Retinal Phenotype. *Stem Cell Reports* **2023**, 18, 5

Boon, N., Alves, C.H., Mulder, A.A., Andriessen, C.A., Buck, T.M., Quinn, P.M.J., Vos, R.M., Koster, A.J., Jost, C.R., and Wijnholds, J. Defining Phenotype, Tropism, and Retinal Gene Therapy using Adeno-Associated Viral Vectors (AAVs) in New-Born Brown Norway Rats with a Spontaneous Mutation in *Crb1*. *Int. J. Mol. Sci.* **2021**, 22, 7, 3563

Boon, N., Wijnholds, J., and Pellissier, L.P. Research Models and Gene Augmentation Therapy for *CRB1* Retinal Dystrophies. *Front. Neurosci.* **2020**, 14, 860

Alves, C.H., **Boon, N.**, Mulder, A.A., Koster, A.J., Jost, C.R., and Wijnholds, J. *CRB2* Loss in Rod Photoreceptors is Associated with Progressive Loss of Retinal Contrast Sensitivity. *Int. J. Mol. Sci.* **2019**, 20, 4069

Buck, T.M., Quinn, P.M.J., Pellissier, L.P., Mulder, A.A., Jongejan, A., Lu, X., **Boon, N.**, [..], and Wijnholds, J. *CRB1* is Required for Recycling by RAB11A+ Vesicles in Human Retinal Organoids. *Stem Cell Reports* **2023**

Möller-Kerutt, A., Rodriguez-Gatica, J.E., Wacker, K., Bhatia, R., Siebrasse, J., **Boon, N.**, [..], Wijnholds, J., Pavenstädt, H., and Weide, T. *Crums2* Is an Essential Slit Diaphragm Protein of the Renal Filtration Barrier. *J Am Soc Nephrol* **2021**, 32, 5, 1053-1070

Dona, M., Slijkerman, R., Lerner, K., Broekman, S., Wegner, J., Howat, T., Peters, T., Hetterschijt, L., **Boon, N.**, [..], and van Wijk, E. Usherin Defects Lead to Early-Onset Retinal Dysfunction in Zebrafish. *Exp. Eye research* **2018**, 173, 148-159

Dudek, A., Boer, J.S., **Boon, N.**, [..], and Verhaegh, G.W. Identification of Long Non-Coding RNAs that Stimulate Cell Survival in Bladder Cancer. *Oncotarget* **2017**, 8, 21

Curriculum Vitae

Nanda Boon was born on February 25th, 1994 in Vught, the Netherlands. After completing high school at Maurick College in 2012, she pursued a degree in Molecular Life Sciences at Radboud University in Nijmegen and obtained her Bachelor's diploma in 2015. Subsequently, she enrolled in the Master's program in Molecular Life Sciences with specialization in Clinical Biology at the Radboud University in Nijmegen. During her Master's studies, she spent half a year studying at University College Cork in Ireland. Additionally, she completed two internships: the first internship (8 months) was at the Department of Human Genetics, and the second internship (7 months) was at the Department of Medical Oncology, both at the Radboud University Medical Centre in Nijmegen.

In 2018, she began her doctoral research as a PhD candidate in the Department of Ophthalmology and the Department of Cell and Chemical Biology at the Leiden University Medical Centre, under the supervision of Prof. Dr. Gré Luyten and Dr. Jan Wijnholds. Throughout her PhD, she focused on studying adeno-associated viral vector mediated gene augmentation therapy approaches for *CRBI* related retinal dystrophies in animal models (mice and rats) as well as in human-derived model systems (retinal organoids).

Currently, she works as a Study Director at Charles River Laboratories in 'S-Hertogenbosch in the Development and Reproductive Toxicology (DART) group.

Acknowledgements

Daar zijn we dan; na een tijd vol uitdagingen, tegenslagen, en ontdekkingen is mijn PhD thesis eindelijk voltooid, en wat ben ik er blij mee. Maar uiteraard heb ik dit niet alleen gedaan, dus ik wil graag degene die mij in deze tijd hebben bijgestaan bedanken.

Allereerst, Jan, bedankt voor je begeleiding, kritisch denken, en levendige discussies tijdens mijn promotietraject. Ik heb heel erg veel geleerd. Ook veel dank aan Prof Gré Luyten, voor alle input tijdens onze meetings én het organiseren van de gezellige kerst diners.

A special thanks has to go to Henrique and Pete: even though we only worked together shortly, I learned a lot from both of you, and I really appreciate all the help over the years! Xuefei and Charlotte, thank you for all the support and fun times in the lab. To the remaining members of the Wijnholds Lab I had the opportunity to work alongside with - Andy, Rossella, Thilo, Michaela, and Carmen - thank you for your valuable input during the meetings and for the enjoyable chats in the lab. To my students - Suzanne, Arend, Lars, Rutger, Rousjan, and Chelsey - thanks for your hard work on the projects.

Van de afdeling Oogheelkunde - Annelies, Pieter, Rogier, Maria - en met name Mieke bedankt voor alle hulp tijdens mijn PhD traject. Ik vond het ook altijd fijn om weer een dagje achter de cryostaat te zitten, mede dankzij Els en Hanneke, was het daar altijd gezellig.

Verder wil ik alle medewerkers van het LUMC Proefdiercentrum bedanken, met name Ben, Fred, Martine, en Marloe voor jullie goede zorgen, zonder jullie had ik veel van mijn experimenten niet kunnen uitvoeren! En ook dank aan Nelleke, Marleen, Jos, Ewout en Jozien voor het helpen met meer organisatorische problemen. Daarnaast wil ik ook de LUMC Microscoop Faciliteit bedanken voor hun harde werk en hun hulp wanneer ik vragen had over een microscoop. In het bijzonder dank aan Aat, Annelies, Carolina, Karien, Lennard, en Willem.

Finally, I would like to extend my thanks to the Department of CCB, the CCB Secretary, and also to the members of the Virus and Stem Cell Biology Section for all the help in the lab and discussions during the vision meetings. Thank you to: Arnoud,

Diana, Hidde, Igno, Iris, Jin, Julia, Kim, Lonneke, Maaïke, Manuel, Martijn, Pauline, Qian, Rob, Sanne, Selas, Sofia, Steve, Timo, Vera, Willemijn and Zhen. Additionally, I want to express my special thanks to Harald and Maria, working in S2-36 with you was always great, and I learned a lot from both of you.

I am also incredibly grateful for all the friends I made during my PhD time in Leiden. The numerous borrels and dinners with you were always a great way to remind us that there is more to life than just work - Leo, Marghe, Fra, Andy, Rossella, Thilo, Dylan, Ale, David, Ale, Ila, Igno, Jessie, Daniel, Sebastiaan, Fredrik, Marcella, and Timo - thank you for the cherished memories! Nicolette, my first friend in Leiden, I am truly grateful that we are still having our monthly movie nights together even across the ocean. Nico, bedankt voor de ontelbare gezellige eet-, sport-, en spelletjes-avonden die we vooral de laatste jaren heel veel hebben gehad! Special thanks goes to Marghe, Leo, and Fra for all the great adventures we had together. And finally, the biggest shoutout goes to my paranymphs: Andy and Fra. You have been such amazing friends and I am happy to have shared my years in Leiden (and beyond) with you.

Nu nog even een stukje in het Nederlands voor mijn lieve vrienden en familie. Maris en Han, bedankt voor alle steun én de gezellige avondjes (ook met Remco en Jasper erbij) door de jaren heen! Lieve Chel, Em, en Lau, ik ben zo blij dat we, ondanks dat we verspreid over heel Nederland zijn, altijd tijd maken om de moeilijke maar zeker ook leuke tijden met elkaar te delen.

Eva en Lara, mijn lieve zusjes, ik ben heel blij dat wij zo'n goede band hebben en dat we altijd voor elkaar klaar staan! Liefste papa en mama; jullie opvoeding hebben me gemaakt tot wie ik nu ben en waar ik sta, en hiervoor ben ik jullie enorm dankbaar. Daarnaast heb ik ook hele leuke bonus-familie: Ank, Sebas, Jeanne, René, Louise, Pepijn, en Xi, die ik graag wil bedanken voor alle support en interesse.

En als laatste, Hugo, woorden kunnen niet uitdrukken hoeveel jij voor mij betekent. Je stond altijd voor me klaar, zowel in goede als in moeilijke tijden, en zonder jou had ik het nooit gered. Daar ben ik je eeuwig dankbaar voor. Ik hou van je!

